Fluctuations in the cosmic microwave background

Anthony John Banday

Fluctuations in the Cosmic Microwave Background

by
Anthony John Banday BSc. (Dunelm)

Being an account of the work undertaken
in the Department of Physics and submitted
in accordance with the regulations for admission
to the degree of Doctor of Philosophy.

December 16, 1991

Abstract

Fluctuations in the Cosmic Microwave Background

The search for fluctuations in the Cosmic Microwave Background (CMB) is one of the most important topics in modern cosmology, since their detection would reveal a great many details about the early universe and, in particular, the nature of the primordial density perturbations giving rise to the galaxies and clusters of galaxies seen in the universe today. However, the search for such anisotropies is not trivial – none have been detected as yet – largely as a consequence of the fact that all radiative astrophysical sources can give rise to anisotropic foregrounds which confuse the search for genuine cosmological signals.

In this thesis, a detailed study is made of the contribution of such foregrounds to searches for CMB fluctuations. After Chapter 1 summarises the theoretical and observational status of the subject, Chapters 2, 3 and 4 consider the foreground resulting from the Galaxy. It is found that frequencies in excess of 20 GHz are required to reduce the Galactic Synchrotron Radiation to a level where genuine anisotropies might be detected (the synchrotron emission is almost certainly responsible for a previously claimed detection), and that dust emission, especially if very cold dust exists which is unseen and possibly untraced by the dust responsible for the emission seen in the IRAS 100 μm passband, can seriously constrain high frequency searches. In Chapter 4 a model is derived for the overall Galactic foreground including a separation of the thermal and non-thermal radio emission in the Galactic plane. Comparison with observations at 10 and 15 GHz suggests that the model is $\sim$ 10% - 20% accurate on average at these frequencies, and maps of the predicted emission at the COBE frequencies 31.5, 53, and 90 GHz are provided. A search is made for a frequency window and sky region which minimises the Galactic contribution to the fluctuation measurements: highly sensitive, high resolution searches should be designed with these values in mind. Chapter 5 investigates the anisotropies resulting from discrete extragalactic sources, in particular, the far-infrared emission from dust in spiral galaxies and the integrated radio emission due to radio galaxies, QSOs etc. A frequency window of $\sim$ 30 - 100 GHz is found to minimise both Galactic and extragalactic foreground anisotropies. Chapter 6 considers several cosmological models which could generate the recently observed large-scale structure in the galaxy distribution: these are constrained by CMB anisotropy limits. It is concluded that genuine cosmological variations in the CMB temperature are now close to detection if the observed galaxy structures are real. Chapter 7 indicates some future projects which should help in the detection and interpretation of CMB fluctuations.

Preface

The work described in this thesis has not been submitted for any degree, diploma or other qualification at any other university. Some of the calculations have been carried out in collaboration with M. Giler, J. Szabelski, B. Szabelska and A.W. Wolfendale, but the majority of that reported is the author's own work.

The following results have been published elsewhere as follows:

Banday, A.J., & Wolfendale, A.W., 1990a. *Proc. 21st I.C.R.C*, **4**, 467.

Banday, A.J., & Wolfendale, A.W., 1990b. *Mon. Not. R. astr. Soc*, **245**, 182.

Banday, A.J., & Wolfendale, A.W., 1991a. *Mon. Not. R. astr. Soc*, **248**, 705.

Banday, A.J., Giler, M., Szabelska, B., Szabelski, J., & Wolfendale, A.W., 1991a. in *Vulcano Workshop 1990: Frontier Objects in Astrophysics and Particle Physics*, p.203, **eds.** Giovannelli, F. & Mannocchi,G., Editrice Compositori Bologna.

Banday, A.J., Giler, M., Szabelska, B., Szabelski, J., & Wolfendale, A.W., 1991b. *Astrophys. J.*, **375**, 432.

Banday, A.J. & Wolfendale, A.W., 1991b. *Mon. Not. R. astr. Soc*, **252**, 462.

Banday, A.J., Giler, M., Szabelska, B., Szabelski, J., & Wolfendale, A.W., 1991c. in *Observational Tests of Cosmological Inflation*, p.419, **eds.** Shanks, T., Banday, A.J., Ellis, R.S., Frenk, C.S., & Wolfendale, A.W., Kluwer Academic Press.

Banday, A.J., Giller, M. & Wolfendale, A.W., 1991. *Proc. 22nd I.C.R.C.*, in press.

Banday, A.J., Giler, M., Szabelska, B., Szabelski, J., & Wolfendale, A.W., 1991d. *Proc. 22nd I.C.R.C.*, in press.

Acknowledgements

I should firstly like to thank my supervisor Professor Arnold Wolfendale for all the help, motivation and suggestions he has provided me with over the past three years. Dr John Osborne has also provided invaluable assistance and advice. For both pleasent chats and helpful discussions, I should like to thank Jacek Szabelski, Tom Shanks, Iain MacLaren, Duncan Hale-Sutton, Dick Fong and all of our group visitors from Poland, Russia and India. For helping me to remain somewhat sane, thanks to Gordon Love, Lilian Graham, Alison Broadbent, Neasa Foley, Sue Watkin and Ken Richardson. Thanks to the Cosmology football team for the success which inspired me to such great heights (?), and to Dominic's team for providing me with a good laugh. Thanks to everyone else in the Department with whom I have had contact for their help and friendship, and a special thank you to Margaret for all the advice and to Pauline for the advice and the drawings.

Now to the part where I thank all those at St. Aidan's for giving me the opportunity for a few laughs (and lots of beers) away from work. So, thanks to:

- the 'A-straight boys' – Weg, Steve P, Gary, Rich, Dinsdale, Pat, Graham, Dave, Steve T, Hans, John W, Lizanne, Shirley, Simon & Paul, Paul (PT), Paddy, Steve Fox and James W.
- The lads ('88 - '90) – Dave ('Ω must equal bloody millions mate'), Gareth, Duncan, Hamish, Bobby P, Duncan H, Chris V, Chris J, Steve Mac and JCP.
- D-house *et al.* – Marc (for useful discussions !), Cath, Caroline, Rich (Norman Psycho Jenkins), Sean, Simon, Andy P, Alex, Crowdie Phil, Steve B, Midge, Karen, Pete (Rocky) Costello, Andy T.
- E-house *et al.* '91 – Cathy, Cath, Kazza, Bobby, Si, Robin, Rufus, Steve, Jason, Laz, Ellie, Ian, Ben, Tom, Louise, JD, Si Lloyd, Jo, Pete, and of course Paul.

Finally, to those closest to me, my parents, Gran, the Giacominis – thanks for all the help and support.

To my family and friends .....

Contents

Chapter 1

Overview of the CMB

1.1 Discovery and Physical Significance of the CMB

The discovery of the Cosmic Microwave Background (CMB) was announced in July 1965 by Penzias & Wilson who, after careful analysis of known sources of noise, identified an isotropic unpolarised component of the sky temperature, measured by the Bell Telephone Laboratories' 20 ft. horn reflector, of 3.5 ± 1 K. A companion paper (Dicke *et al.* , 1965) identified this 3.5 K excess radio noise as the thermal radiation remaining from the hot big bang origin of the universe, as first outlined by Gamow (1948) and his colleagues Alpher & Herman (1948, 1949).

The importance of the CMB lies in its almost unique ability to probe the geometry and physical conditions of the early universe, which provides important clues to the formation of the structure seen in the universe today. The CMB originates at that epoch in the universe's history when the temperature falls to a sufficiently low value to allow the transition from a hot optically thick plasma to a transparent neutral gas at a lower temperature. Prior to this epoch of *recombination*, the photons and electrons were coupled strongly by Thomson scattering. As the universe becomes neutral however, the mean free path of the photons exceeds the size of the universe and they free-stream towards us from what is known as 'the last scattering surface'. The photons appear to originate from this surface, but physically this is not the case – the result is due to the final scattering of the photons occurring at almost the same time across the universe as a whole. Prior to recombination, there

should be fluctuations in the matter component which are the precursors of the structure – galaxies, clusters and superclusters of galaxies – seen today. These fluctuations will be coupled then to fluctuations in the photon distribution (although the precise details of the coupling depends on the overall matter content of the universe, and remains under discussion) such that if they survive the recombination process, the perturbations will be recognised as small temperature variations on the surface of last scattering. Thus, the fluctuations in the CMB sky temperature reflect the physical conditions of the perturbations at recombination. If it were possible to trace the evolution of the matter perturbations, from this epoch through galaxy formation until today, then our theoretical ideas would be on much firmer ground. In practice, the period between decoupling and the formation of galaxies is lost in what might be referred to as the 'cosmic dark ages' since the evolving matter perturbations give off no observable radiation signature (at least until densities rise to such a level that accreting black holes might form). Thus observations of the CMB fluctuations, together with maps of the distribution of galaxies on the sky, must be used to constrain our cosmological models. The connection between an anisotropy of angular size θ and matter fluctuation of mass M can be shown to be

$$\theta \;=\; 9\Omega^{\frac{2}{3}}\,h^{\frac{1}{3}}\left[\frac{M}{10^{15}\,M_{\odot}}\right]^{\frac{1}{3}}\ \text{arcmin}$$

where $h = H_0/100\ \text{kms}^{-1}\ \text{Mpc}^{-1}$ (Davies, 1988). Thus galaxies correspond to fluctuations on a scale of about 20", clusters of galaxies to about 10', and the largest structures yet identified to a few degrees.

The above describes ideas about the CMB in quite general terms, and for the simplest scenario, as summarised in Fig. 1 which is now described in more detail. The figure demonstrates what can be learnt from studying anisotropies in the CMB. The microwave photons free-stream from the surface of last scattering to the observer 'here and now'. Recombination in the standard Big Bang model occurs in the redshift range 1000 - 1500, and as a consequence of the non-instantaneous recombination of hydrogen, the last scattering surface is defined by a transmission factor which is related to the Thomson scattering cross-section and is well approximated by a gaussian peaking at a redshift of ~ 1065 and with a width $\Delta z \sim 80$ (Wyse & Jones, 1985). This corresponds to a comoving distance of $\sim 7\ h^{-1}\ \Omega^{-\frac{1}{2}}$ Mpc (Kaiser & Silk, 1986). The finite width of the shell then smoothes out fluctuations on an-

gular scales $\Delta\theta \leq 8\ \Omega^{-\frac{1}{2}}$ arcmin due to the residual Thomson drag. Again, this is the standard scenario, but in fact the redshift of the surface of last scattering is an important and unknown cosmological parameter – it is possible that the universe did not recombine until much later in its history, or that the matter content was re-ionised at some later epoch (for example, by pregalactic sources such as Population III stars - see Negroponte, 1986). In this case, although sensitive to the amount of baryonic material in the universe, assuming $\Omega_b \sim 1$ and full re-ionisation, the optical depth for Thomson scattering reaches unity at $z \sim 15$ (Partridge, 1988). If the last scattering surface is shifted to lower redshifts, then even large-scale primordial fluctuations are not necessarily preserved. To avoid the considerable uncertainty in the interpretation of fine-scale anisotropy, it is best to observe over an angular scale which exceeds that subtended by the particle horizon at the latest epoch of last scattering. This angular scale $\theta_* \sim (\Omega/z)^{\frac{1}{2}}$ radians, and so, in the conventional model, observations aimed at $\theta \geq 2°$ would be suitable. If $\Omega_b \leq 0.1$, then the minimum last scattering redshift is ~ 30, so angular scales $\geq 10°$ involve the least number of assumptions about the early universe.

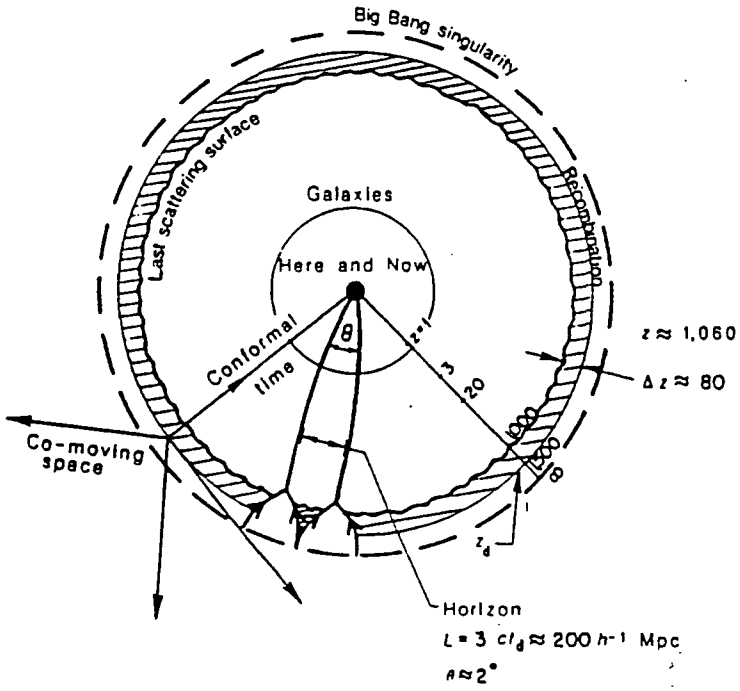

Figure 1.1: Co-moving space/conformal time diagram of the Big Bang. The observer ('here and now') is at the centre. Various important epochs for the CMB are denoted. Taken from Kaiser & Silk (1986).

One last important quantity that the CMB allows us to probe is the velocity of the Galaxy. Since the Doppler effect increases the energy of the photons in the direction of the observer's motion and thus raises the observed intensity and temperature of the CMB, any motion results in a dipole pattern in the observed sky pattern. The best fit dipole (Smoot *et al.* , 1991) has an amplitude 3.3 ± 0.2 mK in the direction $(\alpha , \delta) = (168° \pm 3° , -7° \pm 2°)$.

1.2 The CMB Spectrum

Before considering the nature of CMB anisotropies, which remains the main topic of interest in this thesis, we briefly consider the nature of the spectrum of the CMB and what cosmologically interesting facts it might reveal. If the radiation is left over from a hot, dense phase of the early universe, then the spectrum should be blackbody. This blackbody spectrum is generated during the early phase of thermal equilibrium, and retained during the subsequent expansion of the universe. Since the observed thermodynamic temperature of a Planckian spectrum is independent of frequency, then determining the frequency dependence is a direct test of the hot Big Bang interpretation of the background. However, distortions might be expected to arise at some level in most convincing cosmological scenarios, simply because the universe as observed today is inhomogeneous to some degree. Sources and sinks of radiation are present now, as they undoubtedly were in the past, and may result in deviations from a perfect blackbody spectrum. Considerable effort has been put into theoretical work establishing the nature of such distortions (see Burigama, de Zotti & Danese, 1991, for the most recent work) which might result from such processes as dark matter decay, the dissipation of shock and acoustic waves associated with adiabatic density perturbations, dissipation of gravitational wave energy, phase transitions in the early universe or energy released through the isotropisation of an anisotropic universe. In simple cosmological models the spectrum at recombination is more or less preserved until the present, although redshifted by a factor of ~ 1000, since in a neutral medium neither Thomson scattering nor bremsstrahlung will occur. More complex models may call for substantial energy injection resulting in physically revealing distortions which remain until the present unless there is sufficient time for bremsstrahlung and Thomson scattering to relax the spectrum back to that for a blackbody.

At redshifts greater than a few 10^6, the combined action of bremsstrahlung and radiative Compton scattering tightly couples the matter and radiation fields, thus photon production can take place on a timescale short compared to the expansion time and any non-blackbody features are quickly erased. If the matter is heated with extra energy at redshifts before recombination, but less than $\sim 10^6$, there is cooling below the peak and heating at high frequencies, with bremsstrahlung producing additional low frequency photons. If the energy release occurs in the range $10^5 < z < 10^6$ then the number of Thomson scatterings is insufficient to bring the photons and plasma back into thermal equilibrium and the other radiative processes do not have enough time to add sufficient photons to reestablish a Planckian spectrum. The resulting spectral distortion is Bose-Einstein with a chemical potential μ which is exponentially attenuated at low frequencies. There is a general cooling for frequencies below the peak with the maximum decrease in the range $\sim$ 3 - 10 GHz. At redshifts smaller than $\sim 10^5$, the electron density is no longer high enough for Thomson scattering to establish a Bose-Einstein spectrum. The spectrum assumes a mathematically more complex form, with increased brightness temperature in the Rayleigh-Jeans region due to bremsstrahlung emission from relatively hot electrons, a reduced temperature in the middle Rayleigh-Jeans region where the photons are depleted by Thomson scattering, and a high Wien temperature where the low frequency Thomson scattered photons accumulate. The equations describing these distortions are described in Smoot *et al.* (1988), the interested reader is referred to Danese & de Zotti (1982) for a complete review. The distortions then depend on quantities such as the baryonic content of the universe, thus can help to constrain cosmological parameters. In practice, the equations only approximate the spectral distortions – a proper description requires the solution of the full relativistic Kompaneets equation. This has been performed recently using numerical techniques by Burigama, de Zotti & Danese (1991).

Distortions can also arise from post-recombination physical processes. Comptonisation is the most likely deviation from a blackbody spectrum. If an energy source heats ionised intergalactic material, the hot electrons scatter low energy photons to higher energy, making the CMB cooler at frequencies below the peak, and hotter in the Wien region. This process occurs in X-ray emitting galaxy clusters where it is known as the Sunyaev-Zel'dovich effect. Field & Perrenod (1977) also predicted such a distortion from its association with a hot intergalactic plasma producing the

2 - 50 keV X-ray background. More refined models, and the recent spectral results from COBE seriously restrict the contribution to the X-ray background from such a plasma. Any process which adds photons to the CMB will generate a distortion. Sources of high redshift dust can, in principle, create a sub-mm excess, and were much in favour when Matsumoto *et al.* (1988) found evidence for such an excess. Recent COBE results conflict with this claim, thus limiting the radiative output of dusty objects in the universe (see Chapter 5).

Finally, it is worth noting that spectral distortions can also restrict the primordial fluctuation power spectrum, providing complimentary information to that derived from CMB anisotropies (see Barrow & Coles, 1991).

1.2.1 Observations of the spectrum

The experimental techniques employed to measure the CMB temperature depend on the frequency concerned, and all suffer from systematics of one form or another. At the longest wavelengths, radiometers are used which, as a consequence of the size of the antennas and wave guides involved require the observations to be ground-based. This allows some flexibility in pointing the horn at selected regions of the sky, but must contend with atmospheric emission, reduced by operating the system at a high dry site. Kogut *et al.* (1991) contains a summary of ten years of long wavelength CMB observations by the so-called White Mountain group. At shorter wavelengths, the radiometers may be balloon or rocket mounted, thus enabling the atmospheric contribution to be reduced further. Bolometers may also be employed on and shortward of the spectral peak, these are easily carried above the atmosphere by balloon or rocket. A short review by Staggs & Wilkinson (1991) describes the advantages or otherwise of various experimental techniques.

Fig. 2, taken from Staggs & Wilkinson (1991), but with an additional point at 36.6 cm from Sironi, Bonelli & Limon (1991) summarises the most recent measurements of the CMB temperature. The data shown are well fitted to better than 2σ by a temperature of 2.74 K apart from the Matsumoto *et al.* data denoted by the filled triangle. The disagreement of these points with the COBE and UBC rocket flight data suggests some unknown local radiation contaminating the data. Without significantly improved error bars, there is no compelling evidence for distortions at

any frequency. The detection of a distortion at the longest wavelengths will require detailed modelling of the Galactic contribution to the sky temperature, which is also a problem for many anisotropy experiments.

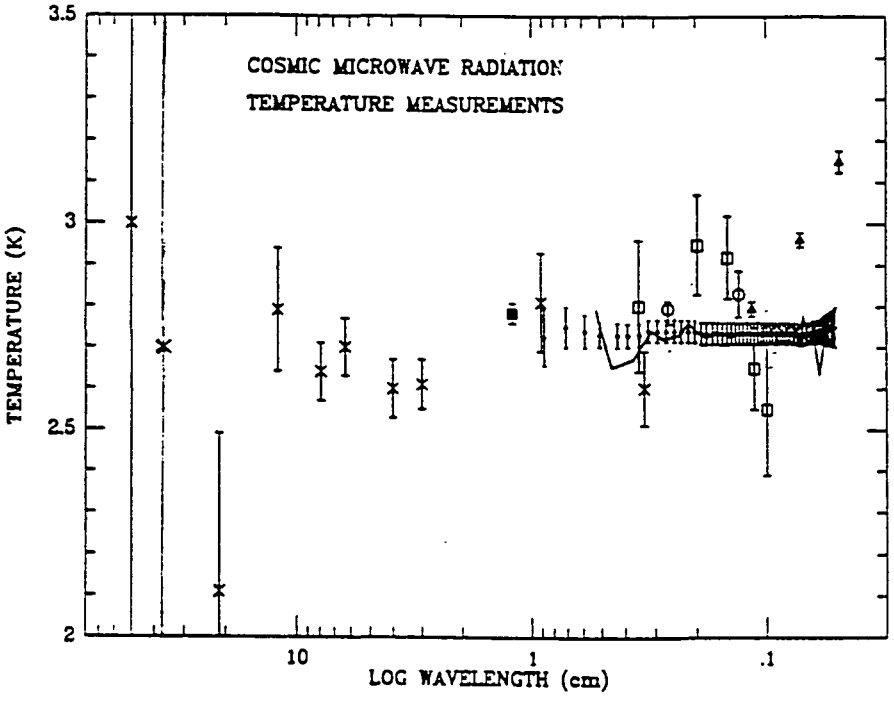

Figure 1.2: Recent measures of the CMB temperature; from Staggs & Wilkinson (1991) – see there for references.

1.3 CMB anisotropies

We have seen previously how anisotropies and their amplitudes are connected to physical processes in the universe such as recombination, and how such fluctuations have characteristic angular scales. However, as a further consequence of the close coupling of the matter and radiation before recombination, and the weak residual coupling during the finite width of the recombination epoch, anisotropies are expected on other characteristic scales associated with the fluctuations in the matter density, and depending on the evolution of the matter through recombination. This evolution itself depends on the exact nature of the perturbations (adiabatic or isocurvature). If the photon entropy per baryon is constant (adiabatic perturbations), then from a simple thermodynamic argument, fluctuations in the temperature $\Delta T/T = \frac{1}{3}\,\Delta\rho/\rho$ are present prior to recombination (Silk, 1967). The amplitude of

these fluctuations, however, is reduced by the substantial optical depth of the universe when perturbations on scales smaller than the comoving width of the last scattering shell become transparent and by the destructive interference of photons received from both peaks and troughs (Sunyaev & Zel'dovich, 1970). The peculiar velocity field associated with the density perturbations gives an additional contribution which dominates for scales close to, but smaller than, the horizon. A precise calculation must take into account the fuzziness of the last scattering surface and the specific strength of anticorrelations between electron velocities in neighbouring regions. Thus, the CMB temperature anisotropies reflect the density contrast in the matter, which on on a given scale is determined by the spectrum of primordial density perturbations. This spectrum is also expected to have several characteristic scales imprinted on it (Silk, 1984). Fluctuations on comoving scales larger than the horizon at the equivalence epoch z_{eq} (equal matter/radiation energy density), $\sim 50h^{-1}$Mpc, grow uninterruptedly, while the growth of smaller scales is suppressed between the time they cross the horizon and z_{eq}. On scales larger than the horizon at last scattering, the dominant source of anisotropy is fluctuations in the gravitational potential.

To properly calculate the amplitude of the anisotropies, the detailed coupling of matter and radiation must be followed. This involves solving the perturbed Boltzmann transport equation for the photon distribution, which is coupled to the matter distribution through Thomson scattering and gravitationally. A number of authors have studied this problem in considerable detail for a variety of cosmological scenarios (Peebles & Yu, 1970; Wilson & Silk, 1981; Bond & Efstathiou, 1984; Efstathiou & Bond, 1986; Bond & Szalay, 1983). Owing to the complexity of the problem, no details are given but the reader is referred to a review by Efstathiou (1990). Instead, we shall briefly comment on the behaviour of the different matter components which affect the radiation pattern. We consider the nature of the perturbations after they have crossed the horizon, since before this the behaviour of adiabatic and isocurvature modes is quite different.

i) **Baryons:** Baryon perturbations which cross the horizon after recombination grow as a consequence of self-gravity, otherwise, however, the coupling to the photons by Thomson scattering generates a counter-pressure to the gravitational interaction. Those perturbations smaller than the Jeans mass oscillate,

the smallest scales undergoing many collisions which essentially wipes them out as a consequence of photons diffusing out of the perturbation. This is known as Silk damping and has important consequences for purely baryonic cosmological models where no mechanisms exist to regenerate fluctuations on these scales. In models with CDM, the CDM perturbations are unaffected by Silk damping and act as seeds to regenerate the baryon perturbations after recombination. After recombination, the Jeans mass falls abruptly and any surviving baryonic perturbations with a mass greater than $\sim 10^6$ $M_\odot$ begin to grow again. If CDM perturbations are already present the baryons fall into them and both components grow together; if $\Omega_b \ll \Omega_{CDM}$ this happens very quickly and the growth of the CDM perturbations is unhindered, if $\Omega_b \sim \Omega_{CDM}$ the growth of the CDM perturbations is slowed by the smoother baryonic component.

ii) **Cold Dark Matter:** The critical scale here is that crossing the horizon at the equivalence epoch $k_{eq}^{hor} \simeq 0.3\,(\Omega h^2)$ Mpc^{-1}. On larger scales which cross the horizon after this time, CDM perturbations grow unaffected by the presence of other components. On smaller scales the CDM perturbations do not grow substantially since the radiation is the dominant component gravitationally, and the baryon-photon fluid oscillates as a consequence of the Thomson coupling. CDM perturbations grow when the energy density approaches that of the radiation. If baryons are gravitationally significant, the CDM growth is slowed until after recombination because of the oscillation of the baryon component. After recombination the baryons fall into the CDM perturbations and both components grow together.

iii) **Massless neutrinos:** These are relativistic collisionless particles, the perturbations in which grow before horizon crossing and free-stream after. They are gravitationally unimportant and merely help to define the equivalence epoch.

iv) **Massive neutrinos:** In the mass range $1eV < m_\nu c^2 < 100eV$, the neutrinos are relativistic initially, becoming nonrelativistic by the recombination epoch. After horizon crossing, relativistic perturbations will decay as a result of cancelling contributions from different directions originating at different locations in the wave. Semirelativistic perturbations will damp as a result of the smearing of fluctuations by a particle velocity dispersion. The largest scales, which

cross the horizon when nonrelativistic grow continuously like CDM. Smaller scales are damped until they become nonrelativistic when growth continues. The critical scale for massive neutrinos is then the scale crossing the horizon when the neutrinos become nonrelativistic. All scales smaller than $k^{hor}_{nonrel} \simeq 6.2 \times 10^{-3}$ $(m_\nu c^2)$ Mpc^{-1} are significantly reduced. The effect of the neutrinos in a hybrid model is to slow the growth of CDM perturbations on scales smaller than k^{hor}_{nonrel} until the CDM and neutrino amplitudes are equal.

The way in which the primordial fluctuation spectrum is modified through recombination is described by the transfer function formalism discussed in Chapter 6. The radiation component is affected by the matter components present; in particular, on large scales crossing the horizon around or after recombination photon perturbations are induced gravitationally by baryon, CDM and neutrino fluctuations (Sachs-Wolfe effect). For models with $\Omega < 1$, the anisotropy amplitude $\Delta T/T$ is increased roughly as Ω^{-1}. This is because the universe becomes curvature dominated at a redshift $\sim 1/\Omega$ and fluctuation growth effectively ceases. Thus normalisation to the observed structure today requires a higher initial fluctuation amplitude, raising $\Delta T/T$ (normalisation is discussed in Chapter 6). If there is a non-zero cosmological constant, the evolution of the perturbations is the same until the expansion of the universe differs from a flat universe. $\Lambda > 0$ increases the expansion rate which has the effect of slowing the growth of fluctuations. By a similar argument to before, $\Delta T/T$ is increased.

1.3.1 Evaluation of Radiation Anisotropy

Having numerically evaluated the perturbations to the photon distribution function, what is required is some measure of the anisotropy of the radiation field. If recombination is considered to occur at a single epoch, τ_{rec}, the perturbations in the radiation field are imposed on a spherical cross-section through the universe at distance $c\tau_{rec}$ centred on our present location. This surface of last scattering then corresponds to the celestial sphere, and since the CMB radiation pattern is generally considered to originate from a Gaussian random field, the anisotropy pattern can be fully described by the temperature autocorrelation function (a.c.f.) $C(\theta) = \left\langle \frac{\Delta T(0)}{T_0} . \frac{\Delta T(\theta)}{T_0} \right\rangle$ with ΔT the perturbation from the mean temperature T_0. Since

the observed radiation pattern is observed on a spherical surface, the correlation function can be expanded in terms of Legendre polynomials

$$C(\theta) = \frac{1}{4\pi} \sum (2l+1)\, C_l\, P_l(\cos\theta)$$

where the discrete function is the power spectrum associated with the l'th component of the radiation temperature seen on the sky. The C_l can the be directly related to the radiation fluctuations $\Delta_{T,l}$ as evaluated numerically from the Boltzmann equation in a plane wave decomposition of the fluctuations, so that

$$C(\theta) = \frac{V}{32\pi^2} \int_0^\infty \sum_{l\geq 2} (2l+1) \mid \Delta_{T,l}(k, \tau_0) \mid^2 P_l(\cos\theta)\, k^2\, dk$$

(Bond & Efstathiou, 1987) where V is a normalisation constant. In practice, the form of $C(\theta)$ is unobservable, requiring infinitessimally small beams. real beams of a finite size act as low pass filters, smoothing out scales much smaller than the beam. What is measured is the beam-modified autocorrelation function, thus theoretical calculations must fold in this smoothing. The smoothed correlation function $C_\sigma(\theta)$ can be evaluated using the small angle approximation of Wilson and Silk (1981) for a gaussian beam profile

$$F(\theta) = \frac{1}{2\pi\sigma^2} e^{-\frac{\theta^2}{2\sigma^2}}$$

where σ^2 is equal to the FWHM/2 ln 2. Then

$$C_\sigma(\theta) \simeq \frac{1}{2\sigma^2} \int_0^\infty C(\phi)\, e^{-\left(\frac{\phi^2+\theta^2}{4\sigma^2}\right)} I_0\left(\frac{\theta\phi}{2\sigma^2}\right) \phi\, d\phi$$

The correlation functions for a wide number of cosmological scenarios have been calculated by several authors, and to ease comparison of results between experiments the accurate a.c.f. calculations have been fitted by a variety of functions. For example, Bond & Efstathiou (1984) consider a wide range of models which they fit by a function of the form

$$C(\theta) = C(0)\,[1 + \frac{(\theta/\theta_c)^2}{2\beta}]^{-\beta}$$

Fits for other models can be found in Bond & Efstathiou (1987), Fukugita, Sugiyama & Umemura (1990), and Holtzman (1989). In Chapter 6, some of these results are used to evaluate anisotropies in several models of large-scale structure. Also in this chapter, details may be found of the technique used by Vittorio & Scaramella (1990) to evaluate the a.c.f. on large angular scales which basically involves an expansion of the correlation function into spherical harmonic components. The amplitude then depends solely on the primordial power spectrum, since on such scales there is little modification to it through recombination.

1.3.2 Secondary Anisotropies

A number of sources of secondary anisotropies are present between us and the surface of last scattering. Primordial temperature fluctuations can be erased on scales up to $\sim 10^\circ$ by a re-ionised intergalactic medium. The new small-scale anisotropies resulting from Thomson scattering off electrons are very small since contributions from the crests and troughs of any plane wave interfere destructively. However, Vishniac (1987) has shown that significant arcminute fluctuations arise as a second order effect due to inhomogeneities in the electron density and peculiar velocity.

Comptonisation by inhomogeneously distributed hot gas, ie. the hot gas component of bound structures is an important source of secondary anisotropies. In a CDM scenario, this effect is dominated by rare clusters of galaxies at moderate redshifts, which might contribute $\Delta T/T \sim 10^{-5}$ on arcminute scales (Cole & Kaiser, 1988).

Dynamic inhomogeneities between the observer and the last scattering surface induce second order Sachs-Wolfe anisotropies (Rees & Sciama, 1968). The profile of the temperature fluctuations is, in general, rather complex, however the effect of multiple inhomogeneities along a given line-of-sight is additive; Dyer & Ip (1988) have shown that it is possible to construct self-consistent models whereby these second order anisotropies are larger than those produced at the last scattering surface. Sanz & Martinez-Gonzalez (1991) are making a detailed study of the problem.

Multiple gravitational lensing by static compact objects at high redshift may reduce the level of fine-scale anisotropy, since the lensing alters the photon trajec-

tories, thereby smearing out the temperature fluctuations. Kashlinsky (1988) has suggested that the cumulative effect of lensing may result in the complete erasure of fluctuations on scales up to several arcminutes.

1.3.3 Observational techniques and results

A good review of the observational status of searches for CMB anisotropies in the CMB is given by Partridge (1988). Considerable time and effort has been invested in the search for fluctuations on a variety of scales, and the exact technique employed depends on the scale in question.

There are two general types of detector which have been employed: heterodyne receivers operating at a fixed frequency between $\sim$ 10 and 100 GHz, and bolometric detectors operating at a fixed frequency with broader bandwidths. More detailed descriptions can be found in the comprehensive review by Weiss (1980). In the case of heterodyne receivers, the sensitivity can usually be expressed as a function of the intrinsic noise generated by the detector (specified as system noise temperature T_{sys} and the bandwidth B employed. For an integration time t, the rms noise is given by

$$T_{rms} = K T_{sys}/\sqrt{B t}$$

where k is a constant depending on the exact nature of the experimental technique used (eg. K = 2 for a two beam differencing method). Representative figures for modern receivers operating at $\sim$ 30 GHz imply sensitivities of $\sim$ 1 mK in 40 s of integration time. The sensitivity of bolometers is achieved through the use of a large bandwidth which more than compensates for the increase in effective system noise over the heterodyne receivers.

Most experiments on large and intermediate scales are based on the Dicke switching radiometer technique (Dicke, 1946) whereby there is a rapid switching between two antennas, or one antenna and a cold reference load. The integrated difference between the two positions can greatly reduce short term gain fluctuations in the receiver. On longer time-scales drifts in the output may result from changes in either the gain or ground pick-up (the antenna detects the ground radiation in its diffraction side lobes), and some technique is usually employed to reduce this effect allowing the required long integration times. This generally takes the form of

either rotating the antennas or nodding them in some way. This results in the production of a triple beam pattern on the sky, which helps to eliminate systematic offsets between the two antennas and their ground radiation response. Fig. 3 shows the principles of the beamswitching technique. The actual physical movement of the detector could itself generate some offset problems, thus some observers (eg. Davies *et al.* , 1987) have chosen to combine first order switching with drift scans to determine the beam pattern. Again, Partridge provides a good review of these techniques, whilst Watson (1989) reviews them in the context of several particular experiments.

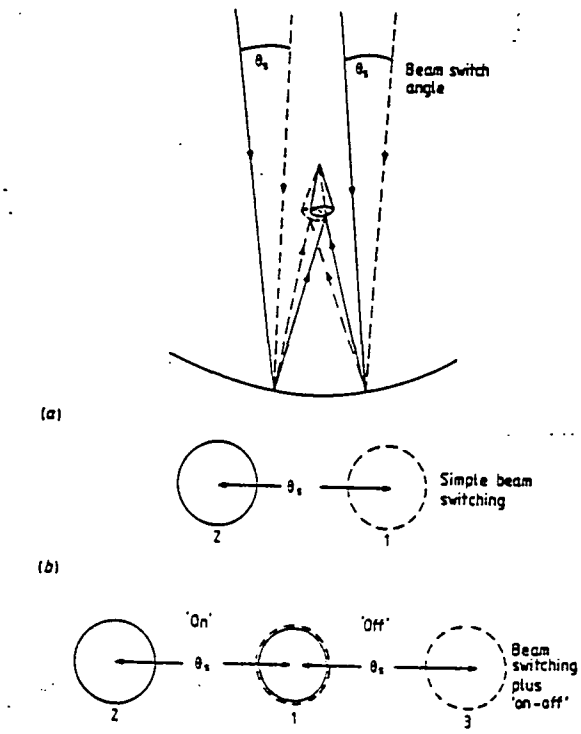

Figure 1.3: The production of two and three beam patterns on the sky. From Partridge (1988).

On small scales, apertures of order 10 m or so are required, thus use is made of existing radio astronomy facilities. On the smallest scales ($\leq$ 1') interferometric techniques are employed, and have achieved remarkably sensitive limits to the sky noise.

Table 1 summarises the most recent upper limits for a number of angular scales, these are also shown in Fig. 4. These limits have imposed some very serious constraints on a number of cosmological models. For example, the Readhead *et al.* (1989) result rules out adiabatic baryonic models with 95% confidence, finds that

isocurvature models with $\Omega < 0.8$ are inconsistent with the limits, and places useful constraints on reionisation in non-standard recombination models; the Vittorio *et al.* (1991) analysis of the UCSB South Pole experiment (Meinhold & Lubin, 1991) constrains the density parameter of CDM universes with $\geq 3\%$ baryon abundance and h = 0.5 to be $\Omega_0 \geq 0.6\ b^{-1}$ where b is the bias parameter.

Reference	ν (GHz)	θ_c	$\Delta T/T$
Meyer, Cheng & Wilkinson (1991)	167	13°	1.6×10^{-5}
Melchiorri *et al.* (1981)	429	6°	4×10^{-5}
Davies *et al.* (1987)	10	4°	3.7×10^{-5}
Watson *et al.* (1988)	10	4°	3×10^{-5}
Lasenby *et al.* (1991)	15	4°	2.5×10^{-5}
Mandolesi *et al* (1986)	10	2° - 6°	$5 - 7 \times 10^{-4}$
Dall'Oglio & de Bernardis (1988)	150	1.3°	2.5×10^{-4}
Timbie & Wilkinson (1990)	43	1.1°	1.1×10^{-4}
de Bernardis *et al.* (1990)	270	45'	2.2×10^{-4}
Fischer *et al.* (1991)	180	30'	1.2×10^{-4}
Meinhold & Lubin (1991)	90	20'	3.5×10^{-5}
Uson & Wilkinson (1985)	20	4'.5	5×10^{-5}
Readhead *et al.* (1989)	20	2'	1.5×10^{-5}
Martin & Partridge (1988)	5	36" - 160 "	1.3×10^{-4}
Martin & Partridge (1988)	5	18" - 80 "	1.7×10^{-4}
Fomalont *et al.* (1988)	5	60"	0.6×10^{-4}
Fomalont *et al.* (1988)	5	30"	0.8×10^{-4}
Fomalont *et al.* (1988)	5	18"	1.2×10^{-4}
Hogan & Partridge (1989)	15	18"	1.6×10^{-4}
Fomalont *et al.* (1988)	5	12"	8.5×10^{-4}
Kreysa & Chini (1989)	230	11"	2.6×10^{-4}
Hogan & Partridge (1989)	15	5.3"	6.3×10^{-4}

Table 1.1: Recent limits (95% confidence level) on $\Delta T/T$ for anisotropies on small and intermediate scales. θ_c is the coherence length for the assumed gaussian correlation function. See also Fig. 4.

It is important to note here that in order to compare these limits with theoretical predictions. it is necessary to take into account the beamswitching technique employed. To relate this to the temperature a.c.f. then, for a beamthrow angle θ_b:

$$\left(\frac{\Delta T}{T}\right)^2_{obs} = 2[C_\sigma(0) - C_\sigma(\theta_b)]$$

for a two beam single subtraction experiment, whilst for a triple beam double subtraction experiment

$$\left(\frac{\Delta T}{T}\right)^2_{obs} = \frac{3}{2}C_\sigma(0) - 2C_\sigma(\theta_b) + \frac{1}{2}C_\sigma(2\theta_b)$$

Even now, it may be necessary to perform more complex theoretical sky reconstruction simulations within the context of a particular cosmological model to take into account the limited sky region surveyed and exact sampling strategy. This, of course, makes the derived limits somewhat model dependent. One way to enable more easy comparison of results on different scales is to assume a gaussian a.c.f. with a characteristic angular scale θ_c. After smoothing, we find

$$C_\sigma(\theta) = \frac{C(0)\,\theta_c^2}{2\sigma^2 + \theta_c^2} e^{-\frac{\theta^2}{2(2\sigma^2+\theta_c^2)}}$$

The intrinsic anisotropy is then C(0), whilst in some cases the quoted anisotropy is $C(0)\theta_c^2/(2\sigma^2 + \theta_c^2)$ where θ_c is that angle which minimises the anisotropy level. Care should be taken in interpreting all limits as to whether the quoted limit includes the smoothing factor or not.

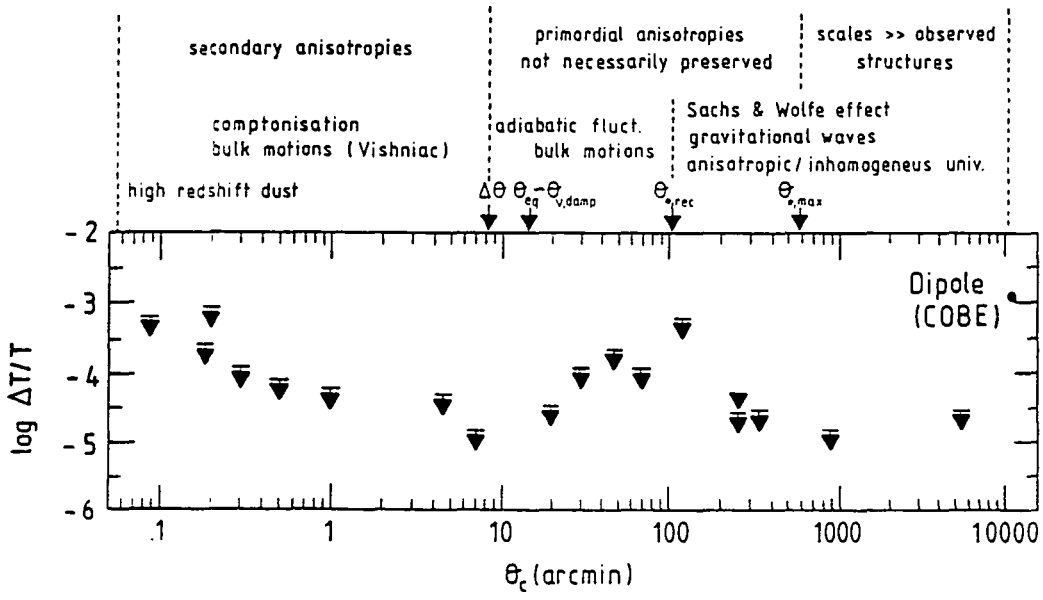

Figure 1.4: Recent measures of CMB anisotropies. A brief (and incomplete) summary of anisotropy generating mechanisms is also shown.

1.4 Problems in Measuring CMB anisotropies

We have seen so far that there are a large number of systematic errors involved in measurements of the CMB. Aside from obvious problems of the internal system noise of the experimental apparatus, ground based radiometer measurements suffer from ground pick-up whereby radiation from the ground is diffracted into the horn antenna and problems with atmospheric emission. Shielding can alleviate the first problem, whilst the operation of the instrument at a high dry site (such as the South Pole) improves the second. Nevertheless, the noise from these effects can never be entirely eliminated. Much more of a problem arises from Galactic and extragalactic radiations which themselves contain anisotropies such that the fractional amplitude is of similar or greater magnitude than those being sought in the cosmic radiation. This then is the subject of this thesis: a detailed study will be made of a number of foregrounds of both Galactic and extragalactic origin, with the intention of determining their contributions to a number of CMB experiments, and prescriptions will be made for the minimisation of the confusion effect.

References

Alpher, R.A. & Herman, R.C., 1948. *Nature*, **162**, 774.

Alpher, R.A. & Herman, R.C., 1949. *Phys. Rev.*, **75**, 1089.

Barrow, J. & Coles, P., 1991. *Mon. Not. R. astr. Soc*, **248**, 52.

Bond, J.R. & Szalay, A.S., 1983. *Astrophys. J.*, **274**, 443.

Bond, J.R. & Efstathiou, G., 1984. *Astrophys. J. Letts.*, **285**, L45.

Burigana, C., de Zotti, G. & Danese, L., 1991. *Astrophys. J.*, **379**, 1.

Cole, S. & Kaiser, N., 1999. *Mon. Not. R. astr. Soc*, **233**, 637.

Dall'Oglio, G. & de Bernardis, P., 1988. *Astrophys. J.*, **324**, 794.

Danese, L. & de Zotti, G., 1982. *Astr. Astrophys.*, **107**, 39.

Davies, R.D., *et al.* , 1987. *Nature*, **326**, 462.

Davies, R.D., 1988. *Q. Jl. R. astr. Soc.*, **29**, 443.

de Bernardis,P., *et al.* , 1990. *Astrophys. J. Letts.*, **360**, L31.

Dicke, R.H., 1946. *Rev. Sci. Instrum.*, **17**, 268.

Dicke, R.H., *et al.* , 1965. *Astrophys. J.*, **142**, 414.

Dyer, C.C. & Ip, S.S., 1988. *Mon. Not. R. astr. Soc*, **235**, 895.

Efstathiou, G. & Bond, J.R., 1986. *Mon. Not. R. astr. Soc*, **218**, 103.

Efstathiou, G. & Bond, J.R., 1987. *Mon. Not. R. astr. Soc*, **226**, 655.

Efstathiou, G., 1990. in *Physics of the Early Universe*, SUSSP.

Field, G.B. & Perrenod, S., 1977. *Astrophys. J.*, **215**, 717.

Fischer, M.L., *et al.* , 1991. in *After the First Three Minutes*, p. 123, eds. Holt, S.S., Bennett, C.L. & Trimble, V., AIP.

Fomalont, E.B., *et al.* , 1988. *Astrophys. J.*, **96**, 1187.

Fukugita, M., Sugiyama, N. & Umemura, M., 1990. *Astrophys. J.*, **358**, 28.

Gamow, G., 1948. *Phys. Rev.*, **74**, 505.

Hogan, C.J. & Partridge, R.B., 1989. *Astrophys. J. Letts.*, **341**, L29.

Holtzman, J.A., 1989. *Astrophys. J. Suppl.*, **71**, 1.

Kaiser, N. & Silk, J., 1986. *Nature*, **324**, 529.

Kashlinsky, A., 1988. *Astrophys. J. Letts.*, **331**, L31.

Kogut, A., *et al.* , 1991. in *After the First Three Minutes*, p. 62, eds. Holt, S.S., Bennett, C.L. & Trimble, V., AIP.

Kreysa, E. & Chini, A., 1989. in *Proc, 3rd ESO/CERN Symposium*, p. 433.

Lasenby, A.N., *et al.* , 1991. in *Observational Tests of Cosmological Inflation*, p. 413, eds. Shanks, T., *et al.* , Kluwer.

Martin, H.M. & Partridge, R.B., 1988. *Astrophys. J.*, **324**, 794.

Matsumoto, T., *et al.* , 1988. *Astrophys. J.*, **329**, 567.

Meinhold, P. & Lubin, P., 1991. *Astrophys. J. Letts.*, **370**, L11.

Melchiorri, F., *et al.* , 1981. *Astrophys. J. Letts.*, **250**, L1.

Meyer, S.S., Cheng, E.S. & Page, L.A., 1991, *Astrophys. J. Letts.*, **371**, L7.

Negroponte, J., 1986. *Mon. Not. R. astr. Soc*, **222**, 19.

Partridge, R.B., 1988. *Rep. Prog. Phys.*, **51**, 647.

Peebles, P.J.E. & Yu, J.T., 1970. *Astrophys. J.*, **162**, 815.

Penzias, A.A. & Wilson, R.W., 1965. *Astrophys. J.*, **142**, 419.

Readhead, A.C.S., *et al.* , 1989. *Astrophys. J.*, **346**, 566.

Rees, M.J. & Sciama, D.W., 1968. *Nature*, **217**, 511.

Sanz, J.L. & Martinez-Gonzalez, E., 1991. in *Observational Tests of Cosmological Inflation*, p. 42, eds. Shanks, T., *et al.* , Kluwer.

Scaramella, R. & Vittorio, N., 1990. *Astrophys. J.*, **353**, 372.

Silk, J., 1967. *Nature*, **215**, 1155.

Silk, J., 1984. in *Proc. 1st ESO/CERN Symposium*, p. 225.

Sironi, G., Bonelli, G. & Limon, M., 1991. *Astrophys. J.*, **378**, 550.

Smoot, G.F., *et al.* , 1988. *Astrophys. J.*, **331**, 653.

Smoot, G.F., *et al.* , 1991. *Astrophys. J. Letts.*, **371**, L1.

Staggs, S. & Wilkinson, D.T., 1991. in *After the First Three Minutes*, p. 85, eds. Holt, S.S., Bennett, C.L. & Trimble, V., AIP.

Sunyaev, R.A. & Zel'dovich, Ya. B., 1970. *Astr. Space Sci.*, **7**, 3.

Timbie, P.T. & Wilkinson, D.T., 1990. *Astrophys. J.*, **353**, 140.

Uson, J.M. & Wilkinson, D.T., 1985. *Nature*, **312**, 427.

Vishniac, E.T., 1987. *Astrophys. J.*, **322**, 597.

Vittorio, N., *et al.* , 1991. *Astrophys. J. Letts.*, **372**, L1.

Watson, R.A., *et al.* , 1988. in *Large Scale Structure and Motions in the Universe*, p. 133, eds. Mezzetti, M., *et al.* , Kluwer.

Watson, R.A., 1989. *Ph.D Thesis*, Victoria University of Manchester.

Weiss, R., 1980. *Ann. Rev. Astr. Astrophys.*, **18**, 489.

Wilson, M.L. & Silk, J., 1981. *Astrophys. J.*, **243**, 14.

Wyse, R.G. & Jones, B., 1985. *Astr. Astrophys.*, **149**, 144.

Chapter 2

Galactic Synchrotron Radiation and the CMB

2.1 Introduction

Observations of the Cosmic Microwave Background (CMB) have been made over a wide range of frequencies in order to determine the thermodynamic temperature of the radiation, and to search for primordial anisotropies on a number of angular scales. A wide range of frequencies is required to verify the blackbody nature of both the spectrum and anisotropies, and to search for spectral distortions which might indicate energy releases at high redshift, or spectral modification by physical processes during more recent epochs (see Smoot *et al.* , 1988 for a recent review). Much of the early work concentrated on observations in the radio frequency region (ie. from a few tens of MHz up to several tens of GHz) although more recently sufficiently sensitive equipment has been available to extend observations beyond these frequencies. However, observations at these frequencies still retain their fundamental importance, not least because the antenna temperature recorded by the experimental apparatus is not far modified from the CMB thermodynamic temperature (at 10 GHz, the antenna temperature for a blackbody at 2.735 K is 2.49 K). The major problem facing such observations is the foreground emission from the Galaxy.

The origin of this emission is the synchrotron radiation from cosmic ray (CR) electrons losing energy in the Galactic magnetic field, and thermal bremmstrahlung from these electrons (the electrons are certainly Galactic in origin, since in ex-

tragalactic space they would lose energy catastrophically due to inverse compton interactions with the CMB). In fact, the radio emission is direct evidence that CR electrons are present throughout the Galaxy and provides information on their distribution. The large-scale emission can be described very simply as follows: there is a central disk of emission centred on the Galactic plane, with features which delineate the spiral arm structure of the Galaxy, surrounded by a weak radio halo (Phillips *et al.* , 1981, have modelled the synchrotron emission evident from the 408 MHz survey of Haslam *et al.* , 1982, and found that a non-spherical halo of emission extending to a distance of order 10 kpc from the plane and having an emissivity $\sim$ 10% of that in the disc is required in all models to explain the high latitude temperature profiles). Features within the emission such as spurs and loops are closely connected with the effects of old supernova remnants on their environment. Up to several tens of GHz, the synchrotron emission dominates the thermal, the domination being complete for directions at more than a few degrees from the plane. The synchrotron emission is thus seen to have a great deal of structure which depends on a number of factors - the nature of the Galactic magnetic field, the electron spectrum in the Galaxy, the distribution of electrons in the Galaxy, variations in the parameters between disk and halo (this is important since according to Lawson *et al.* , 1987, even towards the North Galactic Pole about half of the line-of-sight emission comes from the Galactic disk), and indeed variations of theses parameters from place-to-place within the Galaxy. Even detailed modelling of the synchrotron emission (see, for example, Broadbent, 1989) can only describe the broad distribution of the emission, and although information can be obtained about the spiral arm structure of the Galaxy, the disk and halo by modelling of the low frequency data, detailed structure associated with local variations in, for example, the electron energy spectrum has not been included in such models.

The energy spectrum of electrons in the Galaxy has a power-law form, and as a consequence of this the synchrotron emission varies with frequency as a power-law. The relative contribution of the synchrotron emission to CMB observations thus falls with increasing frequency. Between a few GHz and a few hundred GHz, the CMB signal is dominant, and absolute measurements of the CMB temperature can be made to a level of $\sim$ 1%. At these frequencies, detailed knowledge of the spatial variation of the Galactic Synchrotron Radiation (GSR) is not necessary for spectral measurements at this level of accuracy, knowledge of the broad distribution of emis-

sion is sufficient. This is important since information about the GSR distribution at these high frequencies is not directly available, and extrapolations from lower frequency data must be made by assuming some power-law to scale the data by – the extrapolation and thus spatial distribution of the emission at the higher frequency thus depends on the power-law employed. Kogut *et al.* (1990) observing the CMB at a frequency of 7.5 GHz use a model for the Galactic contribution which extrapolates from the 408 MHz survey using the power-law nature of the emission with frequency and assuming a (probably unphysical) position-independent spectral index. At the highest latitudes, the predicted signal was accurate to better than 0.005 K ($\sim 0.2\%$) which is quite satisfactory. Below a few GHz the Galactic radiation becomes an important fraction of the sky temperature, and dominates below $\sim$ 600 MHz. Thus low frequency measurements of the CMB searching for departures from a blackbody spectrum (see, for example, Sironi *et al.* , 1990) require more accurate foreground subtraction. The major uncertainty posed by GSR, however, arises in the context of anisotropy measurements. Although such searches are made almost exclusively at frequencies beyond 5 GHz, where the foreground temperature is small, $\sim 10^{-3}$ of the blackbody temperature, fluctuations in the foreground are of the order of a few per cent, ie. about 10^{-5} - 10^{-6} in $\Delta T/T$, which is of the same order of magnitude as the primordial fluctuations being searched for.

Subtraction of the Galactic component is very difficult, since comprehensive surveys exist only at low frequencies ($\leq$ 1GHz), and the extrapolation of these data to higher frequencies is problematic since detailed knowledge of the spatial variation of the CR electron spectrum and its variation with energy, and of the Galactic magnetic field is required. Since the CMB observations themselves are of the single- or double-subtraction type, the problem becomes even more complex since the high frequency extrapolation of the GSR contribution must couple 2 or 3 directions respectively, each of which may have considerable variations in their properties. Furthermore, the low-frequency surveys themselves have problems involved with zero-levels, largely due to the lack of absolute measures of the sky temperature. Indeed, until 1985 only four results existed in the literature: near 600 MHz by Howell & Shakeshaft (1967) and Stankevich, Wielebinsky & Wilson (1970), and at 1.4 GHz by Howell & Shakeshaft (1966) and Penzias & Wilson (1967). Only recently has a combined Milan and Berkeley group attempted observations between 0.5 and 2.5 GHz (see Levin *et al.* , 1988; Sironi *et al.* , 1990). It seems that the precise determination of T_{sky} at

a number of points and over a range of frequencies is required for use in cosmology, Galactic astronomy and cosmic ray astrophysics, all of which are connected by studies of the CMB. Of course, the CMB contribution to T_{sky} has been established by COBE as corresponding to the thermodynamic temperature 2.735 ± 0.06 K (Mather *et al.* , 1990).

In this chapter, a number of low frequency radio surveys are considered in some detail, and an attempt is made to predict the fluctuations likely to be seen in higher frequency CMB anisotropy measures, the aim being to produce a prescription whereby genuine anisotropies may be detected in the presence of significant Galactic contamination. To this end, the role of instrumental and atmospheric noise will also be briefly touched upon. An investigation is made into the most comprehensive measures at high frequency so far made – those at 10 GHz by the Jodrell-IAC group, which provide an ideal source for a detailed study of possible Galactic effects (the work is in no sense put forward to disprove the earlier claim for the detection of a genuine CMB anisotropy, although the group itself now recognises that the results can almost certainly be produced by Galactic effects). An alternative method of investigation via CMB and GSR correlation functions is considered, and finally the prospects for future observations are commented upon.

2.2 Properties of the Galactic Synchrotron Radiation

First, it is useful to review the properties of the Galactic synchrotron radiation. This emission results from the energy losses of CR electrons moving relativistically in the Galactic magnetic field. The conventional differential energy spectrum of cosmic ray electrons is represented by a power law form in energy E,

$$N(E)\,dE \propto E^{-\gamma}\,dE,$$

where γ the spectral exponent. The observed radio emission at a frequency ν is given by the integral along the line-of-sight of the volume emissivity,

$$I(\nu) = \int \varepsilon(\nu)\,dl,$$

where the volume emissivity can be shown to be given by,

$$\varepsilon(\nu) \propto B_{\perp}^{(\gamma+1)/2} \nu^{-(\gamma-1)/2} n_e(l).$$

Here, $B_{\perp}$ is the perpendicular component of the effective magnetic field along the line-of-sight and n_e is the relativistic electron density at a given point distance l from the observer along a particular line-of-sight. The observed intensity distribution is clearly dependent on the variations of both the electron density and magnetic fields with position in the Galaxy due to the perturbing and accelerating effects of supernova remnant (SNR) shocks, winds from OB stars etc. The role of SNR in accelerating CR has been considered in detail in Bhat *et al.* (1985), the analysis there relating to the well defined SNR of the major radio Loops. Of more importance here are the non-identified weaker shocks which are postulated to cause the 'continuous acceleration' of cosmic rays -see for example Silberberg *et al.* (1983); Giler *et al.* (1985). The observed brightness (or antenna) temperature of the radiation (as observed by, for example, a horn antenna) seen in a given direction is then given by,

$$T_b = \frac{c^2 I(\nu)}{2\nu^2 k},$$

so that it has a frequency dependence $T_b \propto \nu^{-\beta}$ where $\beta = (\gamma + 3)/2$.

As E rises, the electron spectrum is also expected to steepen as a result of energy losses from the synchrotron emission itself, inverse compton scattering off various radiation fields (important at high latitudes where this process, coupled with the interstellar radiation field, generates a diffuse gamma-ray background), and ionisation and Bremmstrahlung processes. The exact energy at which the spectrum steepens is itself likely to be dependent on position in the Galaxy, through the relation of the electron lifetime to magnetic field etc. However, although an electron of energy E radiates much of its energy in a magnetic field at a critical frequency ν_c, where

$$\nu_c = \left(\frac{E}{m_e c^2}\right)^2 \left(\frac{eB}{2\pi m_e c}\right)$$

there will also be some emission over a distribution of frequencies (the maximum emission occurring for $\nu_m = 0.29\ \nu_c$), thus a sharp change in the spectral exponent

of the electron spectrum will be seen as a more gentle 'roll-over' in the slope of the radio synchrotron emission. It is thus expected that β will vary as a function of both position and frequency in the Galaxy. Webster (1971) has investigated the radio emission of the Galaxy as a function of frequency for the anti-centre region at high latitudes and the inter-arm regions, his work clearly demonstrating variations in the spectral indices between the two regions at given frequencies.

It is worth noting here that in the absence of information about the electron spectrum variations within the Galaxy, it is the observed radio emission and the β -values derived from them which are used to investigate CR electrons. To calculate β , one requires observations at two frequencies, and, using the power-law relation yields,

$$\beta = \log\frac{T_1}{T_2}/\log\frac{\nu_1}{\nu_2}$$

It is thus assumed that β does not vary over the frequency range considered. If this is not the case. the β as defined here is actually the numerical slope between the two frequencies. This should be taken into account when considering the behaviour of spectral indices at higher frequencies, as is done later in the chapter. Fig. 1 indicates the variation of the β -values evaluated between a number of frequencies for a number of latitudes within the indicated longitude ranges. Clearly, as noted previously, the behaviour of β can be rather complex. This is to be expected if it is considered that the acceleration of CR electrons is distributed over their propagation through interstellar space, whereby, after their initial acceleration and during their Galactic confinement, the CR are further accelerated by the weak shocks of widely distributed, somewhat dissipated, old SNRs, which, of course, they are much more likely to encounter than the smaller regions of young remnants.

2.3 The Basic Data

We take as the basic data sets from which extrapolations to higher frequencies are to be made the three low frequency radio surveys at 408, 820, and 1420 MHz (see Lawson *et al.* , 1987 for detailed references to the original surveys). Each survey reports the absolute observed sky brightness temperature, and thus an isotropic component

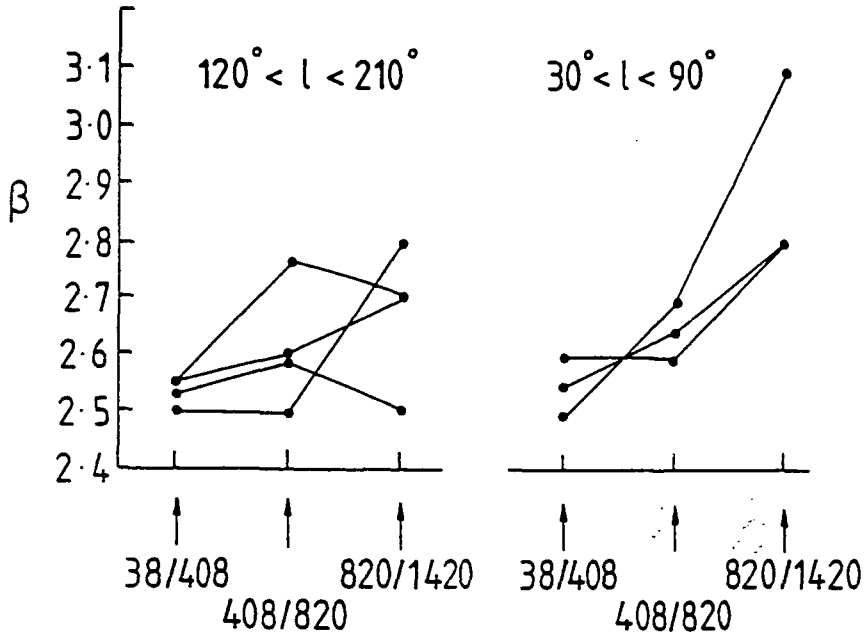

Figure 2.1: Variation of beta values evaluated from pairs of low frequency radio surveys for a number of high latitudes and the longitude ranges shown.

must be subtracted to account for the diffuse radio background of discrete, extra-galactic radio sources and the contribution of the CMB itself. In a comprehensive paper, Lawson *et al.* made a detailed study of the radio continuum emission of the Galaxy in the Northern celestial hemisphere utilising these surveys (amongst others), and they provide details of this diffuse background component. A brief description of each survey follows.

1. 408 MHz: This is an all-sky radio survey in which the component parts were all carried out at the same frequency with telescopes of comparable beam size. The diffuse background component, T_{BG}, amounts to 5.89 K. The basic data provided is convolved to a Full-width-to-half-maximum (FWHM) of 0.85° and can be obtained in either 0.25° × 0.25° pixels or 1° × 1° pixels. The latter are used here.

2. 820 MHz: This survey covers the region $-7° < \delta < 85°$. The FWHM of the antenna was 1°, but regridding resulted in a data base of HPBW 1.2°, again in 1° × 1° pixels. T_{BG} is 4.14 K.

3. 1420 MHz: This survey covers the declination range $-19° < \delta < 90°$, is convolved to a FWHM of 0.85°, and available in $1° \times 1°$ pixels. T_{BG} is 2.93 K.

It should be noted that the original surveys were not absolutely calibrated. Deducing a calibrated version requires consideration of a number of factors – the accuracy of the temperature scales, estimation of zero levels, contributions due to atmospheric and ground radiation, the effect of the telescope sidelobes, and the accuracy of the estimate for the extragalactic component. Lawson *et al.* devoted considerable attention to minimising these base-line errors. The absolute zero level of the 408 MHz survey was established by comparison with the 404 MHz survey of Pauliny-Toth and Shakeshaft (1962) which was absolutely calibrated. The other surveys were compared to a number of horn antenna measures at different frequencies. The next problem is to fix the zero-levels of the surveys in absolute terms. The traditional method is to use a 'T-T' plot, whereby the brightness temperatures of two surveys are plotted against each other over a chosen area of the sky: a straight line fit to the points yields the spectral index between the two frequencies as the slope and the base level of one survey relative to the other as the intercept. The problem here is that there may be genuine variations in the spectral index over the region, making the meaning of the base-level obtained somewhat obscure. Lawson *et al.* adopted an alternative approach. A sky minimum region was found at $20 < \delta < 50$, $130 < \alpha() < 150$; since the spectral index for such a region is the most sensitive to changes in the base-level, a constant value was assumed as given by the 38 and 408 MHz surveys (which have the smallest fractional errors), and the other surveys adjusted to agree. The results are in excellent agreement with those of Kallas *et al.* (1983) which employed the T-T plot method and the 1420 MHz survey as the datum. This gives some confidence in the final versions of the maps as used in this chapter.

After such a lengthy analysis, only small base-line errors remain which are a remnant of the minimisation techniques used at the crossing points of the scans of the original surveys to eliminate base-line drifts from scan-to-scan. These are barely noticeable on the temperature maps. For the 408 MHz survey, the residual errors are < 1.5 K . The effect of the errors is particularly noticable when the ratios of brightness temperatures, hence spectral indices, are calculated. Fig. 2a shows the effect quite clearly, the striping effect running downwards from left to right in this

greyscale map of the spectral indices evaluated between 408 and 1420 MHz. Such an effect is obviously of concern here, where temperatures at high frequencies are to be estimated from lower frequency surveys via the derived spectral indices. The magnitude of the effect may be estimated as follows.

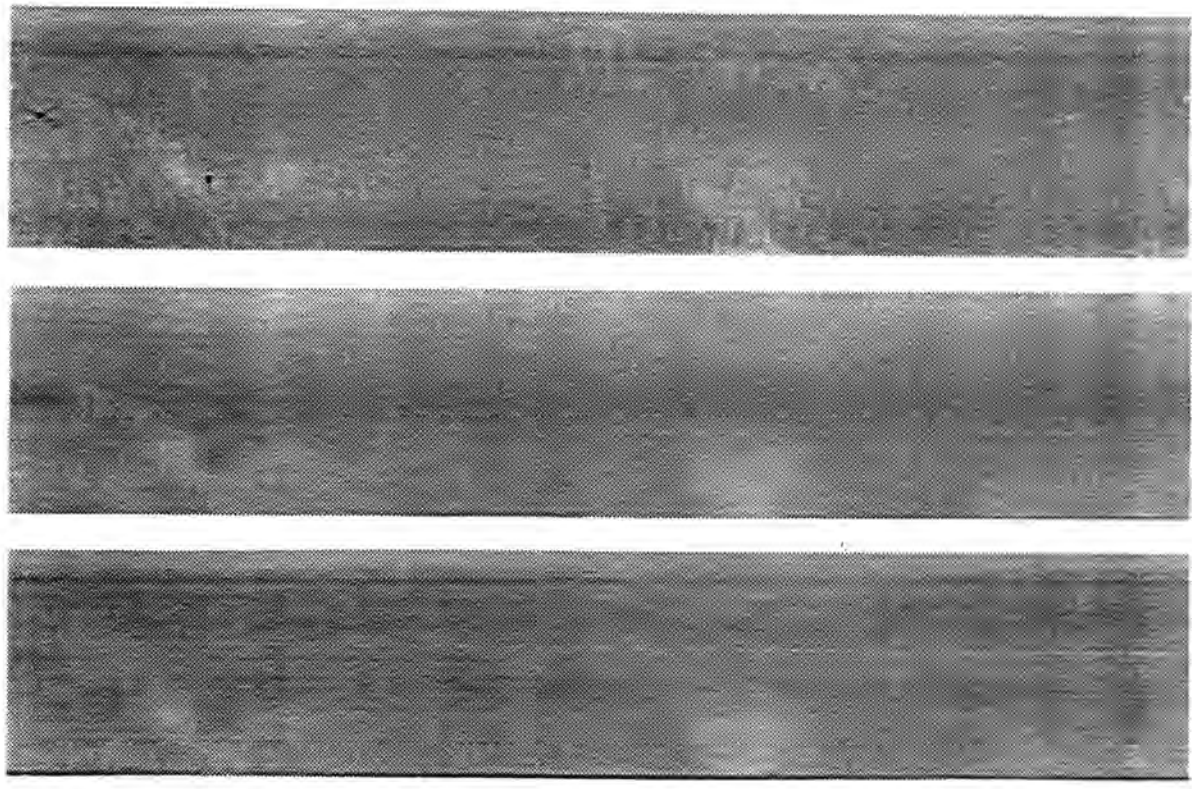

Figure 2.2: Spectral indices calculated between 408 and 1420 MHz. a) original 0.85° FWHM resolution, notice the striping in the data; b)5.6° resolution, striping has gone; c) 8.2° resolution, again no striations.

At a given frequency, we have that

$$T_\nu \propto \nu^{-\beta}$$

If an error in temperature is incurred, then the corresponding error in spectral index is given by,

$$| \Delta T_\nu | \propto | \Delta\beta | \ \nu^{-\beta} \ln \nu$$

(ignoring the weak B-field dependence here). Dividing through by T_ν gives,

$$\frac{| \Delta T_\nu |}{T_\nu} = | \Delta\beta | \ln \nu$$

At high latitudes, a 'typical' value for T at 408 MHz is $\sim$ 15 K (after background subtraction), thus taking $| \Delta T_{408} | \sim 1.5$ K as before, the above relation yields $| \Delta\beta | \sim 0.017$. The effect on the extrapolated temperature values can be estimated in a similar fashion. If we consider that we are scaling from 408 MHz to a frequency ν, it follows from previously that

$$\frac{| \Delta T_\nu |}{T_\nu} = \ln \left(\frac{\nu}{408} \right)^{|\Delta\beta|}$$

If the extrapolation is to 10 GHz (as appropriate to the calculations in this chapter), then an error of $\sim$ 5% can be produced. This is likely to be a lower limit on the possible error, since similar problems are present in the data at the second frequency used to determine the spectral index used for extrapolation, resulting in a larger error in β . Furthermore, since anisotropy measurements are differencing measurements, then the error is increased by combining extrapolations along 2 or 3 lines-of-sight by a factor of $\sim$ 2 - 3. It is obviously of great importance to reduce the significance of the striping as much as possible. In principle, it should be possible to remove the striations by smoothing the data perpendicular to the scanning direction, but because these directions differ from one survey to another, it would not then be possible to compare the different surveys. Lawson *et al.* found by trial-and-error that when the resolution was decreased to 4° or greater, then the striping disappeared from the greyscale images. In what follows, the maps are convolved to the Jodrell-IAC experimental values of FWHM 8.2° and 5.6° before extrapolation, it is then hoped that the baseline errors are minimised. Figs. 2b and c indicate that the striping effect is no longer visible after these convolutions. However, there may still be some false structure in the maps and derived spectral indices, leading to errors in the extrapolated structure, especially in radio quiet regions where the scanning directions of different surveys cross. A possible route to eliminate the problem in the future is to use a Fourier filtering technique, by recognising that the noise in an

image due to the stripes will be given in general by a two-dimensional interference pattern (Malawi, 1989, has used this technique to destripe IRAS images). Such a procedure should ultimately be implemented in order to establish whether there is any false structure present in the extrapolated maps.

Despite these problems, the three data sets as described in Lawson *et al.* are probably the most reliable available at present.

2.4 The 10.46 GHz Jodrell-IAC data

The Jodrell-IAC CMB anisotropy experiment is a twin-horn radiometer experiment which switches the two beams so as to form a triple beam pattern on the sky, with the beamthrow angle between each outlier and the central beam being $\theta_b \sim 8.2°$. The experiment is operated at a high dry site at Izana at an altitude of 2300 m to reduce atmospheric problems. The data with which the synchrotron predictions will be compared are taken from Davies *et al.* (1987), Watson *et al.* (1988), Watson (1989) and Rebolo *et al.* (1989). Full details of the experimental technique can be found in Watson (1989).

2.4.1 Fluctuations in temperature seen by Davies *et al.* (1987)

The original apparatus had a FWHM of 8.2° , and after a large-area survey of the northern sky at declinations between -15° and +55° at 5° intervals, two long integration scans were made at declinations 0° and 40° . Here, the results for δ = 40° are considered. Fig. 3a shows the experimental points, together with a running gaussian mean with FWHM as for the horn antenna, each point on the line being averaged over 11 points from the recorded data (as prescribed in Watson 1989). A number of points should be mentioned.

i) despite very careful experimentation the noise in the observations is, inevitably, rather large; specifically it has standard deviation $\sigma \sim 0.22\,\mathrm{mK}$ taking adjacent points of one degree separation (the dispersion here is inevitably noise since the beamwidths are much greater than this). It should be remarked that,

hopefully, later observations with improved apparatus will reduce the value of σ by an order of magnitude.

ii) the smoothed distribution (smoothed, following the technique prescribed in Watson, 1989, by a gaussian of standard deviation 3.5°) is seen to be characterised by two peaks separated by $\theta_s \sim 25°$ in R.A., and with FWHM of $\theta_c \sim$ 10° and 6°. One of these peaks (at $\sim$ 220°) is significant but the other is not (as demonstrated by a jack-knife type analysis in Vittorio *et al.* , 1989); nevertheless, Figure 3a represents the actual data and we need to examine the likelihood of deriving similar patterns from GSR.

iii) the peak amplitude is $\sim 0.2\,\mathrm{mK}$.

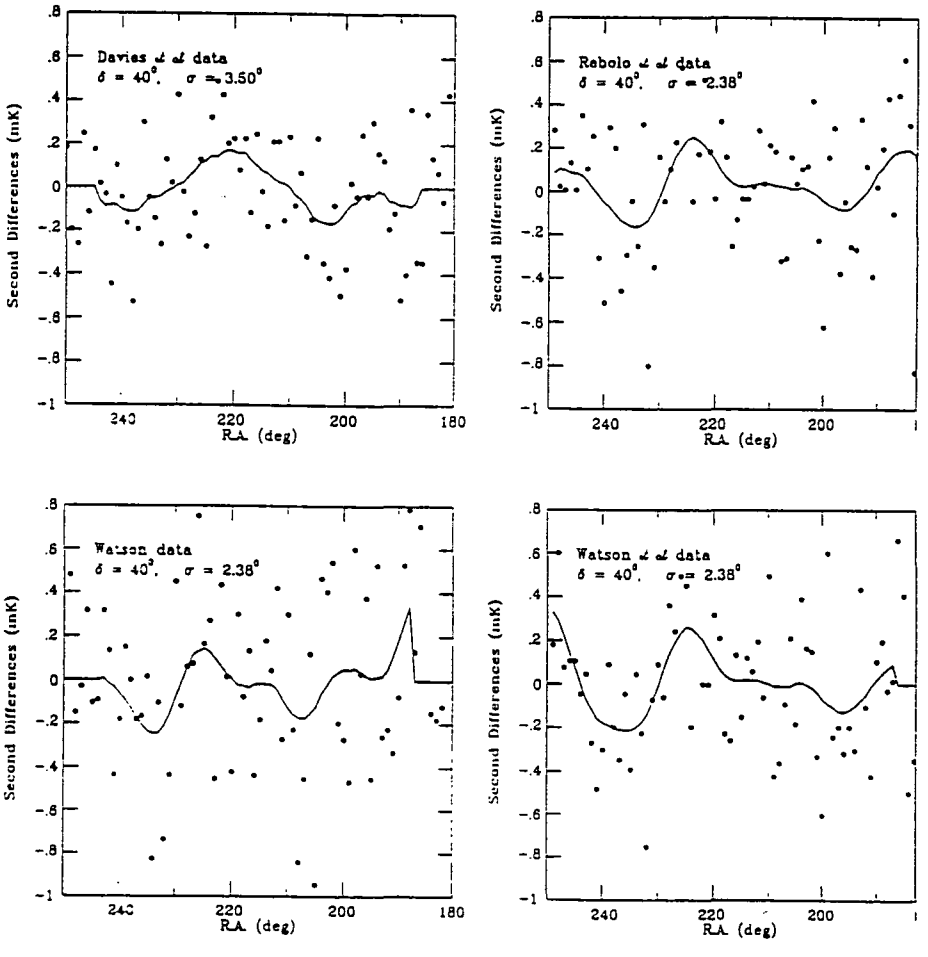

Figure 2.3: Scans at declination 40° from the Jodrell-IAC anisotropy experiment.

Analysis of their data led Davies *et al.* to claim a cosmological signal of $\Delta T/T = 3.7 \times 10^{-5}$. This value was obtained from a likelihood ratio (LR) analysis of the data assuming a gaussian covariance function. Recall from Chapter 1 that, after allowance for the finite width of the observing beam, this has the form

$$C_\sigma(\theta) \;=\; C_\sigma(0)\, e^{-\theta^2/2(\theta_c^2+2\sigma^2)}$$

where θ_c is the coherence angle, and the smoothed fluctuation level is related to the intrinsic anisotropy level by $C_\sigma(0) = C(0)\theta_c^2/(\theta_c^2 + 2\sigma^2)$. The LR analysis found that for $\theta_c = 4^\circ$, $\sqrt{C_\sigma(0)} = 0.1$ mK, then assuming a CMB temperature of 2.7 K gives the published result. The 'likely' contribution of the Galactic synchrotron radiation was also evaluated, from an extrapolation to 10.46 GHz using a constant spectral exponent of 2.8. The lack of correlation between the observations and predictions resulted in the rejection of the hypothesis that GSR could be the source of the fluctuations, Davies *et al.* further claiming that a spread of spectral indices greater than that observed between 408 and 1420 MHz would be required to explain the observed structure in the observations. This is what will later be determined.

2.4.2 Fluctuations in temperature in the 5.6° experiment

The modified version of the original experiment retains the 8.2° beamthrow of the original, but has a FWHM of 5.6° . Scans were again made over a range of declinations, the results being shown in Figs. 3b - d for declination 40° (scans from three different sources) and Figure 4 for scans separated by 2.5° in declination. Again there are some points to note.

i) The noise in the observations is again rather large, specifically $\sigma \sim 0.27$ mK per 1° separation in R.A. at $\delta = 40^\circ$.

ii) For those declinations where several sets of published data are available (particularly declination 40°) the differences between the sets are due either to differing analyses of the same results, or more data being included. Note that the differences in the experimental profiles at the same declination, although not negligible, are smaller than the differences between separate points, giving some confidence in the measurements.

iii) On comparing profiles from adjacent declinations differing by only 2.5° , there is an absence of correlations between them probably due to either incorrect data processing or to the measurements being dominated by atmospheric or instrumental noise.

iv) The smoothed distribution (by a gaussian of standard deviation 2.8°) at declination 40° is again characterised by 2 peaks, at $\sim$ 222° (R.A.) and a second near to 190° . However, the scans show more structure than those from the original system (even allowing for the smaller extent of smoothing due to the smaller beamwidth). Again, only the peak at $\sim$ 222° appears significant, the second peak being present at differing amplitudes from one data set to another presumably as a result of noise effects or the data reduction technique employed. The significant peak has FWHM $\sim$ 15° and peak amplitude slightly greater than 0.2 mK, suggesting that the structure responsible has a characteristic angular scale comparable to the smaller beam used here.

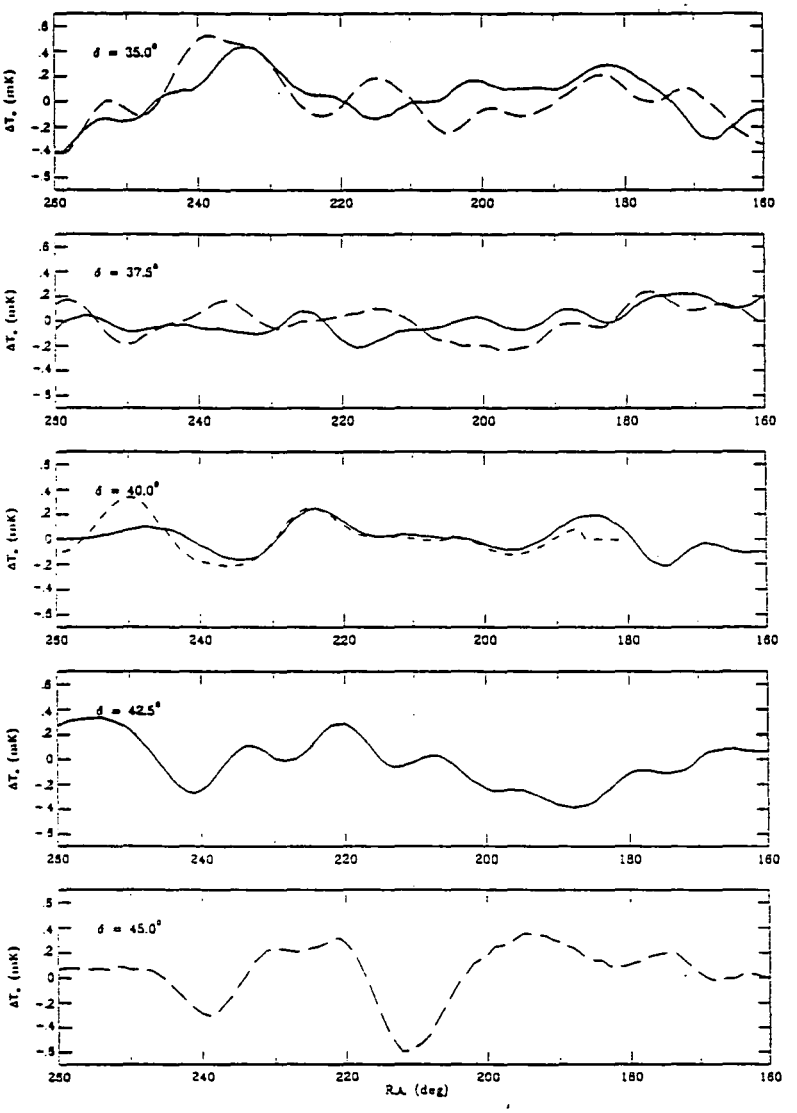

Figure 2.4: Scans from the Jodrell-IAC 5.6° experiment for a number of declinations.

The results have been analysed in the same way as the original data set and limits of 4 - 8 $\times 10^{-5}$ set for the range of declinations in Rebolo *et al.* (1989). The effect

of point sources, more important for the new configuration, has been investigated in Watson *et al.* (1988) and found to have little effect in the region of interest (the effect of point sources will be returned to in Chapter 4). The feature at dec 40° is also unlikely to be due to the large void in Boötes where it crosses at dec 40° , or to the unusual string of galaxies at this position (Tago *et al.* , 1986).

The objective now is to examine the extent to which the results can be explained by GSR.

Figure 2.5: Colour plot of the 408 MHz survey at original 0.85° resolution.

2.5 Fluctuations at the Standard Frequencies

2.5.1 Fluctuations at 408 MHz

Since the 408 MHz survey was performed by comparable telescopes, and since it is an all-sky survey, it is generally regarded as superior to the the other surveys used in this paper. In addition, as discussed previously, the small baseline errors arising at the crossing points of the upward and downward scans are $< 1.5\,\mathrm{K}$, which is barely apparent in the brightness temperature maps (Fig. 5 shows a colour image

of the 408 MHz survey, in its original FWHM of 0.85° . Convolving to 5.6° and 8.2° , as is appropriate to the Jodrell-IAC work, is thought to reduce the base-line problems to a minimum). From the Galactic synchrotron standpoint then, the 408 MHz survey is probably the best *initial* indicator of the smoothness of the interstellar medium (ISM). In order to determine the sky region of minimum fluctuations then, we examine the sky brightness temperature in the 408 MHz survey.

We need now to more explicitly define what we mean by fluctuations, and since we intend to pay particular attention to measurements at 10.46 GHz, fluctuations will be defined as 'second differences' in the manner of Davies *et al.* and the experimental configurations adopted. Signals detected by the twin-horn drift-scan apparatus are combined in such a manner that a triple beam pattern is formed on the sky. That is, if the temperature seen by one horn is denoted T_C and that seen by the other T_E, the difference $T_C - T_E$ is measured by the equipment. Then as the sky rotates through the horn separation (beamthrow θ_b), the horns will then record T_W and T_C respectively, say; the second difference is then defined as

$$\Delta T = \frac{1}{2}[(T_C - T_E) - (T_W - T_C)]$$

We therefore look to determine these second differences at 408 MHz in order to gain a first order idea of the sky fluctuations with a view to identifying the least disturbed region. The 408 MHz data were convolved to a FWHM corresponding to a gaussian dispersion of $\sigma = 3.5°$ and 2.8° , and a beamthrow of 8.2° was adopted. Cells were then chosen in R.A. of size 55° in real sky angle centred on 215° R.A. (so that the region at declination 40° corresponds to the region in Davies *et al.*) and 135° R.A. taking care to avoid the Galactic plane, and at 5° intervals in declination, from $\delta = 30°$ to 70° . The evaluated root mean square of the second differences are recorded as ΔT values in Table 1.

It is clear from these values (and calculations from a number of smaller regions of about 40° real sky angle) that we should identify the $\delta = 40°$, R.A. = 180° to 250° range as the 'best' sky minimum 'best' region, coinciding with the 'preferred' region from the Jodrell-IAC studies. This region is, in fact, that identified by Bridle (1967) as 'the interarm' and so, insofar as disturbing phenomena such as supernova remnants are expected to be infrequent there, such a quiet region is not unexpected.

It is thus likely that if a cosmological signal is to be detected at 10.46 GHz, then this is the region where it is most probably going to show above the Galactic foreground, and so calculations are concentrated on this region (for the other declinations, the 10 GHz signal is almost entirely due to a combination of GSR and noise, and so we can gain some guidance for our declination 40° calculations from these regions). We shall also initially concentrate on the 8.2° experiment, for which the point sources have a smaller effect, returning later to the 5.6° results (though in slightly less detail). Fig. 6 shows a contour map of the 408 MHz sky, the 'quiet' region enclosed by a box. It is clear that this is a relatively undisturbed region for GSR phenomena.

declination	8.2° FWHM		5.6° FWHM	
δ (°)	Region 1	Region 2	Region 1	Region 2
30	0.54	0.80	0.72	0.96
35	0.61	0.80	0.84	0.89
40	0.33	0.88	0.42	1.03
45	0.36	0.85	0.67	1.04
50	0.39	0.81	0.64	0.88
55	0.50	0.87	0.68	0.99
60	0.58	0.85	0.71	0.98
65	0.72	0.92	0.94	1.14
70	0.70	1.20	0.87	1.73

Table 2.1: R.M.S. second differences in kelvin at 408 MHz. Region 1 centred on R.A. 215° ; region 2 on R.A. 135° . Each region is of 55° real sky angle.

2.5.2 Fluctuations expected from GSR: angular scales

All searches for CMB fluctuations using GHz data will rely on a knowledge of the expected GSR fluctuations on these same angular scales. Specifically, it will be necessary to use lower frequency data to predict the expected GSR pattern at the frequency of interest. The problem then arises as to the extent to which the pattern of the GSR is displaced from that at lower frequencies. The question then is the angular scale over which coherent values of the mean CR electron intensity ($< j(E_e) >$) and the effective mean magnetic field ($< B_\perp >$) exist.

There is some guidance for the latter from γ-ray astronomy. For example, in analysis of COS-B and SAS-II data, Bhat *et al.* (1986) estimated coherence lengths

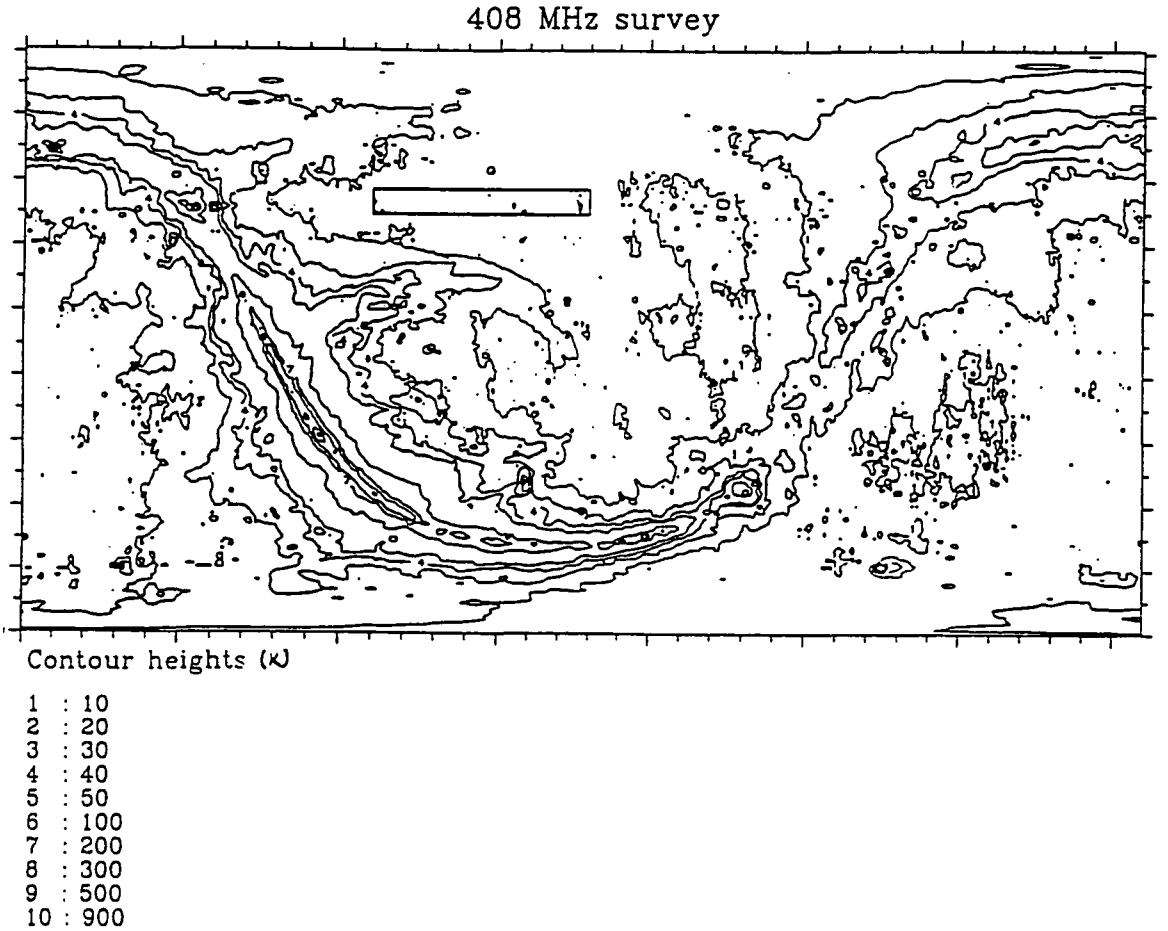

Figure 2.6: The 408 MHz sky at 0.85° FWHM. The region enclosed by the box is the 'preferred' region of Davies *et al.* (1987), which has been shown to be a quiet region on the sky.

for electrons and protons in the Outer Galaxy and low latitudes which suggest the presence of 'cells' of enhanced intensity with $\theta_c \approx 5° - 10°$ at the higher latitudes of concern here. One would expect rather similar values for $< B_\perp >$; indeed, Simonetti *et al.* (1984) find angular scales for rotation measure variations up to 5° at high Galactic latitudes.

Another feature of the angular scale is the separation of the cells and the synchrotron data themselves are relevant here. At 10.46 GHz and along declination and R.A. cuts away from the preferred region, the separation of the peaks $< \theta_s >$ is very approximately 17°. Another indicator of interstellar turbulence comes from

HI data. In particular, we have looked at the HI column density at a number of latitudes from the HI data of Stark *et al.* (1991) convolved to a FWHM of 2.5° . These scans show a similar value for the separation of peaks, $\langle\theta_s\rangle$ being $\sim 15°$, the spread in values running from 5° to 25° (see Fig. 7). The cell sizes as suggested by the FWHM of the peaks also appear to be of order 5° - 10° as suggested by the γ-ray data.

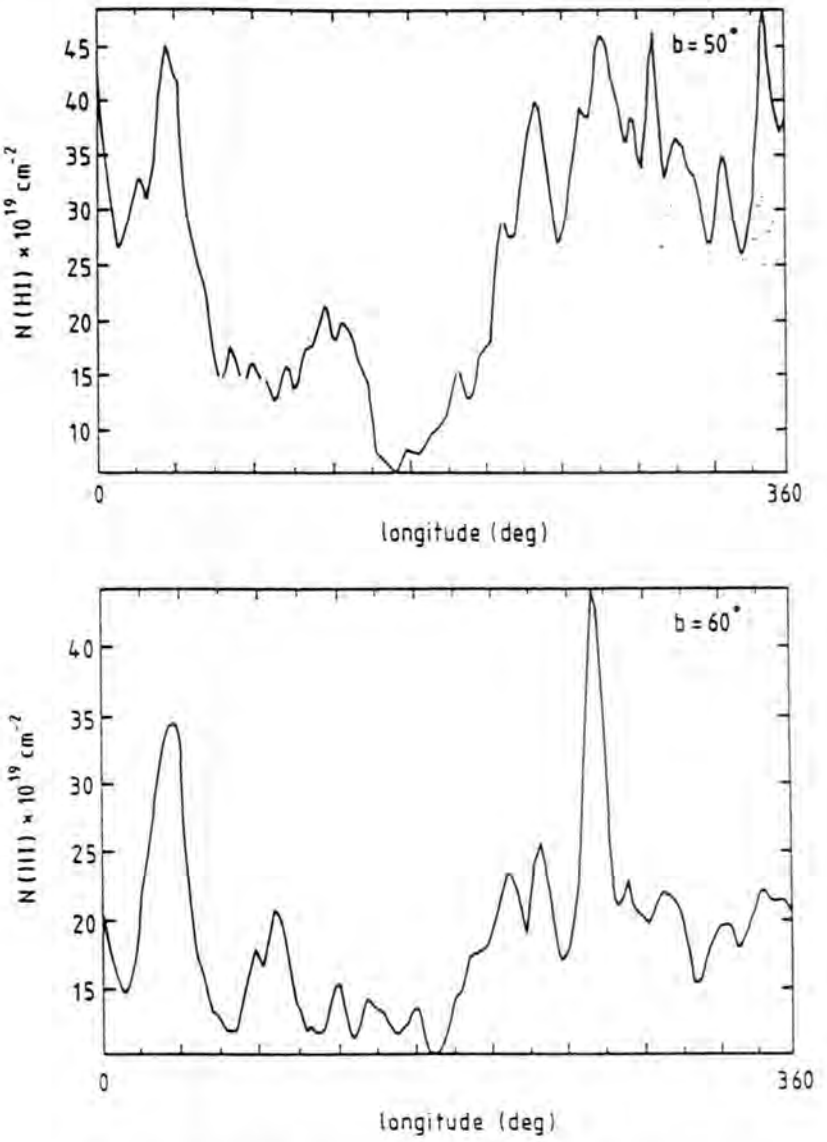

Figure 2.7: HI column densities from Stark *et al.* (1991).

Briefly, we expect $\theta_c \approx 7°$ and $\theta_s \approx 20°$, values rather close to those seen in the quiet region. A more detailed analysis now follows.

As remarked previously, the pattern at 10 GHz would be accurately predictable if the T-values were known at the lower frequencies with great accuracy and the

value of β was also known for each point for the region between the datum low frequency and 10 GHz. None of these parameters is known with any accuracy but we can examine each in turn.

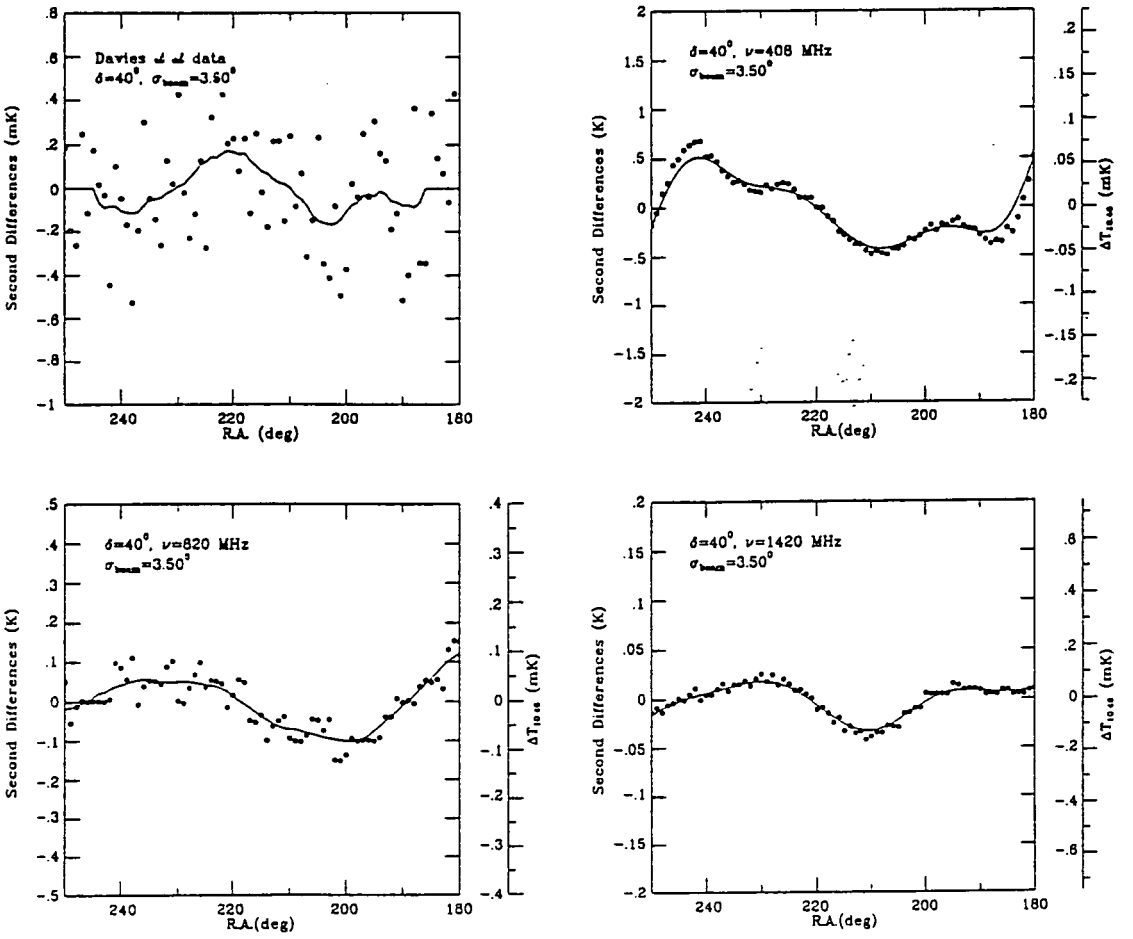

Figure 2.8: a) Observed second differences at 10.46GHz from Davies *et al.* (1987). Solid line is a running gaussian mean. b) -d) second differences at 408, 820, 1420 MHz. Right hand scales give temperatures at 10.46 GHz extrapolated using β = 2.8.

Figs. 8b - d give ΔT vs R.A. for each of the lower frequencies, the data being processed in the standard manner in each case. The scale of $\Delta T_{10.46GHz}$ is also given where the conversion is made assuming a constant value for β of 2.8 (as in Davies *et al.*, 1987; Lasenby & Davies, 1988) in each case. Comparison with Fig. 8a shows that the general characteristic parameters — the θ_c- and θ_s-values — are not dissimilar, but the scales are different; specifically, the amplitudes of $\Delta T_{10.46GHz}$ are 'predicted' to be $\sim$ 0.05, 0.05 and 0.07 mK from the 408, 820 and 1420 MHz data, respectively, to be compared with the observed amplitude (Fig. 8a) of $\sim$ 0.2 mK. The reason for the bigger observed amplitude is clearly connected with the fact that the assumption of a constant exponent (2.8) is unphysical, and the next section

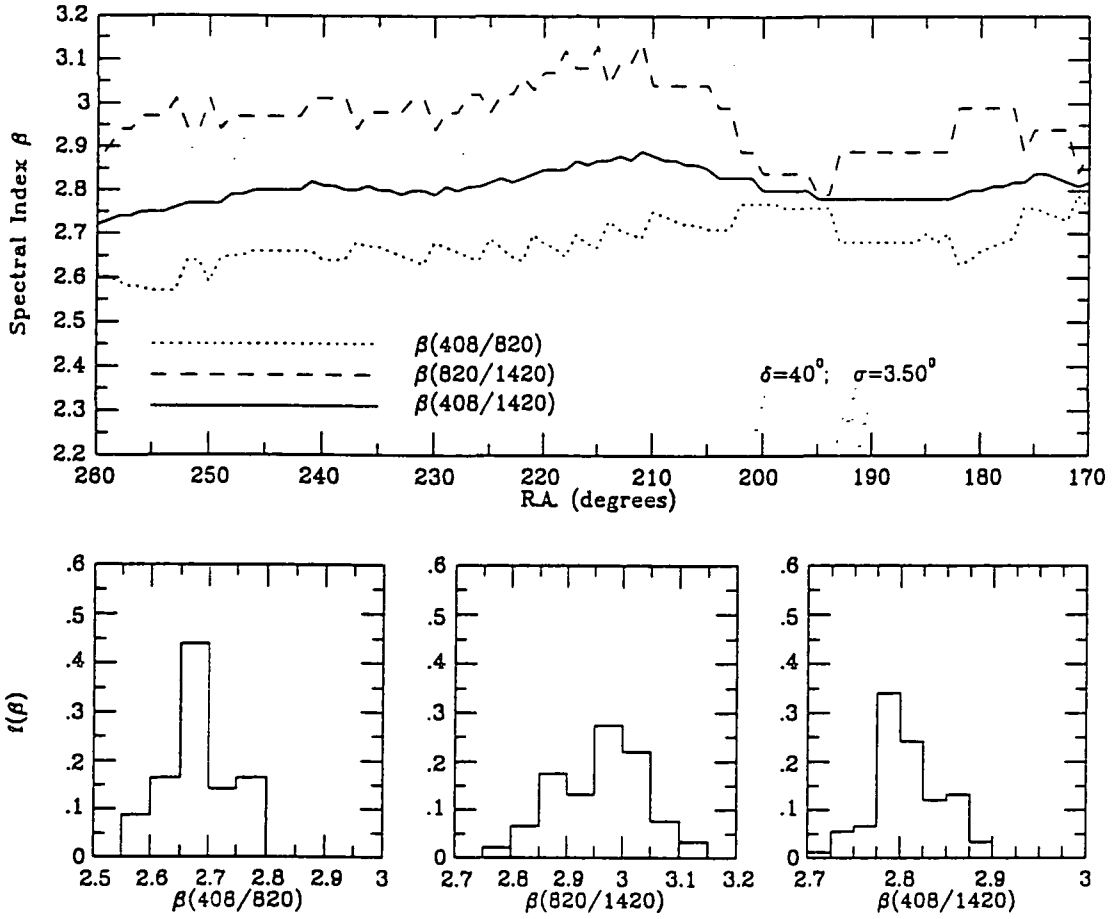

Figure 2.9: a) Distribution of spectral indices between pairs of frequencies at declination 40° in the R.A. range 180° - 250° . b) - d) histograms of spectral index probability distributions for pairs of frequencies.

adopts a more realistic treatment.

2.5.3 Fluctuations in spectral slope as a function of frequency

It should be possible to make more accurate predictions of the GSR fluctuations using the combined data at lower frequencies, ie using the knowledge on the radio spectral slopes evaluated from the three data sets.

We have seen in Section 2 that the observed brightness temperature T_b is a

function of frequency of the form $\nu^{-\beta}$. β has been evaluated for the frequency pairs 408/820, 820/1420 and 408/1420 each data set being convolved to $\sigma = 3.5°$, the background components recorded in Section 3 also being subtracted, and the results are shown in Fig. 9a. It is clear that whilst in some regions there appears to be some correlation between $\beta(408/820)$ and $\beta(820/1420)$ eg. a general uniform steepening, in other regions there is little or no correlation. $\beta(408/1420)$ is obviously a weighted average of the other two β-distributions, and shows less intrinsic variance.

In Figs. 9b, c and d the distributions of β are shown for the preferred region, plus ten degrees either side since the second difference measurements sample from these regions too. The mean value of β is seen to increase with frequency. Also, the width of the distribution is a function of the 'frequency throw', ie. 408/820, 820/1420. Although it is unclear what the actual form of the distribution of β is with respect to frequency throw in either case, or indeed whether the distribution changes significantly with frequency throw, extrapolation to higher frequency throws, specifically for 1.42/10.46 GHz, yields σ_β in the range 0.05 - 0.1. Such behaviour is to be expected in a continuous acceleration model of CR electrons.

As remarked already, accurate prediction of the likely GSR contribution to CMB measurements at high frequencies needs extrapolation of the lower frequency measurements to the frequency (10 GHz) in question. This, in fact, requires a knowledge of the actual β-values point-by-point for the Galactic range in question. The importance of choosing the correct β-values should be obvious, since each second difference measurement contains a contribution from three lines-of-sight, over which β may vary significantly. It is completely unclear then, as to the precise values of spectral indices to adopt in the extrapolation to higher frequencies, especially in view of the structure seen in Fig. 9a

In view of the uncertainties we proceed by adopting a variety of procedures in the hope that thereby the sensitivity to the assumptions will be apparent and a best estimate will appear. It is appreciated that the effect of uncertainties in the measured temperatures will give rise to corresponding errors, often enlarged, in the derived $\Delta T_{10.46\,GHz}$ values, and the predicted amplitudes will thus probably be overestimates. Nevertheless, the general errors would not be expected to be too large and furthermore these are offset (to an uncertain extent) by the intrinsic errors

in the 10.46 GHz data itself.

i) Lower limit: since the structure seen in the distribution of $\beta(408/1420)$ is less than for the other frequency pairs, then it seems reasonable that a lower limit might be set on the 10 GHz fluctuations by extrapolating directly from 408 MHz adopting β derived point-by-point from the 408/1420 data. The second differences are then calculated and the results shown in Fig. 10b. (the datum, observed second differences from Fig. 2a, is repeated again as Fig. 10a for ease of comparison). This procedure gives a lower limit because the steepening due to cosmic ray electron energy losses is expected to occur above 1420 MHz, losses being very small at the corresponding lower energies.

ii) In the second case, a direct extrapolation is made from 1420 MHz using $\beta(820/1420)$, the result is shown in Fig. 10c. The peak amplitude here is $\simeq 0.29\,\mathrm{mK}$, somewhat higher than for the first case, and the dispersion of the points is greater. These features lead us to believe that the 408 MHz data are of higher quality than the 820 MHz results.

iii) Direct extrapolation from 408 MHz is made using $\beta(408/820)$, and the result shown in Fig. 10d. The peak amplitude here is again $\simeq 0.40\,\mathrm{mK}$. The dispersion in the points is larger still, an indication of the inferior nature of the 820 MHz survey.

iv) This time, it is acknowledged that there is a general steepening in the spectrum ($< \beta >$ increases with ν) and that β changes somewhat with R.A.

The 'final' method then involves the following: an extrapolation is made from 408 MHz to 10.46 GHz using a spectral index given by

$$\beta = \beta_{(408/1420)} + \Delta\beta_{\mathrm{Steepening}} + \Delta\beta_{\mathrm{Random}}(\Delta\theta)$$

$\Delta\beta_{\mathrm{Random}}(\Delta\theta)$ is a random component selected by Monte Carlo techniques from a gaussian distribution of dispersion σ_β which has as its origin the spread in β-values referred to previously. The value of $\Delta\theta$ is connected to the coherence of cosmic ray effects in a given region of the sky: as we have seen, this scale runs from $6^\circ - 10^\circ$ and cells of this scale are placed at random on the sky. $\Delta\beta_{\mathrm{Steepening}}$ is the steepening in index expected between 1420 MHz and

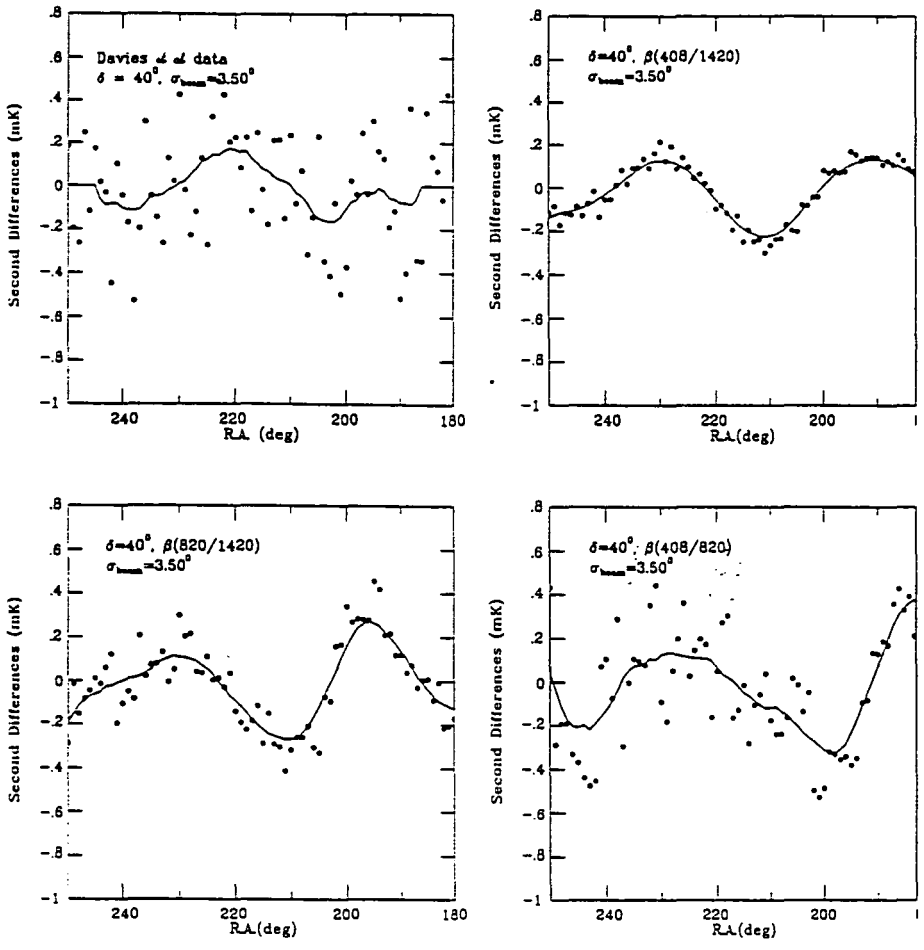

Figure 2.10: a) Observed second differences at 10.46 GHz. b) - d) extrapolations using spectral indices calculated from frequency pairs from the higher frequency to 10.46 GHz.

10.46 GHz due to the increased energy losses of the CR electrons, its value being determined as follows.

As remarked previously, the average spectral index of the GSR increases with frequency as a consequence of the energy loss of the electrons. The evaluation of the steepening relevant to GSR at high frequencies is somewhat difficult, since this requires detailed knowledge of the electron spectrum in the region under investigation over a range of energies, since electrons at a number of energies contribute to the radiation at a given frequency. In addition, as the energy of the electrons increases, the scale-height of the electron distribution above the plane decreases, thus it is rather difficult to determine the appropriate value for the magnetic field strength as required to calculate the GSR intensity, although it is likely that the effective value increases. The region of interest is, however, close to the North Galactic Pole (NGP), and certainly at high latitudes, so for the frequency in question - 10.46 GHz - the electrons pro-

ducing the radiation are almost certainly local. As a first attempt to evaluate $\Delta\beta_{\text{Steepening}}$, consider the radio spectrum at the NGP, constructed from data in Webber (1983) and from 5 GHz and 10 GHz measurements at Jodrell Bank (as shown in Fig. 11a). Using the observed intensities, the spectral index can be determined for pairs of frequencies as required. The curve denoted 'b $\sim 90°$ ' in Fig. 11b shows the derived β values (relative to 408 MHz); at the highest frequencies a value of ~ 3.05 is found.

As a second estimate of the spectral index behaviour, use is made of the locally measured electron spectrum (see Giler, Wdowczyk & Wolfendale, 1978). Since for a given frequency, most of the radiation arises from electrons of energy E, where

$$\nu(\text{MHz}) \;=\; 16\,\text{B}_{\perp}(\mu\text{G})\,\text{E}_{\text{e}}^{2}(\text{GeV}^{2})$$

(Webber, 1983), then combining the effective energy E_e with spectral information from the local electron spectrum for a choice of magnetic fields again allows β to be evaluated. Values for the magnetic field of 1 μG and 6 μG have been used here – this spread should account for for any possible variations (the higher value was favoured for GSR in an analysis by Chi & Wolfendale, 1990). Fig. 11b is then probably sufficiently accurate to give the very large scale β -variations as a function of frequency and enable an estimate of $\Delta\beta_{\text{Steepening}}$ to be made above 1420 MHz. Also shown in the figure are the mean values of β (408/820) and β (408/1420) (the low value for the 408, 820 MHz pair may arise from the 820 MHz temperatures being overestimated, this would account for the steep values between 820 and 1420 MHz as well). Additional data are shown from fits to the GSR required by observations of the CMB temperature at a number of frequencies. The data from Sironi *et al.* (1990) at declination 46.5° shows good agreement with the calculations, lending support to the claims here. The points from de Amici *et al.* (1988), and Kogut *et al.* (1990) are not in such good agreement, but the points are more relevant to latitudes nearer the Galactic plane, where the spectral indices are unlikely to be as steep.

For the frequency range 408/1420, the average measured value of β for the quiet region is ~ 2.8, differing from the asymptotic value 3.05 by 0.25, This then is the value adopted for $\Delta\beta_{\text{Steepening}}$. It is important to realise that this

value is only likely to be appropriate for high latitude inter-arm regions, as is the case here. In other, more active regions of the Galaxy, where there are more supernovae and more continuous acceleration, β may remain rather flat, $\sim$ 2.8 - 2.9, to quite high frequencies, and the steepening could certainly be more gradual.

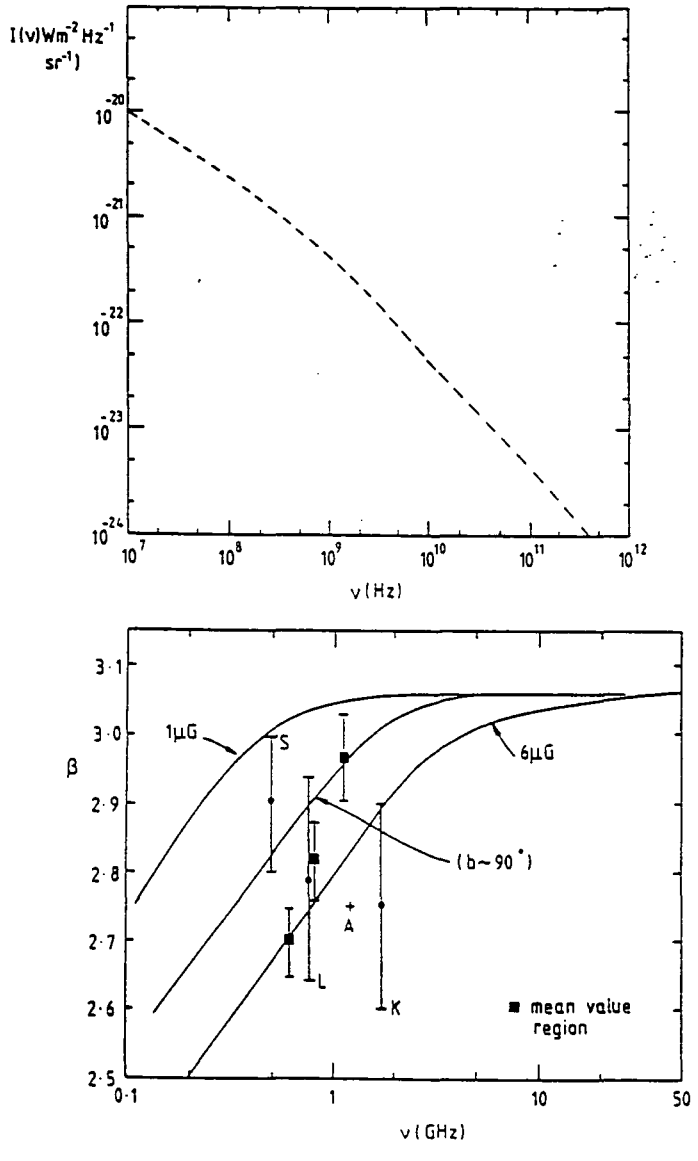

Figure 2.11: a) the radio spectrum at the NGP; b) average spectral index as a function of frequency - see text for details.

1000 simulations were run, and the resulting ΔT-values at 10.46 GHz had white noise added to them (rms amplitude 0.22 mK) so as to more closely simulate the experimental situation. Fig. 12 shows typical sets for the likely extremes of $\Delta\beta_{\rm Random}$, that is, for σ_β equal to 0.05 or 0.1. It will be noted that the latter gives amplitudes which are too large; those for σ_β of 0.05 are

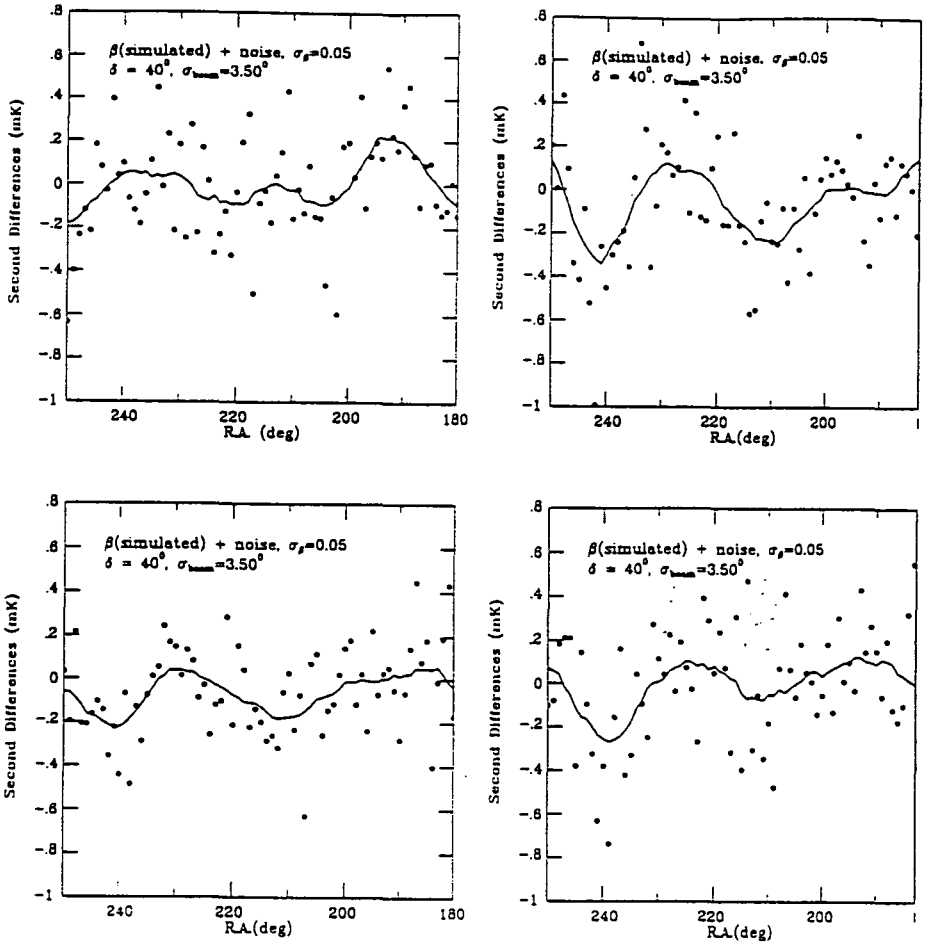

Figure 2.12: Simulations of second differences at 10.46 GHz for the region of interest using $\beta(408/1420)$ and allowing for steepening, a random component in the spectrum, and instrumental noise.

acceptable, however. In particular, the root-mean-square of all the points (1° separation) about zero for this set of results is 0.26 ± 0.03 mK, which is consistent with the same quantity estimated by us for the Davies *et al.* data of ~ 0.25 mK.

2.5.4 Detailed comparison of observation and prediction

It has been shown that several different methods of predicting the ΔT distribution at 10.46 GHz give results rather similar to observation. The similarity extends to there being usually only two or three peaks in the smoothed distribution — as observed — and amplitudes of similar magnitude ($\simeq 0.2$ mK). The major difference is that the major peak in the observed distribution is at R.A. $\simeq 220°$ whereas those predicted are nearer 230°. Such an important result — which could mean that the 220° peak

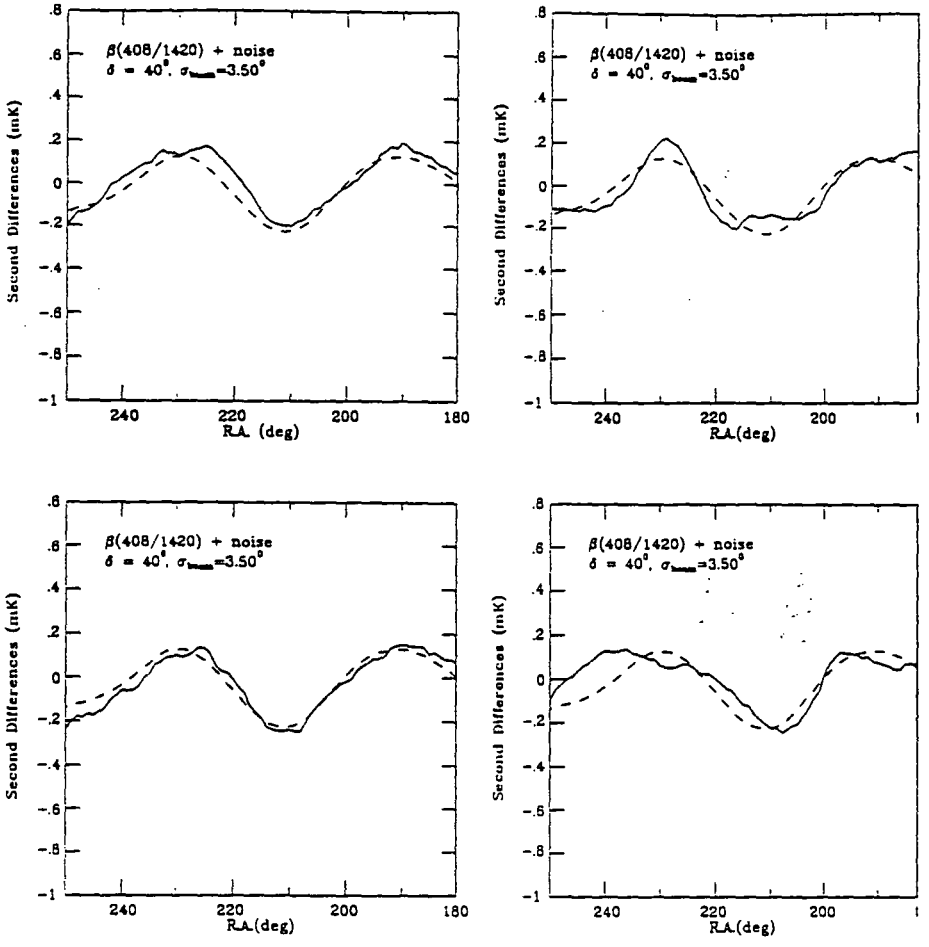

Figure 2.13: Examples of the effect on peak amplitude and position found by adding noise to the simple extrapolation from 408 and 1420 MHz (4 from 1000 simulations). The dashed line is the extrapolation without noise.

was of genuine cosmological origin — needs checking, and this has been done.

The effect of the instrumental noise on the location and amplitude of the predicted peak was ascertained in a simple manner, by adding such noise to the simple extrapolation using $\beta(408/1420)$ in 1000 simulations. Some examples are given in Fig. 13.

Fig. 14 is a plot of the major peak positions against peak amplitudes for the two halves of the region of interest. It is clear that instrumental noise alone may shift the peaks by $\sim 4°$, and affect the amplitudes by a factor of ~ 2.

The problem of deriving the probability of the observed second difference distribution (Fig. 2a) arising by chance is not a trivial one insofar as we are dealing with *a posteriori* statistics. Instead, a random set of plots of the type shown in Fig. 12a were examined and several picked out that have sufficient similarity to arouse

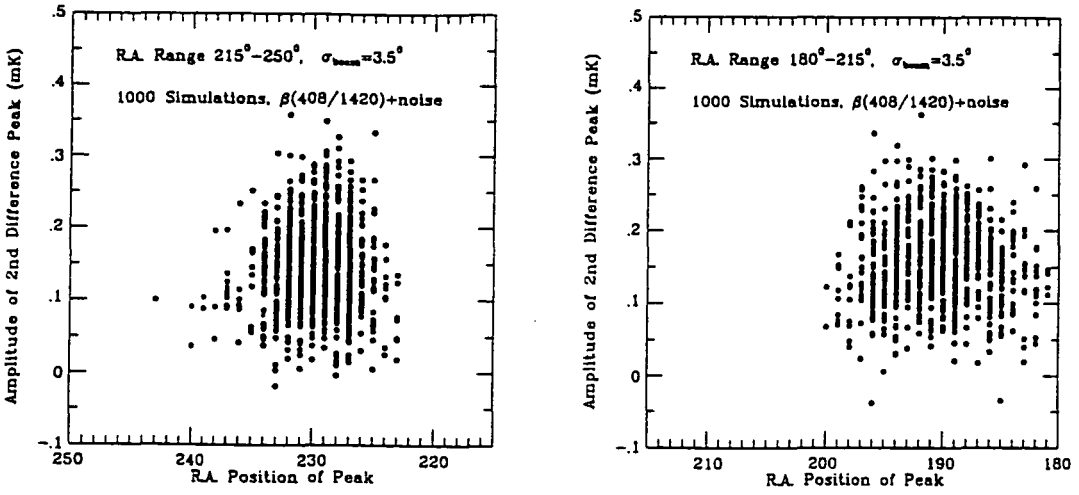

Figure 2.14: Plot depicting the peak amplitude against the peak position for the 1000 Monte Carlo simulations of the effect of instrumental noise on the extrapolations.

comment. A set of four chosen from 1000 is shown in Fig. 15. Bearing in mind the large number of degrees of freedom inherent in a posteriori studies we conclude that there is quite a strong likelihood that GSR fluctuations are responsible for the results.

2.5.5 An Investigation of the 5.6° results

Having established that GSR fluctuations can explain the observed ΔT fluctuations in the original experiment, attention is now turned to the newer results for the modified system with FWHM 5.6° . This will be instructive since data are available over a wider range of declinations, which will allow a more convincing determination of both the role of GSR in the observations, and the influence of instrumental noise.

Returning to the analysis, the rms values of $< \Delta T_s^2 >^{\frac{1}{2}} \equiv \sigma_s$ divided by the brightness temperature (represented as σ_s/T) are plotted in Fig. 16 as a function of frequency. This graph reflects mainly the decrease with increasing frequency of the relative contribution of the GSR to the total radio flux. The upper curve represents the extrapolation to higher frequency assuming power law spectra as derived for each position from the two frequencies 408 and 1420 MHz. The lower curve allows for a steepening of the spectra at higher frequency as considered in detail above. The expected range of CMB anisotropy for a CDM type model with primordial spectral index n = 1 (both adiabatic and isocurvature models) is indicated

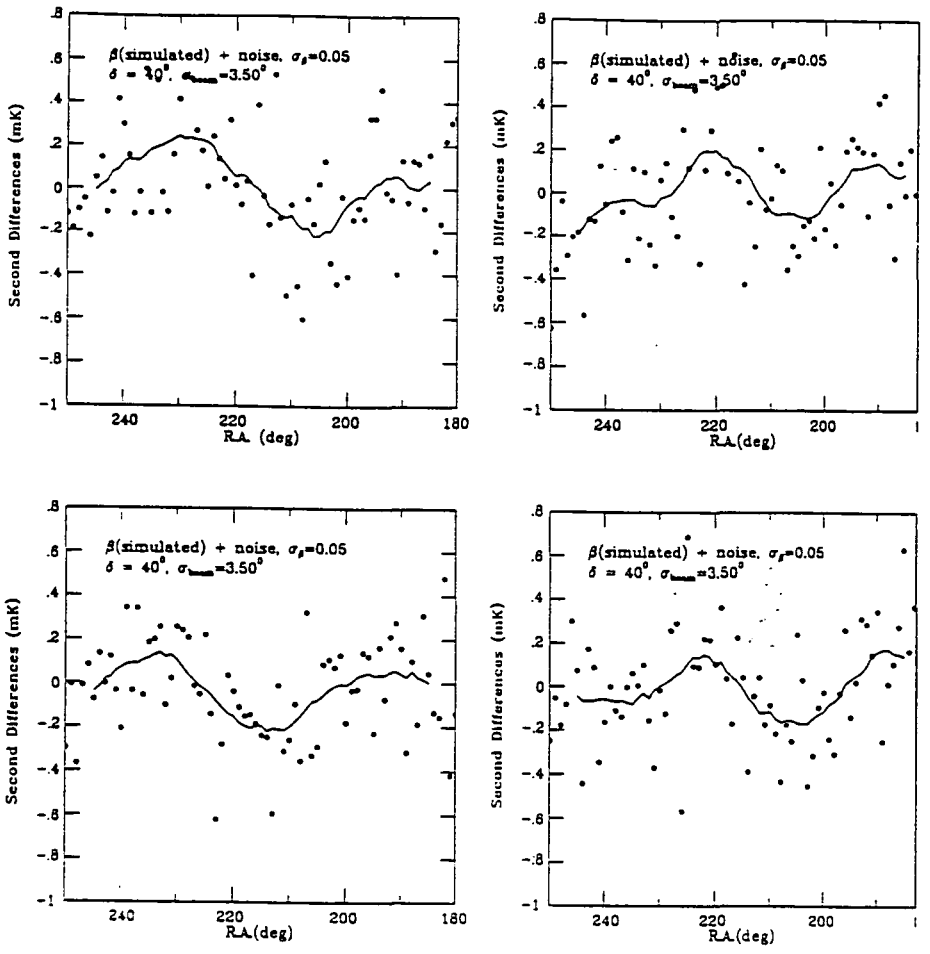

Figure 2.15: Four Monte Carlo results, of the type shown in Fig. 12a, which bear a similarity to the observed second difference results.

by the two horizontal lines. The range shown allows for a small increase in the standard normalisation amplitude as may be required by recent measures of large-scale structure in the universe, and as is discussed in detail in Chapter 6 where the appropriate calculations leading to the indicated values may be found (the small frequency dependence is accounted for in the range).

The actual fluctuation values are $\sigma_s = 0.42\,\mathrm{K}$ and $0.020\,\mathrm{K}$ for 408 MHz and 1420 MHz respectively. The average GSR brightness temperature over the considered part of the sky are $13.7\,\mathrm{K}$ and $0.41\,\mathrm{K}$, correspondingly, which result in relative GSR fluctuations of about 3.1 % at 408 MHz and 4.9 % at 1420 MHz. Taking the rms temperature (ΔT) variation as a measure of GSR fluctuations shows a strong increase of their relative values with frequency (12.4 % and 13.9 % respectively). This conclusion is also true for other parts of the Galaxy and provides interesting information about the propagation of cosmic ray electrons, in particular, about the manner in which the propagation characteristics depend on energy (basically

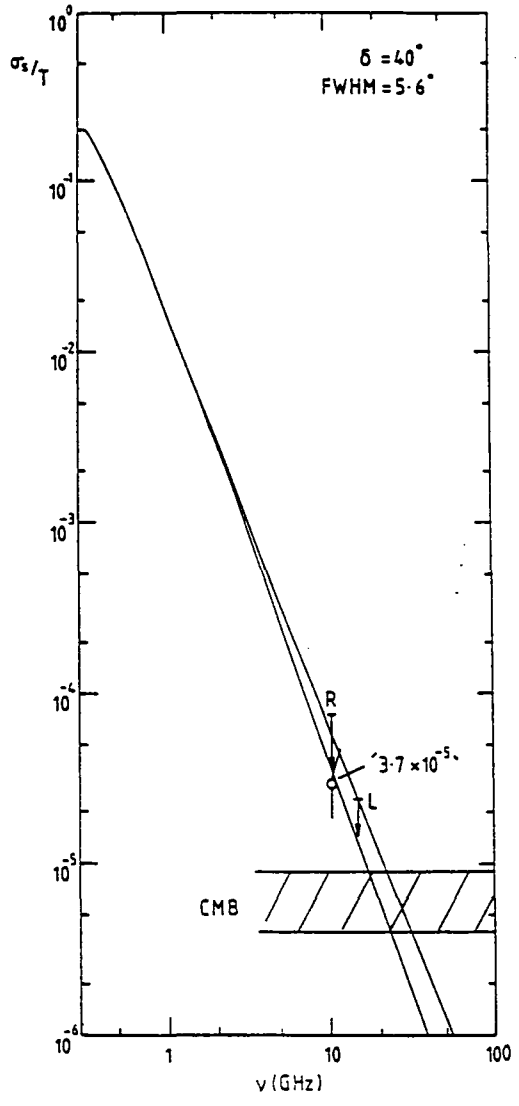

Figure 2.16: Predicted GSR anisotropy vs. frequency. The values relate to the rms second differences divided by T = 2.7 K , and arise from an extrapolation of the measured T_{408} and T_{1420} maps. Also shown are upper limits from the Jodrell-IAC experiments.

it suggests that whilst there is a trend towards a steepening spectral index, the rate at which the turn over occurs varies with position in the Galaxy. This is also indicated by the increasing spread in spectral indices with frequency as has already been noted).

The situation with respect to the observations at 10.46 GHz is not completely clear. The original Davies *et al.* (1987) observations (with FWHM 8.2° rather than the later 5.6°) gave prima facie evidence for fluctuations at a level $\sigma_s/T \sim 3.7\times10^{-5}$ but Rebolo *et al.* (1989) quote 95% upper limits in the range $(4\text{-}8)\times10^{-5}$. Both are plotted in the figure although in fact the former should be increased in

magnitude to correspond to the smaller FWHM considered in this section. The actual values plotted in the figure are scaled by an amount appropriate to the fact that the quoted limits correspond to $C_\sigma(0)$ for a gaussian autocorrelation function, whereas the values required correspond to the rms second difference. For a double subtraction experiment, this is given by,

$$\sigma_s^2 = \frac{3}{2}C(0) - 2C(\theta_b) + \frac{1}{2}C(2\theta_b)$$

so the scaling factors are 0.96 for 5.6° , and 0.80 for 8.2° . Also shown is a new limit at 15 GHz, again using the 5.6° equipment. It is apparent that the predicted level of fluctuations due to GSR is similar to that observed.

Fig. 17 represents the observed ΔT_s profiles (averaged over 10° in right ascension to minimize experimental noise, as described in Watson, 1989) and those predicted from GSR for the various declinations. The predictions are made using a simple extrapolation of the GSR spectra from 408 MHz to 1420 MHz onward to 10.46 GHz without an increase in slope. In fact, the slope will increase, on average, as discussed above, and as allowed for in Fig. 16, but the result of this effect alone is to simply scale down the predicted amplitude slightly.

Inspection of Fig. 17 shows no obvious correlations between observation and prediction. The figure indicates that displacements between the observed and predicted second difference peaks of 5° - 10° are not uncommon. That there should be some differences is to be expected because of the undoubted fact that there is curvature in the radio spectrum of a magnitude that depends on position in the sky. This was taken into account in our simulations for the 8.2° experiment, but only on a statistical basis.

As the ΔT_s profiles, extrapolated to 10.46 GHz using information about 408 and 1420 MHz intensities only, do not correlate with the measurements, we have next used the 820 MHz data to attempt to improve our predictions at 10.46 GHz. Fig. 18 shows the expected profiles from extrapolations from pairs of frequencies for the 408, 820 and 1420 MHz data. However the new ΔT_s profiles do not show better agreement with the observations. If our predictions are not far from being correct then the discrepancies must be due to experimental errors. The absence of correlations between scans from neighbouring declinations separated by 2.5° suggests that

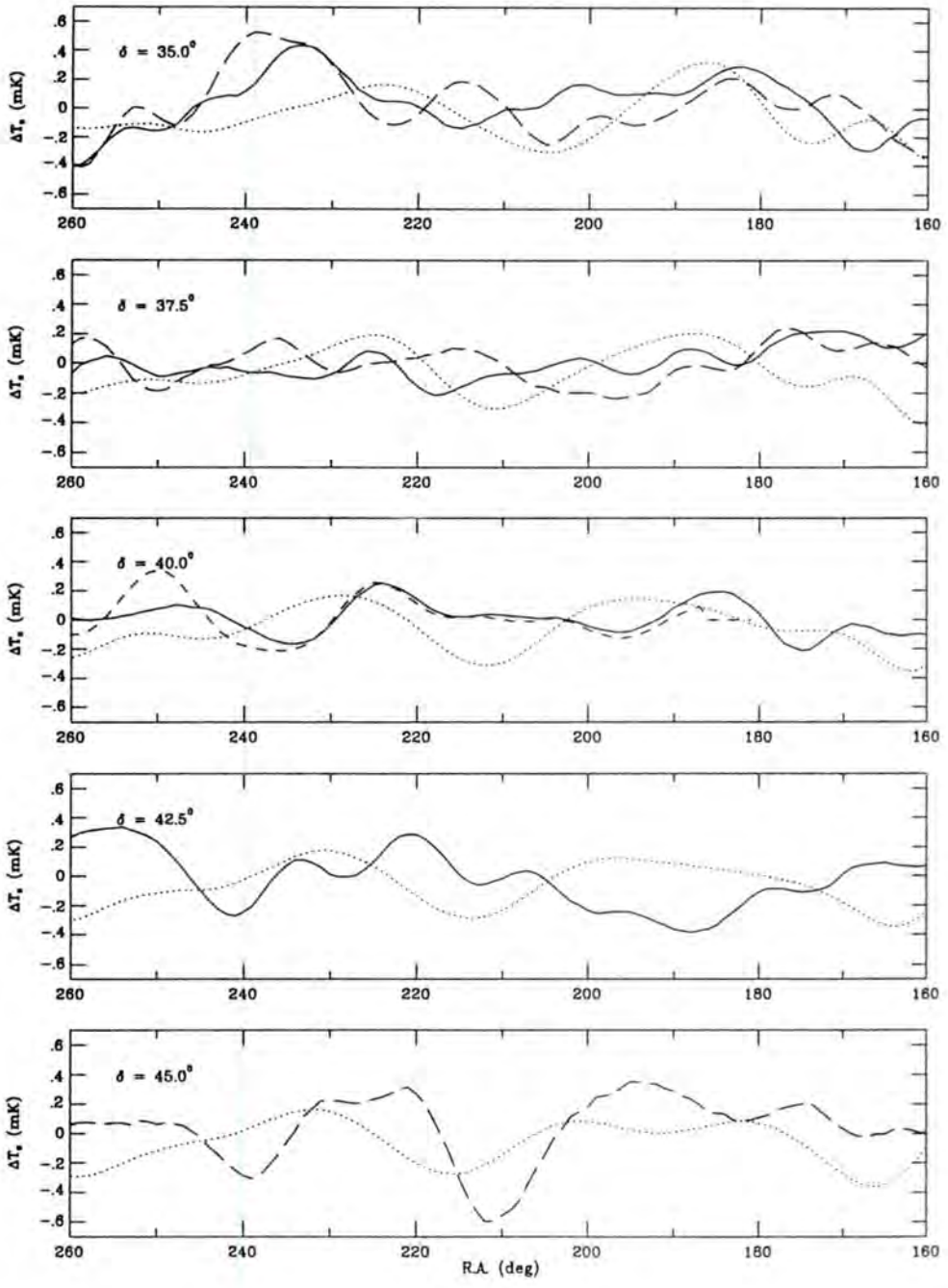

Figure 2.17: Comparison of observed and predicted second differences at 10.46 GHz. Dotted line: predictions; solid line: Rebolo *et al.* (1989); long dash: Watson (1989); short dash: Watson *et al.* (1988).

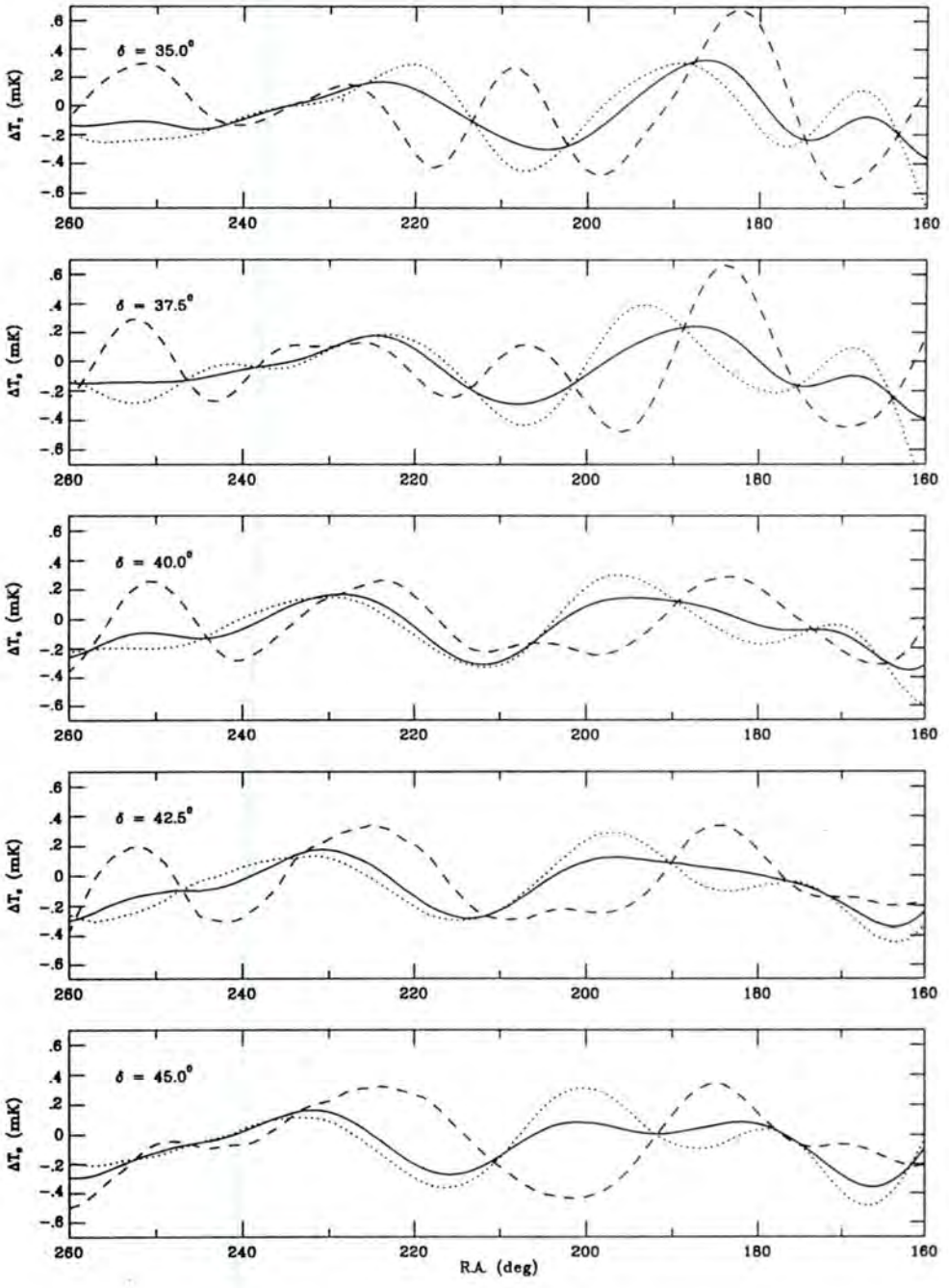

Figure 2.18: Predicted second differences at 10.46 GHz. Solid line from 408/1420; dashed line from 408/820; dotted line from 820/1420.

the measurements are indeed dominated by instrumental or atmospheric noise.

It is accordingly necessary now to consider the extent to which the experimental noise may dominate the measurements. The Jodrell-IAC experiment has a quoted uncertainty per second difference point of $\simeq 0.27\,\mathrm{mK}$ (Watson *et al.* 1988) at declination 40° , and this alone results in a (spurious) $\Delta T_s/T$ value of several times 10^{-5} at 10.46 GHz. We have performed a statistical analysis to calculate the probability that the observed peak in $\Delta T_s/T$ at $\delta = 40°$, R.A. $\simeq 225°$ has occurred by chance. This was achieved by assuming that the instrumental noise could be represented by an uncorrelated Gaussian signal (which may not be correct since there will be some correlated effects such as atmospheric disturbances in the real data), with a dispersion equal to the quoted error. 1000 simulations were performed, with 71 points per simulation arranged in degree pixels. Each set of points was then smoothed by a running Gaussian mean of dispersion 2.38°, and the amplitude and location of the peaks compared to the Watson *et al.* (1988) data smoothed in the same manner. The result is $\sim 11\%$ for achieving a peak of magnitude at least as big as that observed. Immediately it is apparent that measurements of greater precision are needed, as well as there being a need for a fuller understanding of the GSR fluctuations.

2.6 The Likely Situation at Higher Frequencies

It is self evident that investigations at higher frequencies should make the CMB ΔT_s measurements easier, insofar as GSR effects fall rapidly with increasing frequency. Unfortunately, however, atmospheric effects cause the noise level to increase and a limiting frequency is soon reached.

Insofar as the effect of noise will always be of significance we have examined it in more detail. 1000 simulations were run for a region similar to that of the region of interest, and analysed after smoothing in the usual fashion. The results are shown in Fig. 19, where the solid line and the dashed line represent the amplitude of the biggest peak in the simulations above which there is a 10% and 3% probability of seeing a larger peak respectively. It will be seen that even with a random σ_{noise}-value as low as $25\,\mu\mathrm{K}$ it is not unlikely to find a (spuriously) interesting excess of

$\Delta T_s/T \geq 10^{-5}$ for an experiment with 5.6° FWHM.

In the following, we examine the situation from the stand-point of GSR and noise alone. Later on in Chapter 5 we go on to consider what may be an important contributor at low $\Delta T_s/T$ levels: extragalactic sources.

2.6.1 The role of GSR and instrumental noise

The result of evaluating the rms spurious signal as a function of instrumental noise value and frequency is shown in Fig. 20. Here we have adopted a mean GSR prediction from Fig. 16 and the noise has been taken as the error per pixel – typically 200 μK – divided by $\sqrt{5}$, so as to correspond to the noise in 5° smoothed data. It is apparent that if the genuine signal is $\Delta T/T \simeq 8\times10^{-6}$ then a frequency as high as 20 GHz appears necessary, together with improved precision, viz. $\sigma \leq$ 20 μK. It is possible to go a little way below the curves, if the correlation length is greater than 5° .

Use of interferometric techniques reduces the contamination due to atmospheric effects somewhat, as well as allowing a better signal-to-instrumental-noise ratio at higher frequencies. For example, Timbie and Wilkinson (1988, 1990) employ a low-noise interferometer system to determine the level of CMB anisotropy at a frequency of 43 GHz and over angular scales of 0.5° - 5°. By adopting a symmetric beam pattern, large scale gradients in the atmospheric emission are eliminated. However, changes in higher order derivatives of the atmospheric emission over scales of a few degrees will affect the radiometer output. Clouds give large signals typically of magnitude 1 mK on this angular scale on a time scale of 100 s. Since the instrumental noise, ΔT_{rms}, is given by $13\,mK/s^{1/2} < \Delta T_{rms} < 15\,mK/s^{1/2}$, it can be seen that the atmospheric contribution on this time-scale is then comparable to the instrumental noise. It is obviously important to observe on clear days. The result of the particular experiment of Timbie and Wilkinson (1990) is that the data are consistent with temperature fluctuations in the sky with ΔT_{rms} of 180 μK or less, but instrumental noise is clearly the limiting factor in the experiment. The interferometric technique reduces the atmospheric noise to a negligible level but the residual instrumental noise will remain significant. At the frequency of interest, it is hoped that all Galactic contamination effects are below 30 μK in magnitude.

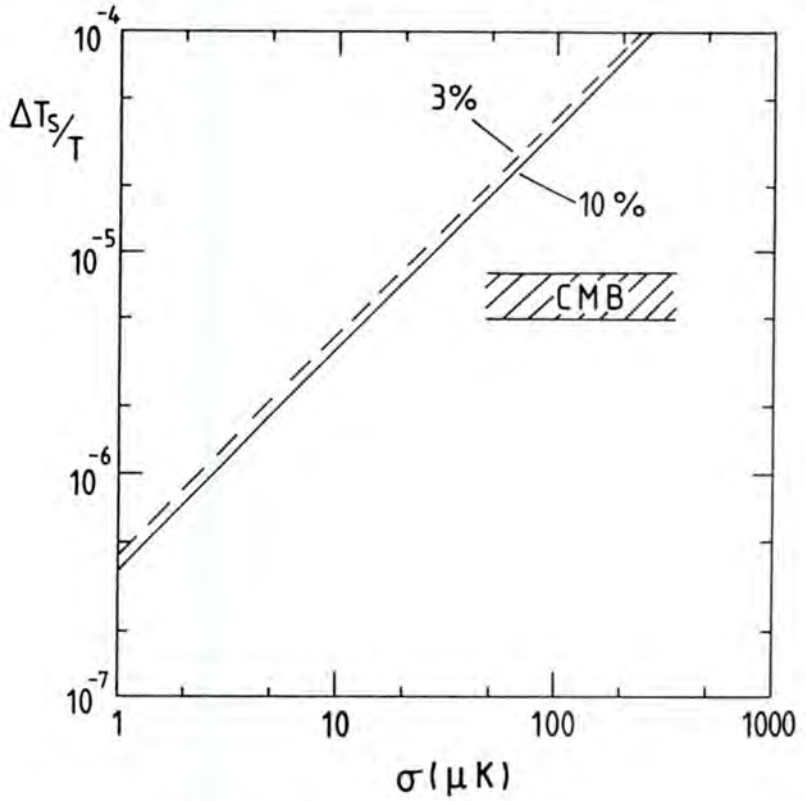

Figure 2.19: The values of $\Delta T_s/T$ generated by noise in an experiment with 5° FWHM for a region comparable in size to that of the region of interest.

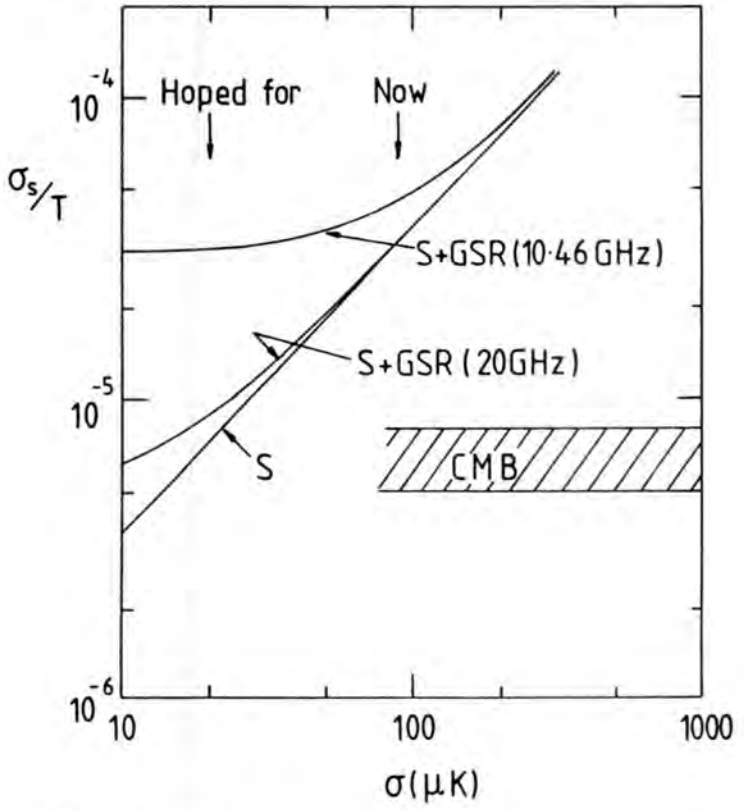

Figure 2.20: The (noncosmological) σ_s/T, vs rms error of measurement, σ, for two frequencies.

2.7 An Alternative Method: Comparison of CMB and GSR correlation functions

Many predictions have been made for the correlation functions expected from different cosmological scenarios, see, for example, Bond & Efstathiou (1984, 1987), Efstathiou (1990). Scaramella & Vittorio (1990) have noted that, as a consequence of the long-range nature of the gravitational interactions and the assumed primordial power spectrum (see Chapters 1 and 6), our microwave sky does not constitute a fair sample for the large scale CMB anisotropy. Thus even an angular average over the whole sky will not coincide with ensemble average theoretical prediction, constituting a very obvious handicap for comparison of observation with theory. An even more important practical point arises, however, viz, that the background over the sky against which the anisotropies are sought varies considerably and so far, at least, attention has been devoted to specific background-quiet regions. Specifically, the Jodrell-IAC experiment refers to $\simeq 70°$ in longitude. The significance of taking such a small region of the sky is that, with correlation lengths of order 10°, there will be big fluctuations in $C(\theta)$ from region to region in the CMB sky. Since the correlation function is directly related to the observed sky temperature fluctuations, such variations in $C(\theta)$ correspond to variations in the second differences from region-to-region on the sky. Such an effect is obviously of great importance when one is trying to extract a genuine cosmological signal from a Galactic foreground which does show large spatial variations. As an example, we adopt the isocurvature (IC) model of Bond & Efstathiou (1987), and compare the angular correlation functions for this model with that found observationally for GSR at different frequencies. Fig. 21 indicates the variations in $C(\theta)$ expected for five 70° longitude strips for a CMB sky generated in an approximate fashion The 'LSA' refers to the ensemble average theoretical prediction taken directly from Bond & Efstathiou. The data have a resolution of 5° .

A useful parameter describing the correlation function is the value of $\theta_{0.3}$ at which $C(\theta_{0.3})/C(0) = 0.3$. We see from Fig. 21 that for the five regions considered $\theta_{0.3}$ covers the range 4.5° to 12°; a greater number of samples would doubtless yield a somewhat larger range of values.

Turning to GSR temperature correlation functions we have, of course, only one

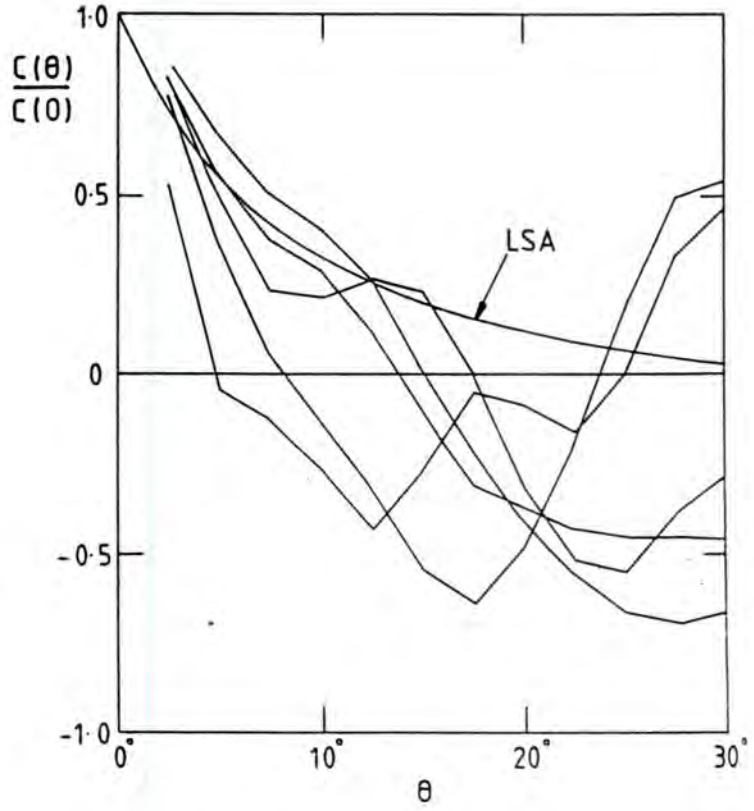

Figure 2.21: Correlation functions for CMB temperature for the isocurvature model of Bond & Efstathiou (1987). The data were binned in 2.5° intervals, and have a resolution of 5° .

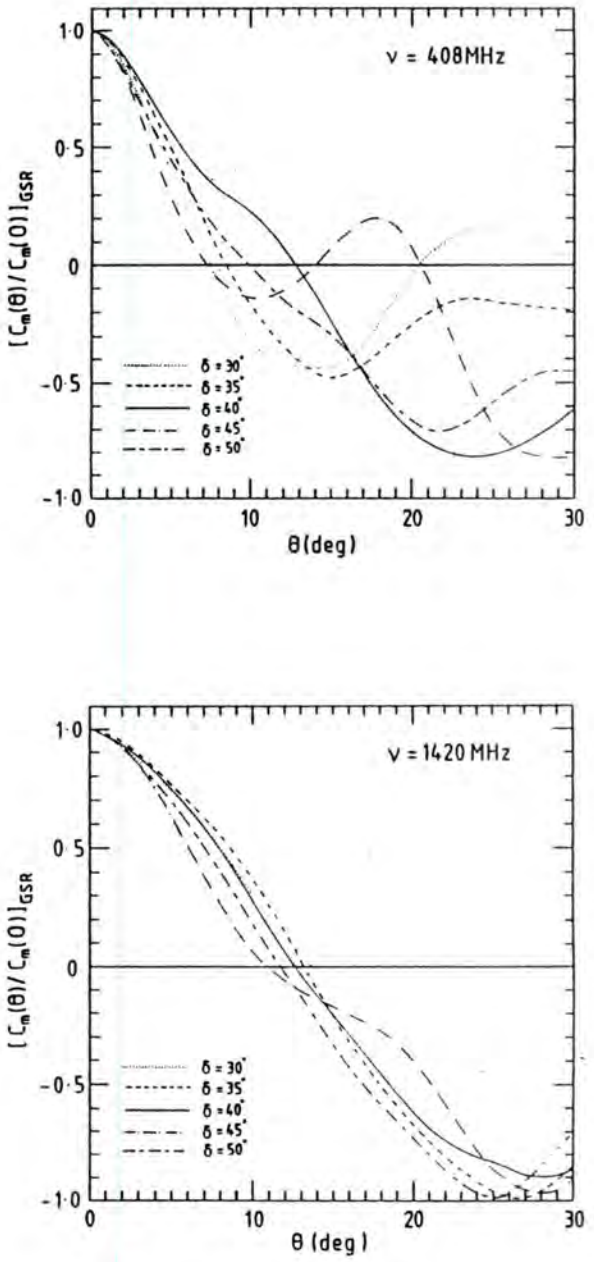

Figure 2.22: Correlation functions for the GSR along declination bands bordering 40° for two frequencies (data smoothed to 5.6° FWHM).

map for each region of the sky (at each frequency) and therefore cannot predict a range of $C(\theta)$ values similar to those in Fig. 21. However, a representative set can be achieved by taking temperature profiles for a variety of δ-values, not too far from $\delta = 40°$. The corresponding results are shown in Fig. 22 for two frequencies: 408 and 1420 MHz, the results coming from the maps reported by Lawson *et al.* (1987). In each case the linear best fit to the temperature profiles along R.A. has been taken out of the data.

A number of features are apparent and can be considered in turn.

i) The value of $\theta_{0.3} = 8°$, for $\delta = 40°$, is in the middle of the range found for the sample of five CMB 'predictions' shown in Fig. 21.

ii) The range of $\theta_{0.3}$ for GSR shown in Fig. 22, 5° to 9° for 408 MHz and 8° to 11° for 1420 MHz, is again similar to that for CMB.

It has already been seen that the amplitude $C(0)$ for GSR extrapolated to higher frequency is of the order of the theoretically predicted cosmological fluctuations. So, if the shape of the correlation function is preserved up to highest frequencies then it will not be possible to rule out GSR anisotropies on the basis of correlation function alone, at least for the IC model: both CMB and GSR have anisotropies of similar angular scales. Indeed, not only is the mean value of the correlation function (characterised by $\theta_{0.3}$) for GSR at $\delta = 40°$ similar to the mean for CMB, but the range from declination to declination is similar to the range for independent regions for CMB. It is necessary to point out that although there is preoccupation at present with the radio-quiet region ($\delta \sim 40°$), when measurements are made at higher frequencies a wider region of the sky will need to be studied to enable firmer conclusions about the magnitude of the CMB anisotropy to be drawn. This will make extraction of the genuine CMB signal even more difficult against a GSR contribution varying considerably over the sky.

2.8 Discussion and Conclusions

We have used the low frequency sky maps, dominated by GSR to predict its contribution to measurements of the brightness temperature fluctuations at higher frequen-

cies ($\geq$ 10 GHz), aimed to detect fluctuations of the cosmic microwave background. Our sky region of interest was that where recent measurements at 10.46 GHz claimed some evidence for a detection of cosmological fluctuations. However, we have shown that the level of the fluctuations due to GSR is the same as that measured. Moreover the correlation functions $C_\sigma(\theta)$ for GSR at 408 and 1420 MHz have similar shapes to the correlation function calculated in the framework of a theoretical model. If $C_\sigma(\theta)$ preserves its shape at 10 GHz then the GSR would smear the cosmological fluctuations on angular scales from a few to some 20°. The GSR fluctuations can explain the observed ΔT fluctuations, but we have been unable to demonstrate that they do. Such a situation, which is clearly unsatisfactory, is due to the simple reason that the actual, as distinct from statistically-derived, $\Delta\beta$ changes are not yet known. The case for there being changes has been made, but the actual topography of the changes is not yet clear. The evidence that the observed second differences at 10.46 GHz are due to Galactic Synchrotron Radiation is already quite strong (the contribution to the signal is certainly significant enough to require its inclusion in any analysis of the data to extract information on, for example, primordial density perturbation spectra. The analysis of Vittorio *et al.*, 1989, is thus deficient in this respect). It certainly seems likely that the signal is more easily explained in terms of Galactic emission than by any of the cosmological proposals (see, for example, Scaramella 1990). Indeed the Jodrell-IAC group themselves now agree that the 10 GHz fluctuations are likely to be the result of a combination of GSR fluctuations, together with discrete sources (which we return to in Chapter 5) and instrumental noise. A likelihood analysis of the 5.6° results including the contribution from GSR, as estimated from a straightforward extrapolation from the 408 and 1420 MHz data, yields an upper limit on the residual sky fluctuations of $\Delta T/T < 3 \times 10^{-5}$, although not at a high confidence level. Furthermore, new work at 15 GHz detects lower sky fluctuations strongly supporting the claim that GSR is the major contaminent of the data (Lasenby *et al.* , 1991). Fig. 23 shows the preliminary 15 GHz data taken from Lasenby *et al.* , together with our simple extrapolation using the 408 and 1420 MHz data. The 10 and 15 GHz results analysed together should enable the removal of the GSR contribution at higher frequencies allowing stronger limits to be placed on the intrinsic sky fluctuations.

However, there is no convincing evidence so far from experimental measurements for fluctuations in either of these two radiations at high frequencies. More work is

needed both to understand GSR phenomena and to be able to predict what the GSR anisotropies should be at the higher frequencies, and so measurements in the 5 GHz - 20 GHz region are of the greatest importance. These measurements need to be of such quality that the maps at lower frequencies (which themselves would benefit from absolute calibration and the removal of scanning effects) can be used to predict the bulk of the features seen at the higher frequencies and the reasons for the residual discrepancies can be understood. Only then will it be possible to trust the predicted GSR maps at the very highest frequencies and thereby allow the discrepancies seen there to be interpreted as arising from cosmological effects. Such measurements should see a gradually decreasing role for the Galactic Synchrotron Radiation with increasing frequency (a feature not yet seen) and detailed understanding will enable the GSR contribution to be predicted at the highest frequencies. We estimate that the GSR fluctuations at frequencies higher than about 20 GHz should be small enough ($\sigma_s/T \leq 5 \times 10^{-6}$) not to dominate the cosmological effect.

The measurements of Galactic Synchrotron Radiation and therefore of cosmic ray electron intensity (and/or magnetic field) at these high frequencies are very interesting by themselves and may give a better understanding of cosmic ray propagation and source problems, topics which might themselves have cosmological implications when related to other, distant galaxies.

Although observations above 20 GHz will give improved prospects a detection of CMB anisotropies still requires an understanding of the cosmic ray effects, particularly when it is appreciated that Fig. 16 refers to a quiet region of the sky. In fact, measurements are needed over a wider region of the sky in order to test the statistical nature of the temperature fluctuation distribution and thus gain information about the nature of the initial perturbation spectrum and the physics of the early universe.

From Fig. 16, it would appear that the Cosmic Background Explorer (COBE) operating at 31.5, 53 and 90 GHz should not have too much trouble with GSR for a sensitivity per sky pixel of $\sim 10^{-5}$ (although we recognise that Fig. 16 is not strictly accurate since the beamthrow for COBE is 60° compared to the 8.2° used here). However, for any data analysis involving averaging over sky pixels, the contribution from regions not as quiet as investigated here are still likely to be significant.

Furthermore, the far-infrared emission from the Galaxy becomes important at the higher frequencies, as is discussed in the following chapter.

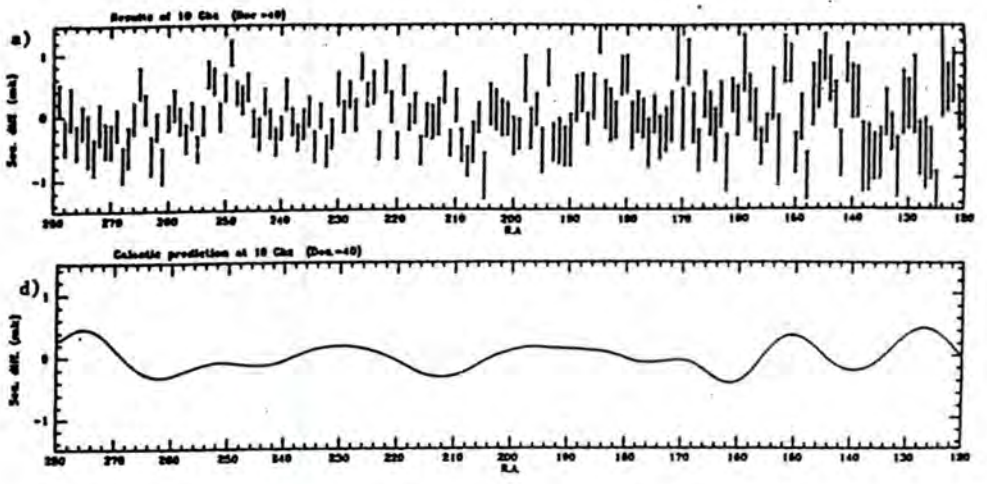

Figure 2.23: 15 GHz results from Lasenby *et al.* (1991), together with a simple extrapolation of the GSR contribution from lower frequency data.

References

Bhat, C.L. *et al.* , 1985. *Nature*, **314**, 515.

Bhat, C.L., Issa, M.R., Mayer, C.J., Wolfendale, A.W., & Zan, M., 1986. *J. Phys. G*, **12**, 1067.

Bond, J.R. & Efstathiou, G., 1984. *Mon. Not. R. astr. Soc*, **285**, L45.

Bond, J.R., & Efstathiou, G., 1987. *Mon. Not. R. astr. Soc*, **226**, 655.

Bridle, A.H., 1967. *Mon. Not. R. astr. Soc*, **136**, 219.

Broadbent, A., 1989. PhD Thesis, University of Durham.

Chi, X. & Wolfendale, A.W., 1990. *J. Phys. G.*, **16**, 1409.

Davies, R.D., Lasenby, A.N., Watson, R.A., Daintree, E.J., Hopkins, J., Beckman, J., Sanchez-Almeida, J., & Rebolo, R., 1987. *Nature*, **326**, 462.

de Amici, G. *et al.* , 1988. *Astrophys. J.*, **329**, 556.

Efstathiou, G., 1990. in *'Physics of the Early Universe'*, eds. Heavens, A.F. *et al.* , SUSSP.

Giler, M., Wdowczyk, J., & Wolfendale, A.W., 1978. *J. Phys. G*, **4**, L269.

Giler, M. *et al.* , 1985. *Proc. Int. Cosmic Ray Conf.*, **3**, 324.

Haslam, C.G.T. *et al.* , 1982. *Astron. Astrophys. Suppl.*, **47**, 1.

Howell, T.F. & Shakeshaft, J.R., 1966. *Nature*, **210**, 1318.

Howell, T.F. & Shakeshaft, J.R., 1967. *Nature*, **216**, 753.

Kallas, E. *et al.* , 1983. *Astr. Astrophys.*, **128**, 268.

Kogut, A. *et al.* , 1990, *Astrophys. J.*, **355**, 102.

Lasenby, A.N., & Davies, R.D., 1988. *Large scale Motions in the Universe*, eds. Coyne, G.V., & Rubin, V.C., Vatican Press.

Lasenby, A.N., *et al.* , 1991. in *Observational Tests of Cosmological Inflation*, p. 413, eds. Shanks, T., *et al.* , Kluwer.

Lawson, K.D., Mayer, C.J., Osborne, J.L., & Parkinson, M.L., 1987. *Mon. Not. R. astr. Soc*, **225**, 307.

Levin, S. *et al.* , 1988. *Astrophys. J.*, **334**, 14.

Longair, M.S., 1981. in *'High Energy Astrophysics'*, CUP.

Malawi, A.A.S., 1989. PhD Thesis, University of Manchester.

Mather, J.C. *et al.* , 1990. *Astrophys. J.*, **354**, L37.

Pauliny-Toth, I.I.K. & Shakeshaft, J.R., 1962. *Mon. Not. R. astr. Soc*, **124**, 61.

Penzias, A.A. & Wilson, R.W., 1967. *Astron. J.*, **72**, 315.

Phillips, S. *et al.* , 1981. *Astr. Astrophys.*, **103**, 405.

Rebolo, R., Watson, R.A., & Beckman, J.E., 1989. *Astrophys. Space Sci.*, **157**,333.

Scaramella, R., 1990. *Astrophys. J.*, **346**, 607.

Scaramella, R., and Vittorio, N., 1990, *Ap.J.*, **353**, 372.

Silberberg, R. *et al.* , 1983. *Phys. Rev. Lett*, **51**, 1217.

Simonetti, J.H., Cordes, J.M., & Spangler, S.R., 1984. *Astrophys. J.*, **284**, 126.

Sironi, G. *et al.* , 1990. *Astrophys. J.*, **357**, 301.

Smoot, G. *et al.* , 1988. *Astrophys. J.*, **331**, 653.

Stankevich, K.S., Wielebinsky, R. & Wilson, W.E., 1970. *Austr. J. Phys.*, **23**, 529.

Tago, E., Einasto, J. & Saar, E., 1986. *Mon. Not. R. astr. Soc*, **218**, 177.

Timbie, P.T., and Wilkinson, D.T., 1990, *Ap.J.*, **353**, 140.

Timbie, P.T., and Wilkinson, D.T., 1988, *Rev.Sci.Instrum.*, **59**, 914.

Vittorio, N., De Bernadis, P., Masi, S., & Scaramella, R., 1989. *Astrophys. J.*, **341**, 163.

Watson, R.A., Rebolo, R., Beckman, J.F., Davies, R.D., & Lasenby, A.N., 1988. ***Large Scale Structure and Motions in the Universe***, p.133, ed. Mezzetti *et al.*, Kluwer Academic Publishers.

Watson, R.A., 1989. *Ph.D Thesis*, University of Manchester.

Webber, W.R., 1983. in *'Composition and Origin of Cosmic Rays'*, p. 83, ed. Shapiro, M.M., Reidel.

Webster, A.S., 1971. *PhD Thesis*, University of Cambridge.

Chapter 3

Galactic Dust Emission

3.1 Introduction

It is important to extend measurements of the CMB to frequencies upwards of a few tens of GHz in order to continue to verify the blackbody nature of the spectrum. Measurements of the CMB spectrum near the peak of the Planck curve at $\sim$ 160 GHz are of particular interest since it contains most of the photon energy in the universe. Furthermore, it is necessary to verify the existence or otherwise of distortions representing energetic physical processes in the early universe. At such frequencies, however, measurements become increasingly difficult very rapidly as a result of a combination of factors, including the decrease in antenna temperature of the CMB and increasing problems with emission from the apparatus (essentially a blackbody at $\sim 300\,\mathrm{K}$). Atmospheric effects are also a problem, as a result the apparatus is usually established at high dry sites such as the South Pole, or carried above the atmosphere by balloon or rocket. At frequencies below $\sim$ 90 GHz, the well established technology of heterodyne receivers employed in the more traditional radio region can still be utilised, and many of the more sensitive results have been achieved with such apparatus. For frequencies above 90 GHz, new receiver technology – that of bolometric photometers – have been employed, but whilst the detectors are more sensitive in principle, they are less well developed thus far. Some of the more interesting results of recent years have appeared at high frequencies. In 1988, Matsumoto *et al.* reported evidence for an excess of flux beyond the blackbody peak. Whilst the observed sky flux fell with frequency, it did not do so as rapidly as expected for a blackbody. Such a result suggested the possibility of spectral mod-

ification by Compton scattering of the CMB photons from hot electrons, or as a consequence of the re-radiation of starlight from exotic massive stars forming early in the universe's history by dust. Such a result aroused considerable interest and theoretical speculation; however, later investigation found problems with the data, and the COBE FIRAS instrument ruled out such a large distortion when it confirmed the blackbody nature of the spectrum to better than 1% over a large range in frequency.

Of more relevance to this thesis, anisotropy measurements have also moved to higher frequencies, where the maximum level of anisotropy flux is expected. Beyond 30 GHz, the contribution from Galactic Synchrotron Radiation is expected to fall considerably, and to be of little importance as a foreground at a level much above $\Delta T/T \simeq 10^{-6}$ (see Chapter 2). However, at the frequencies in question a new problem arises from the foreground emission from dust in the Galaxy, which is present even at the highest latitudes. Indeed, some of the first evidence for dust emission at high latitudes, and for structure in it, came from attempts to measure CMB anisotropies at high frequencies (Melchiorri *et al.* , 1981; de Bernardis *et al.* , 1984). As is the case with GSR, structure in the dust emission may give rise to features which can mimic genuine cosmological anisotropy signals, so it is important to analyse this possibility in some detail. Furthermore, since the contribution from the dust is still rising as the CMB intensity begins to fall, accurate models of the dust emission are also important for spectral measurements. Wright (1991) has demonstrated the necessity for adequate foreground modelling if COBE is to detect spectral distortions corresponding to a Thompson parameter of y = 0.0001. De Bernardis *et al.* (1988) have shown how the diffuse Galactic emission can give rise to a spurious dipole anisotropy. Recent measurements of CMB anisotropies in the frequency range upwards of 30 GHz have found great problems with the subtraction of the Galactic emission. Furthermore, although Meyer *et al.* (1991) find clear evidence for anisotropy in their data at 170 GHz at the $1 - 3 \times 10^{-5}$ level, their extrapolations of the IRAS 100 μm data with a spectrum observed by them for a plane crossing at $l = 42°$ yields fluctuations at a similar level. Confirmation or otherwise of the cosmological nature of this anisotropy will depend on measurements at other frequencies and accurate foreground subtraction.

In the present chapter we concentrate on Galactic dust insofar as our main

concern is to estimate the effect on scales of several degrees. The objective is to estimate the overall radiation spectrum at high Galactic latitudes at the frequencies in question and to go on to estimate the magnitude of the anisotropy in this radiation field which cannot yet be predicted and therefore subtracted.

Since Galactic dust emission provides the large-scale foreground at frequencies beyond the CMB blackbody peak, in principle, the IRAS data should be of considerable value. Comprehensive maps are available at 60 and 100 μm which enable much of the dust to be mapped. In particular, maps are available binned to 0.5 ° resolution with zodiacal light subtraction as in Rowan-Robinson *et al.* (1990). These have been synthesised from HCONs 1, 2 and 3, the binning procedure allowing any gaps in the coverage to be smoothed over (the 100 μm maps in this chapter have been generated from software kindly provided by Prof Rowan-Robinson, and all calculations will make use of these). The problem then resolves itself into answering the question: how accurately can the IRAS (and other) data be used to predict the high latitude radiation field in the 30 - 100 GHz region? The presence of the FIR 'cirrus' at high latitudes, a discovery of IRAS, and the possibility of the existence of grains with unusual dielectric properties and complex emissivities indicates immediately that the problem is not a trivial one.

We start by reviewing the properties of dust in various environments, and the nature of the overall Galactic foreground.

3.2 Dust-grain properties in the Galaxy

In the IR part of the spectrum, we consider that dust radiates as a greybody, that is, its spectrum is that of a blackbody at temperature T_d modified by a frequency-dependent emissivity Q_ν, conventionally represented as $K\nu^\alpha$. The determination of the exact nature of Q_ν (such as the possible dependence of α on frequency) requires knowledge of the composition and structure (both atomic and geometric) of the grain, so that its dielectric properties can be calculated satisfying the Kramers-Kronig dispersion relations. Once Q_ν is calculated, then it is a simple matter to derive the equilibrium temperature T_d in an interstellar radiation field of energy density u_ν, since in the 'steady-state' grain heating by photon absorption can be

equated to cooling by photon emission,

$$c \int_0^\infty u_\nu Q_\nu \, d\nu \; = \; 4\pi \int_0^\infty B_\nu[T_d] \, Q_\nu \, d\nu \, ,$$

where $B_\nu[T_d]$ is the Planck function at temperature T_d. In practice, we can write the ISRF as the sum of several dilute blackbodies, each with its' own characteristic temperature and dilution factor, plus a UV contribution from early-type stars which dominates in the region 912 - 2500Å (Mathis, Mezger & Panagia, 1983). Since a mixture of grain types is present, the FIR radiation due to dust must be evaluated by first determining the temperature T_d which each grain species acquires through radiative balance with the ISRF.

Table 3.1: Theoretical and laboratory determinations of grain properties. Laboratory measures in references 3, 5 and 6, the remainder are theoretical calculations constrained by observations

Material	α	Reference	Comments
Amorphous Carbon	1.0 - 1.7	1	
		2	frequency dependence for α : 1.0 for λ = 5 - 200 μm , steepening further towards 2.0 beyond 1000 μm .
		3	
Graphitic Carbon	2.0	1	
		2	for long wavelength response.
Fused Quartz	1.6	4	
	1.0 - 1.8	5	Spectra depend on grain size a: a = 400Å- 1.8 μm , $Q_\nu \propto \nu^2$ as for bulk material; a below 400Åα falls finally to $\sim$ 1.0 for a $\sim$ 60 - 70Å.
Amorphous Silicates	1.2 - 1.5	1	
		6	for λ = 100 - 300 μm , 2 compounds showed α = 1.25 and 1.5 respectively.
Crystalline Silicates	1.9 - 2.2	1	
		4	
Silicate core/iron mantle	2.2 - 3.5	4	

References: 1 - Tielens & Allamandola (1987); 2 - Martin & Rogers (1987); 3 - Koike *et al.* (1980); 4 - Aannestad (1975); 5 - Koike *et al.* (1987); 6 - Day (1976).

Table 1 summarises the situation for a variety of grain compositions. Calculations (Seki & Yamamoto, 1980) and laboratory experiments (Koike *et al.* , 1987) also suggest that the observed spectral properties of the dust grains will be a function of grain size. Seki & Yamamoto (1980) have calculated that, for amorphous silicates, larger grains demonstrate a ν^2 dependence whilst smaller grains show less steep spectra, whilst for a fixed grain size, α changes from 2 to 1 as frequency decreases (though this cannot be true to arbitrarily low ν from elementary Kramers-Kronig

considerations) with the critical frequency at which the slope changes increasing with decreasing grain size. For the smallest grains, quantum effects become important, and the grains do not achieve an equilibrium temperature, instead being transiently heated to very high temperatures (their contribution to the diffuse Galactic emission has been evaluated by Draine & Anderson, 1985). The presence of such small grains is required to explain the excess emission seen at 12 and 25 μm (and to a lesser extent at 60 μm) by the IRAS satellite. The presence of a distribution of grain sizes and compositions obviously leads to a complex frequency dependence for the dust emission.

The observed spectral emission of a source can be used to attempt to evaluate grain temperatures, cloud masses and the dust/gas ratio, and to impose constraints on the grain composition by the derivation of the spectral index of FIR emissivity. In this situation, α and T_d must be fitted together to the continuum emission, since varying α affects the spectrum significantly. Considerable variation in the observed spectra among sources is expected as a consequence of the variability of the grain composition and hence spectral properties of the grain, and the variation in the radiation fields heating the dust from source-to-source. Table 2 indicates the observed dust parameters for a variety of sources in the Galaxy. The great range of observed values of α is indicated in Fig. 1. In a recent review, Helou (1989) also derived α for a number of external galaxies (Fig. 2). With FIR flux uncertainties of the order of 30 %. he claims that the problem of evaluating α , T_d is quite severe, and that therefore there is no evidence for α varying with ν, or that it lies outside the range 1 - 2. Fig. 1 demonstrates the considerable range of α -values which have been observed however, and which will complicate any large-scale modelling of Galactic emission if they are genuine.

Table 3.2: Dust parameters in the Galaxy inferred from observations. In all cases α and T_d are determined by empirically fitting a modified blackbody spectrum to the data.

Source	α	T_d	λ	Reference	Comments
Dust forming stars	1.0	375 K	50 - 1000 μm	Campbell et al. (1976)	1
	1.0 (assumed)	250 K	35 - 175 μm	Harvey et al. (1978)	2
	1.0		12, 25, 60, 100 μm	Rowan-Robinson et al. (1986)	3
Galactic centre	1.0	80 K (1pc) - 50 K (10pc)	30, 50, 100 μm	Gatley et al. (1977)	4
M42, OMC-1	1.2		1300 μm + other data	Gordon (1987)	
3 compact dust complexes	1.8 - 2.0				
Compact HII sources	1.75 $\pm$ 0.2 long λ		0.35, 0.8, 1.1, 3.3mm	Gear et al. (1988)	5
	0.80 $\pm$ .15 short λ				6
	1.0		FIR	Tokunaga et al. (1978)	7
30 HII regions	$\geq$	$\sim$ 26 K	1.3mm	Chini et al. (1986a)	
12 star forming regions	2.0 $\pm$ .4		350, 1300 μm	Chini et al. (1986b)	
Molecular clouds	2.2 - 2.6		mm wavelengths	Schwartz (1982)	8
	1.0	48 K	62 - 400 μm	Schwartz et al. (1983)	9
	1.0	49 K (central cloud)	50 μm - 1mm	Richardson et al. (1985)	10
Kleinmann-Low nebula	1.0 ($\lambda > 150$ μm)	85 K	100 - 500 μm	Pipher et al. (1978)	
Large-scale Galactic FIR emission	1.8 $\pm$ .2	17 $\pm$ 2 K	200, 400, 620, 3000 μm	de Bernardis et al. (1984)	11
	2.0	28 K	227, 323, 1250 μm	Halpern et al. (1988)	12
	2.0	22.1 $\pm$ .7 K	0.44, 0.63, 1.1, 1.8mm	Page et al. (1990)	13
	$\simeq$ 1.5		2.5 μm - 1cm	Hauser et al. (1991)	14

Comments:

1 - Observation of IRC 10216. Errors in flux $\sim$ 30%. Dust emission from molecular cloud heated by compact source at core.

2 - Observations of η Carinae. $Q_\nu \propto \nu$ considered most likely from previous observations.

3 - IRAS observations of circumstellar dust shells around late-type stars.Grains likely to have amorphous structure. Some sources have excess 100 μm emission due to a dust-shell or Oort cometary cloud?

4 - Peak of brightness distribution coincides with Sgr A West.

5 - Excess at long λ, possibly due to a new cool/cold dust component not associated with dust seen at higher frequencies.

6 - Excess at short λ: small grain component.

7 - Observations of S140IR. Good fit to spectrum assuming $Q_\nu \propto \nu$.

8 - Observations of NGC 2264, S140, NGC 6334N. $\alpha > 2$ implies the presence of silicate core grains with thin ice mantles.

9 - FIR and sub-mm mapping of S140IRS. Beyond 400 μm α approaches 2.

10 - Detailed structure evident in cloud.

11 - Clear evidence for structure in the Galactic emission at high latitudes.

12 - Considerable structure in Galactic emission. Evidence for an excess at $\nu < 18\text{cm}^{-1}$ in the region $b = 20^\circ$, $40^\circ \leq l \leq 120^\circ$, possibly indicating the presence of a cold dust component with parameters $\alpha = 1.1$, $T_d = 6$ K .

13 - Structure in the Galactic plane emission at $l = 42^\circ$ for $\nu < 15$ cm^{-1} suggesting the presence of a cold dust component ($T_d \sim 4$ K).

14 - Galactic emission greater than expected for $Q_\nu \sim \nu^2$, $\alpha \sim 1.5$ gives a reasonable fit to preliminary data. Evidence of discrepancies with IRAS data. DIRBE results towards the South ecliptic pole substantially fainter than the IRAS results at 60, 100 μm. More detailed investigation shows errors in the zero point calibration resulting in large overestimates of 100 μm fluxes in faint regions.

A more detailed approach to the problem of the total Galactic emission has been made by Rowan-Robinson (1990, 1986) who has developed a model consisting of multiple grain types of discrete sizes, each with its own emissivity characteristic of their composition. When a suitable model of the ISRF is adopted (see, eg., Mathis, Mezger & Panagia, 1983) which allows for variation in the heating within the Galaxy, such a procedure provides an excellent fit to high frequency data both in the plane and at high latitudes. An alternative approach is to assume a mixture of grain types with a power law distribution of sizes f(a) $\propto a^{-3.5}$ for $0.005 \leq a \leq 0.25\,\mu$m (Mathis, Rumpl & Nordsieck, 1977). In both cases, the effect of small grains is required to explain the 12, 25 and part of the 60 μm IRAS fluxes.

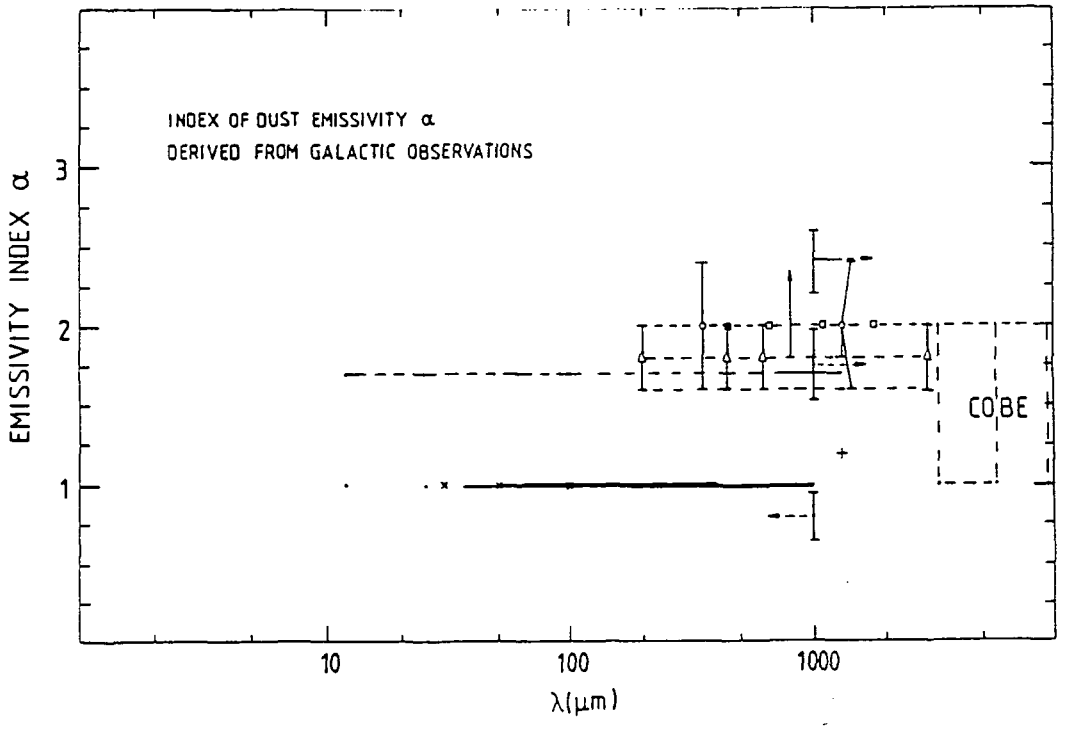

Figure 3.1: Observed emissivity exponents for Galactic objects, plotted against the frequencies of observation from which they were derived.

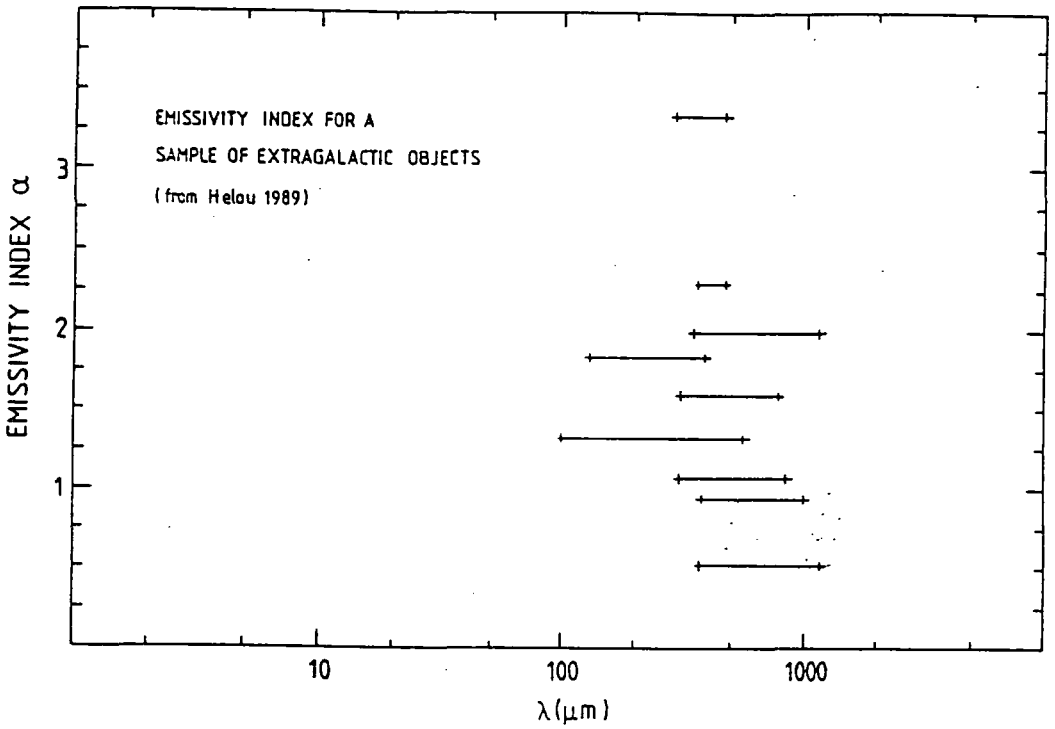

Figure 3.2: As figure 1, for external galaxies, derived from the review by Helou (1989).

3.3 Nature of the Galactic Foreground

Diffuse emission from interstellar dust contributes from 10 - 30% of the radiative output of the Galaxy. The integrated spectral energy distribution shows two peaks - one at $\sim 100\,\mu$m corresponding to grain temperatures T_d in the range 15 - 40 K , and a secondary peak near $10\,\mu$m indicating a component with $T_d \sim 200$ - 500 K (see Fig. 3). Detailed interpretation of the emission requires knowledge of the dust characteristics, spatial geometry of the dust and sources of energy input, and the correlation between the dust and sources. However, the FIR peak seems consistent with thermal emission from grains in equilibrium with the Interstellar Radiation Field (ISRF), the mid-infrared excess arising from small particles undergoing non-equilibrium transient heating by absorption of individual energetic photons. The overall spatial structure of the Galactic IR emission shows a number of strong peaks, all of which seem to be associated with bright GMC/HII complexes, spiral arms or the Galactic Centre, superimposed upon a continuous ridge. This diffuse emission component can be well described by a multi-component dust model, in which a warm component of dust, $T_d \sim 30$ K , heated by OB stars dominates the $100\,\mu$m emission

(Cox & Mezger, 1987, their Fig. 2; see also Broadbent *et al.* , 1989) in the plane; at high latitudes the dust being heated by the general ISRF.

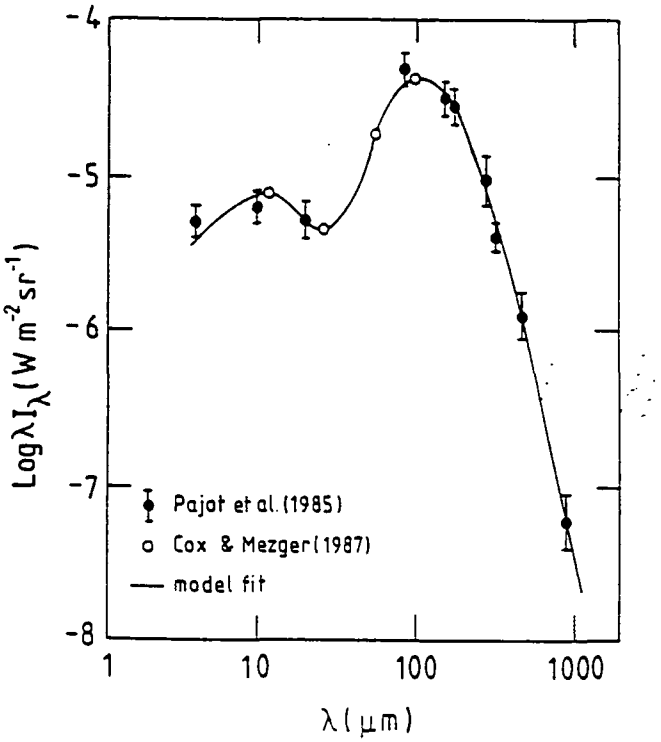

Figure 3.3: Integrated spectral energy distribution for the Galaxy. Derived from Cox & Mezger (1988).

One of the major discoveries of the IRAS mission was the large-scale filamentary emission at 60 and 100 μm arising not only in the Galactic disk, but also in regions of intermediate and high latitude. Indeed, Hauser *et al.* (1984) found that the Galaxy made an unexpectedly large contribution to the 100 μm brightness and showed direct evidence for smooth Galactic emission for $|\, b \,| > 30°$, superimposed upon which Low *et al.* (1984) detected extended sources of FIR emission — the so-called 'cirrus' referred to already. The cirrus may also be associated with molecular clouds, from which emission is also seen in CO (Blitz, Magnani & Mundy, 1984; Weiland *et al.* , 1984). The average brightness at 100 μm is in good agreement with predictions based on classical dust models, but emission at 12 μm and 25 μm requires the presence of small grains and/or large molecules such as polyaromatic hydrocarbons (PAHs) as proposed by Leger & d' Hendecourt (1988). The fact that the small grains are thought to also contribute to the 60 μm flux means that the commonly used technique of determining dust temperatures from the 60 μm and 100 μm intensities is inaccurate. A systematic study of the emission has been carried out by Boulanger

& Pérault (1988) who find that away from molecular clouds and heating sources there is generally a good correlation between 100 μm emission and HI column density (this also being the case for the other IRAS wavelengths), and that on scales of $\sim$ 100 pc the ISRF and dust abundance are roughly uniform. The emission also follows a cosec b law for $|\ b\ | > 10^\circ$ up to the poles provided a large enough bin in longitude is selected. However, there is still some scatter in this distribution corresponding to variations in the IR emission per H atom by a factor of $\sim$ 3 from one field to another. The greatest variations occur in the vicinity of OB stars, lower variations in the direction of the anti-centre: this behaviour is undoubtedly due to changes in the ISRF. The cosec b law is also found to overestimate the values of the pole emission, eg. in their version of the 100 μm data with zodiacal light subtraction the cosecant fit implies at the north Galactic pole an intensity of 1.7 ± 0.4 MJy sr^{-1} compared to the observed flux of 1.1 ± 0.5 MJy sr^{-1}. A more recent study by Rowan-Robinson *et al.* (1991) uses a physical model to subtract the zodiacal light background from the IRAS data rather than the empirical fit attempted in Boulanger & Pérault, and thus should give better results as it accounts for variations in the scan profile during observation (this, as mentioned previously, is the data employed in this chapter). Detailed maps of both 100 μm emission and HI column density are presented. which largely confirm the results of Boulanger & Pérault, and in particular, a good linear relationship is found between the FIR emission and HI distribution. In particular, over 90% of the sky there is good agreement with the relationship derived in Boulanger & Pérault, I(100 μm)[MJy sr^{-1}] = 0.85 $\times$ 10^{-20} N(HI)[cm^{-2}], which holds to about 30%. A similar cosecant slope has been derived for b $> 30^\circ$ in bins 55° length along bands in longitude, and the result of the fit is that the intensity at the north Galactic pole is again overestimated, by $\sim$ 30%. The maps reveal that 100 μm emission is present over virtually all of the sky, but that there are two substantial areas with low 100 μm column densities centred at (l,b) = (160° , 55°) and (85° , 75°). These may be of use in searches for fluctuations in the CMB (as well as for galaxy counts etc. where low extinction is desirable). Fig. 4 shows the 100 μm sky in Galactic coordinates. There are several large loops and filaments present, which can also be traced on HI maps (see Heiles, 1975; Heiles & Jenkins, 1976). Amongst such features is the north polar spur at l = 30° extending up to b = 30° and faintly to higher latitudes. Individual bright sources include the LMC, SMC, M31 and M33. More details can be found in Rowan-Robinson *et al.* (1991), and a

table of extended sources in Boulanger & Pérault. For comparison, Fig. 5 shows the HI map for declinations above -40° from Stark *et al.* (1991) from observations made with the Bell Labs antenna of FWHM $\sim 2°$. Considerable structure can be seen at the highest latitudes in the 100 μm map. This is the IR cirrus which may be associated with high latitude molecular clouds, which can also be seen in the map. Désert, Bazell & Boulanger (1988) found that IR-excess clouds have a typical diameter of order 3pc and are found at a mean distance of 100pc, corresponding to an angular scale of $\sim 1°$. Such clouds have a range of intensities, comparable to or a few times that of the diffuse foreground over these restricted angles. For example, Weiland *et al.* (1986) found evidence for a large loop-like structure near the North ecliptic pole with an intensity about 1.8 times that of the diffuse foreground and with an angular scale of 1° (the topic of molecular clouds will be returned to later).

In Fig. 6, a number of measures of the emission at the Galactic poles are given, together with the CMB spectrum for reference. Some of the most accurate measures of the Galactic foreground and of anisotropies at the frequencies under consideration have been made by Lubin, Meinhold & Chingcuanco (1990) (to be referred to as LMC) at the South Pole on an angular scale of $\sim 1°$. They have found that the total emission reaches a minimum in the range 30 - 100 GHz. Measurements at other frequencies are shown also in Fig. 6. The points at 24.5 and 37 GHz obviously contain some contribution from GSR, so a single component dust model will not fit the data at these points. LMC also quote a correlation between their 90 GHz data and the IRAS 100 μm data such that the signal at 90 GHz is 10 μK per MJy sr^{-1} at 100 μm (although a more recent publication - Meinhold & Lubin, 1991 - claims that calibrating to a Galactic plane crossing gives a correlation $17 - 18\,\mu$K per MJy sr^{-1}, although this may be due to thermal bremsstrahlung emission as well as dust). Purely as an empirical description of the observations at long wavelengths, we shall follow what seems to be standard practice as far as modelling a dust background to CMB measures are concerned, and fit the data with a single dust component in the FIR region ($\lambda > 100\,\mu$m) with constant emissivity down to 90 GHz (rather than pursuing a theoretical model since many parameters such as the long wavelength behaviour of dust grains are uncertain). If α between 1 and 2, then T_d lies between $\sim 22\,$K and $\sim 13.6\,$K .

Considering the Lubin, Meinhold & Chingcuanco data at the pole in some detail,

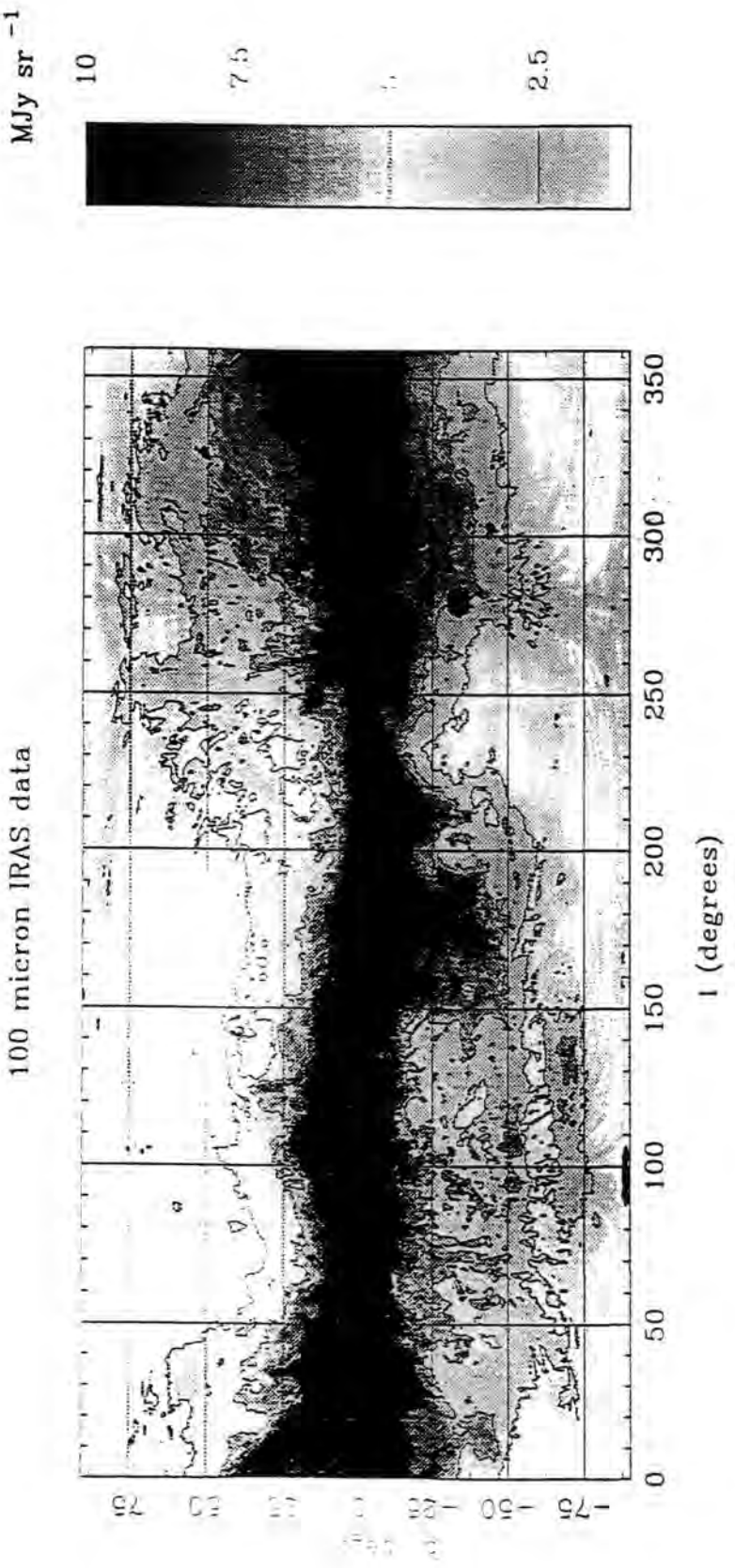

Figure 3.4: The 100 μm IRAS survey with zodiacal subtraction as in Rowan-Robinson (1990).

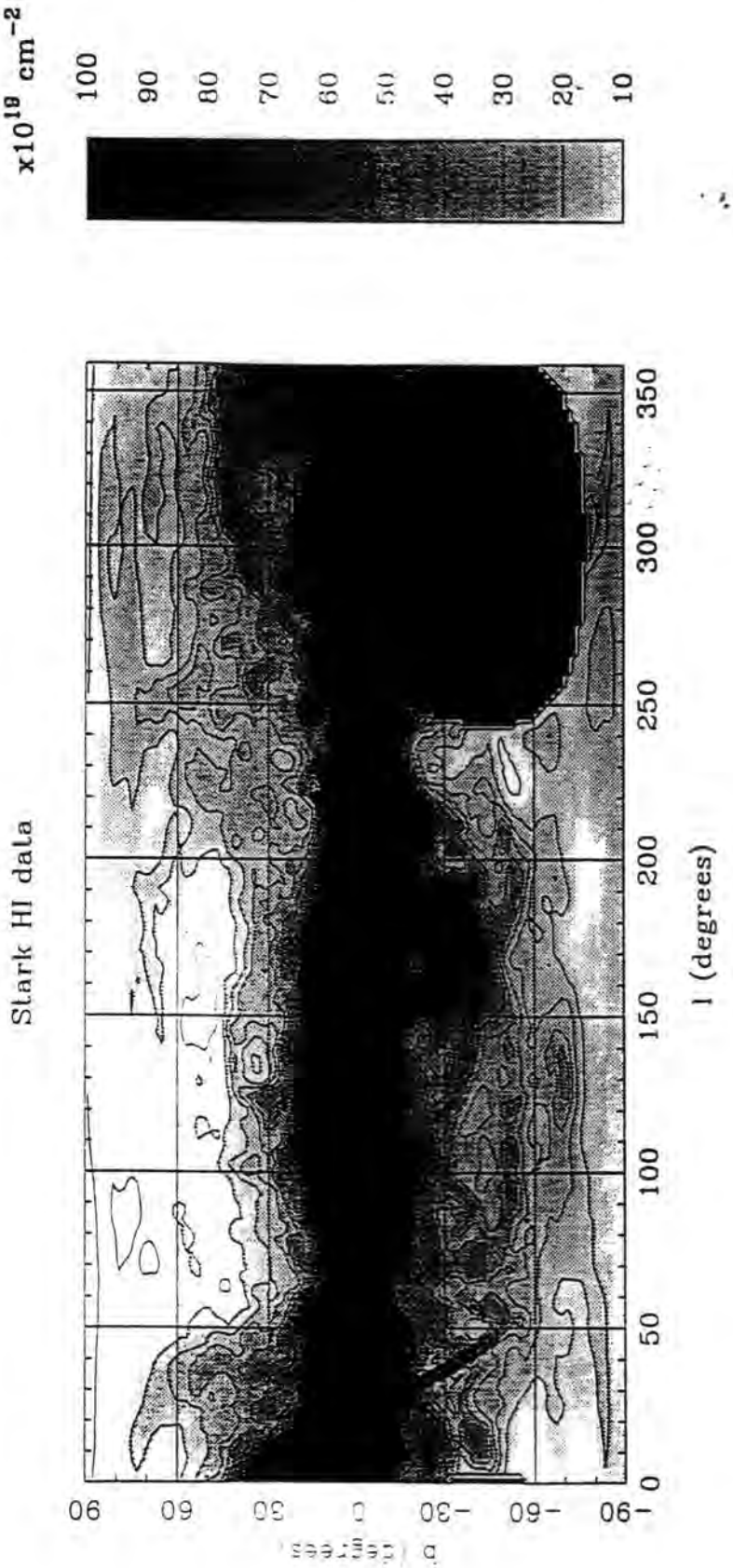

Figure 3.5: The HI survey from Stark *et al.* (1991) for declinations above -40° .

then if we assume that all of the 24.5 GHz signal is due to synchrotron radiation (which almost certainly is not the case), the extrapolation of the SGP antenna temperature at 408 MHz requires a spectral index β ($T_a \propto \nu^{-\beta}$) of 2.72, which will only explain about 60% of the 37 GHz signal. The residual is clearly indicative of an excess above the assumed dust extrapolation at low frequencies – the low frequency data would be better fitted by a three component model: synchrotron radiation with a spectral index slightly steeper than that derived here, a warm dust component with α in the range 1 - 1.5 (to fit the higher frequency data), and an additional cold dust component. Alternatively, the two dust components might be replaced by a single one with emissivity varying smoothly from 2 to 1 at longer wavelengths. It is interesting to note that the derived spectral index β for the synchrotron component is significantly flatter than the typical values used in Chapter 2 to explain the Davies *et al.* (1987) result. However, local variations are also expected for the synchrotron emission, and the Davies *et al.* region was identified as a quiet region where β could certainly steepen towards the asymptotic value of $\sim$ 3 (from II), so there is no contradiction. There is also the possibility that the index is flat due to the presence of some thermal emission. Although at high latitudes the contribution is expected to be small, the low frequency surveys are not sensitive enough to detect the emission, so there may be some present. Additionally, since the data are calculated from cosecant fits to the large-scale anisotropy maps, some thermal emission nearer the plane may affect the overall extrapolation to the pole. As with other published data, one must ensure that the use of additional maps from other sources to help spectral analysis is consistent with the data by convolving to the appropriate FWHM and averaging the maps in the same way as the data.

The best fit to all the data is given by 2 dust components with parameters α =1, T_d =22.1 K and α =1, T_d =4 K , and by a synchrotron component extrapolated from the 408 MHz survey with spectral index β of 2.75. This is very flat, as mentioned above, and may result from the cosec b fit to the data and extrapolation to the pole. This will undoubtedly overestimate the polar flux since the Galactic plane data will flatten the predicted spectrum. In future calculations, the cold dust component is dropped and indeed, fitting by eye to the data in Fig. 6 we find α = 1, T_d = 22.1 K to be an excellent fit, as shown in the figure.

Other measurements have been made away from the pole and extrapolations

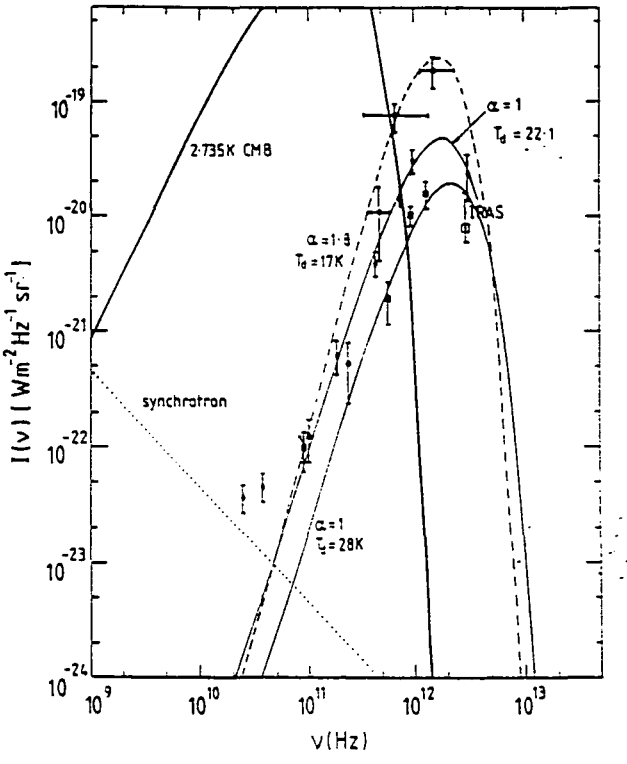

Figure 3.6: Derived Galactic emission at b=90° from different sources. Points marked by circles: de Bernardis *et al.* (1984); squares: Halpern *et al.* (1988); diamonds: Lubin *et al.* (1990). IRAS points at 100 μm : point with errors from Boulanger & Pérault (1988); open square from Rowan-Robinson *et al.* (1990).

made again utilising the (oversimplified) cosec b law to give the points as shown (which may be overestimates as in Boulanger & Pérault) Only the IRAS point at 100 μm denoted by the square box is an absolute measure of the intensity, and comes from the IRAS data with a zodiacal light best fit removed, as in Rowan-Robinson *et al.* (1990, 1991); all other points being extrapolations from lower latitude data. In particular, the point at 100 μm denoted IRAS is from Boulanger & Pérault (1988): I(100 μm) = 1.1 $\pm$ 0.5 MJy sr^{-1} (consistent with the Rowan-Robinson *et al.* figure of 0.8 MJy sr^{-1}). The best cosecant fit for b > 20° would give a somewhat higher value. The other sets of data points from de Bernardis *et al.* (1984) and from Halpern *et al.* (1988), should not be contrasted directly since the FWHM of the experimental beams are different: 5.6° and 17° respectively. The agreement of the $\alpha = 1$, $T_d = 28$ K curve with the IRAS point is purely fortuitous. The extrapolated emission could depend quite sensitively on the FWHM of the experiment and on the latitude and longitude in view of the presence of variations in the dust/gas ratio from place-to-place and that of the ISRF (large scale variations in the dust/gas ratio in the Galaxy and for other galaxies have been discussed by Issa *et al.* , 1990).

Such variations will be crucial to the success or otherwise of the searches for genuine CMB fluctuations in the 30 - 100 GHz region. Fig. 7 shows the calculated dust/gas ratio derived from the 100 μm and HI maps in 2° pixels. The maps appear quite smooth, but there are variations from region to region indicating variations in the ISRF affecting the dust temperature. There will also be a contribution due to dust associated with H_2.

There is in fact also evidence for a longitude dependence; Halpern *et al.* (1988) found that their prediction of the Galactic emission was significantly improved by the inclusion of a $\cos^4(l/2)$ dependence in their model. The de Bernardis *et al.* result suggests that in the region $140° < l < 180°$, the Galactic emission can be described by a near uniform distribution of dust together with a patchy distribution corresponding to ~ 4 cirrus clouds per square degree. Finally, the Halpern *et al.* points for $\nu < 500$ GHz taken together indicate excess emission, which might be attributable to a cold dust component (the slope probably being too flat to arise from a change in α).

Evidence for cold dust, or at least regions of remarkably low α , is borne out by observations of specific dust complexes and particular regions away from the Galactic plane, as we discuss below. Whatever the cause, in fact, there is often an excess at low frequencies such that the spectrum is quite complicated – its shape depending on the frequency of observation. Fig. 8 presents data from three sets of measurements, which we have normalised so that the best fit curves claimed by the authors give a flux of 1 in arbitrary units at 100 μm . The Halpern *et al.* experiment was designed to measure large angular scale variations in the CMB temperature, but found that thermal emission from dust was easily seen. In particular, there is evidence that the Galactic plane is broader at 1 mm. than at shorter wavelengths, and that a low surface brightness extended object is seen in the low frequency map at $b = 20°$, $40° \leq l \leq 110°$. This object was also seen by Cottingham (1987) at 19 GHz, and coupled with limits from the 240 GHz map, the object is seen to have an emissivity proportional to $\nu^{1.1}$ and a temperature $T_d \leq 6\,K$, if adoption of a single temperature is correct. Fig. 8 shows the best fit $T_d = 28\,K$, $\alpha = 1$ spectrum for the high frequency points, the large-dashed line indicating the spectrum if the cold component is included. The Page *et al.* (1990) experiment has a much smaller beamwidth of 25' FWHM, but also finds evidence for excess emission in its scan across the Galaxy at l

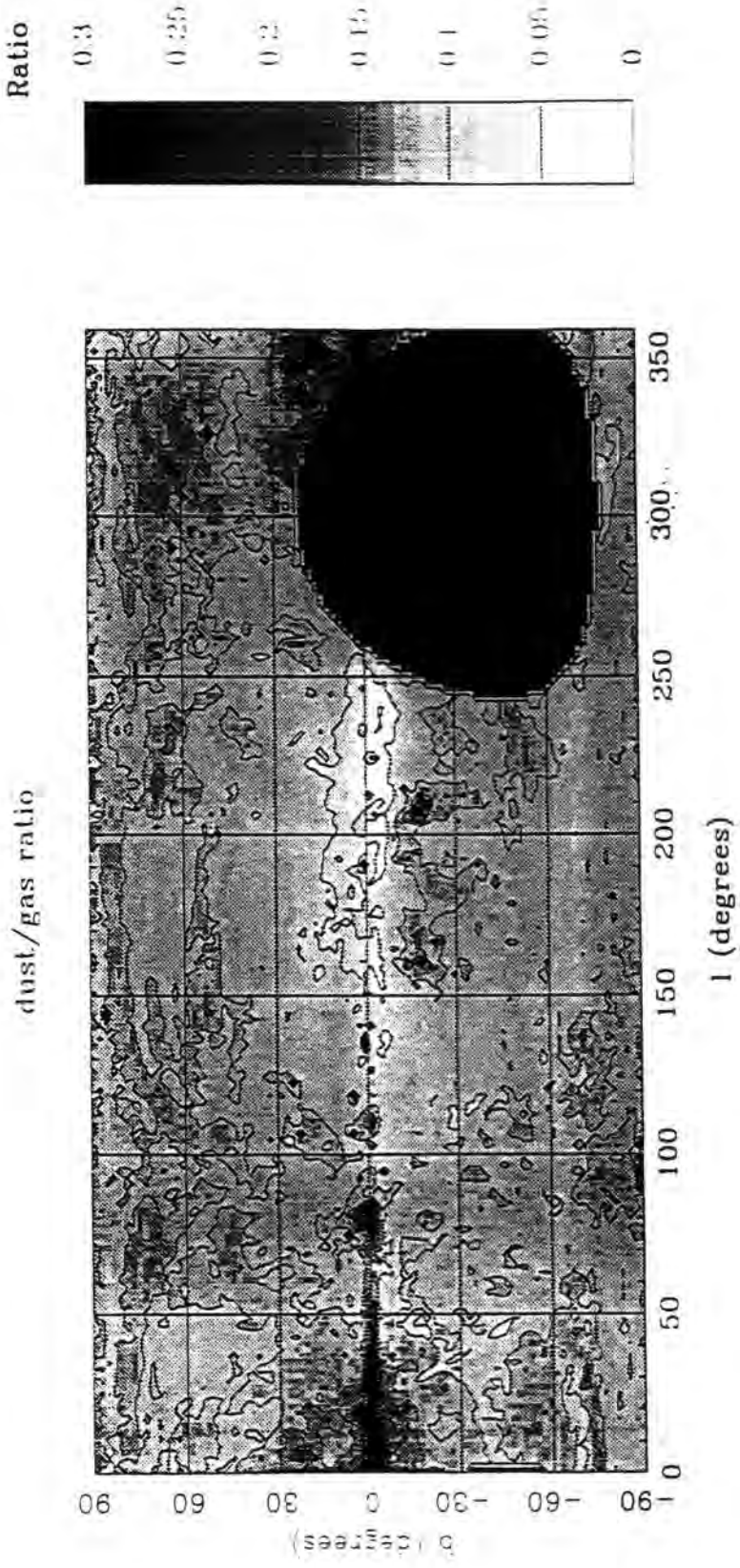

Figure 3.7: Dust/gas ratio in the Galaxy.

$= 42°$. The best fit curve has grain temperature $22.1 \pm 0.7\,\mathrm{K}$ with a ν^2-dependence for the emissivity which provides a very good fit to the data above 450 GHz. Below this frequency, there is excess emission which might signify a change in Q_ν , or may indicate the presence of another dust component. Such a component would have a temperature $\leq 4\,\mathrm{K}$ for a ν^2 emissivity. Free-free emission cannot explain this excess. The final points on the plot are from Andreani *et al.* (1991 – paper I) and represent observations of various clouds and cloud complexes. Fitting curves to the highest frequency data they find $\alpha = 2$ and T_d in the range 22 - 24 K , thus the points may be compared favorably to the solid curve with T_d of 22.1 K and α of 2 (all of the experimental points being scaled according to the actual best fit curve for the cloud in question).

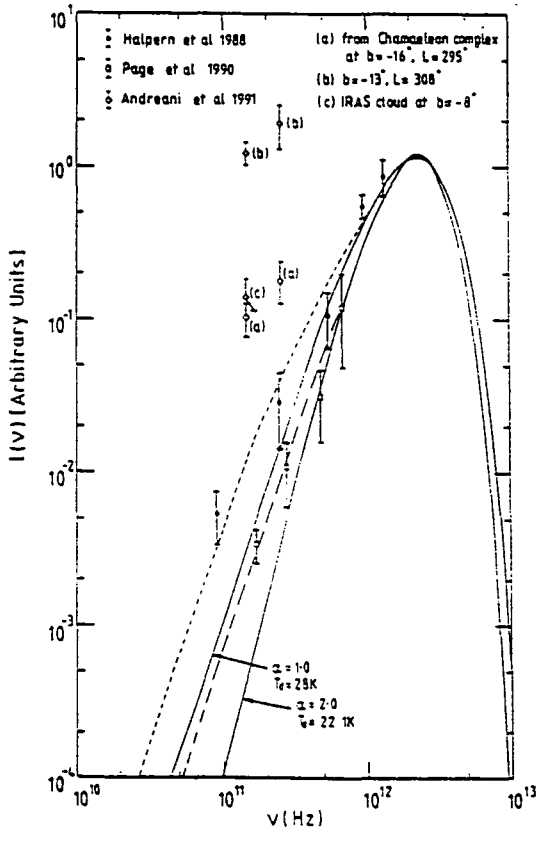

Figure 3.8: Dust spectra with best fitting curves (solid lines) from observations of different regions of the Galaxy. All points are normalised so that the $100\,\mu$m intensity is one in arbitrary units for all curves. There is evidence for cold dust at low frequencies. See text for details of dashed lines.

It is clear that in some directions there are considerable excesses at low frequencies, although the Andreani *et al.* data are for observations near the plane where the ISRF is higher which would explain some of the excess. The existence of a cold dust component, as opposed to a low value of α , whilst not conclusively demonstrated, cannot be considered too unlikely from an energetics point-of-view. Large

($\geq 0.1\,\mu$m) silicates or needle-shaped grains can attain a sufficiently low equilibrium temperature (Wright, 1981; Wright & Hawkins 1988), whilst non-spherical grains could show a frequency dependent emissivity (Wright, 1987). Hoyle & Wickramasinghe (1988) have proposed the existence of needle-shaped iron ejecta from supernovae — these would have a low equilibrium temperature and a blackbody emissivity (ie, $\alpha = 0$). It should also be noted that recent observations of a cirrus cloud at $l = 120°$, $b = 20°$ by Myerdierk, Brouillet & Mebold (1990) show that whilst most of the cloud has a kinetic temperature of ~ 21 K as would be expected, associated with the centre of the cloud is a clump of high molecular abundance with a temperature of only ~ 7 K . Larger clumps of such material may well account for the low frequency excess in the IR emission, the low temperatures arising from paucity of heating by the interstellar radiation field as a consequence of dust shielding in the outer layers of the cloud.

There is no doubt that the nature of the Galactic emission is complex, resulting from a multicomponent grain medium, the likelihood of a variable dust/gas ratio and variable ISRF, which could cause considerable variation in both the derived T_d and α for an empirically fitted curve. Nevertheless, a datum level is needed and for this we take the LMC spectrum of Fig. 6 (although we keep in mind that this may not apply over the whole Galaxy). For comparison, Fig. 9 shows the data again, together with a single component empirical fit reported in Wright (1991) but attributed to Lubin, and also the physically realistic model of Rowan-Robinson (1990 - scaled to fit the data at high frequencies). The latter two models seriously underpredict the intensities for $\nu < 450$ GHz. The Rowan-Robinson model provides an excellent fit above this frequency, however, and since the emissivity is not well known below $100\,\mu$m , the excess may be explicable extending the frequency range for which a $Q_\nu \propto \nu$ type emissivity holds (especially for the $0.1\,\mu$m grains considered). Otherwise, the poor fit could be considered further evidence of another dust component.

3.4 Fluctuations in the Foreground

3.4.1 Statement of the problem

We now turn to the likely level of fluctuations to be expected in high latitude CMB observations due to Galactic emission. Such fluctuations are, of course, variations in the dust emission with longitude due to variations in the ISRF. The problem is to extrapolate the variations in the IRAS 100 μm data down to 90 GHz and below. Such extrapolation requires knowledge of the dust spectrum at these frequencies, largely unknown at present. The amplitude of the extrapolated intensity will depend on the spectrum adopted at any point, which may vary with the ISRF etc. If cold dust is present too which is not well correlated with the IRAS dust, then use of the IRAS data will be inaccurate. Obviously, the fluctuations will be strongly frequency-dependent compared to genuine CMB anisotropies for which $\Delta T/T$ is essentially frequency-independent. Before continuing we note that it is not the thermodynamic temperature which is measured, but rather the antenna temperature T_a of the horn apparatus used for the observations. This quantity relates to the intensity of the radiation fields, the relation between the fluctuation in antenna temperature and the equivalent fluctuation $\Delta T/T$ in the CMB being

$$\frac{\Delta T_a}{T_a} = \frac{\Delta I}{I} = \frac{x\, e^x}{e^x - 1}\frac{\Delta T}{T}$$

where $x = h\nu/kT$, T being the CMB temperature 2.735 K . Thus the observed fluctuations in antenna temperature for genuine CMB anisotropies are also frequency-dependent. The equation demonstrates how to relate fluctuations in the Galactic dust emission not recognised as such to an upper limit on CMB anisotropy: if ΔI is the excess unsubtracted dust component then relating this to the expected CMB intensity I at that frequency gives the limit on $\Delta T/T$ from the relation.

A further complication in treating the Galactic subtraction results from the nature of the CMB observations — that they are by necessity **difference** measurements as discussed in Chapter 1. In general, for observations at the frequencies in question here it appears that the experiments adopt a single-subtraction technique (as opposed to the double-subtraction used by Davies *et al.* - see Chapter 2). That is, the signal from two different regions of the sky are compared by switching the

beam between the two regions, such that the recorded signal

$$\Delta T_a = T_a(\theta_1) - T_a(\theta_2)$$

where $\mid \theta_2 - \theta_1 \mid = \theta_b$, the fixed beamthrow angle. The actual way in which the 2-beam pattern is formed on the sky itself varies between different experimental configurations. One technique is the drift scan method as used in lower frequency radio measurements, whereby the apparatus is fixed in position and the two-beam pattern formed by switching rapidly between two positions on the sky separated by θ_b in the scanning direction. In a recent experiment, de Bernardis *et al.* (1990) switched between two positions on the sky placed symmetrically at $\sim 45°$ to the scan direction, so that their sky separation is θ_b. Balloon and rocket borne experiments achieve their sky coverage as a consequence of their flight plan. It is obvious from the previously detailed properties of the Galactic dust emission that switching between different regions of the sky, particularly if the angle θ_b is large (greater than $\sim 1°$), multiplies the problem of foreground subtraction, since it may be that the two regions under consideration contain clouds of very different properties (in α say), or regions of different dust/gas ratio. The scans are also more sensitive to gradients in the Galactic emission. It is to be hoped that the future multi-frequency observations by satellites such as COBE will utilise the frequency coverage to enable more accurate subtraction, but again coupling different regions of sky with different frequency dependences may still may make the procedure a difficult one.

We have assumed a datum (DC) level – in Fig. 9 – it is now necessary to estimate the fluctuations around this value, and thereby the expected value of $\Delta T/T$ on a statistical basis for angular scales of $\sim 5°$ and above, and beamwidths of similar scale. It is these fluctuations which are truly of importance for observations of anisotropies in the CMB. Table 3 summarises a number of Galactic fits determined from anisotropy measurements from a number of sources, together with numerical factors to scale the fluctuations in antenna temperature at $100\,\mu$m seen in the IRAS maps to the COBE frequency channels for each fit.

spectral parameters		scaling factor from 100 μm to			
α	T_d	90 GHz	53 GHz	31.5 GHz	Reference
1	22.1	2.829	1.736	1.057	Fit to Fig. 9
2	20	0.151	0.055	0.020	de Bernardis *et al.* (1990)
1	28	0.923	0.561	0.340	Halpern *et al.* (1988)
composite grain model		0.688	0.292	0.107	Rowan-Robinson (1990)
2	22.1				Page *et al.* (1990)
+ cold dust[a]		0.428	0.184	0.073	
1.5[b]	21.75	0.535	0.252	0.118	
1.65[c]	23.3	0.219	0.095	0.041	Wright *et al.* (1991)
2[d]	20.4				
+ cold dust[e]		0.277	0.110	0.042	

Table 3.3: Spectral fits from a number of sources. *Notes:* a) $\alpha = 2$, $T_d = 4\,K$; b) average at high latitudes; c) including Galactic plane data; d) as c); e) $\alpha = 2$, $T_d = 4.77\,K$.

3.4.2 Estimates of the 'AC' fluctuation level at b $\sim 90°$

Extrapolations from the 100 μm data

The basic idea here is to use the IRAS 100 μm data appropriately scaled to the frequency of observation by assuming an α and T_d to give an estimate of the likely level of contamination for a given region. This method has been used by Lubin *et al.* (1990), and de Bernardis *et al.* (1990). However, there are likely to be variations in the scaled amplitudes for the reasons we have already stressed: variations in T_d with location, variations in cloud composition and hence Q_ν from point-to-point, and the possibility of a cold dust component not evident in the 100 μm survey which may or may not be physically associated with the clouds observed in this survey. Searching for a detailed correlation between the structure expected in difference calculations using IRAS data and observed first differences at another frequency will also prove unfruitful in general for the same reasons: whilst there may be regions where there is a good correlation, there will be others where it is not so strong. De Bernardis *et al.* (1990) find a good correlation for the region $\delta = 7.46°$, R.A. = 335° - 355° , but a much worse correlation for other neighbouring declinations, especially around R.A. = 340° , the overall correlation being 0.57 ± 0.07. Andreani *et al.* (1991 – paper I) also find correlations lying between 0.58 and 0.83 depending

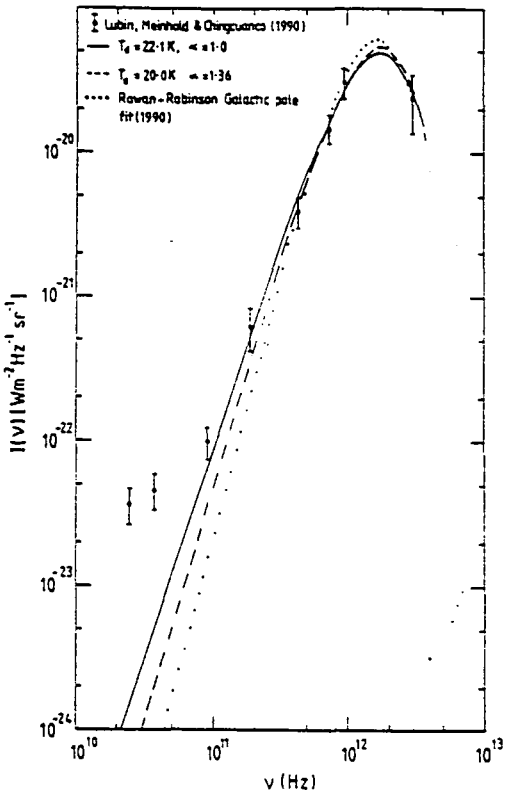

Figure 3.9: Lubin *et al.* data together with three fits: two empirical from large scale data sets, and the physically motivated model of Rowan-Robinson (1990).

on the cloud under observation. Indeed, detailed correlation should not be expected if, as suggested by Deul & Burton (1990), cirrus features seen in the IRAS data are commonly line-of-sight superpositions of kinematically different structures. It seems likely that the 100 μm data will provide a useful estimate on contamination when other frequency measures are used to determine the appropriate spectrum, unless a new component of the interstellar medium is found which is not correlated with HI, in which case it will not be possible to use it as an accurate tracer of the emission at lower frequencies. Andreani *et al.* (1991 - paper II) have found that observations of the CMB at 150 GHz are constrained by the thermal emission from very cold dust, the contribution from which is, to first order, traceable by the 100 μm data scaled in an appropriate fashion, but the detailed spatial distribution of which remains as yet unknown.

The fluctuations in the IRAS 100 μm maps with zodiacal light subtraction as in Rowan-Robinson *et al.* (1990) have been evaluated. The zodiacal light is relatively unimportant at the frequencies considered here, and since it is modelled by grains at temperatures of $\sim 250\,\mathrm{K}$, would need subtraction and separate extrapolation even if it were important. In particular, the fluctuations expected for the COBE

satellite have been evaluated after convolving the data to 7° FWHM, and taking scans along lines of constant latitude for longitude ranges of $\sim$ 100° in width, and a beamthrow of 60° real sky angle. Fig. 10 gives some examples. In these regions, the intrinsic fluctuations in intensity range from $\sim$ 20% at b = 30° to 40% at b = 45° , then falling to $\sim$ 20% by b = 70° . However, there is no reason why these statistics should be reproduced in other sky regions, or in the southern part of the sky (the fluctuations may be larger here since Malawi, 1989 has shown that the cirrus in this part of the sky lies closer to the plane. This would also explain why the intensity at the south Galactic pole is higher than at the north, since the dust is heated by an ISRF which is on average stronger). $\Delta I/I$ can range from $\sim$ 80% to $\sim$ 20%. Assuming the LMC spectrum for the dust emission, then typical rms variations in ΔI at 90 GHz would correspond to variations in antenna temperature of a few - 10 μK.To determine the corresponding limit in $\Delta T/T$ from fluctuations in antenna temperature, assuming T = 2.735 K the scale factors at 90, 53 and 31.5 GHz are respectively 0.448, 0.393 and 0.375. So a fluctuation of 10 μK at 90GHz corresponds to $\Delta T/T \sim 4 \times 10^{-6}$, which although not immediately significant compared to the expected sensitivity per pixel of $\sim 10^{-5}$ is not negligible. When averaging over pixels to derive the spherical harmonic components of the CMB temperature fluctuations, the significance of this contribution will increase being comparable to the projected COBE sensitivity per spherical harmonic component of $\sim 3 \times 10^{-6}$. Note also that cuts at constant declination will inevitably result in larger fluctuations since the large beamthrow angle ensures that the Galactic plane is crossed in any given scan.

We have also attempted to determine the fluctuations relevant to a number of other experiments. For the de Bernardis *et al.* (1990) configuration (25' FWHM, $\theta_b = 1.8°$), we have verified the level of fluctuations expected as in their figure 2. Fig. 11 also shows the scan appropriate to the UCSB South Pole experiment of Lubin *et al.* at declination -73° . The level of fluctuations is in agreement with that claimed by Lubin *et al.* , specifically the maximum pixel excursions correspond to an antenna temperature at 90 GHz of $\sim$ 10 - 20 μK adopting their scaling (which is in agreement with our fit to the spectral data). This is less than the noise of 60 μK per pixel, but not negligible.

Dust contamination under these assumptions could be a problem at the limiting sensitivity of the considered experiments, except possibly at the highest latitudes.

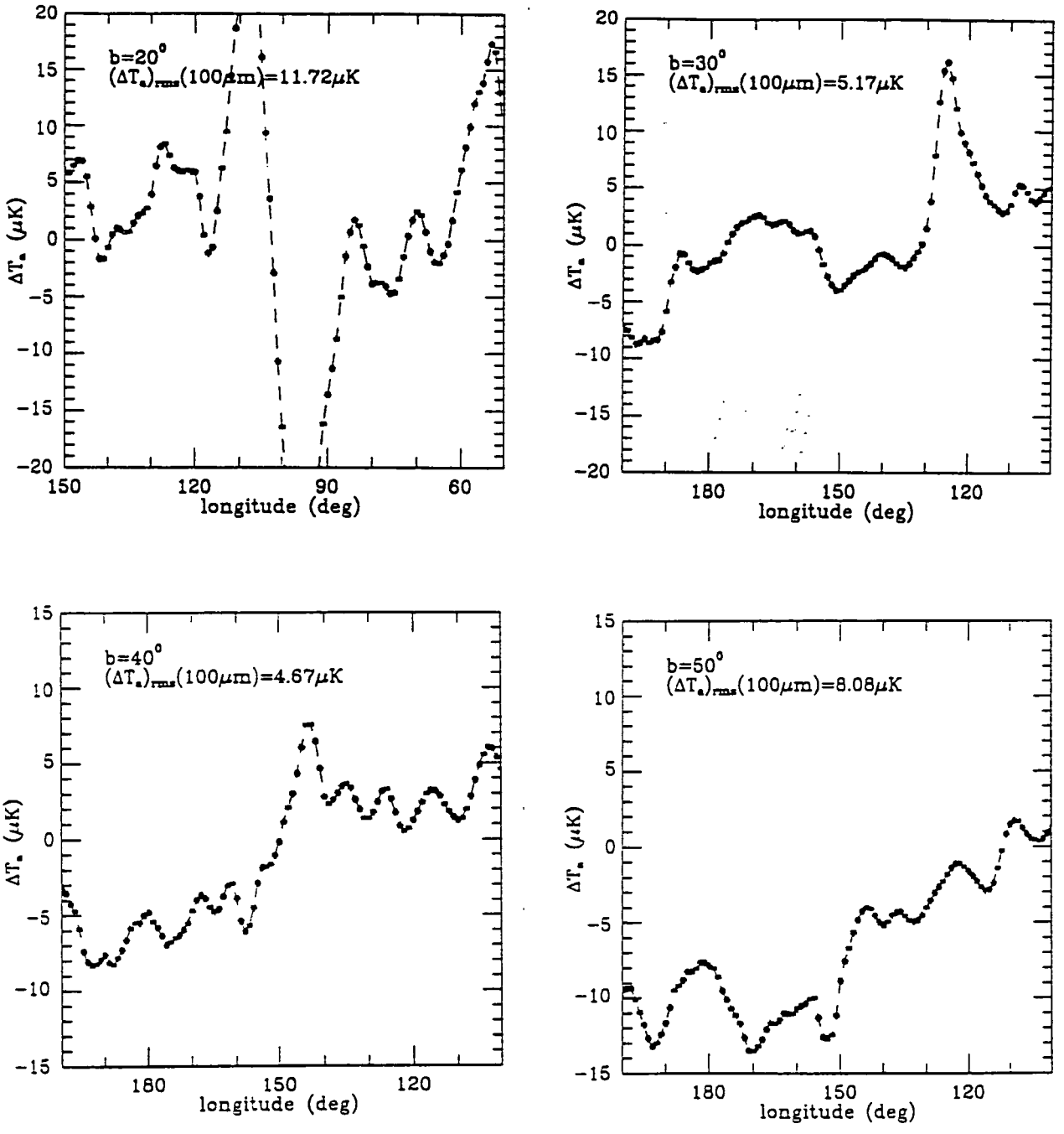

Figure 3.10: Fluctuations in the IRAS 100 μm survey as appropriate for COBE calculated at a number of latitudes.

However, as we have repeatedly remarked, such an extrapolation need not be appropriate, and we should find alternative methods to estimate the fluctuations.

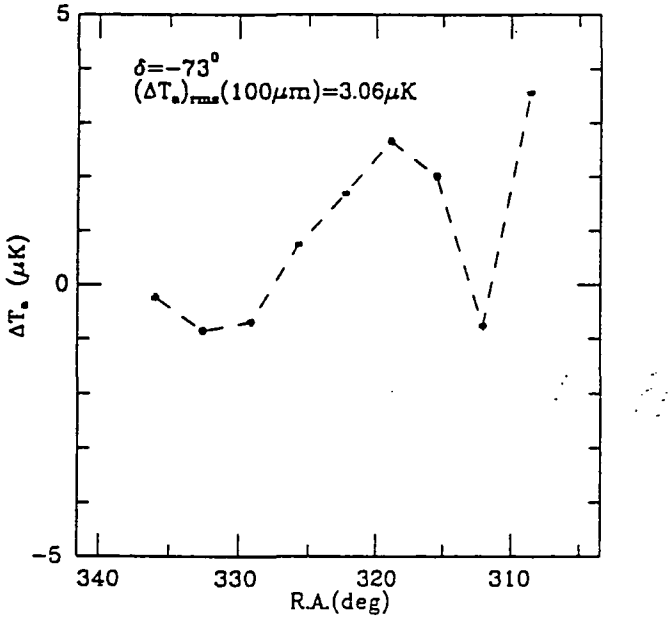

Figure 3.11: Fluctuations in the 100 μm survey appropriate for comparison to the Lubin *et al.* result.

An alternative method via HI and molecular clouds

One approach to a more realistic estimate of $\Delta T/T$ is to compare the maps of 100 μm and N(HI) at high latitudes and thereby to estimate the variation of 100 μm to N(HI) with position. Most of this will arise from changes in the mean dust/gas ratio and temperatures rather than from molecular clouds. On angular scales of 5° the variation appears to be about 10%. The contribution from the dust/gas ratio alone can be estimated by examining the Copernicus data of Bohlin *et al.* (1978) concerning the relationship between interstellar HI and colour excess E(B-V) to specific stars. This is also related to the clumpiness of the ISM having a strong effect on the ISRF in the UV part of the spectrum. This analysis leads to a median spread of 'dust-to-gas' values of $\sim$ 35% for the data presented; we have endeavoured to allow for random errors in N(HI) and E(B-V) and the undoubted fact that the fluctuations become smaller as the angle between lines-of-sight diminishes, and estimate that the

residual uncertainty is only roughly 10% although the derivation of this value makes an assumption about the magnitude of the observational error. It should be no surprise that the level of fluctuations is of the order of that due to cirrus, since Blitz, Bazell & Désert (1988) have shown that the high latitude clouds identified by Désert, Bazell & Boulanger (1988) from their excess emission above that expected from the correlation between 100 μm emission and the HI column density are present in number and with column densities similar to those clouds identified by Bohlin, Savage & Drake; it is likely that they form the same group of objects.

Thus, most of the variation arises from changes in the effective mean temperature. Coupled with the possible changes in α from one line-of-sight to another the variations predicted at 100 GHz could be bigger than $\sim$ 15%. Only a little guidance comes from the actual measurements at 100 GHz, of course (this is why we are extrapolating back from the 100 μm data), and the final value is very imprecise. We estimate that I_{DC} has fluctuations on it of $\sim$ 30%. To this variation must be added a contribution from unresolved molecular clouds. The contribution from dust associated with molecular gas is clearly potentially important. Having presumably taken account of the contribution from known molecular clouds, such as those documented by Désert, Bazell & Boulanger (1988) and as we have likely done with our analysis of the Bohlin *et al.* data, then contributions to the noise will come from unidentified (small) molecular clouds and, again, dust-to-gas variations. Knapp & Bowers (1988) found a class of very small molecular clouds associated with Betelgeuse relatively close to the plane, but such clouds must exist at high latitudes, so far escaping detection because of their small size ($\sim$ a few arcminutes). These small clouds are unlikely to be seen in CO either; as pointed out by Blitz, Bazell & Désert (1988), for surface brightnesses < 4 MJy sr^{-1}, CO is not self-shielding and so the clouds have low column density in CO. The clouds in question here will have lower 100 μm brightnesses still. An estimate of the fluctuation level can be made by examining the likely mass spectrum of the clouds. If the mass spectrum in the cirrus clouds follows the same 'law' as that for GMCs in the Galactic Plane, and indeed for the sub-clumps of material within them, namely $N(m) \propto m^{-1.6}$, and if clouds below 30 $M_\odot$ are not recorded efficiently (a figure derived from the CO observations of Blitz, 1990), the corresponding unidentified material is $\sim$ 5% assuming $m_{max} \sim 10^5 M_\odot$ as locally. The effect of varying α and T_d is presumably not too different from that for HI. The HII associated dust should be a small component

and the rare 'large' clumps should be recognised by way of their large HII radio recombination line signal.

The conclusion is that the overall fluctuation is $\sim$ 35 - 40 per cent of the DC level.

3.5 Discussion and Conclusions

We have estimated the likely range of values of AC signals expected in the frequency range 30 - 500 GHz for $\Delta T/T$ searches, the condition being that the directions chosen should be away from currently known cirrus cloud complexes. It appears that the lowest $\Delta T/T$ achievable is $\sim$ (2 - 4) $\times 10^{-6}$ at 90 GHz, a range not sufficiently below the likely bona-fide signal strength of (5 - 8) $\times 10^{-6}$ in CDM scenarios. The problem now is to estimate the extent to which one can extract a meaningful CMB signal from the measurements by invoking an understanding of the origin of the Galactic signal. In Chapter 2 it was pointed out that at 10 GHz the Galactic synchrotron signal could not be corrected and a genuine signal extracted as yet. The situation here appears to be the same at present, that is, sufficiently comprehensive measurements have not yet been made at higher frequencies from which to extrapolate back to the important 50 - 100 GHz region.

It is clear that detailed allowance for Galactic dust emission is of great importance if genuine CMB anisotropies are to be detected in the FIR, and that point-by-point modelling of the emission will be required to achieve this. Since such modelling requires knowledge of α , T_d then detailed multifrequency observations are required. COBE, observing at 31.5, 53 and 90 GHz — where the the Galactic emission from both synchrotron radiation and dust is expected to be at a minimum — has a good chance of identifying this contamination. The likely level from the Galaxy is expected to be $\sim$ a few times 10 μK for COBE which is on the limits of its sensitivity. After subtraction of a component correlated with the IRAS 100 μm emission de Bernardis *et al.* found residual fluctuations at 270 GHz of $\Delta I \simeq 3.26 \times 10^{-21}$ MJy sr^{-1} (for FWHM of 25' on a scale θ_b of 1.8°). This residual is obviously attributable to the very subject we have been discussing, variations of dust parameters along a given line-of-sight. Extrapolation of this residual to 90 GHz is obviously uncertain

as we have seen, but if we assume it is due to cold dust (for example) then $\Delta T \sim 68$ μK, assuming a T_d of 4 K and α of 2 (as in Page *et al.* , 1990), and ~ 106 μK, assuming a T_d of 6 K and α of 1.1 (as in Halpern *et al.*). Such signals would certainly be a problem for COBE, and future more sensitive experiments will undoubtedly require detailed mappings of the spatial fluctuations of the dust in order to detect anisotropies on the 10^{-6} level even at frequencies close to the minimum in Galactic foreground emission.

What is clear is that COBE is likely to produce at least as much information about the Galaxy as it does for the CMB. Indeed, the factor of 3 discrepancy with the IRAS 100 μm amplitude at the SGP is already interesting. The preliminary results (Wright *et al.* , 1991) suggestive of $\alpha < 2$ is indicative of either a change in slope with frequency, or the presence of a cold dust component. However, the best fit dust spectra to the COBE FIRAS data imply a lower flux at $\leq$ 90 GHz than the Lubin *et al.* cosecant fits suggest. In fact, they find that the ratio of the 3mm antenna temperature to 100 μm flux is 1.5 ± 0.5 MJy sr^{-1} – a factor of $\sim$ 10 - 15 down from the Lubin *et al.* correlation. There is also clear evidence that the dust spectrum does change with position, reinforcing the conclusion of this chapter that detailed knowledge of the spatial fluctuations in the dust spectrum at a number of frequencies is required to achieve the sensitivity necessary to test cosmological models such as CDM.

References

Aannestad, P.A., 1975. *Astrophys. J.*, **200**, 30.

Andreani,P., Dall'Oglio, G., Martinis, L., Piccirillo, L., Pizzo, L., Rossi, L. & Venturino, C., 1991. *Astrophys. J.*, **375**, 148. (paper I)

Andreani, P., *et al.* , 1991. *Astr. Astrophys.*, **249**, 299. (paper II)

Blitz, L., Magnani, L. & Mundy, L., 1984. *Astrophys. J.*, **282**, L9.

Blitz, L., Baxell, D. & Désert, X., 1988. *Astrophys. J. Letts.*, **352**, L13.

Blitz, L., 1990. *preprint.*

Bohlin, R.C., Savage, B.D. & Drake, J.F., 1978. *Astrophys. J.*, **224**, 132.

Boulanger, F. & Pérault, M., 1988. *Astrophys. J.*, **330**, 964.

Broadbent, A., MacLaren, I. & Wolfendale, A.W., 1989. *Mon. Not. R. astr. Soc*, **237**, 1075.

Campbell, M.F., Elisa, J.H., Gezari, D.Y., Harvey, P.M., Hoffman, W.F., Hudson, H.S., Neugebauer, G., Soifer, B.T., Werner, M.W. & Westerbrook, W.E., 1976. *Astrophys. J.*, **208**, 396.

Caux, E. & Serra, G., 1986, *Astr. Astrophys.*, **165**, L5.

Chini, R., Krügel, E. & Kreysa, E., 1986a. *Astr. Astrophys.*, **167**, 315.

Chini, R., Kreysa, E., Mezger, P.G. & Gemünd, H.-P., 1986b. *Astr. Astrophys.*, **157**, L1.

Cottingham, D., 1987. *PhD Thesis*, Princeton University.

Cox, P. & Mezger, P.G., 1987. *Star Formation in Galaxies*, p.23, ed Lonsdale-Perrson, C.J., NASA Conference publication no. 2466.

Davies, R.D., Lasenby, A.N., Watson, R.A., Daintree, E.J., Hopkins, J., Beckman, J., Sanchez-Almeida, J. & Rebolo, R., 1987. *Nature*, **326**, 462.

Day, K.L., 1976. *Astrophys. J.*, **210**, 614.

de Bernardis, P., Masi, S., Melchiorri, B., Melchiorri, F. & Moreno, G., 1984. *Astrophys. J.*, **278**, 150.

de Bernardis, P. *et al.* , 1988. *Astrophys. J.*

de Bernardis, P., Amicone, L., de Luca, A., de Petris, M., Epifani, M., Gervasi, M., Guarini, G., Masi, S., Melchiorri, F., Natale, V., Boscaleri, A., Natali, G. & Pedichini, F., 1990. *Astrophys. J.*, **360**, L31.

Désert, F.X., Bazell, D. & Boulanger, F., 1988. *Astrophys. J.*, **334**, 815.

Deul, E.R., & Burton, W.B., 1990. *Astr. Astrophys.*, **230**, 153.

Draine, B.T. & Anderson, N., 1985. *Astrophys. J.*, **292**, 494.

Fixsen, D., Cheng, E.S. & Wilkinson, D.T., 1983. *Phys. Rev. Letts.*, **50**, 620.

Gatley, I., Becklin, E.E., Werner, M.W. & Wynn-Williams, C,G., 1977. *Astrophys. J.*, **216**, 277.

Gear, W.K., Robson, E.I. & Griffin, M.J., 1988. *Mon. Not. R. astr. Soc*, **231**, 55P.

Gordon, M.A., 1987. *Astrophys. J.*, **316**, 258.

Halpern, M., Benford, R., Meyer, S., Muehlner, D. & Weiss, R., 1988. *Astrophys. J.*, **332**, 596.

Harvey, P.M., Hoffman, W.F. & Campbell, M.F., 1978. *Astr. Astrophys.*, **70**, 165.

Hauser, M.G., Gillett, F.C., Low, F.J., Gautier, T.N., Beichman, C.A., Neugebauer, G., Aumann, H.H., Brand, B., Boggess, N., Emerson, J.P., Houck, J.R., Soifer, J.T. & Walker, R.G., 1984. *Astrophys. J.*, **278**, L15.

Hauser, M.G., Kelsall, T., Moseley, S.H., Silverberg, R.F., Murdock, T., Toller, G., Spiesman, W. & Weiland, J., 1991. to appear in *After the First Three Minutes*, eds. Holt, SS., Bennett, C.L. & Trimble, V., AIP Proceedings.

Hawkins, I. & Wright, E.L., 1988. *Astrophys. J.*, **324**, 46.

Heiles, C., 1975. *Astr. Astrophys. Suppl.*, **20**, 37.

Heiles, C. & Jenkins, E.B., 1976. *Astr. Astrophys.*, **46**, 333.

Helou, G., 1989. *Interstellar Dust*, p. 285, eds Allamandola, L.J. & Tielens, G.G.M., IAU Symposium no 135, Kluwer Academic Publishers.

Hoyle, F. & Wickramasinghe, N.C., 1988. *Astrophys. Space Sci.*, **147**, 245.

Issa, M.R., Maclaren, I. & Wolfendale, A.W., 1990. *Astr. Astrophys.*, **236**, 237.

Knapp, G.R. & Bowers, P.F., 1988. *Astrophys. J.*, **330**, 684.

Koike, C., Hasegawa, H. & Hattori, T., 1987. *Astrophys. Space Sci.*, **134**, 95.

Koike, C., Hasegawa, H. & Manabe, A., 1980. *Astrophys. Space Sci.*, **67**, 495.

Leger, A. & d' Hendecourt, L.B., 1988. in *Dust in the Universe*, eds. Bailey, M.E. & Williams, D.A., Cambridge University Press.

Low, F.J., Beintema, D.A., Gautier, T.N., Gillett, F.C., Beichman, C.A., Neugebauer, G., Young, E., Aumann, H.H., Boggess, N., Emerson, J.P., Habing, H.J., Hauser, M.G., Houck, J.R., Rowan-Robinson, M., Soifer, J.T., Walker, R.G. & Wesselius, P.R., 1984. *Astrophys. J.*, **278**, L19.

Lubin, P. *et al.* , 1985. *Astrophys. J. Letts.*, **298**, L1.

Lubin, P., Meinhold, P.R. & Chingcuanco, A.O., 1990. *The Cosmic Microwave Background - 25 Years Later*, p. 115, eds Mandolesi, N. & Vittorio, N., Kluwer Academic Publishers.

Martin, P.G. & Rogers, C., 1987. *Astrophys. J.*, **322**, 374.

Mathis, J.S., Mezger, P.G. & Panagia, N., 1983. *Astr. Astrophys.*, **128**, 212.

Mathis, J.S., Rumpl, W. & Nordsieck, K.H., 1977. *Astrophys. J.*, **217**, 425.

Matsumoto, T. *et al.* , 1988. *Astrophys. J.*, **329**, 567.

Meinhold, P. & Lubin, P., 1991. *Astrophys. J. Letts.*, **370**, L11.

Melchiorri, F. *et al.* , 1981. *Astrophys. J. Letts.*, **250**, L1.

Meyer, S.S., Cheng, E.S. & Page, L.A., 1991. *Astrophys. J. Letts.*, **371**, L7.

Myerdierks, H., Brouillet, N. & Mebold, U., 1990, *Astr. Astrophys.*, **230**, 172.

Page, L.A., Cheng, E.S. & Meyer, S., 1990. *Astrophys. J.*, **355**, L1.

Pajot, F. *et al.* , 1989. *Astr. Astrophys.*, **223**, 107.

Pipher, J.L., Dathie, J.G. & Savedoff, M.P., 1978. *Astrophys. J.*, **219**, 494.

Richardson, K.J., White, G.J., Gee, G., Griffin, M.J., Cunningham, C.T., Ade, P.A.R. & Avery, R.W., 1985. *Mon. Not. R. astr. Soc*, **216**, 713.

Rowan-Robinson, M., Lock, M., Walker, D.W. & Harris, S., 1986. *Mon. Not. R. astr. Soc*, **222**, 273.

Rowan-Robinson, M., Hughes,J., Vedi, K. & Walker, D.H., 1990. *Mon. Not. R. astr. Soc*, **246**, 273.

Rowan-Robinson, M., Hughes,J., Leech, K., Vedi, K. & Walker, D.H., 1991. *Mon.*

Not. R. astr. Soc, **249**, 729.

Rowan-Robinson, M., 1986. *Mon. Not. R. astr. Soc*, **219**, 737.

Rowan-Robinson, M., 1990. in *Interstellar Medium in Galaxies*, p.121, eds Thronson, H.Jr & Shull, M., Kluwer, Dordrecht.

Schwartz, P.R., 1982. *Astrophys. J.*, **252**, 589.

Schwartz, P.R., Thronson, H.A., Lada, C.J., Smith, H.A., Glaccum, W., Harper, D.A. & Knowles, S.H., 1983. *Astrophys. J.*, **271**, 625.

Seki, J. & Yamamoto, T., 1980. *Astrophys. Space Sci.*, **72**, 79.

Stark, A.A. *et al.* , 1991. *Astrophys. J. Suppl., submitted.*

Tielens, A.G.G.M. & Allamandola, 1987. *Interstellar Processes*, p. 397, eds Hollenbach, D.J. & Thronsen, H.A., Reidel, Dordrecht, The Netherlands.

Tokunaga, A.T., Erickson, E.F., Caroff, L.J. & Dana, R.A., 1978. *Astrophys. J.*, 224, L19.

Weiland, J.L., Blitz, L., Dwek, E., Hauser, M.G., Magnani, L. & Rickard, L.J., 1986. *Astrophys. J.*, 306, L101.

Wright, E.L., 1981. *Astrophys. J.*, **250**, 1.

Wright, E.L., 1987. *Astrophys. J.*, **320**, 818.

Wright, E.L., 1991. to appear in proceedings of the Texas-ESO-CERN symposium.

Wright, E.L. *et al.* , 1991. *Astrophys. J.*, **381**, 325.

Chapter 4

The Overall Galactic Foreground

4.1 Introduction

In the previous two chapters, a detailed study has been made of the Galactic foregrounds dominating the contamination signal in searches for CMB anisotropies at both low frequencies (GSR) and high frequencies (Galactic dust emission). The aim now, of course, should be to combine the information on these two foregrounds, and then to estimate a 'frequency window' or range of frequencies over which a given sensitivity in $\Delta T/T$ is achievable. In addition, it would also be useful to identify quiet sky regions where the foregrounds in such a window correspond to a particularly low contribution to the measured anisotropy. It should then be possible to make searches for anisotropies in such regions with a much improved chance of success, although the interpretation of the anisotropy limits for these small sky regions would not be immediately obvious with respect to the imposition of constraints on various cosmological models, especially those such as CDM where the long-range nature of the gravitational interactions and the assumed power spectrum implies that even an all-sky map of the microwave sky from our location in the universe does not represent a fair sample of the fluctuations (Scaramella & Vittorio, 1990). Furthermore, deriving constraints on the lower order multipole moments, such as the quadrupole, requires the sky coverage to be as great as possible, necessarily covering regions where the foregrounds are significantly higher than in the quiet regions. Of course, to set the best limits on multipole moments, data for the whole sky would need to be considered, requiring a model of the Galactic plane emission. However, in the plane, thermal bremmstrahlung emission from hot electrons makes

a significant contribution to the radio emission at low frequencies, with the brightest HII regions dominating the emission. Broadbent, Haslam & Osborne (1989) estimated that the thermal luminosity corresponds to $\sim 2.5\%$ of the non-thermal luminosity at 408 MHz, and this fraction increases with frequency since the thermal emission has a power-law frequency dependence which is flatter than that for the synchrotron emission. A rough estimate from the work of the previous 2 chapters would suggest that the foreground emission should be at a minimum between ~ 30 and 100 GHz, and extrapolating the luminosity ratio indicates that the thermal component becomes dominant at a frequency which depends on the spectral index of the non-thermal emission, but which for reasonable values lying between 0.7 (as is likely for the plane) and 1.0 (plausible at the highest latitudes) ranges from ~ 195 GHz down to 25 GHz. Thus, it is quite obvious how important the thermal emission from the plane (which dominates the thermal luminosity as a consequence of the small scale height of the HII component in the interstellar medium) is to the overall foreground in the important frequency range. Even at the highest latitudes there may be low surface brightness regions of thermal emission not obvious in the low frequency surveys due to their low sensitivity, which are glowing faintly and can contribute significantly to any observed anisotropy at higher frequencies.

Previous attempts to model the Galactic sky temperature at a given frequency have been made by groups attempting to measure the CMB sky temperature or the dipole and quadrupole moments. Fixsen, Cheng & Wilkinson (1983) adopted a model extrapolating from the 408 MHz all-sky survey to 24.5 GHz with a constant spectral index of 2.75 and added a thermal component based on 5 GHz surveys of HII regions in the plane. Similarly, Kogut *et al.* (1990) utilised the 408 MHz survey with β equal to 2.75 and a compilation of thermal sources at 2.7 GHz, finding good agreement with the measured signal at 7.5 GHz to within 0.01 K, certainly of sufficient accuracy for spectral measurements at such a frequency in the absence of any small spectral distortions (see also Levin *et al.* , 1988; de Amici *et al.* , 1988, 1990). In what follows, an improved model will be derived using the 408 and 1420 MHz radio maps together with the IRAS 100 μm survey, and estimating the thermal component in the plane by a technique developed by Broadbent, Haslam & Osborne (1989), and Broadbent (1989) from data kindly provided by Dr A. Broadbent (1991 – private communication). An attempt is also made to estimate the high latitude thermal emission from the associated Hα line emission. Sky maps are the generated

at the COBE frequencies, and quiet regions looked for in the data.

4.2 Thermal Emission in the Galaxy

Thermal emission in the Galaxy is classically with the localised regions of continuum radiation referred to as 'compact' HII regions. Such regions are the ionised remnants of gas associated with O-type stars, and typically have a radius of a few parsecs, and electron density $n_e \sim 10^4$ cm^{-3} (Schraml & Mezger, 1969). However, analysis of the Westerhout (1958) 1.39 GHz survey at low resolution revealed an underlying diffuse background which Mezger (1978) associated with extended low density (ELD) HII regions which have evolved beyond the compact radio phase, but whose gas is still fully ionised. Most of the interstellar space in the Galaxy appears to be filled with this extended low density fully ionised gas which extends ~ 13 kpc from the Galactic centre and ~ 100 pc from the plane with $n_e \sim 5$ - 10 cm^{-3} (Matthewson *et al.* , 1962). Observations of compact HII regions imply that they have been observed at a number of stages of evolution, supporting the hypothesis that compact HII regions form from the ionised remnants of O stars which subsequently evolve to less compact regions of lower density when the O stars leave their progenitor gas clouds and their surrounding spheres of ionisation begin to merge. Gordon & Cato (1972) concluded that the bulk of the diffuse emission comes from the inner Galaxy. Matthews *et al.* (1973) showed that the diffuse recombination line emission (eg. H 109α , He 109α) originates in the same ELD gas responsible for the thermal continuum radiation. This fact, as we shall see later, enables an estimate of the thermal continuum radiation at high latitudes to be made from the associated Hα emission.

The thermal emission itself has its physical origin in the free-free emission (bremsstrahlung) of electrons in the region of ionised gas. To derive the frequency dependence of the brightness temperature in a given direction, consider a homogeneous emission nebula of temperature T_e, and optical depth τ. The brightness temperature is given by

$$T = T_A + T_B + T_e(1 - e^{-\tau})$$

where T_A and T_B are the temperatures due to regions in front of, or behind, the

nebula. These terms are generally negligible for frequencies above a few hundred MHz. If the gas is optically thin, as is usually the case for the frequencies considered, the expression reduces to

$$T = T_e \tau$$

The optical depth for free-free emission is (Oster, 1961),

$$\tau = K \left(\frac{T_e}{K}\right)^{-1.5} \left(\frac{\nu}{GHz}\right)^{-2} \{\ln[4.955 \times 10^{-2} \left(\frac{\nu}{GHz}\right)^{-1}] + 1.5 \ln \left(\frac{T_e}{K}\right)\} \left(\frac{\int n_e^2 ds}{pc\, cm^{-6}}\right)$$

where $K = 3.014 \times 10^{-2}$. This can be written as,

$$\tau = 8.235 \times 10^{-2}\, a(\nu, T_e) \left(\frac{T_e}{K}\right)^{-1.35} \left(\frac{\nu}{GHz}\right)^{-2.1} \left(\frac{\int n_e^2 ds}{pc\, cm^{-6}}\right)$$

where the expression without the factor $a(\nu, T_e)$ is the approximation from Altenhoff *et al.* (1960) which always deviates no more than 24% from the exact relation, and $a(\nu, T_e)$ is a correction factor as derived and tabulated in Mezger & Henderson (1967). This is the origin of the power-law nature of the thermal emission with frequency, which only breaks down if the source is optically thick.

The importance of the thermal contribution lies, of course, in the extrapolation of low frequency radio data to higher frequencies where the search for CMB anisotropies is made. The observed radio continuum comprises both thermal and non-thermal components, and although it is obvious that the thermal component in the plane is important due to the number of strong HII sources observed, even at high latitudes the thermal emission may begin to become important at high enough frequencies. The effect of the thermal emission is to flatten the observed spectral index from the synchrotron value which lies in the range 2.3 - 2.8 between 408 and 1420 MHz. As an example, consider a region at 408 MHz where the thermal component amounts to $\sim$ 2% of the observed brightness temperature. If the true non-thermal spectral index is 2.7, then the extrapolated flux at 10 GHz is such that that a naive calculation assuming that the emission is entirely non-thermal would require $\beta = 2.67$. If the 2.7 index was retained, the 10 GHz flux would be underestimated by $\sim$ 9%. Even at the highest latitudes, where the thermal contribution may still be of order 0.5% of the non-thermal, and if $\beta = 3$ is more appropriate for the non-thermal component

up to 30 GHz, then a naive extrapolation would require $\beta = 2.95$, resulting in about a 20% flux error if the non-thermal index was assumed. It is thus obviously of importance to consider the likely thermal contribution at higher frequencies.

4.2.1 Modelling the Thermal Component in the plane

We have seen how important the thermal contribution may be at high frequencies, and thus the importance of deriving a model for this emission, especially in the plane where the free-free emission dominates the radio continuum at frequencies above $\sim$ 2 GHz. Surveys at low frequencies are available, but the use of spectral index techniques to separate the thermal and non-thermal components is subject to considerable error, since the non-thermal spectral index needs to be known a priori, but does, as has been discussed in Chapter 2, vary from region-to-region on the sky. Here, an alternative method has been adopted.

In 1987, Haslam & Osborne noted the detailed correlation in the spatial intensity distributions of the emission from the inner Galactic plane as recorded by the 60 μm IRAS survey and high frequency (5 GHz) radio surveys at a similar resolution. The correlation with the thermal emission suggests that the dust responsible for the diffuse IR emission in the plane is mixed in with the ionised gas in the ELD regions where it assumes a temperature of 30 - 40 K. Such a model has been developed by Cox & Mezger (1988) to explain the large-scale infrared emission of the Galaxy. At high latitudes, the amount of ionised gas is less, and the dust has a lower temperature of order 20 - 25 K. If the dust were associated with molecular clouds, then the FIR emission would be preferentially correlated with the ^{12}CO line emission, which was found not to be the case. Broadbent (1989), and Broadbent, Haslam & Osborne (1989) developed the technique of using the correlation as an independent means of separating the thermal and non-thermal continuum on a Galactic scale, essentially by using the 60 μm emission as a tracer of the thermal radio component. By quantifying the the IR-radio correlation (after removing the zodiacal light contribution and that part of the IR emission arising from dust correlated with the general HI distribution), the thermal contribution could be subtracted from radio surveys at low frequencies using the appropriately scaled residual 60 μm emission. Since the free-free emission has a flat spectrum over a range of $\sim$ 100 MHz to tens of GHz,

once the scaling was established at one high frequency where the thermal emission is dominant, it is then easy to evaluate the component at lower frequencies where the non-thermal emission is more significant using the power-law frequency dependence of the emission. The subtraction was carried out at 408 MHz after scaling the thermal contribution from either 2.7 or 5 GHz. In the inner Galaxy, some obvious minima in the resultant non-thermal emission could be discerned which were located in the vicinity of strong HII complexes. This was found to result from the assumption that all of the sources were optically thin down to 408 MHz, producing an overestimate of the thermal component. Using data on the optically thick regions from Shaver & Goss (1970), a correction was made. We have used the corrected 408 MHz thermal map to derive the non-thermal component in the plane, and scaled the uncorrected data to 1420 MHz to produce the non-thermal data at that frequency (the strong HII sources – W51, W43, M17, RCW127, G333 -0.2, RCW74, RCW57 and Carina – were first investigated at a number of frequencies to check the optically thin assumption at 1420 MHz. Only Carina is likely to be in error, but since the source lies outside the range of the 1420 MHz survey no correction has been made). The resultant components should allow a better estimate of the high frequency emission than has been achieved so far using just the 408 MHz survey and catalogues of HII regions, since it should account more fully for the ELD component.

4.2.2 Modelling the High-latitude Thermal emission

At high latitudes, the contribution of the thermal component is rather small, the brightness temperature at 408 MHz being dominated by the non-thermal emission due to its greater scale height. In fact, the determination of the thermal component from low frequency surveys is difficult since the average level of emission may be of the order of the errors in the surveys. As an alternative method of determining the high-latitude contribution, one can consider the recombination-line emission which also traces the warm ionised interstellar medium. Sivan (1974) observed the general Hα emission in the plane, noting that it formed an intense diffuse background connecting the classical compact HII regions. In fact, the diffuse Galactic Hα emission appears to be present over the whole sky with an intensity ranging from 3 - 12 R (where 1R is the isotropic intensity emitted by 10^6 recombinations per second) near the Galactic equator with a mean of 6 R , to 0.25 - 0.8 R at

the poles. The emission originates from the low density 2 - 3 kpc thick layer of warm ionised interstellar gas where the thermal continuum emission is produced. High resolution Hα photography (see Reynolds, 1990, for a comprehensive review and references) reveals a complex morphology – filaments and diffuse patches of enhanced emission are seen on a fainter, more uniform background present in areas between bright HII regions, and sometimes far from the Galactic plane. Reynolds (1990), presents a map of this Hα emission synthesised from Fabry-Perot data from a number of sources down to declination -20° . This map is very undersampled and only large-scale features are apparent. In order to more accurately estimate the thermal background, a similar map is required with better sampling and higher angular resolution, but at this time such a survey is limited by the long integration times required to reach the desired sensitivity. From the present data however, it is apparent that for $|\,b\,| > 5°$, the Hα intensities vary generally as $I_\alpha \sin b = 1$ R. At a given latitude there are real variations in intensity from one direction to another by a factor of ~ 3 from peak-to-trough, and for $|\,b\,| > 60°$ there is some evidence that the csc b law from lower latitude measures overpredicts the emission by a factor of ~ 2. Since no detailed measures of the Hα emission are available, we have made use of the csc b form of high latitude emission to estimate the likely thermal continuum radiation. In particular, the observed Hα line intensities yield estimates of the emission measure (EM) given by

$$EM = \int n_e^2 \, dl = 2.75 \, T_4^{0.9} \, I_\alpha$$

where T_4 is the temperature of the ionised medium in units of 10^4 K, and I_α is given above. Recalling our earlier expression for the thermal brightness temperature in the optically thin case, $T = T_e \tau$ where τ is given by the approximation to Oster's formula, it follows that,

$$T = 5.688 \times 10^{-5} \, a(\nu, T_e) \, T_e^{0.55} \left(\frac{\nu}{\mathrm{GHz}}\right) \left(\frac{1}{\sin b}\right)$$

where T_e is of order 7000 K (Shaver, 1976). We have put down a rectangular grid of points in celestial coordinates at high latitudes of the appropriate temperatures. When convolved to 8.2° as for the original Davies *et al.* (1987) experiment, we find that for the region of interest the pixel values lie in the range ~ 20 - 30 μK as noted in Davies *et al.* (1989). However, the actual second difference estimate for the

region is only of order 2 μK, due to the smoothly varying nature of our model. It is unlikely that this could be increased by more than the factor 3 peak-to-trough intensity variation as estimated by Reynolds (1990), so the contribution to the 10 GHz measurement is small compared to the likely GSR signal.

4.2.3 The complete model

The complete model for the Galactic emission at a given frequency has been evaluated by combining the model for thermal emission with the derived non-thermal components at 408 and 1420 MHz, and the IRAS 100 μm data. In order to test how reasonable the model is, the data have been extrapolated in the appropriate fashion (see Chapters 2, 3) to 10.46 GHz and second difference calculations performed to compare to the plane crossing observations in Watson (1989) for a number of declinations. The crossings at declinations to 40° in the inner Galaxy encounter the Cygnus complex, which although being a large thermal source, also contains a number of non-thermal sources. At 408 MHz, Broadbent (1989) remarked how well the thermal model fitted the emission in this region, even though it lay outside the area where the radio-FIR correlation had been established. Being such a complex region, it might be expected that the fit would show some deviations from the extrapolated model. Indeed, it is found that the estimate of the second difference amplitude for the inner Galaxy crossing is $\sim$ 105 mK, compared to the observed amplitude of 82 mK recorded in Watson (1989). This could be explained if the thermal spectral index near the Cygnus region is a little steeper than the theoretical value of 2.1 (since the Cygnus complex, although containing a number of sources – see Wendker, 1984 – is still predominantly thermal, the discrepancy is likely to be rooted in the thermal model). In fact, the more recent 15 GHz measurements (Lasenby – private communication) give a second difference amplitude for this crossing of $\sim$ 34 mK. If account is made of the steep spectral index non-thermal sources' contributions to the 10 and 15 GHz data, then the use of a thermal index of $\sim$ 2.2 is found to adequately reproduce the Jodrell-IAC data. The inclusion of a detailed thermal model is obviously an improvement on using the simple extrapolation from the 408/1420 MHz spectral indexes directly, which would have predicted a second difference amplitude at 10 GHz of $\sim$ 40 mK. For the other declinations at which comparisons have been made – namely 45° , 42.1° , 35.2° , 5° , 0° , -2° and -5° – the differences between

the model features and observations at 10 GHz are smaller, typically being of order 10%, and all of the general features are reproduced (although the observations are noisier away from the plane crossings, so there appears to be more structure in the observed fluctuations), especially well in the outer Galaxy (the largest errors are for the inner Galaxy crossings). It is likely that more detailed catalogues of strong HII sources at a number of frequencies are needed to improve the model. This supports remarks we have made in previous chapters that multi-frequency observations are essential to help accurately subtract the foreground. Figs 1a and b give two examples of the observed and predicted second differences. If simple extrapolations are made for the plane crossings using the spectral indices calculated directly from the 408 and 1420 MHz surveys, then the amplitudes are in error by a factor of about 2. A comparison has also been made with the difference scan measurement at 3.7 GHz in de Amici *et al.* (1988) at declinations 38° and 36° . If account is made for the atmospheric contribution, then there is reasonable agreement once again ($\sim$ 10 - 20% accuracy).

4.3 Sky Maps at the COBE frequencies

We now procede to generate sky maps from the lower and higher frequency surveys. This is achieved by scaling the thermal map according to a $\nu^{-2.1}$ power-law, the non-thermal component is evaluated by calculating the spectral index β point-by-point from the 408 and 1420 MHz non-thermal maps as determined above and scaling the 408 MHz map by a $\nu^{-\beta}$ power-law, and finally the dust contribution by assuming a $\nu^{\alpha}\, B_{\nu}[T_d]$ type spectrum for the dust. Of course, such maps themselves cannot possibly hope to reproduce the exact nature of the Galactic foreground at a given frequency, but are hopefully some of the better estimates made to date. In particular, there may be small changes as a consequence of the steepening of the non-thermal index (which has not been considered here - see Chapter 2) and its variation on the sky, departures from the theoretical thermal spectral index of 2.1, and the assumption of a constant dust temperature and emissivity across the sky (which is most clearly wrong near the plane where it is expected that the dust is warmer as a consequence of additional heating in the ionised HII regions associated with O stars).

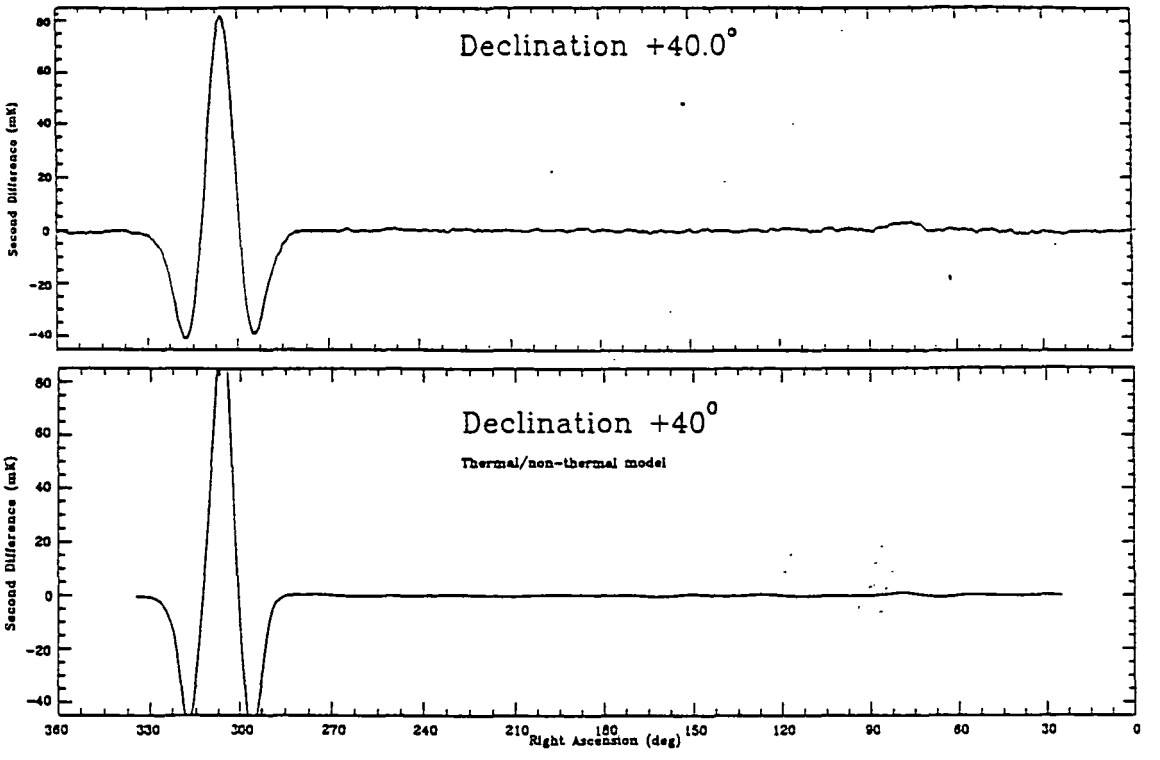

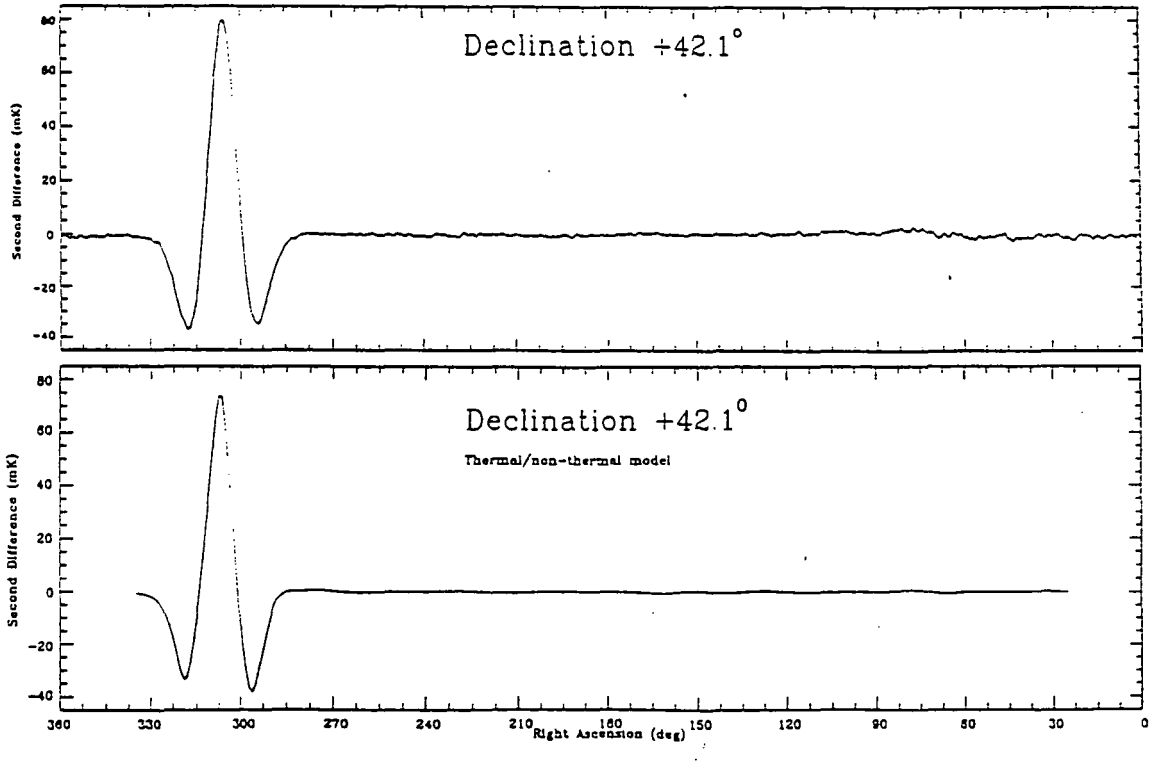

Figure 4.1: a) second difference scan at declination 40° . Upper figure is experimental data from Watson (1989), lower is model prediction. b) as a) for declination 42.1°

Furthermore the use of the 408 and 1420 MHz surveys to provide extrapolations to higher frequencies has been questioned by Watson & Gutiérrez de la Cruz (1991), so we reconsider the problem here. As discussed in Chapter 2, the problems with the low frequency surveys is a consequence of the slight offsets occurring in adjacent scans as a result of changes in the atmosphere, receiver noise, and ground pick-up. Corrections for this are attempted by minimisation techniques using overlapping scans from different directions. However, the residual effects appear as small vertical bands in the 408 MHz survey, and curving ripples at 45° to lines of constant declination at 1420 MHz. As discussed earlier and in Lawson *et al.* (1987), the effects appear most clearly in spectral index maps calculated between the two frequencies where striations are easily seen for the maps at FWHM 0.85°, but these seem to be eliminated after convolving to FWHMs greater than 4° . Watson & Gutiérrez de la Cruz use the two low frequency maps to evaluate a second difference map at 10 GHz, and claim that the ripples now seen are again a consequence of the baseline effects. A simple calculation using the likely baselevel errors at the two frequencies for a 5.6° FWHM beam does indicate that the effect could give rise to structure at about the level observed in the calculations. However, we have also looked at second difference maps at the two frequencies for both 0.85° and 5.6° resolution, as well as at the 10 GHz extrapolations. At 0.85° resolution, there do appear to be some spurious striping effects in the 1420 MHz data, although these do not persist over the whole area surveyed ($25° < \delta < 80°$; $270° > \alpha > 90°$), and the presence of baselevel effects in the 408 MHz survey is not so immediately obvious. On convolving to 5.6° , as in Fig. 2, the ripples seen by Watson & Gutiérrez de la Cruz are apparent in both maps, but the question of whether these are artifacts of baseline errors depends on the coherence of the errors across the 5.6° beamwidth. Furthermore, although in the 1420 MHz map there is a striping effect in the same position as seen in the higher resolution map, there are certainly regions showing similar enhancements or depreciations at the same positions for both frequencies. Such an effect is unlikely to be a consequence of baseline errors due to the differing scanning techniques employed in the two surveys, thus it seems likely that in the 10 GHz extrapolation there remains a considerable amount of genuine structure. Obviously, any weak false structure present at lower frequencies will be amplified by the large factor in the ratio of frequency differences between 408, 1420 and 10,460 MHz, but it seems too soon to entirely reject the low frequency surveys as first order

approximations of higher frequency structure.

The conclusion of Watson & Gutiérrez de la Cruz that a simple extrapolation does not appear to be good enough to establish the likely synchrotron emission at 10 GHz at the required sensitivity may well be an accurate assessment, but we consider that this is most likely a consequence of the variations in the spectral indexes beyond 1420 MHz and rather less the result of propagated baseline errors. Indeed, the more recent 15 GHz measurements (Lasenby *et al.* , 1991) would certainly seem to support the view that any structure present is most likely the result of non-thermal Galactic emission. The 10 GHz measurements will be important in aiding the assessment of the 15 GHz GSR contribution, and in fact it appears that the 10 GHz work is most readily identified as a high frequency Galactic synchrotron radiation survey.

In the following maps, it is considered that any structure resulting from the extrapolations of low frequency data is genuine and not connected with flaws in the baseline offsets. Any false structure present will be at a lower level than that discussed for the Davies *et al.* experiment since there is no error escalation as temperature second differences are not calculated.

In Figs. 3a to c, sky maps are presented in a rectangular projection of celestial coordinates for the sky at 31.5, 53 and 90 GHz, for a beam of FWHM 7° as appropriate for the COBE differential microwave radiometers. The maps cover declinations -10° to +90° as a consequence of the incomplete sky coverage of the 1420 MHz survey, and RA runs from 359° to 0° . The dust contribution is estimated from the 100 μm IRAS survey using a preliminary COBE result (Wright *et al.* , 1991) for the dust parameters of $\alpha = 1.5$, $T_d = 21.75$ K. This excludes data from the plane, where the dust is expected to be hotter, so the extrapolation will be slightly low for that part of the sky. The maps show the general decrease in the Galactic contribution with frequency as seen in the COBE maps of Smoot *et al.* (1991), and the dominance of the emission from the plane above that in other sky regions. The temperature scale is such that white corresponds to all regions brighter than 0.6 mK. As discussed with reference to the 10 GHz sky scans, the thermal contribution is subject to small corrections near bright HII regions. Clearly, the model whilst being useful to first order still requires additional input from other frequency channels, and the foreground subtraction still requires point-by-point modelling of the

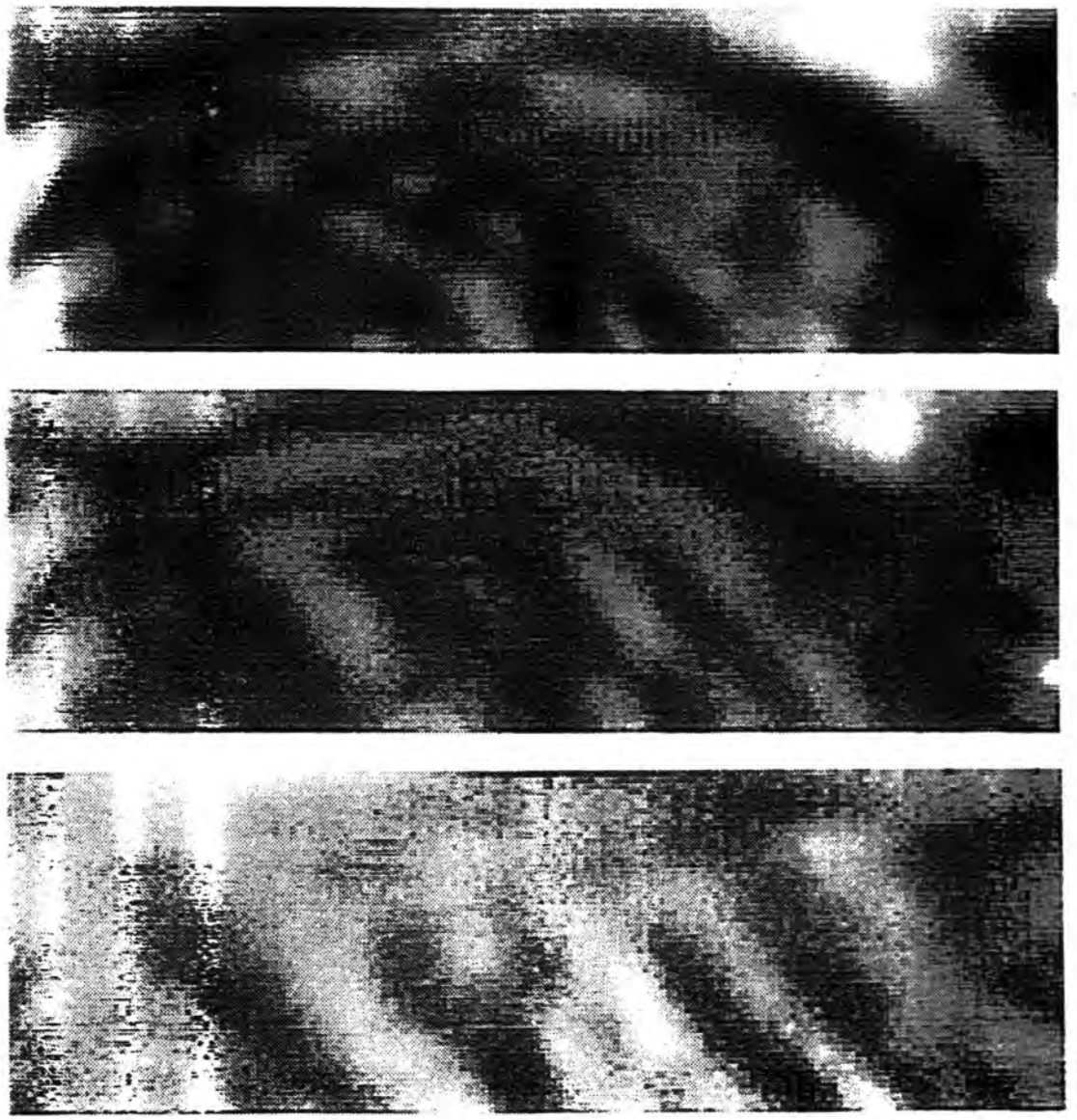

Figure 4.2: a) Second differences at 408 MHz for the region $25° < \delta < 80°$, $270° > \alpha > 90°$ for FWHM 5.6° and beamthrow 8.2°; b) at 1420 MHz; c) at 10 GHz.

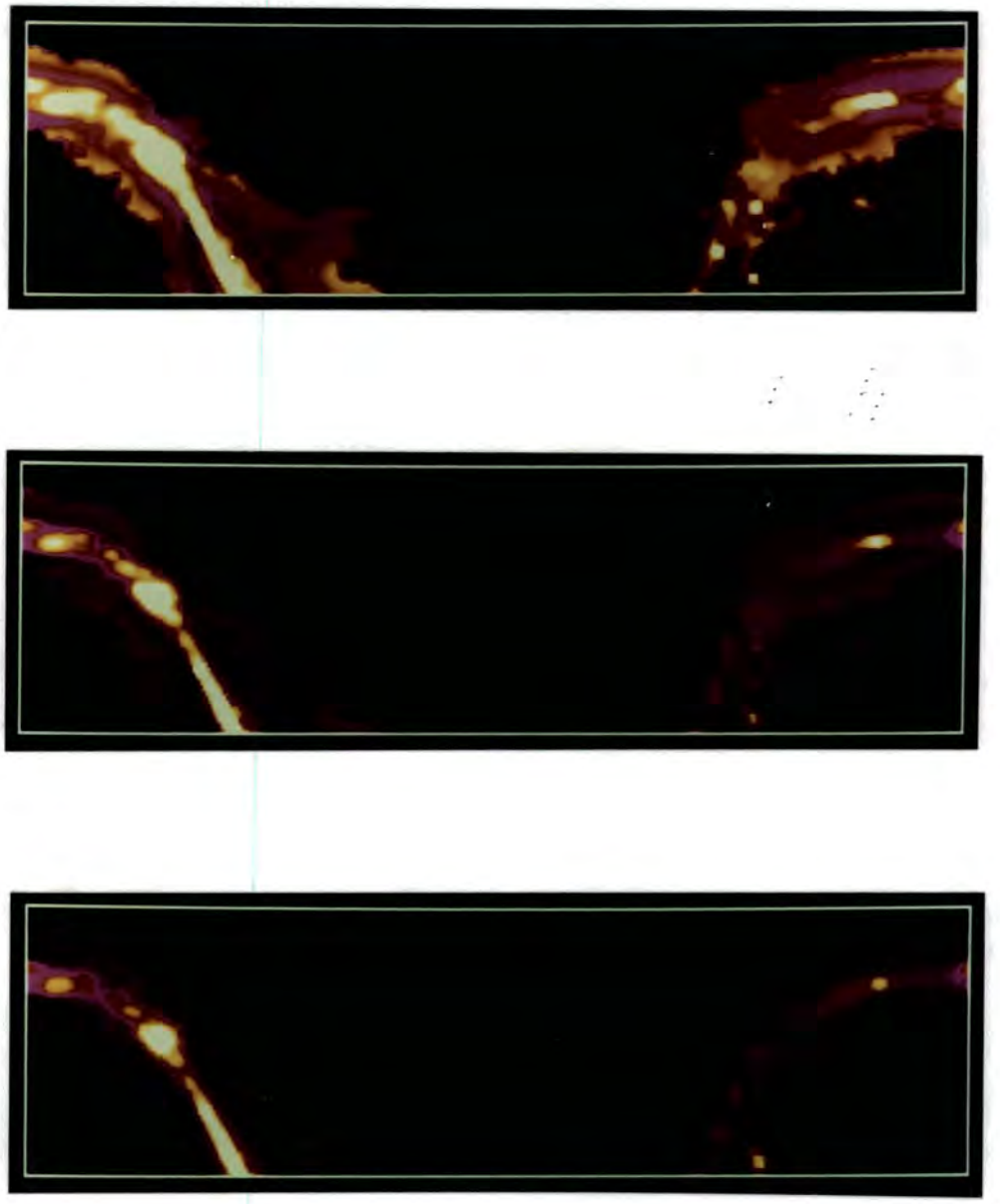

Figure 4.3: Predicted sky temperature a) at 31.5 GHz for a beam of FWHM 7° ; b) at 53 GHz; c) at 90 GHz.

emission.

4.4 Quiet regions on the sky

We have already noted that there may exist quiet regions on the sky where the Galactic foregrounds are at a minimum and therefore it may be of advantage to look for CMB anisotropies. Although such regions are likely to be relatively small, and therefore limits on low order multipole moments unreliable, good limits on anisotropies may be achievable as long as careful comparisons of the data obtained are made with theoretical predictions which account for the limited sky coverage (as in Vittorio *et al.* , 1991) – comparison with the theoretical ensemble rms value for a given cosmological model would clearly be at worst meaningless, and at best rather difficult to interpret. Another obvious advantage of looking at a quiet region is that observations may be repeated on a shorter timescale leading to improved signal-to-noise levels and greater sensitivity in a given time. Whilst all-sky surveys are certainly desirable for better statistics to compare with CMB predictions, a sensitive survey over a small sky region could find use as a calibrator for the all-sky data.

Masi *et al.* (1991) have considered the problem of finding a good 'window' on the sky for mm. and sub-mm. observations by looking at the IRAS 100 μm survey and recording those regions which constitute the lowest 10% of the sky intensity distribution. In Fig. 4a, we present our calculation of these regions, seen as black in the greyscale representation, which is in excellent agreement with Masi *et al.* . All of the points in the regions have sky fluxes below 1.67 MJy sr^{-1}. In Fig. 4b, we show a similar greyscale image for the 408 MHz sky temperature, where all pixels in the quiet regions have temperatures below 12.2 K. Masi *et al.* suggested that the clean sky regions in the 100 μm survey were also likely to be clean at radio frequencies on the basis of a statistically significant correlation between the 408 MHz and 100 μm surveys. However, the two figures indicate that this is not necessarily the case, as would be expected since the two physical components giving rise to the emission – the dust and cosmic-ray electrons – have quite different scale heights; the correlation probably arises from the general csc b trend in both sets of data. Nevertheless, there are two regions where the intensities are within 10% of the minimum:

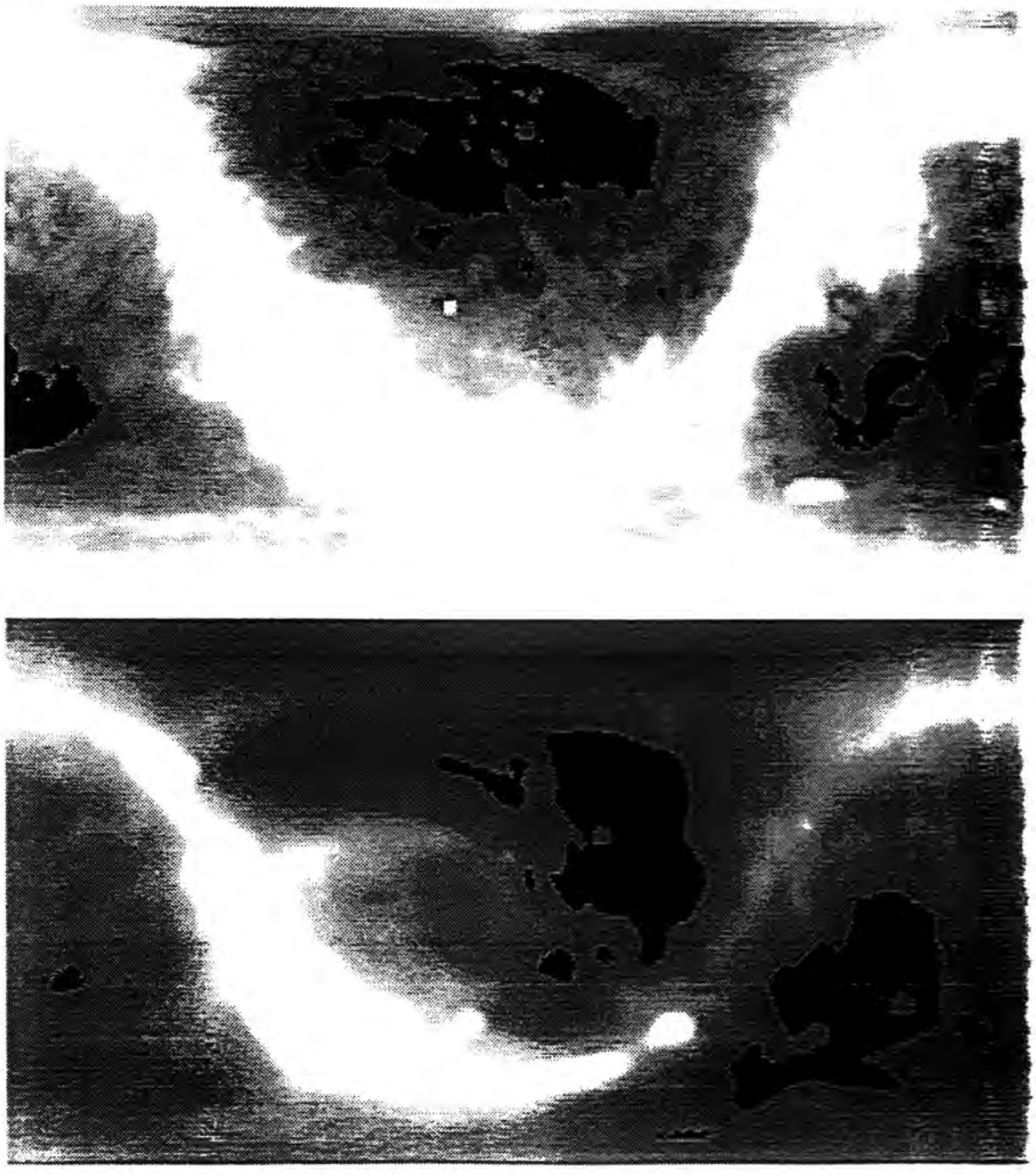

Figure 4.4: a) 100 μm IRAS survey: regions in black constitute the lowest 10% of the sky intensity; b) 408 MHz survey with minimum sky regions again shown in black.

$27° < \delta < 47°$, $134° <$ RA $< 170°$ and $-34° < \delta < -22°$, $36° <$ RA $< 60°$. These would be ideal regions in which to make sensitive multifrequency observations. However, it is still necessary to take into account the effects of beamswitching, which relates more to the variation of intensities about a mean value in a given region than to the absolute minimum pixel values, since the DC level is removed by the switching process. Although the indicated regions are likely to show small variations, it is worth recalling that in the synchrotron case for the Davies *et al.* (1987) and Watson *et al.* (1988) experimental set-ups with $\theta_b = 8.2°$, the region $180° <$ RA $< 250°$ at declination 40° appeared to be the quietest on the sky. We have repeated the second difference scans for strips of size 55° real sky angle at constant declination for the IRAS survey, with the results in Table 1.

declination (deg.)	Region 1	Region 2
30	1.63	3.11
35	1.46	4.14
40	1.63	2.77
45	1.12	1.96
50	1.42	2.51
55	0.90	4.14
60	1.05	6.26
65	2.05	7.19
70	6.62	8.55

Table 4.1: rms second differences in μK at 100 μm for FWHM 5.6° and beamthrow 8.2° . Region 1 centred on R.A. 215° ; region 2 on R.A. 135° . Each region corresponds to a real sky angle of 55° at constant declination.

Although the Davies *et al.* strip this time is not the lowest in value, it still corresponds to one of the quietest regions on the sky, and since considerable effort has already been employed in establishing limits on the anisotropy level at both 10 and 15 GHz (efforts which are still in progress) with plans to extend the investigation to a third frequency – namely 30 GHz – it may be worth considering additional work in this region at yet other frequencies, and its use as a calibrator for all-sky surveys. If a number of neighbouring scans are made at interval in declination of not more than 2.5° , it will be possible to reconvolve the declination 40° data to the 7° resolution of the COBE experiment and make use of the 31.5 GHz data, as well as the 19 GHz work of Boughn *et al.* (1990). Fig. 5 shows the fluctuations at

100 μm for the Watson *et al.* configuration.

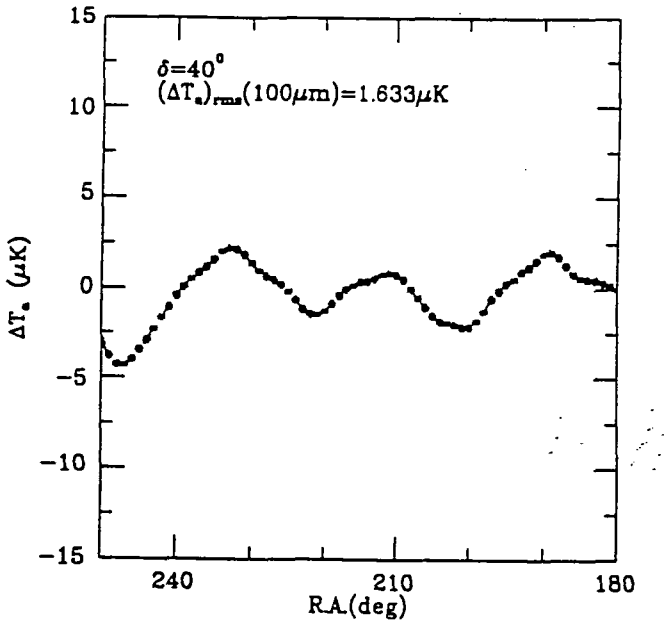

Figure 4.5: Expected second difference measurement at declination 40°

Assuming the COBE preliminary result for the dust parameters, this corresponds to a $\Delta T/T$ of 3.9×10^{-7} at 90 GHz, well below the expected CDM signal, although the peak pixel values reach of order 10^{-6}. Future work might like to consider multi-frequency observations in the common quiet regions with sufficient coverage to allow good foreground modelling. Figs 6a to c show the sky temperature distribution in the quiet region of the sky defined as $30° < \delta < 50°$, $250° > \alpha > 180°$ for the COBE frequencies and resolution. The temperature scale runs from 1.97 to 6.16 μK. At the lowest frequency, the sky temperature is greater than 5 μK across the whole region, at the higher frequencies, the competing effects of the synchrotron and dust emission can be seen: there is a region of very low temperature, but structure still exists on the μK level over the entire region.

4.5 Discussion and Conclusions

We have derived sky maps at the COBE frequencies and found good general agreement with the sky as seen by COBE. In particular, the sky is very quiet off the

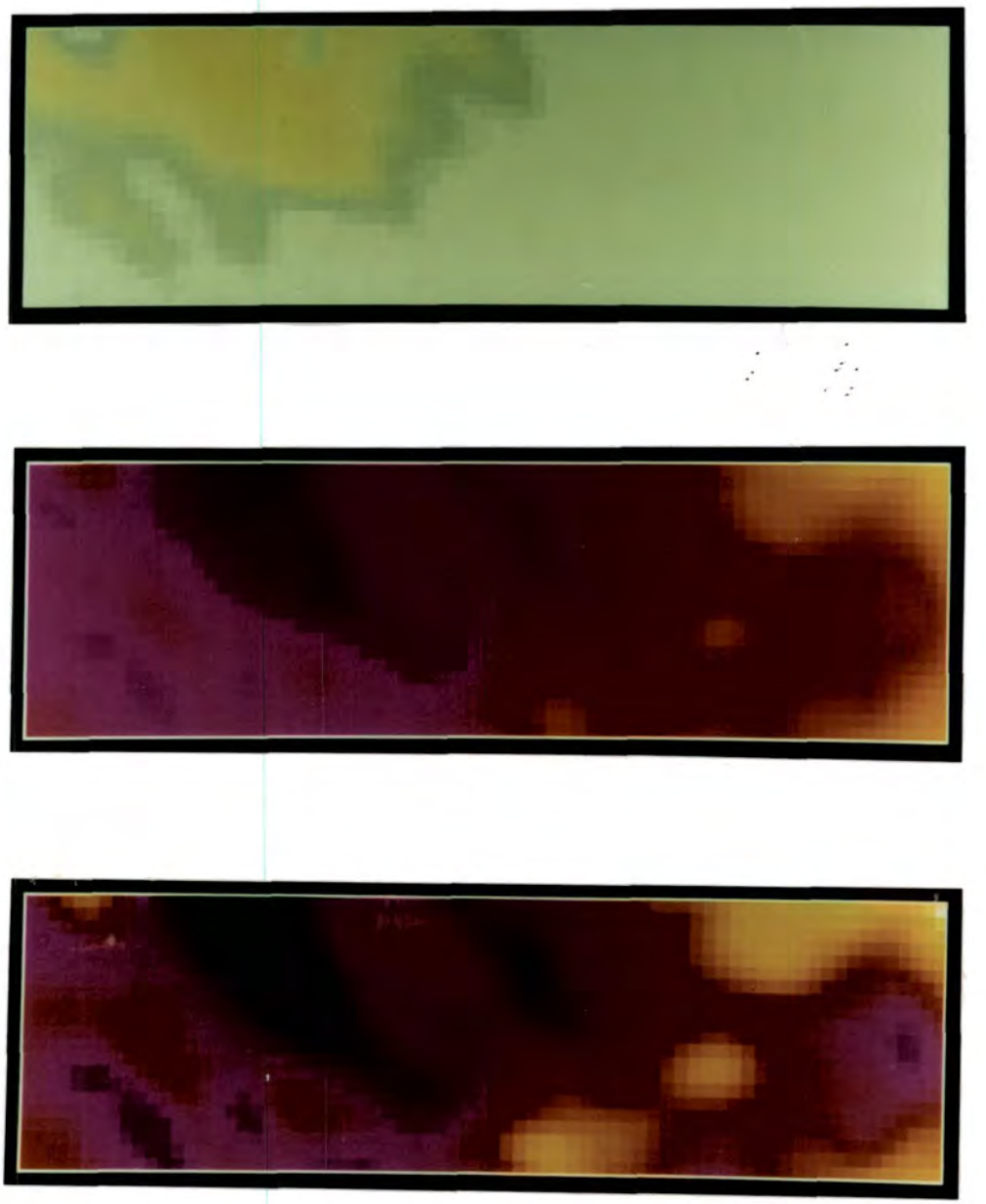

Figure 4.6: Sky temperature distribution a) at 31.5 GHz for the quiet region (see text); b) at 53 GHz; c) at 90 GHz.

plane. However, there are a number of difficulties with the extrapolations used, and it is clear that observations of the sky temperature over a range of frequencies are needed in order to allow Galactic foreground subtraction. The discussion of the errors in the low frequency radio surveys suggests that whilst the 408 MHz survey, after some form of Fourier cleaning to remove residual baseline effects and a check on the absolute calibration, may remain of some use as a guide to the foreground emission, the 1420 MHz survey with its limited sky coverage and more obvious baseline deficiencies needs replacing by a new full sky absolutely calibrated survey at $\sim$ 5 GHz, or better still by several at, say, 2 GHz and 7.5 GHz. Here, improvements in detector technology may be required in order to achieve the required sensitivity. Obviously, the data provided by the COBE-DIRBE experiment should allow modelling of the dust contribution to sufficient accuracy for the DMRs to achieve their intended sensitivity at 90 GHz, and the 150 μm and 240 μm maps will also trace the quiet regions for sub-mm measurements more accurately than has been possible here. Masi *et al.* have derived a fit to measurements of the Galactic emission over a number of frequencies and suggested that taking the non-thermal index as 2.91 together with dust parameters $\alpha = 1.25$ and $T_d = 26$ K everywhere provides an excellent description of the high latitude emission. However, although they have considered the variation in intensities at 100 μm in order to estimate the likely contribution to a given measurement of $\Delta T/T$ (see de Bernardis *et al.* , 1991), it is the fact that the measurements are differential, coupling together different lines-of-sight, and that the spectral parameters may vary along each lie-of-sight which will amplify the variations seen at one frequency when an extrapolation is made. This was particularly evident in Chapter 2, of course, where it was found that the straightforward extrapolation of the 408 MHz data to 10 GHz did not fit the Davies *et al.* data, but that allowing for spectral variations a reasonable fit could be found.

The need for point-by-point spectral modelling will become increasingly important as the stage is reached where the topology of CMB fluctuations can begin to be investigated. Figs. 7a to c show the topology of Galactic anisotropies expected at the three COBE frequencies in an imaginary experiment of 7° FWHM and 8° beamthrow forthe region -10° $< \delta <$ 80°., 270° $>$ R.A. $>$ 90° . The variations, seen as contours of $\Delta T/T$ ($\times 10^6$), can be compared to CMB predictions in various cosmological models (the topology will be sensitive to θ_b). It is interesting to note the change in the structure of the fluctuations with frequency, and that at

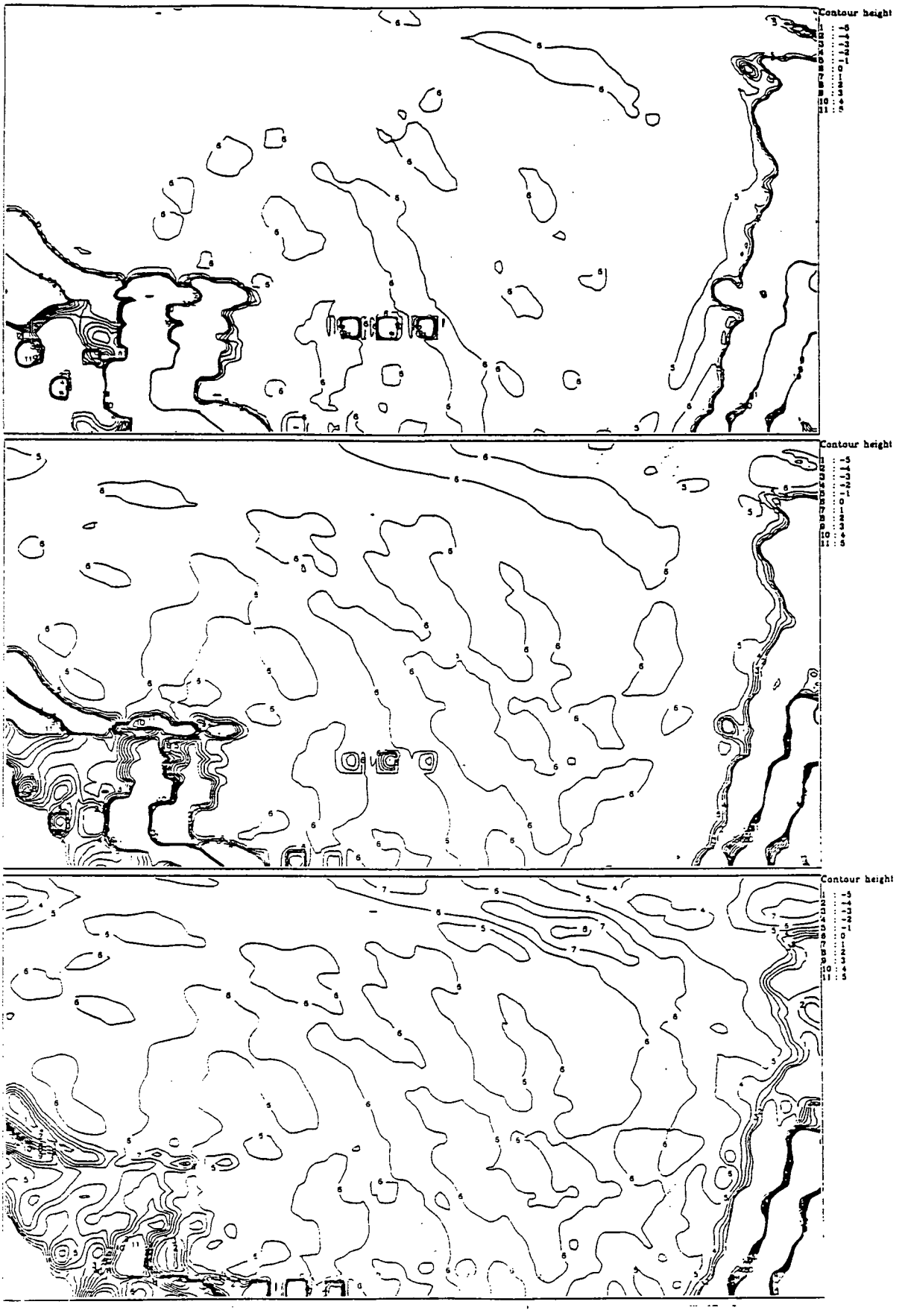

Figure 4.7: a) $\Delta T/T$ variations for FWHM 7° and second differencing with $\theta_b =$ 8° at 31.5 GHz in units of 10^{-6}; b) at 53 GHz; c) at 90 GHz.

$\sim$ 50 GHz there appears to be a minimum in the Galactic emission (away from the plane). At such a frequency, there appears to be a great number of regions away from the plane where the anisotropy level is $\sim 10^{-6}$ or less, although this value depends on the exact spectral model assumed for the different Galactic components.

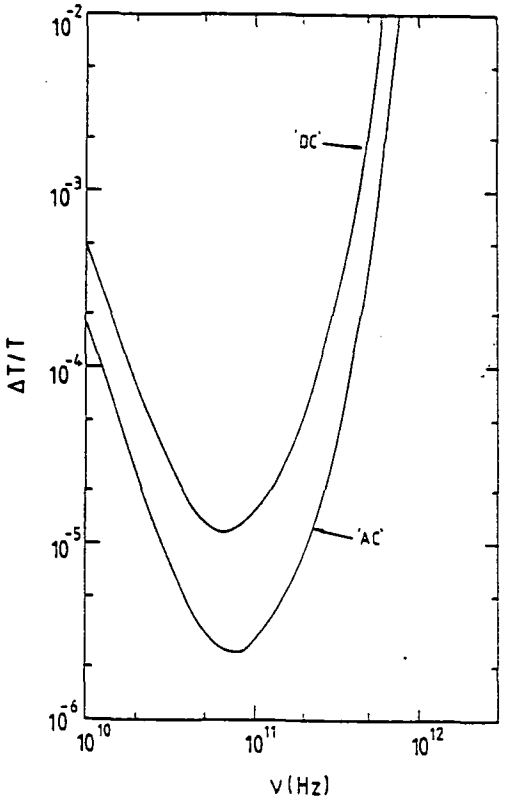

Figure 4.8: The 'best' estimate of the Galactic contribution to $\Delta T/T$ at a number of frequencies. DC corresponds to the situation at b = 90° . AC corresponds to difference measurements for COBE in quiet regions of the sky away from the Galactic plane (see text).

To close the section on Galactic foregrounds, Fig. 8 indicates the expected contribution to the measured $\Delta T/T$ due to the Galaxy in quiet regions of the sky away from the Galactic plane. The estimate here is a little higher than would be expected from Fig. 7 since the dust emission is described by the fit to the LMC data described in Chapter 3, which is towards the upper end of the values employed for dust emission, and certainly greater than the preliminary COBE result used in this chapter and in Fig. 7. Since there remains the possibility that there is a component of cold dust not well correlated with the IRAS dust, then this figure should give a conservative estimate on the Galactic contribution to the anisotropy measures in that it may overestimate the foreground (ie. it preserves some wariness in the interpretation of fluctuations on the 10^{-6} level). The lowest $\Delta T/T$ achievable is $\sim 2 \times 10^{-6}$ at $\sim$ 60 GHz, rather close to the 5 - 8×10^{-6} expected in CDM models.

It is clear that detailed Galactic modelling is still required even at the frequency of lowest Galactic contribution. If the preliminary COBE fit to the dust emission is assumed, then the minimum $\Delta T/T$ level may fall by a factor of ~ 2 - 3, but foreground subtraction will still be required for the unequivacol identification of cosmological fluctuations. Nevertheless, 50 - 70 GHz appears to be the optimum range of frequencies to reduce the Galactic foregrounds to a minimum, the exact $\Delta T/T$ values depending on the experimental configuration adopted.

References

Altenhoff, W., *et al.* , 1960. *Veröff, Sternwärte, Bonn*, **59**, 46.

Boughn, S.P., *et al.* , 1990. *Rev. Sci. Instrum.*, **61**, 158.

Broadbent, A., 1989. *Ph.D. Thesis*, University of Durham.

Broadbent, A., Haslam, C.G.T. & Osborne, J.L., 1989. *Mon. Not. R. astr. Soc*, **237**, 381.

Cox, P. & Mezger, P.G., 1988. in *Comets to Cosmology*, p. 97, ed. Lawrence, A., Springer-Verlag.

de Amici, G., *et al.* , 1988. *Astrophys. J.*, **329**, 566.

de Bernardis, M., *et al.* , 1990. *Astrophys. J. Letts.*, **366**, L31.

Davies, R.D., *et al.* , 1987. *Nature*, **326**, 462.

Davies, R.D., *et al.* , in *The Galactic and Extragalactic Background Radiation*, p. 398, eds. Bowyer, S. & Leinert, C.

Fixsen, D.J., Cheng, E.S. & Wilkinson, D.T., 1983. *Phys. Rev. Letts.*, **50**, 620.

Gordon, M.A. & Cato. T., 1972. *Astrophys. J.*, **176**, 587.

Haslam, C.G.T. & Osborne, J.L., 1987. *Nature*, **327**, 211.

Kogut, A., *et al.* , 1990. *Astrophys. J.*, **355**, 102.

Lasenby, A.N., *et al.* , 1991. in *Observational Tests of Cosmological Inflation*, p. 413, eds. Shanks, T., *et al.* , Kluwer.

Lawson, K.D., *et al.* , 1987. *Mon. Not. R. astr. Soc*, **225**, 307.

Levin, S.M., *et al.* , 1988. *Astrophys. J.*, **334**, 14.

Masi, S., *et al.* , 1991. *Astrophys. J. Letts.*, **366**, L51.

Matthews, H.E., *et al.* , 1973. *Mon. Not. R. astr. Soc*, **165**, 149.

Matthewson, M., *et al.* , 1962. *Aust. J. Phys.*, **15**, 354.

Mezger, P.G. & Henderson, A.P., 1967. *Astrophys. J.*, **147**, 471.

Mezger, P.G., 1978. *Astr. Astrophys.*, **70**, 565.

Oster, L., 1961. *Rev. Mod. Phys.*, **33**, 525.

Reynolds, R.J. 1990. in *The Galactic and Extragalactic Background Radiation*, p. 157, eds. Bowyer, S. & Leinert, C.

Scaramella, R. & Vittorio, N., 1990. *Astrophys. J.*, **353**, 372.

Schraml, J. & Mezger, P.G., 1969. *Astrophys. J.*, **156**, 269.

Shaver, P.A. & Goss, W.M., 1970. *Aust. J. Phys. Astron. Suppl.*, **14**, 133.

Shaver, P.A., 1976. *Astr. Astrophys.*, **49**, 1.

Sivan, J., 1974. *Astr. Astron. Suppl.*, **16**, 163.

Smoot, G.F., *et al.* , 1991. *Astrophys. J. Letts.*, **371**, L1.

Vittorio, N., *et al.* , 1991. *Astrophys. J. Letts.*, **372**, L1.

Watson, R.A., *et al.* , 1988. in *Large Scale Structure and Motions in the Universe*, p. 133, eds. Mezzetti, M., *et al.* , Kluwer.

Watson, R.A., 1989. *Ph.D. Thesis*, Victoria University of Manchester.

Watson, R.A. & Gutiérez de la Cruz, 1991. in *Physical Cosmology*, p. 565, eds Blanchard, A., *et al.* , Editions Frontiers.

Wendker, 1984. *Astr. Astrophys. Suppl.*, **58**, 291.

Westerhout, G., 1958. *Bull. astr. Inst. Neth.*, **14**, 215.

Wright, E.L., *et al.* , 1991. *Astrophys. J.*, **381**, 325.

Chapter 5

Discrete Sources and CMB Observations

5.1 Introduction

In this chapter, attention is shifted from the foreground contamination emission due to the Galaxy to that arising from discrete extragalactic sources, such as radio galaxies. Again, it is important to consider the likely discrete source contribution as a function of both frequency and angular scale, since by appropriate choices of both it may be possible to minimise the effects. Although the Galaxy is certainly dominant on large angular scales, $\theta \geq 1^{\circ}$, it is still important to determine the extragalactic foregrounds on such scales, as well as on the smaller scales ($\sim$ a few arcminutes) where they dominate. Indeed, the integrated spectra of all extragalactic sources is an interesting topic in its own right, providing information on the formation and evolution of baryonic structures in the universe. Since it is likely that any sources which do form will demonstrate clustering at some level or other, then the presence of anisotropies in the foreground radiation is inevitable, and it is these anisotropies which must be understood to avoid confusion with genuine CMB anisotropies. In this chapter, particular effort will be made on estimating the likely fluctuations on degree scales, although reference will be made to limits on small-angle anisotropies. An estimate will be made of the fluctuations in an rms sense from a number of models; ultimately, of course, the detailed spatial characteristics of the sources will be required if an attempt is to be made to uncover the detailed topology of the genuine CMB sky variations, but at the moment such details are only known for

relatively strong, and thus generally nearby, sources. These sources do contribute the largest fraction of the anisotropy level (as will be seen later), thus the use of catalogues to synthesize their contributions is of great importance (this has been done for strong radio sources at 10 GHz by Watson *et al.* , 1988). However, the remaining variations due to faint unresolved sources also needs estimation using reasonable physical models.

Here, the fluctuations due to emission from dusty galaxies out to high redshifts, and dust in clusters of galaxies will be considered, and the a review given of the contribution from radio galaxies, including recent faint source counts and their consequences for anisotropy measures.

5.2 Fluctuations from discrete Infrared Sources

Observations of the extragalactic background light (EBL) are expected to provide information on the cosmic 'dark ages' – the period between recombination and the epoch of galaxy formation – and many pregalactic sources of radiation have been proposed. There could be many kinds of astrophysical generators in the infra-red during the period $z = 10$ - 10^3, namely primaeval galaxies, population III stars, accreting massive black holes, large-scale explosions, or decaying particles. The resultant radiation would, in general, reside in the near-IR, which is of course of no consequence for CMB observations; however, if the universe were filled with dust, the radiation would be reprocessed into the FIR. Such models have been investigated extensively in the literature, in particular see Bond, Carr & Hogan (1988, 1991), Negroponte (1986) and McDowell (1986). However, there is no firm evidence for the existence of either intergalactic dust or pregalactic astrophysical sources, so the emission from ordinary galaxies remains the most plausible precursor of extragalactic far-infrared radiation. Recent observations of extinction (Boyle, Fong & Shanks, 1988) towards distant clusters and groups of galaxies suggests the presence of dust in the intracluster medium, which is a second plausible source for FIR radiation. Observations of such foregrounds directly will be difficult due to the presence of emission from the Galaxy: zodiacal light, starlight, interplanetary dust and interstellar dust emission, but none-the-less they remain an important systematic in the search for CMB anisotropies. In what follows, simple models

for the galactic and cluster radiations are investigated, and anisotropies therein estimated by considering the clustering properties of the sources. To constrain the models, a number of recent EBL limits are used; these are summarised in Table 1.

Reference	ν (10^{12} Hz)	I_ν (MJy sr^{-1})
Lange *et al.* (1988)	1.09	< 2.66
	2.22	2.48 ($\pm$0.72)
	3.00	< 1.07
Hauser *et al.* (1991)	1.25	5.62 ($\pm$3.21)
	1.99	6.53 ($\pm$3.52)
	3.13	3.84 ($\pm$1.60)
	5.45	4.22 ($\pm$1.83)
Rowan-Robinson *et al.* (1990)	3.00	2.20 ($\pm$0.20)

Table 5.1: Recent extragalactic background light limits.

Upper limits over a wider range of frequencies may be found by consulting the tables in Negroponte (1986) and McDowell (1986). The results from Lange *et al.* come from an analysis of the high frequency observations in Matsumoto *et al.* (1988). The experiment was rocket-borne, and thus the sky coverage rather small, leading to possible errors in the estimation of the Galactic contribution to the flux. It is thus rather difficult to estimate how accurate these upper limits are. The Hauser *et al.* results are from a preliminary analysis of the DIRBE sky maps at the South Ecliptic Pole (a region of low overall sky brightness in the FIR), and correspond to the total sky flux (ie. it contains the local contributions from the Galaxy and the solar system). The Rowan-Robinson *et al.* value arises from a fit of the zodiacal light emission to the IRAS 100 μm data, corresponding to an offset in the data which may or may not be attributable to the EBL. Constraints on the anisotropy level in the FIR region come from the Kreysa & Chini (1989) observation at 230 GHz of $\Delta T/T < 2.6 \times 10^{-4}$ on a scale of 30 arcseconds using a beam of FWHM 11 arcseconds. Although the VLA results are more restrictive concerning genuine CMB anisotropies, this result will constrain models of the FIR foreground.

5.2.1 Contribution from dust in 'normal' galaxies

Far-infrared radiation is expected from a normal spiral galaxy by a variety of mechanisms. Dust associated with hydrogen in the general interstellar medium heated by the interstellar radiation field radiates predominantly at $\sim 100\,\mu$m , and in the Galaxy has been referred to as infrared 'cirrus' (Low *et al.* , 1984). It is also seen at $60\,\mu$m , and surprisingly strongly at 25, $12\,\mu$m requiring the presence of a grain population hotter than the equilibrium temperature – either very small grains or very large molecules heated transiently to high temperatures by the incoming photons. Active 'starburst' galaxies may differ from spirals only in the proportions of the different dust components, whilst Seyferts and quasars are expected to produce additional radiation in the 1 - $10\,\mu$m range with a power-law spectrum. Rowan-Robinson & Crawford (1989) have used such a 3-component spirals + starbursts + Seyferts model to account for the variations in galaxy spectra in a sample of IRAS galaxies. Similarly, Beichman & Helou (1991) have used this model together with an empirical fit to the IR-luminosity function to predict the foreground due to IR-luminous galaxies. Since we are predominantly interested in the mean intensity and anisotropies at wavelengths longer than $100\,\mu$m , it is the cirrus component which is of greatest importance. Models of this emission have been constructed for the Galaxy using a number of grain components of different temperatures (Cox, Krugel & Mezger, 1986), whilst others employ empirical fits to the observed spectrum. Rowan-Robinson & Crawford suggest a fit of the form $a\nu\ B_\nu[30\ K] + b\nu\ B_\nu[210\ K]$, where $B_\nu[T]$ is the Planck function at temperature T, and a, b are constants adjusted to fit the data. In the following calculations, it is implicitly assumed that all galaxies would have similar properties to our own if observed at the present epoch – that is, no allowance is made for a spread in luminosities, dust emissivities or dust temperatures. A recent review by Helou (1989) suggests that this may not be such a bad approximation: IRAS measurements provide no clear evidence for systematic variations in the emissivity exponent α between Galactic and extragalactic dust, α always lying between 1 and 2 (see Fig. 3.2). In particular, there is no reason to believe that the Milky Way is not a typical galaxy in its IR properties. To model the galactic emission then, an empirical fit to the COBE data up to $100\,\mu$m has been employed from Wright *et al.* (1991). For a galaxy spectrum of the form $\nu^\alpha\ B_\nu[T_d]$, a fit to data including the plane gives $\alpha = 1.65$, $T_d = 23.3$ K, which should be

appropriate for extragalactic sources. However, if recent evidence (see Chapter 3) for the existence of excess flux at low frequencies due to a very cold dust component is confirmed, then the estimates here may be too low.

The sky brightness at a given frequency due to the integrated effect of dusty galaxies along a line-of-sight is given by

$$I_\nu = \frac{c}{4\pi} \int_t^{t_0} \left(\frac{a(t)}{a_0}\right)^3 j[\nu a_0/a(t)]\, dt$$

where $j[\nu a_0/a(t)]$ is the luminosity density within a given redshift shell, and the cubic term in the expansion factor $a(t)$ accounts for the dilution of monochromatic surface brightness by the expansion of the universe. The luminosity density thus depends on the evolution of galaxy luminosity with epoch, and the evolution of the number of effective IR-luminous galaxies with redshift (which is the convolution of the galaxy formation rate and the dust forming rate within each galaxy). The problem now is to quantify the evolution.

Little is known about the evolution of the infrared luminosity with redshift, but from the 60 μm IRAS counts (Saunders *et al.* , 1990) there is strong evidence for evolution in either luminosity, number density, or both. However, the IRAS sample is not particularly deep, and the results on evolution may be dominated by the starburst galaxies, so it is unclear how the normal galaxy cirrus component might evolve. Wang (1990a) has developed a model for the time evolution of the mean luminosity of galaxies by considering several models of star-formation within the galaxy. It is preferred here to leave the luminosity evolution as a parameter constrained only by the EBL upper limits, and is given the form $L(z) \propto (1 + z)^\beta$. Since the dust temperature depends on the luminosity of the galaxy by the relation $L \propto T_d^{4+\alpha}$, with α the emissivity as above, the temperature must clearly evolve as $(1 + z)^{\beta/(4+\alpha)}$.

To account for the evolution of the number of dusty galaxies, Wang (1991b) has utilised his model of dust formation in a given galaxy together with a particular model for the galaxy formation rate. Of course, different cosmological models predict different epochs for galaxy formation. As a complementary approach, and since the evolution of dust is directly connected with the chemical evolution of the interstellar medium because the dust is mostly composed of heavy elements (C,N,O,Si ...), it

is considered that the observed rate of evolution of heavy element absorption lines is indicative of the overall dust/galaxy evolution problem. In particular, Steidel, Sargent & Boksenberg (1988) have followed the evolution of the CIV absorption line towards a large sample of quasars, and found that by representing the number density of effective absorbers as $n(z) = n_0\ (1 + z)^{(3+\delta)}$ (where δ equals zero if there is no evolution with redshift other than that due to the expansion effect), then δ = -1.5 for $1 \leq z \leq 4$ and 0 for $z < 1$ (assuming that $\Omega = 1$). The upper redshift limit of 4 can be considered some kind of 'switch-on' epoch, and lies conveniently within the presently favoured redshift range for galaxy formation.

Substituting for all quantities in the previous equation, and assuming an $\Omega = 1$ universe explicitly, then

$$I_\nu \propto \frac{n_0\, c}{4\pi\, H_0} \int_0^{z_{max}} \nu^{3+\alpha}\, (1+z)^{\frac{1}{2}+\alpha+\beta+\delta}\, [e^{h\nu(1+z)^\kappa/kT_d} - 1]^{-1}\, dz$$

where $\kappa = (1 - \frac{\beta}{4+\alpha})$. The intensity is normalised to the 60 μm local luminosity density from Saunders *et al.* (1990). This may result in an overestimate of the intensity at lower frequencies if there is a significant contribution from small grains to the 60 μm datum.

The next important step is to evaluate the anisotropy in the FIR radiation field arising from the discrete nature of the sources and clustering therein. The luminosity density can be represented a the sum of point-like terms $j_\nu = \sum_{i=1}^{n} L_i \delta(\vec{r} - \vec{r_i})$, so that its autocorrelation is given by

$$\langle \delta j(\vec{r_1}).\delta j(\vec{r_2}) \rangle = n \left\langle L^2 \right\rangle \delta(\vec{r_1} - \vec{r_2}) + n^2 \langle L \rangle^2\, \xi(\vec{r})$$

with ξ the galaxy correlation function. The first term corresponds to a shot noise arising from the light concentration within individual galaxies. This is dominated by nearby galaxies, but these are hopefully already catalogued and their effect can be subtracted. The second term results from the clustering of the discrete sources. To evaluate it more specifically, it is useful to rewrite in a form similar to that for the mean foreground intensity.

$$\delta I_\nu(\vec{n}) = \frac{c}{4\pi} \int j[\nu a_0/a(t)] \left(\frac{a(t)}{a_0}\right)^3 \delta(\vec{n})\, dt$$

where $\delta(\vec{n}) = (\delta n_g/n_g)_{\vec{n}}$ is the fluctuation in the galaxy number density in the direction $\vec{n}$. Then, the autocorrelation function is

$$\langle \delta I_\nu(\vec{n_1}).\delta I_\nu(\vec{n_2})\rangle \propto \int\int j[\nu a_0/a(t_1)]\, j[\nu a_0/a(t_2)] \left(\frac{a(t_1)}{a_0}\right)^3 \left(\frac{a(t_2)}{a_0}\right)^3 \langle \delta(\vec{n_1}).\delta(\vec{n_2})\rangle \, dt_1 dt_2$$

The evaluation of this integral is made simpler by replacing the light cone correlation with an equal time correlation (Bond, Carr & Hogan, 1986). Again, $\langle \delta(\vec{n_1}).\delta(\vec{n_2})\rangle$ is recognised as the galaxy autocorrelation function, which may be written as

$$\xi(r) = \left(\frac{r}{r_0}\right)^{-\gamma} (1+z)^{-3-\epsilon}$$

r is the comoving separation between the galaxies, r_0 is the comoving correlation length and the term $(1+z)^{-\epsilon}$ allows for any evolution in the clustering pattern. It can then be shown (Wang, 1991b) that the fractional intensity autocorrelation $C(\theta)$ is given by

$$C(\theta) = \frac{\langle \delta I_\nu(\vec{n_1}).\delta I_\nu(\vec{n_2})\rangle}{I_\nu^2} = B(\frac{1}{2}, \frac{\gamma-1}{2})\, I(\gamma)\, (\sin\theta)^{1-\gamma}$$

where

$$I(\gamma) = \frac{\int_0^{x(t_0)} j^2[\nu(1+z)]\,(1+z)^{-8-\epsilon}\, x(x/r_0)\, dx}{[\int_0^{x(t_0} j[\nu(1+z)]\,(1+z)^{-4}\, dx]^2}$$

assuming $\Omega = 1$. The parameter x is given by

$$x(t) = \int_t^{t_0} \frac{c}{a(t)}\, dt = \frac{2c}{H_0}(1 - \frac{1}{\sqrt{1+z}})$$

Realistically, account must be made of the finite resolution of the beams, of dispersion σ. In the small angle approximation, it follows that

$$C(\theta;\sigma) = B(\frac{1}{2}, \frac{\gamma-1}{2})\, I(\gamma)\, \frac{1}{2\sigma^2} \int_0^\infty (\sin\phi)^{1-\gamma}\, I_0(-\frac{\theta\phi}{2\sigma^2})\, e^{-\left(\frac{\theta^2+\phi^2}{4\sigma^2}\right)}\, \phi\, d\phi$$

For a single beam experiment, the observed fluctuation in intensity corresponds to

$$\left(\frac{\delta I_\nu}{I_\nu}\right) = [2^{1-\gamma}\, \Gamma(\frac{3-\gamma}{2})\, B(\frac{1}{2}, \frac{\gamma-1}{2})\, I(\gamma)]^{\frac{1}{2}}\, \sigma^{(1-\gamma)/2}$$

so that the rms fluctuation is a power-law as the function of the beam size. In practise, for $\sigma > \theta_0$, where θ_0 corresponds to the angle subtended by r_0, the shot-noise contribution (which was previously dropped) scales as σ^{-1}, and can dominate. However, again if the shot-noise is itself dominated by the effect of nearby catalogued galaxies, its effects can be accounted for. The residual fluctuations in the beam are then due to the clustering effects of the sources.

Finally, the observed fluctuations are related to the 2/3 beam geometry of the differencing experiment and converted to the equivalent thermodynamic fluctuations for the CMB. Thus,

$$\frac{\Delta T}{T} = \frac{\Delta I}{I}\frac{I}{I_{CMB}}\frac{e^x - 1}{xe^x}$$

where $x = h\nu/kT_{CMB}$ and

$$\left(\frac{\Delta I}{I}\right)^2 = 2[C(0;\sigma) - C(\theta_b;\sigma)]$$

for a single-subtraction experiment,

$$\left(\frac{\Delta I}{I}\right)^2 = \frac{3}{2}C(0;\sigma) - 2C(\theta_b;\sigma) + \frac{1}{2}C(2\theta_b;\sigma)$$

for a double-subtraction experiment. However, in the calculations which follow, the quoted results refer to the **intrinsic** anisotropy $C(0;\sigma)^{\frac{1}{2}}$. The anisotropy can then be shown to be simply proportional to $\sigma^{(1-\gamma)/2}$.

A number of models have been considered. Initially, the luminosity was allowed to evolve with β taking values between 0 and 4 and the resulting spectral distribution compared to the EBL limits. It is clear that with the assumptions made by the model, the luminosity evolution is constrained to have a power law dependence $\beta \leq 1.5$ to satisfy the Lange *et al.* upper limits (this allows for some lenience in the interpretation of the limits). In fact, the best fit corresponds to $\beta = 1$. For the purposes of establishing upper limits on anisotropies, however, $\beta = 1.5$ will be retained (this is weaker than the $\beta = 3$ used in Banday & Wolfendale, 1990, simply because the upper limits have been reduced), and compared to calculations for $\beta = 0$. This no evolution model is that favoured by deep radio source counts, and applies here if there is a tight correlation between the FIR and radio emission in the sources. Fig. 1 shows the predicted fluxes for the two models.

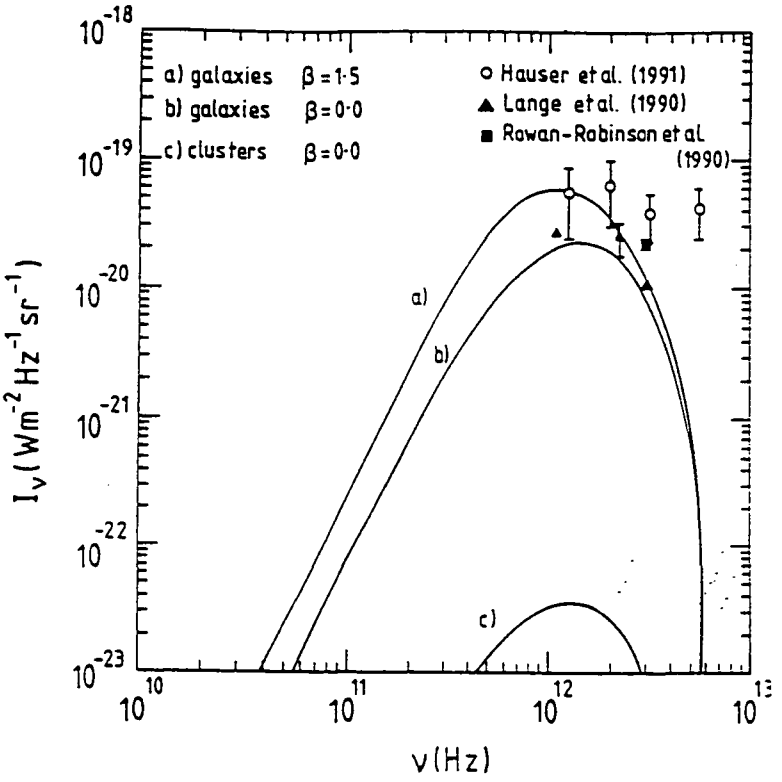

Figure 5.1: Far-infrared spectra for both evolving and non-evolving galaxy models, and for a non-evolving cluster model. See text for details.

To evaluate the anisotropy level, we need to adopt appropriate values for the clustering parameters r_0, γ. For an optically selected sample, r_0 is usually considered to be of order $5h^{-1}$Mpc, with $\gamma \sim 1.7$ - 1.8. recent observations (Shanks *et al.* , 1989) have found evidence for a shoulder feature in the correlation function at about $1.6h^{-1}$Mpc and a break to a steeper slope at $7h^{-1}$Mpc. However, since spiral galaxies tend to avoid the cores of rich clusters, they demonstrate less clustering than ellipticals or non-morphologically separated samples, thus it is to be expected that r_0 will be smaller for spirals. A simple power-law model is adopted, with r_0 set equal to $4h^{-1}$Mpc and the slope to 1.7 (Lahav, Nemeroff & Piran, 1990), the effect of the shoulder feature and break being left for future work. Two possibilities are considered for the clustering: $\epsilon = 0$ corresponds to the clustering remaining fixed in proper coordinates, ie. it is dynamically bound and stable at small scales; ϵ = -1.2 describes a clustering pattern which is fixed in comoving coordinates as is roughly the case for theories such as biassed CDM.

In Table 2, results are recorded for 4 models:

Model 1: No luminosity evolution ($\beta = 0$); no cluster evolution ($\epsilon = 0$)

Model 2: No luminosity evolution ($\beta = 0$); cluster evolution (ϵ = -1.2)

Model 3: Luminosity evolution (β = 1.5); no cluster evolution (ϵ = 0)

Model 4: Luminosity evolution (β = 1.5); cluster evolution (ϵ = -1.2)

The results are applicable to a beam of FWHM 7° as is appropriate to the COBE satellite.

	$\Delta T/T$ ($\times 10^6$)			
ν (GHz)	Model 1	Model 2	Model 3	Model 4
31.5	0.010	0.015	0.024	0.050
53.0	0.024	0.035	0.055	0.116
90.0	0.062	0.086	0.136	0.284
167.0	0.238	0.318	0.490	1.000
230.0	0.616	0.780	1.195	2.391
417.0	10.06	12.13	15.91	29.64
750.0	1643	1837	1845	2935

Table 5.2: Predicted anisotropy due to dust emission from galaxies back to redshift of 4. See text for details of models.

The contributions to all of the COBE frequencies are less than 10^{-6}, so the effect of dust emission from galaxies is effectively negligible. Two other large scale measures against which the results may be compared are those of Melchiorri, Melchiorri & Ceccarelli (1981), who set an upper limit at 417 GHz of 4 $\times$ 10^{-5} for a FWHM of 5° , and Page, Cheng & Meyer (1990) who at 167 GHz and for a FWHM of 3.7° found a monochromatic anisotropy limit at 10° of 1 $\times$ 10^{-4}; this limit would be larger still if convolved with the beam resolution function. Using the $\sigma^{(1-\gamma)/2}$ dependence of the intrinsic anisotropy, the results for 7° at the appropriate frequencies in Table 1 have been scaled to the appropriate resolution. All of the models are unconstrained by the upper limits, although with $\Delta T/T$ = 3.3 $\times$ 10^{-5} model 4 is getting quite close to the Melchiorri, Melchiorri & Ceccarelli upper limit, particularly when it is realised that there is likely to be some contribution from the Milky Way's own dust emission. Once a firm estimate of this contribution can be made, then it may be possible to further constrain dust evolution models for external galaxies. The 230 GHz result can be scaled to the 11 arcsec resolution of the Kreysa & Chini experiment found an upper limit of 2.6 $\times$ 10^{-4}. This limit does not significantly constrain the models. At sub-mm wavelengths, it can be seen that dust emission from external galaxies dominates the CMB fluctuations, thus any measured anisotropies at λ $<$ 0.5 mm are most likely due to the extragalactic sources, which thereby will constrain the FIRB and dust evolution. Finally, using more modest

luminosity evolution of the form $e^{\beta\cdot\tau}$, where β^{-1} is the evolution time-scale in units of the Hubble time, and τ is the look-back time, then for $\beta = 4.3$ (as suggested in Franceschini *et al.* , 1988, for the rapidly evolving component of the radio source counts) then models with and without clustering evolution have anisotropy levels down on the power-law luminosity models by a factor between 3 and 4.

5.2.2 Dust in clusters of galaxies

The existence of dust in the intracluster medium (ICM) has been indicated by extinction observations. Zwicky (1962) estimated the extinction of light from distant clusters of galaxies by nearby ones, whilst more recently Boyle, Fong & Shanks (1988) have found a value of $A_B = 0^m.2$ from a deficiency of UV excess objects behind clusters and groups of galaxies. The existence of dust in the ICM implies that it may be possible to detect its presence through any FIR emission, thus creating another foreground against which the CMB must be observed. Since the ICM is pervaded by hot gas with a temperature usually $\geq 10^7$ K, the dust grains are heated by collisional interactions with the hot plasma. In principle, of course, the intracluster radiation field due to the emission from galaxies within the cluster could contribute to the heating of the dust in the same manner as the interstellar radiation field and dust grains within our Galaxy are in thermal equilibrium. In practice, this effect is negligible compared to the collisional heating, and is likely to remain so even if the galaxy luminosities evolved with redshift as discussed in the previous section. However, such dust grains will be continuously sputtered by the ambient hot gas, so that if any IR emission is to be detected, there must be a continuous replenishment of the grains. Ferrini, Barsella & Greenberg (1987) have demonstrated that the radiation pressure due to the ISRF in a galaxy can result in the ejection of certain dust grains from the galaxy; alternatively dust may be removed from individual galaxies as a result of collisional drag by the predominantly gaseous galactic wind. The actual level of the FIR emission will then depend on the detailed balance of the the injection and sputtering rates in the hot gas. Based on the study of dust grain interactions with a hot gas Burke & Silk (1974) found a typical grain temperature of ~ 30 K, as did Pustil'nik (1975). In the early calculations, the dust temperature was assumed to attain an equilibrium value given by equating the collisional heating rate of the dust to its cooling rate by IR emission. However, Dwek (1986) demonstrated

that below a certain grain size, this breaks down and the particle is stochastically heated by the ambient plasma, so that its temperature will fluctuate. In a detailed study, Dwek, Rephaeli & Mather (1990) consider the FIR emission from the Coma cluster of galaxies, considering the spatial distribution of the dust and its resultant sputtering, and accounting for a variation of grain temperature within the cluster. This temperature dependence results from the variation of the gas density within the cluster, since at the high temperatures which prevail in the ICM an analytic approximation to the dust temperature is given by (Dwek, 1987) $T_d \simeq 57\ n^{0.18}$. The consequence of the model is that the dust is more depleted towards the core of the cluster, so that the observed extinction towards Coma requires a large mass of gas and dust in the outer regions of the cluster.

To estimate the integrated EBL due to cluster dust, and anisotropies therein, it is assumed in what follows that, as a first order approximation, the dust temperature is constant throughout the whole cluster, with a temperature of 20 K which is equal to the estimated cluster core temperature for Coma (Dwek, Rephaeli & Mather, 1990), and that the dust emissivity is the same as that observed in the Galaxy by COBE, namely $\alpha = 1.65$ (although this might not be the case if the efficiency of expulsion of grains from the galaxies within the cluster was a function of grain type in which case the averaged emissivity could depart from the value observed within a given galaxy). The other factors of importance concern the density and luminosity evolution. Since there is little evidence for any X-ray luminosity evolution with redshift, and since the FIR luminosity is connected directly to L_X as both are functions of the properties of the ICM, then a no evolution model is preferred. This makes the integrated flux easier to determine, since if there is no evolution in the gas density and temperature, the dust temperature is the same at all epochs. The density evolution can then be taken as the same as for the individual galaxies which are the source of the IC dust. If there were luminosity evolution, the dust evolution would necessarily have to account for the variation in sputtering rate with redshift, which would modify the density evolution from the galactic values. The cluster spectrum is calculated by assuming a local space density of galaxy clusters of $2 \times 10^{-4} h^{-3} Mpc^{-3}$, $h = 1$, and that the 100 μm intensity of a cluster at the present epoch is 0.2 MJy sr^{-1}, in agreement with the value calculated for the Coma cluster core in Dwek, Rephaeli & Mather.

For the anisotropy calculation, the correlation parameters r_0 and γ are required. Bahcall & Soneira (1984) found from the redshift data for the nearest 100 Abell clusters that a good fit was given by $\xi_{cc} = \left(\frac{r}{25 h^{-1}}\right)^{-1.8}$. This large enhancement of the cluster correlation function over that for galaxies is rather difficult to reconcile with popular models of structure formation, such as CDM. However, several authors have found peculiarities in the Abell catalog which might give rise to excess correlations on large scales. In particular, Sutherland (1988) corrected for large anisotropies in the clustering pattern in redshift space, leading to the reduction of the correlation length to $\sim 14 h^{-1}$Mpc. More recent work (Dalton *et al.* , 1991) using the APM galaxy cluster catalog finds $r_0 = 12.9 \pm 1.4 h^{-1}$Mpc, $\gamma = 2$, whilst the correlation function for cD clusters (West & van den Bergh, 1991) has $r_0 \sim 22 h^{-1}$Mpc, $\gamma = 1.7$. In the calculations which follow, the cluster-cluster correlation function is taken as $\xi_{cc} = \left(\frac{r}{14 h^{-1}}\right)^{-1.8}$. If the Abell determination were correct, the anisotropy amplitude would need to be raised by a factor of $\left(\frac{25}{14}\right)^{1.8} \sim 2.8$.

For the assumed values of the cluster parameters, and allowing no luminosity evolution, the anisotropy expected due to dust emission in clusters of galaxies is of the order 10^{-10} at 31.5 GHz and 5×10^{-10} at 90 GHz. Thus the contribution to the COBE measurements is entirely negligible. At sub-mm wavelengths, the contribution may rise to $\geq 10^{-5}$, but this will still be dominated by the anisotropy due to the dust emission from galaxies. The increase in anisotropy if the clustering of clusters evolves as -1.2 (as with the galaxies themselves) is only $\sim$ 30 - 40%, whilst allowing both luminosity and clustering evolution (ignoring the modifications to the dust equilibrium temperature and densities which this would imply) increases the anisotropy by a factor of order 6 - 8. It seems that if the properties of clusters assumed here is correct (ie. that they are similar to those estimated for Coma) then cluster dust emission is unimportant for CMB observations. If the amount of dust in the cluster core is significantly depleted compared to that in the outlying parts of the cluster, then taking account of the radial temperature profile might lead to a broader dust spectrum at lower frequencies (contributions from lower temperature dust components), however it is not likely that this could raise the predicted anisotropy level by more than an order of magnitude, the cluster dust contribution to CMB observations thus remaining negligible.

5.2.3 Summary

Whilst the cluster dust emission is unlikely to be a problem for CMB observation, the anisotropies resulting from dust in galaxies is certainly of importance at frequencies of a few hundred GHz. CMB limits in this region will help to constrain the evolution of dust in these galaxies as well as primordial anisotropies, and in addition will constrain radio source evolution as as consequence of the tight correlation between the FIR and radio emission from these sources. The integrated radio background itself provides a background against which CMB observations are to be made, and in the next section a review is given of the important results concerned with this problem. Improved calculations concerning the dust contribution to anisotropy measurements requires a detailed model of all the IR emission features of galaxies, and the possible contributions from starburst galaxies (although the effect from such galaxies may not be too different from regular spirals at the COBE frequencies where the cirrus emission is likely to be dominant).

5.3 Fluctuations due to discrete radio sources

The presence of discrete radio sources is of great importance from a number of astronomical standpoints. Firstly, the integrated radiation due to the sources gives a component of the sky brightness which must be removed when attempting to determine either the temperature of the Galactic Synchrotron Radiation, or indeed, the CMB brightness temperature. The brightness temperature T_{ex} of the extragalactic radio emission is well described by

$$T_{ex}[\nu\,(\mathrm{MHz})] \;=\; (23 \pm 5)\,[\frac{\nu}{178}]^{-(2.75\pm0.05)}\,\mathrm{K}$$

where $T_{ex}(178)$ was originally estimated by Longair (1966) and remains in good agreement with the recent analysis of de Zotti & Toffalatti (1989) from which the above equation is taken. At frequencies of the order of a few hundred MHz, all three of the above radiations (away from the Galactic plane) have similar brightness temperatures, and the assumption of two of the values can lead to large errors in the third. Difficulties in the estimation of both T_{ex} and that due to Galactic Synchrotron Radiation at $\nu \sim 500$ MHz has resulted in large error bars on T_{CMB}, making it

problematic to assess the existence or otherwise of a spectral distortion in the CMB (see Sironi, Bonelli & Limon, 1991). Physically, the radio emission results from non-thermal electrons generating synchrotron radiation. The brightness sources, which have been cataloged at a number of frequencies for the whole sky, comprise QSOs and radio galaxies, with the flat spectrum sources corresponding to 'compact' self-absorbed sources. These sources are important in their own right from a cosmological point of view, since, with the assistance of multi-frequency observations, optical identifications and the measurements of redshifts, the evolution of astrophysical sources in the universe has been followed. Such sources were originally studied in a bid to determine cosmological parameters such as q_0 and H_0 by evaluating the variation of the number counts on the sky with flux density. These counts were subsequently found to differ from that expected either for a universe with a 'Euclidean' geometry or a conventional relativistic cosmology, which led to the conclusion that the radio sources were evolving either in luminosity, space density, or both with redshift. Although this leaves the determination of q_0 and H_0 somewhat intractable, it does leave the possibility of determining a formation redshift for galaxies. Since the source surface density increases rapidly with decreasing flux, then a small sky sample may be adequate statistically to determine the properties of faint sources, provided the overall distribution is uniform. The faint sources comprise the QSOs and radio galaxies which make up the bright sources, plus at the faintest flux densities a population of blue galaxies with an as yet uncertain nature. These blue galaxies are responsible for the flattening of the counts at low densities. The interpretation of source counts in general is complicated by the fact that that the sources are an inhomogeneous collection of quasars, radio galaxies, extended and compact sources, all of which may have different local luminosity functions, lifetimes and cosmic evolution.

However, it is the fluctuations which these discrete radio sources impose on the CMB which are of interest in this chapter, and which are now reviewed. On small angular scales, of order a few arcminutes or less, where anisotropy measures are sensitive to both primordial fluctuations and the fluctuations produced by the development of structure at intermediate redshifts, the most accurate work has been performed at the VLA operating at 5 GHz by Martin & Partridge (1988) and Fomalont *et al.* (1988). Fomalont *et al.* have concluded that all of the observed fluctuations are consistent with extrapolated source counts after the removal of

known bright sources from the region of interest. Here, we are interested in the contribution to larger scale anisotropies. A theoretical study of the problem has been made by Franceschini *et al.* (1989) who have taken models which reproduce the observed number counts and convolved the results with a gaussian beam response. Fig. 2 is taken from their paper, and indicates that for the COBE DMRs, the contribution to the intrinsic smoothed anisotropy should lie below 10^{-6}. Similarly, for the Watson *et al.* (1988) observations the discrete source contribution is expected to lie below the 10^{-5} level, such that the Galactic Synchrotron Radiation should still be of the greater importance at 10 GHz.

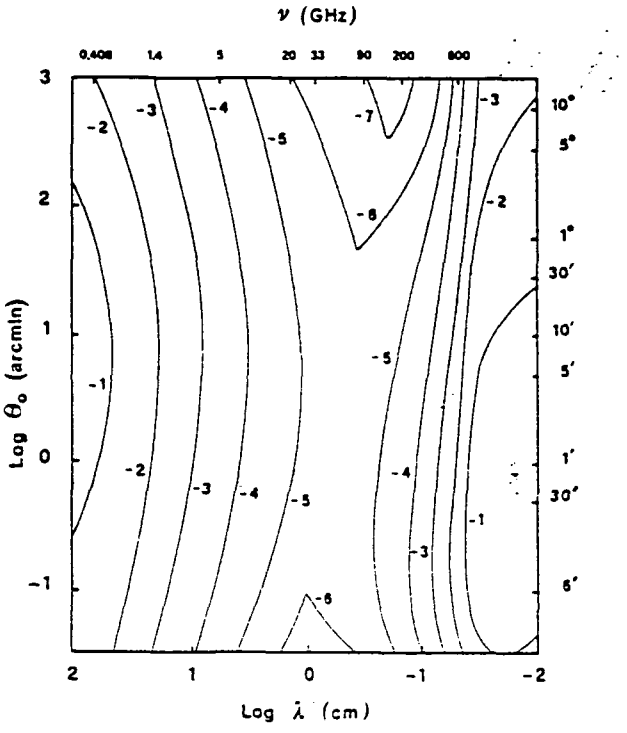

Figure 5.2: Discrete source contributions to single beam measures of $\Delta T/T$ as a function of frequency and angular resolution. Taken from Franceschini *et al.* (1989).

These calculations do not include the effect of clustering, which decreases the effective number of objects in randomly placed cells, and consequently enhances the cell-to-cell fluctuations. An estimate of this effect could be made using the same techniques as for IR luminous galaxies. The correlation functions of radio galaxies are still somewhat uncertain, but recent observations suggest that some classes must be strongly clustered (Peacock & Nicholson, 1991). This implies that although models of the point source contribution to the CMB may need revision, the anisotropic radio background offers the possibility of mapping out large-scale

structure in the universe.

In larger scale experiments, the actual observed temperature differences due to the known sources will almost certainly be required to be evaluated, since although relatively quiet sky regions can be sought, it is unlikely that all bright sources may be avoided, as may be the case for small angle observations. As an example, Watson *et al.* (1988) and Watson (1989) remove all known sources from their survey region using the 10.7 GHz catalog of Kuhr (1981) and spectral information therein. Fig. 3 taken from Lasenby *et al.* (1991) shows the overall fluctuations measured at dec. 40° for the 10GHz 5.6° experiment, together with the point source contributions from Watson *et al.* (the sources have no effect in the region where a claim was originally made for a cosmological signal, and so the conclusions of Chapter 2 regarding the Galactic Synchrotron contribution remain unaltered).

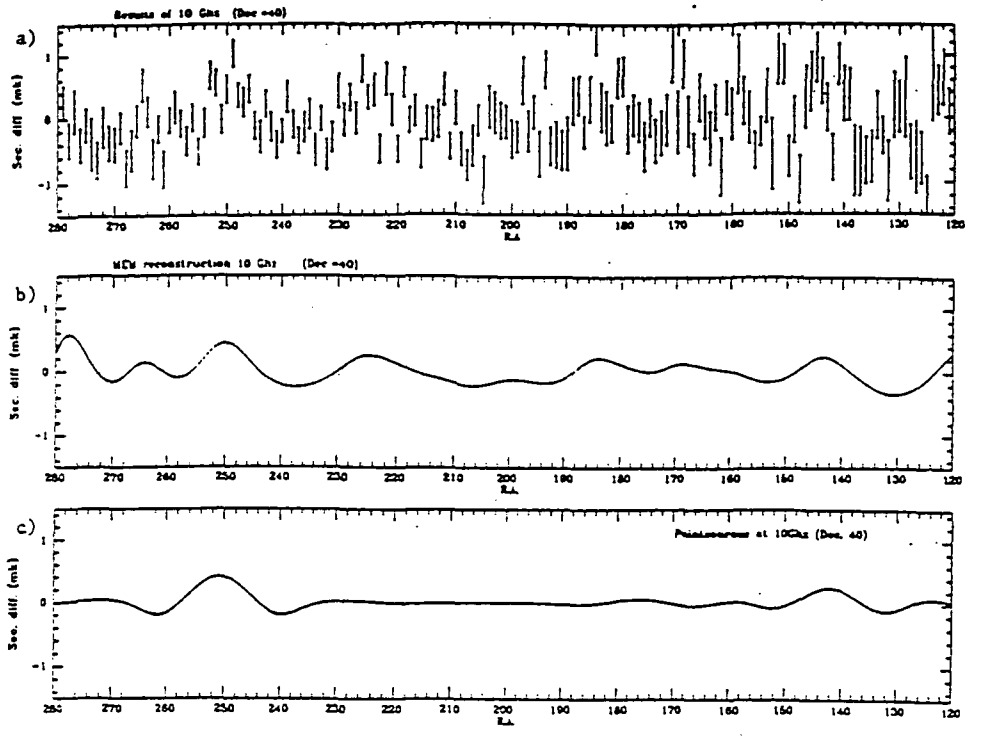

Figure 5.3: From Lasenby *et al.* (1991), the fluctuations seen at 10 GHz using the Jodrell-IAC 5.6° configuration, and the estimated contribution to the second differences from point sources.

Such a procedure will remove bright sources, but fluctuations might also arise from concentrations of many weaker radio sources. The assessment of this contribution requires a complete catalog of all radio sources convolved with the beam profile for observations at a given declination. Unknown strong sources not included in

existing catalogs are rather unlikely since they would need to have highly inverted spectra to avoid detection at the lower frequencies, and such objects are expected to be rare. Again, as in the small-angle anisotropy case, the contribution from weak sources can be assessed statistically from source counts. Banday *et al.* (1991) attempted an alternative method to deduce the contribution from both known and weak unidentified sources. Since for a given catalog, there is a limiting flux below which identifications cannot be made, the object is to relate this limit to the possible induced fluctuations. The problem was studied using the 5 GHz catalog of Langston *et al.* (1990) which lists sources with fluxes above 40 mJy with 99.9% completeness. In particular, second differences for a 5.6° FWHM beam with θ_b of 8.2° were determined for the region R.A.: 270° - 170° , dec: 34° - 39.15° for all sources, and for 4 subdivisions of the sources. The results are reproduced here in Fig. 4 Source by

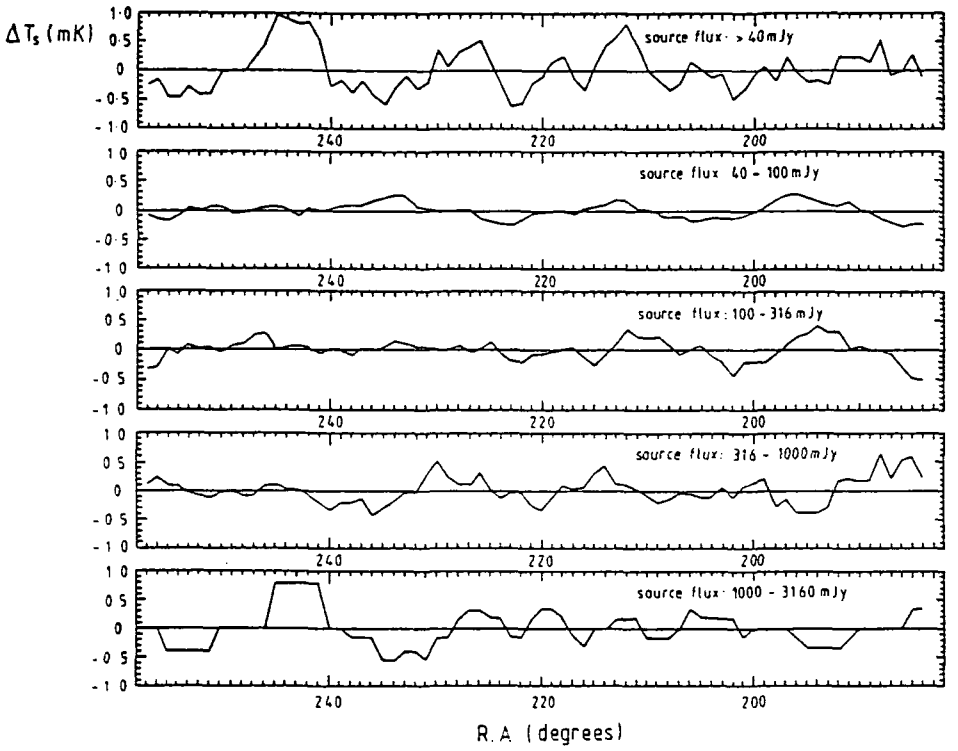

Figure 5.4: Predicted second difference values for radio sources at 5 GHz from the catalog by Langston *et al.* (1990), assuming a FWHM of 5.6° and $\theta_b = 8.2°$. Different source power ranges are indicated.

source extrapolations were then made using published spectral indexes, the results are shown in Fig. 5. To derive the likely contribution from sources below the 40 mJy threshold S_{min}, it was noted that the contribution from the 4 flux bands considered is comparable (within 20%) to the highest band alone, thus it is not unreasonable to assume that the contribution from those sources with $S < S_{min}$ is comparable

to the first flux band above S_{min}. From Fig. 5 then, the limit set by unidentified sources with flux densities less than 40 mJy at 5 GHz is $\sim 5 \times 10^{-6}$ at 10 GHz and 5° resolution, and $\sim 10^{-5}$ for 2° resolution at the same frequency. These results are within a factor of 2 of those in Franceschini *et al.* (which do not include the effects of clustering which are inherent in the catalog, or the beamswitching effect). As the frequency increases, the expected contribution will diminish such that by 20 GHz if all known sources with $S_{5GHz} > 40$ mJy are removed, then the residual discrete source contribution will be of order 10^{-6}, so that beyond 20 GHz point sources should be relatively unimportant until the sub-mm region where the integrated dust emission in galaxies rises rapidly. Some care may need to be taken with time varying sources and flat spectrum sources, although a compilation of bright sources at 31.4 GHz exists (Witzel *et al.* , 1978) enabling their removal from high frequency observations by COBE etc.

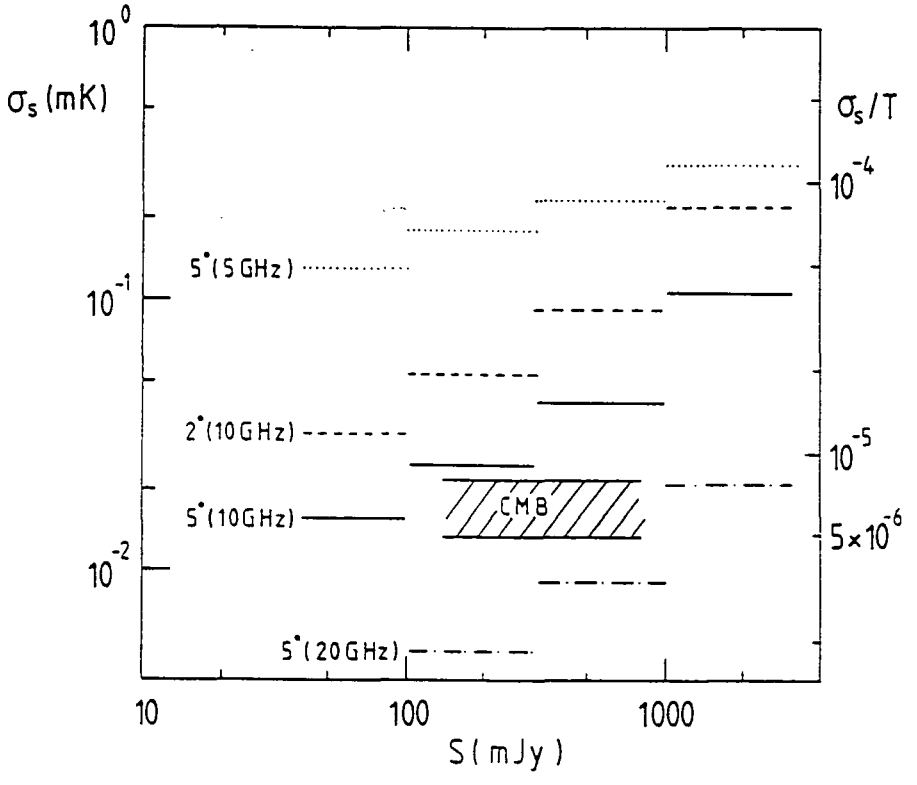

Figure 5.5: rms fluctuation values from the observed 5 GHz point sources and those predicted by extrapolation to 10 and 20 GHz. The contributions from different source power ranges are indicated as are the angular scale and the frequency. The shadowed area indicates the expected cosmological temperature fluctuations.

5.4 Conclusions

As has been found for Galactic emission, the presence of discrete sources emitting at both radio and IR frequencies leaves only a small frequency window for which to make CMB observations without any contamination at greater than the 10^{-6} level. This window is slightly wider than in the Galactic foreground case, here being of order 30 - 300 GHz (for FWHM $\sim 5^{\circ}$), and does depend a little on the experimental resolution. More work on cataloging faint sources remains to be done to confirm these predictions, and the elimination of flat-spectrum and time varying sources is desirable. Radio sources may yet prove to be one of the greatest stumbling blocks to the detection of anisotropies on the scale of a few arcminutes, or even up to degree scale, since clustering may enhance the predicted $\Delta T/T$ given by Franceschini *et al.* .

References

Bahcall, N.A. & Soneira, R.M., 1983. *Astrophys. J.*, **270**, 20.

Banday, A.J. & Wolfendale, A.W., 1990. *Mon. Not. R. astr. Soc*, **245**, 182.

Banday, A.J., *et al.* , 1991. *Astrophys. J.*, **375**, 432.

Beichman, C.A. & Helou, G., 1991. *Astrophys. J. Letts.*, **370**, L1.

Bond, J.R., Carr, B.J. & Hogan, C.J., 1986. *Astrophys. J.*, **306**, 428.

Bond, J.R., Carr, B.J. & Hogan, C.J., 1991. *Astrophys. J.*, **367**, 420.

Boyle, B.J., Fong, R. Shanks, T., 1988. *Mon. Not. R. astr. Soc*, **231**, 897.

Burke, J.R. & Silk, J., 1974. *Astrophys. J.*, **190**, 1.

Cox, P., Krugel, E. & Mezger, P.G., 1986. *Astr. Astrophys.*, **155**, 380.

Dalton, G.B., *et al.* , 1991. *Preprint*, University of Oxford.

Davies, R.D., *et al.* , 1987. *Nature*, **326**, 462.

de Zotti, G. & Toffalatti, L., 1989. *Highlights Astr.*, **8**, 232.

Dwek, E., 1986. *Astrophys. J.*, **302**, 363.

Dwek, E., 1987. *Astrophys. J.*, **322**, 812.

Dwek, E., Rephaeli, Y. & Mather, J.C., 1990. *Astrophys. J.*, **350**, 104.

Fomalont, E.B., *et al.* , 1988. *Astron. J.*, **96**, 1187.

Franceschini, A. *et al.* , 1988. in *Comets to Cosmology*, p. 348, ed. Lawrence, A.,

Springer-Verlag.

Franceschini, A., *et al.* , 1989, *Astrophys. J.*, **344**, 35.

Hacking, P.B. & Soifer, B.T., 1991. *Astrophys. J. Letts.*, **367**, L49.

Hauser, M.G., *et al.* , 1991. in *After the First Three Minutes*, p. 161, eds. Holt, S.S., Bennett, C.L. & Trimble, V., AIP

Helou, G., 1989. in *Interstellar Dust*, p. 285, eds. Allamandola, L.J. & Tielens, A.G.G.M., Kluwer.

Kreysa, E. & Chini, R., 1989. in *Proceedings of the Third ESO-CERN Symposium: Astronomy, Cosmology & Fundamental Physics*, p. 433, eds. Caffi, M., *et al.* , Kluwer.

Kuhr, H., *et al.* , *Astr. Astrophys. Suppl. Ser.*, **45**, 367.

Lange, A.E., *et al.* , 1990. *Preprint.*

Langston, G.I., *et al.* , 1990. *Astrophys. J. Suppl.*, **72**, 621.

Lasenby, A.N., *et al.* , 1991. in *Observational Tests of Cosmological Inflation*, p. 413, eds, Shanks, T., *et al.* , Kluwer.

Longair, M.S., 1966. *Mon. Not. R. astr. Soc*, **133**, 421.

Low, F.J., *et al.* , 1984. *Astrophys. J. Letts.*, **278**, L19.

Martin, H.M. & Partridge, R., 1988. *Astrophys. J.*, **324**, 794.

Matsumoto, T., *et al.* , 1988. *Astrophys. J.*, **329**, 567.

McDowell, J.C., 1986. *Mon. Not. R. astr. Soc*, **223**, 763.

Melchiorri, F., Melchiorri, B.O. & Ceccarelli, C., 1981. *Astrophys. J.*, **217**, 425.

Negroponte, J., 1986. *Astrophys. J.*, **222**, 19.

Page, L.P., Cheng, E.S. & Meyer, S.S., 1990. *Astrophys. J. Letts.*, **355**, L1.

Peacock, J.A. & Nicholson, D., 1991. *Mon. Not. R. astr. Soc*, **253**, 307.

Pustil'nik, S.A., 1975. *Soviet. Astr. Lett.*, **1**, 49.

Rowan-Robinson, M. & Crawford, J., 1989. *Mon. Not. R. astr. Soc*, **238**, 523.

Rowan-Robinson, M., *et al.* , 1990. *Mon. Not. R. astr. Soc*, **246**, 273.

Saunders, W., *et al.* , 1990. *Mon. Not. R. astr. Soc*, **242**, 318.

Shanks, T., *et al.* , 1989. *Mon. Not. R. astr. Soc*, **237**, 589.

Silk, J. & Burke, J.R., 1974. *Astrophys. J.*, **190**, 11.

Sironi, G., Bonelli, G. & Limon, M., 1991. *Astrophys. J.*, **378**, 550.

Steidel, C.S., Sargent, W.L. & Boksenberg, A., 1988. *Astrophys. J. Letts.*, **333**, L5.

Sutherland, W.J., 1988. *Mon. Not. R. astr. Soc*, **234**, 159.

Wang, B., 1991a. *Astrophys. J.*, **374**, 456.

Wang, B., 1991b. *Astrophys. J.*, **374**, 465.

Watson, R.A., *et al.* , 1988. in *Large-Scale Structures and Motions in the Universe*, p. 133, eds Mezzetti, M., *et al.* , Kluwer.

Watson, R.A., 1989. *PhD Thesis*, Victoria University of Manchester.

West, M.J. & van den Bergh, S., 1991. *Astrophys. J.*, **373**, 1.

Witzel, A., *et al.* , 1978. *Astron. J.*, **83**, 475.

Zwicky, F., 1962, in *Problems of Extragalactic Research*, p. 149, ed. MacVittie, G.C., New York: MacMillan.

Chapter 6

Large Scale Structure and CMB Observations

6.1 Introduction

Very recently, several large-scale galaxy surveys have become available which probe to a sufficient depth in the universe to make claims about the existence or otherwise of large-scale structure. Most conventional observations of, for example, the galaxy 2-point correlation function have shown little evidence for structure on scales greater than $\sim 10\ h^{-1}$Mpc, in contrast to the auto-correlation function of Abell clusters which remains positive out to scales $\sim 100\ h^{-1}$Mpc. The angular 2-point correlation function of the APM survey (Maddox *et al.* , 1990) the counts in cells analysis of the QDOT IRAS survey (Efstathiou *et al.* , 1991), observations from the CfA2 survey (Baumgart & Fry, 1991), the evidence for quasi-periodicity in the galaxy distribution on scales of $\sim 100 h^{-1}$(Broadhurst *et al.* , 1990), and the POTENT reconstructions of galaxy peculiar velocities on scales of up to 60 h^{-1}Mpc (Bertshinger *et al.* , 1991) offer support for greater power on large scales than previously demonstrated. The importance of these observations relates to the presently accepted 'standard' model of galaxy formation and evolution. In 'standard' Cold Dark Matter (CDM) theory, it is considered that the universe is closed, ie. $\Omega = 1$, with the difference between the dynamical estimates of Ω_b from, for example, nucleosynthesis arguments, and the

closure density being accounted for by the existence of fundamental particles which are non-relativistic at the epoch of decoupling. The subsequent dynamical evolution of structure in the universe is dominated by these particles. In 'standard' CDM (see Davis *et al.* , 1985) the predicted galaxy 2-point correlation function seems much more in accord with traditional measures on scales greater than 10 h^{-1}Mpc which show little power (ie. a correlation function consistent with zero correlation).

In this chapter, linear theory is employed to test the predictions of CDM, together with some alternative models, against the observations with the intention of matching the observations on the largest scales and determining the consequences for CMB anisotropies. That is, for a given model, we attempt to determine a consistent normalisation based on the observations, and verify its validity by comparison with observational microwave background upper limits. In retrospect, the problem may lie in the area of normalisation of the model power spectra. This is usually done on scales of $\sim$ 8-10 h^{-1}Mpc, where it is assumed that linear theory applies. It may be (and recent theoretical work demonstrates some support for this viewpoint) that even on these scales there exist some residual non-linear effects and that consequently the normalisation should be made on a larger scale where linear theory is more likely to be applicable. This is investigated in some detail. Finally, a discussion is given of the significance of the large scale observations, and the consequences of each of the models considered. It is concluded that the observation of fluctuations in the CMB will provide the cleanest test for the existence of such structure.

6.2 A primer in linear theory: transfer function formalism

It is generally considered that a spectrum of density perturbations is imprinted on the contents of the universe during its earliest stages, and that this spectrum is assumed to be power-law in form, that is, the Fourier components are given by $|\delta_k|^2 \propto k^n$. In the inflationary scenario, which is currently considered to be very promising, these fluctuations arise as quantum fluctuations in scalar fields generated during the inflationary epoch become density fluctuations. A fairly natural outcome of such a scenario is that the initial power-law fluctuations are scale-invariant (ie. for adiabatic perturbations n = 1, for isocurvature fluctuations n = -3). The sub-

sequent evolution of this spectrum then depends critically on the matter content of the universe, since the associated physical processes modify the initial spectrum to a non-power law spectrum by the end of the recombination epoch. Using linear perturbation theory, the fluctuations can be decomposed into scalar, vector (vorticity) and tensor (gravitational wave) modes, although only the scalar modes are likely to be important for structure formation. Numerical integration of the perturbation equations then allows the evolution of the components to be followed. Since each Fourier component evolves independently of the others, an immediate outcome of such calculations is the transfer function for density fluctuations, T(k), which relates the fluctuations at the present epoch t_0 to the fluctuations at the time t_i when they were generated. For adiabatic fluctuations,

$$\delta_k(t_0) \;=\; \delta_k(t_i)\,T(k)$$

For isocurvature fluctuations, the transfer function is defined in terms of the initial spectrum of entropy fluctuations,

$$\delta_k(t_0) \;=\; \delta S_\gamma(t_i)\,T(k)$$

The transfer function thus maps the early universe (post-inflation) power spectrum into the pre-nonlinear post-recombination one, and is characterised by a set of scales reflecting the physical processes which occur once the fluctuation wavelength exceeds the Hubble length.

The form of such a transfer function is given by analytic fits to the linear perturbation calculations. Detailed analysis of such calculations has been performed by a number of authors, and analytic fits to the transfer function in CDM, HDM and WDM cosmologies with varying cosmological parameters (Ω, Ω_b, Ω_{CDM}, Ω_ν, m_ν, Λ) can be found, for example, in Bond & Efstathiou (1984), Bardeen *et al.* (1986), Holtzman (1989) and Efstathiou (1990).

In Fig. 1, an example is given of the power spectra arising from CDM, HDM and WDM scenarios (the spectra are actually presented as the variance, $\Delta^2(k) = \frac{k^3}{2\pi^2} \mid \delta_k \mid^2$, which provides a measure of the density fluctuations $(\delta\rho/\rho)^2_\lambda$ on a scale λ, where $k = \frac{2\pi}{\lambda}$). The transfer functions reflect characteristic scales which depend on the particle content of the universe (see chapter 1 for a relevent discussion).

The calculation of T(k) is clearly a pre-requisite for N-body simulations of non-linear gravitational clustering in particular cosmological models. However, if we are considering observations on sufficiently large scales, then nonlinear evolution should be negligible, and it is valid to compare a linear calculation using the transfer function formalism to the observations. In this chapter, this is the procedure adopted.

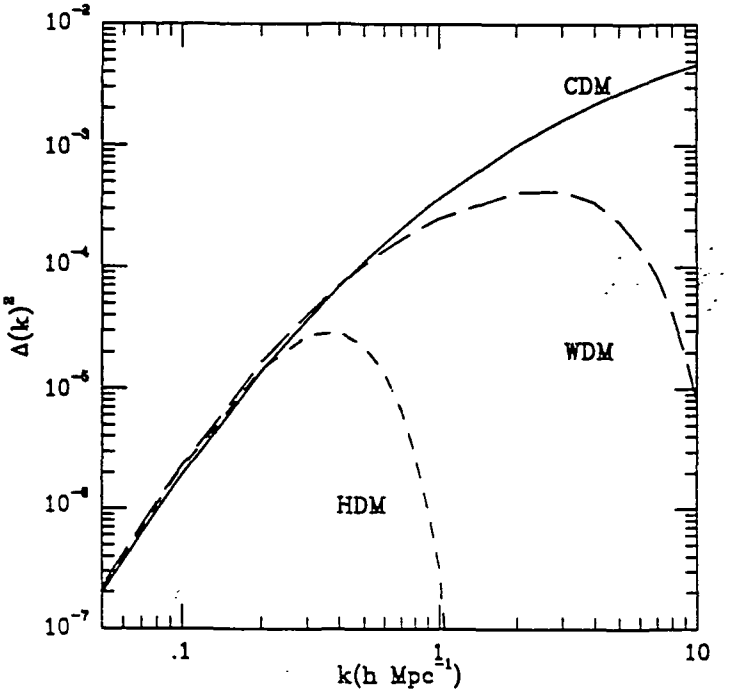

Figure 6.1: CDM, HDM and WDM adiabatic post-recombination power spectra.

6.3 Normalisation

Although the combination of the primordial perturbation spectrum and transfer function fully determines the shape of the pre-nonlinear spectrum, the overall normalisation amplitude still has to be fixed. In principle, this would be determined from the details of the fluctuation generation mechanism in the early universe — for example, the inflation potential in an inflationary scenario. In practice, we must introduce a parameter to characterise the amplitude of the linear spectrum. The most natural normalisation would be to the mass in this case, but unfortunately, there is as yet no completely reliable measure of this. If we consider, for example, the variance of galaxy counts, then an assumption has already been made - that the distribution of galaxies is the same as the underlying mass distribution. The

bulk motions of galaxies on large scales would trace the mass distribution, but it is questionable whether sufficient numbers of observations exist to provide a usable rms value. Similarly, fluctuations in the CMB, which can be directly related to the linear theory amplitude, have yet to be detected. To account for the 'light-traces-mass' problem, a biasing factor b_ρ has been introduced, which is unity if mass does trace the galaxy distribution, and greater than one if galaxies are more clustered than the mass.

To fix the normalisation, two methods have been widely used. The first is based on the second moment of the mass correlation function ξ_ρ,

$$J_3 = \int_0^R r^2 \xi_\rho \, dr = b_\rho^{-2} \int_0^R r^2 \xi_{gg} \, dr$$

where ξ_{gg} is the galaxy 2-point autocorrelation function. This turns out to be a very useful measure of the linear fluctuation amplitude since if R is chosen in the regime where $\xi_\rho \ll 1$ then the integral grows according to linear theory even if the fluctuations on scales $\ll$ R are very nonlinear (Groth & Peebles, 1976). The form for J_3 in terms of the power spectrum is given in the next section. Normalisation is then fixed by comparison with J_3 estimated from the CfA redshift survey. From an analysis of the spatial correlation function Davis & Peebles (1983) find,

$$J_3(10\,h^{-1}\ \mathrm{Mpc}) \simeq 270\,h^{-3}\ \mathrm{Mpc}^3$$

with 10 h^{-1}Mpc being about the largest scale on which J_3 may be estimated from this survey. Note that, by using this normalisation, one is assuming consistency between the shape of the observed correlation function and that predicted by linear theory. The data may still not be good enough to make such a direct comparison.

The second method involves the variance of the mass distribution when sampled in randomly placed spheres of radius R. The predicted variance of the density field is then,

$$\sigma_\rho^2(R) = \sum_k |\, \delta_k \,|^2 \, W^2(kR) = b_\rho^2 \sigma_{gal}^2$$

where W(kR) is the Fourier Transform of the spherical window function (see next section). The galaxy distribution has unit variance when sampled in spheres of

radius $\sim 8\ h^{-1}$Mpc. Normalisations performed by both methods generally agree to $\sim 10\%$ for non-pathological power spectra.

Unfortunately, 8 $h^{-1}$and 10 h^{-1}Mpc may not be sufficiently large scales for the normalisation to be reliable – linear theory may not be valid on these scales. Normalisations should more likely be made on larger scales where linear theory is more nearly correct. Until recently, observations on large scales have been sufficiently uncertain to exclude this procedure, but with the advent of the newer deeper surveys it may now be possible to normalise in a more linear regime. In this chapter, predictions from various models normalised in the standard $\sigma^2(8\,h^{-1})$ fashion are compared to the new observations allowing the consistency of the normalisation to be challenged. The effect of normalising on larger scales is also investigated for the standard CDM model, particularly with respect to CMB upper limits.

Normalising on larger scales in linear theory will itself result in the overestimation of quantities on smaller scales. However, this can simply be attributed to non-linear evolution of fluctuations on the scales where it has been recognised that linear theory may not apply – the theoretical understanding of the complicated nonlinear gravitational dynamics and possible hydrodynamic processes is still in its infancy. By use of the Zel'dovich approximation to calculate the evolution of density perturbations in an $\Omega = 1$ universe, Hoffman (1987) has noted that the use of linear theory on a scale of 8 h^{-1}Mpc overestimates the normalisation amplitude by a factor of $\sim \left(\frac{5}{3}\right)^2$. This would seem to imply that, if normalised on a larger scale where linear theory is applicable, the linear theory calculation on 8 h^{-1}Mpc should be scaled by a factor of order $\left(\frac{5}{3}\right)^{-2}$. This will also be investigated. Similar investigations by Martínez-González & Sanz (1991) reach similar conclusions (they suggest that the overestimate is $\sim 0.55^{-2}$ and also demonstrate an Ω-dependence for the correction). The conclusions reached by these methods are themselves subject to doubt, however, since the Zel'dovich approximation may well be no more accurate than the linear calculations. The question of normalisation is then still a subject for debate. Indeed, the normalisations discussed above themselves may not be appropriate for models which are not of the gravitational clustering hierarchy type. Peebles *et al.* (1991) have suggested that using the value $\sigma^2(20\,h^{-1}) = 0.25$ would provide a normalisation more suitable to explain the large-scale structure claimed in recent surveys.

6.4 Quantities in linear theory

From this point unless otherwise stated, reference to the power spectrum will imply the post-recombination power spectrum – $| \delta_k |^2 = A\ k^n\ T^2(k)$ where it is assumed that the primordial spectrum is of power law form, and A is the normalisation constant. Several quantities will now be defined in linear theory in terms of the power spectrum,

i) J_3 integral: on a scale R the J_3 integral is defined as

$$J_3 = \int_0^R r^2\, \xi(r)\, dr$$

Since ξ is the Fourier Transform of the power spectrum, it follows that,

$$J_3 = \left(\frac{1}{2\pi^2}\right) \int_0^\infty | \delta_k |^2\ (\sin kR - kr \cos kR)\, \frac{dk}{k}$$

This is to be compared to the values determined from the CfA survey.

ii) Variance in the mass distribution: The variance in the mass distribution on a given scale refers to the rms fluctuation on that mass scale. Determination of this quantity is done as follows: consider a volume V_W which on average contains a mass M, place it at all points in space, then evaluate the rms mass fluctuation. The actual volume considered is determined by the window function which smoothly defines both the boundaries of the volume V_W and the mean mass $\overline{\rho}\ V_W$ such that

$$V_W = 4\pi \int_0^R r^2\, W(r)\, dr$$

The mass fluctuation on the mass scale $M = \overline{\rho}\ V_W$ is then given in terms of the density contrast and window function by,

$$\left\langle \left(\frac{\delta M}{M}\right)^2 \right\rangle = \sigma^2 = \left\langle \left(\int \delta(\vec{x} + \vec{r})\, W(r)\, d^3r \right)^2 / V_W^2 \right\rangle$$

and after a little Fourier algebra this turns out to be,

$$\sigma^2(R) = \frac{1}{2\pi^2} \int_0^\infty k^2\ | \delta_k |^2\ \frac{| W_k |^2}{V_W^2}\, dk$$

where W_k is the Fourier Transform of the window function.

Three window functions will be employed in this chapter - spherical, gaussian and cubic to be compared to measures from the CfA survey and the QDOT IRAS galaxy redshift survey. The simplest window function is the spherical which refers to the mass variance in spherical volumes with a sharply defined surface at radius R. the top hat function as it is also referred to is defined by,

$$W(r) = \begin{cases} 1 & r \leq R \\ 0 & r > R \end{cases}$$

$$V_W = \frac{4}{3}\pi R^3$$

$$W_k = 4\pi R^3 [\frac{\sin kR}{(kR)^3} - \frac{\cos kR}{(kr)^2}]$$

Thus we define the variance in a spherical volume of radius R as,

$$\sigma_s^2(R) = \frac{1}{2\pi^2}\frac{9}{r^6}\int_0^\infty \mid \delta_k \mid^2 [\sin kR - kR\cos kR]^2 \frac{dk}{k^4}$$

The gaussian window function has been used by Saunders *et al.* (1991) to analyse the QDOT IRAS survey. The window function is of the form $W(r) = e^{-r^2/2R^2}$ leading to the result,

$$\sigma_g^2 = \frac{1}{2\pi^2}\int_0^\infty k^2 \mid \delta_k \mid^2 e^{-k^2R^2} dk$$

The final window function – the cubic– was employed by Efstathiou *et al.* (1990) also to analyse the QDOT IRAS survey. The aim with this function is the determination of the mass variance in a cubic cell of side L. It can be shown that,

$$\sigma_c^2(L) = \frac{1}{(2\pi)^3}\int\int\int \mid \delta_k \mid^2 \frac{\sin^2(k_xL/2)}{(k_xL/2)^2}\frac{\sin^2(k_yL/2)}{(k_yL/2)^2}\frac{\sin^2(k_zL/2)}{(k_zL/2)^2} d^3k$$

As usual, if galaxies do not trace the mass distribution, all results should be scaled by $b_\rho{}^{-2}$.

iii) Peculiar Velocities: Determination of the peculiar velocity field provides a direct probe of the underlying mass distribution, since no assumption needs to be made about the relationship between mass and light – the galaxies in this case merely act as test particles to measure the local gradient of the gravitational field. The actual observation of peculiar velocities is difficult since the relative errors increase with distance,but new techniques may now be producing some reliable results. In a linear analysis of the evolution of density perturbations, the peculiar velocity of a particle can be decomposed into an irrotational and rotational part. The rotational part does not couple to the density inhomogeneities and can be shown to decay away as the cosmological scale factor, $a(t)^{-1}$. The rotational piece does couple to the density field of the universe as,

$$\vec{v_{\|}}(k) = \frac{a(t)}{ik}\,\dot{\delta}_k + \frac{\vec{const}}{a(t)}$$

where the constant decays away as with its rotational counterpart. The peculiar velocity is then solved for as,

$$\vec{v}(\vec{r},t) = \frac{\vec{const}}{a(t)} + \frac{2}{3}\,(\Omega_0\,H_0)^{-1}\,\left(\frac{d\,\ln\delta}{d\,\ln a}\right)\,\vec{g}(\vec{r},t)$$

$\vec{g}$ defining the peculiar acceleration field. It is then possible to compute the rms peculiar velocity in terms of the power spectrum, but far more convenient is the rms peculiar velocity averaged over a volume defined by the window function W(r) and its Fourier Transform W_k,

$$v_p^2(r) \;=\; \frac{H_0^2}{2\,\pi^2}\,\left(\frac{d\,\ln\delta}{d\,\ln a}\right)^2\,\int_0^\infty\,\mid\delta_k\mid^2\,\frac{\mid W_k\mid^2}{V_W^2}\,dk$$

where a is the cosmological expansion parameter. A good analytic approximation to $\left(\frac{d\,\ln\delta}{d\,\ln a}\right)$ is $\Omega^{0.6}$ (Peebles, 1980). Both gaussian and spherical window functions have been employed, and a combination of the two, the gaussian providing smoothing of data on small scales so that linear theory is applicable, is also possible.

iv) Anisotropies in the CMB: In Chapter 1 the theoretical framework for evaluating CMB anisotropies has been briefly described. Here, the calculation of values is related to the transfer function formalism as closely as possible. Recall that temperature fluctuations in the CMB arise from 5 distinct physical effects:

1. our peculiar velocity with respect to the cosmic rest frame (dipole anisotropy)
2. fluctuations in the gravitational potential on the surface of last scattering (Sachs-Wolfe effect)
3. fluctuations intrinsic to the radiation field itself on the last scattering surface
4. the peculiar velocity of the last scattering surface
5. damping of anisotropies during a reionisation epoch after decoupling

The natural angular scale dividing the contributions from the physical effects is given by the Hubble scale at decoupling which subtends an angle of,

$$\theta_{\rm dec} = 0^{\circ}.87\,\Omega_0^{\frac{1}{2}}\,(z_{\rm dec}/1100)^{-\frac{1}{2}}$$

Angular scales smaller than this correspond to comoving lengths smaller than the horizon at decoupling where the last three effects dominate the contributions to the anisotropy, larger scale anisotropies correspond to super-horizon scales at decoupling.

- Sachs-Wolfe anisotropies: These arise as stated above from fluctuations in the gravitational potential on the last scattering surface. Such anisotropies are simple to evaluate since they probe lengths that are super-horizon sized at decoupling and are therefore insensitive to microphysical processes taking place during the recombination epoch. Thus, for scales $\geq 1^{\circ}$, we need only consider the primordial perturbation spectrum (ie. $\mid \delta_{\rm k} \mid^2 \propto {\rm k}^{\rm n}$) in calculations.

  The theoretical expectation for the rms value of $\Delta T/T$ can be evaluated rather simply in terms of the temperature auto-correlation function $C(\theta)$. Observationally, however, it is the smoothed correlation function $C_\sigma(\theta)$ which is important, the smoothing arising from the finite beamwidth of the antenna (the beam is generally assumed to be gaussian in shape). This implies that the FWHM of the beam $\simeq 2.35\ \sigma$. As noted in Chapter 1, the observed rms temperature fluctuations observed for a two-beam experiment with beamthrow $\theta_{\rm b}$ is,

$$\left(\frac{\Delta T}{T}\right)^2 \;=\; 2\,[C_\sigma(0) - C_\sigma(\theta_{\rm b})]$$

whilst for a three beam experiment,

$$\left(\frac{\Delta T}{T}\right)^2 = \frac{3}{2} C_\sigma(0) - 2\, C_\sigma(\theta b) + \frac{1}{2} C_\sigma(2\theta_b)$$

To calculate anisotropies in the Sachs-Wolfe regime, it is best to construct the temperature fluctuations on the sky in terms of the spherical harmonic decomposition of the plane-wave components,

$$\frac{\Delta T}{T} = \frac{1}{4} \sum_k \sum_l (2l+1)\, \Delta_l(k, t_0)\, P_l(\mu)\, e^{i\mathbf{k}.\mathbf{x}}$$

where $\Delta_l(k,t_0)$ is the brightness fluctuation. Writing $\Delta T/T$ in spherical harmonics

$$\frac{\Delta T}{T} = \sum_m \sum_l a_{lm}\, Y_{lm}(\theta, \phi)$$

where θ, ϕ are spherical angles on the sky, the predicted auto-correlation function for two antennae whose response is well-modelled by a gaussian of angular width σ is given by

$$C_\sigma(\theta) = \left\langle \frac{\delta T(\mathbf{x_1})}{T} . \frac{\delta T(\mathbf{x_2})}{T} \right\rangle = \frac{1}{4\pi} \sum_{l=2}^{\infty} (2l+1) \left\langle |\, a_{lm}\, |^2 \right\rangle P_l(\hat{\mathbf{x}}_1.\hat{\mathbf{x}}_2)\, e^{-[(l+\frac{1}{2})\sigma}$$

where $\hat{\mathbf{x}}_1.\hat{\mathbf{x}}_2 = \cos\theta$. The coefficients a_{lm} can be shown to be given by

$$\left\langle |\, a_{lm}\, |^2 \right\rangle = \frac{1}{2\pi} \int_0^\infty |\, \tilde{h}\, |^2\, j_l^2(k\tau)\, \frac{dk}{k^2}$$

with τ the conformal time, and h the scalar metric perturbation (fluctuation in the gravitational potential) in linear theory (see Efstathiou, 1990, p.56 for more details). For a power law spectrum of perturbations, $|\, h\, |^2 \propto k^n$, the above equation reduces to,

$$\left\langle |\, a_{lm}\, |^2 \right\rangle = \left\langle |\, a_2\, |^2 \right\rangle \frac{\Gamma(9-n)/2}{\Gamma[(3+n)/2]} \frac{\Gamma[(2l+n-1)/2]}{\Gamma[(2l-n+5)/2]}$$

where a_2 the rms quadrupole moment. This is a rather convenient form in which to cast $\Delta T/T$, since we can relate a_2 to the amplitude of linear perturbations at the present epoch. If we write the fractional density perturbation in the matter at epoch τ as

$$|\, \delta_k\, | = B(k) \left(\frac{\tau}{\tau_0}\right)^2$$

(the factors of τ arising since the metric grows with conformal time as τ^2) then the amplitude of the quadrupole moment is

$$| a_2 |^2 = \frac{8}{\pi} \frac{1}{\tau_0^4} \int_0^\infty | B(k) |^2 \, j_2^2(k\tau_0) \frac{dk}{k^2}$$

where $\tau_0 = 2c/H_0$ ($\Omega = 1$), the shape of B(k) being fixed by the initial perturbation spectrum and the transfer function. The amplitude can be evaluated by the usual normalisation procedures (though if $\Omega \neq 1$ account must be made for the slower rate of growth of perturbations in such a universe).

- Small-angle anisotropies: The evaluation of $\Delta T/T$ on angular scales $\leq 1^\circ$ is a more complex procedure, since certain physical effects conspire to modify the photon perturbations on different scales. In particular, one must consider the 'washing-out' of anisotropies due to the finite thickness of the last scattering surface, the damping of small-scale fluctuations arising from the imperfect coupling between baryons and photons, and the generation of temperature fluctuations for those perturbations with wavelengths smaller than the Jeans length at recombination by photons scattering off moving electrons. An accurate computation of these processes requires the numerical solution of the collisional Boltzmann equation for the photons. The approach to such calculations is described in some detail in Bond & Efstathiou (1987). From this one obtains the Fourier transform of the temperature fluctuation on the last scattering surface $\delta_T(\mu,k)$ (where μ is the direction cosine of the propagation direction of the plane wave); it is then relatively straightforward to calculate the CMB correlation function. For two antennae,

$$C_\sigma(\theta) = \frac{1}{4\pi^2} \int_0^\infty k^2 \, dk \int_{-1}^1 | \delta_T(\mu, k) |^2 \, e^{-4k^2 H_0^{-2}(1-\mu^2)\sigma^2} \, j_0[2kH_0^{-1}(1-\mu^2)^{\frac{1}{2}}\theta]$$

Such calculations have been performed by a number of authors, some of whom have provided analytic fits to the unsmoothed correlation functions for a variety of models (including models with non-closure density and positive cosmological constants – see Bond & Efstathiou (1984), Holtzman (1989), Efstathiou (1990) and Fukugita, Sugiyama & Umemura (1990) for example. Such fits will be employed where appropriate, however these can only be found for scale-invariant spectra.

When analytic fits are not available, the method outlined in Fukugita & Umemura (1989) could be employed to determine the small-scale anisotropy level. However, this is only accurate to within a factor of 2 - 3 and so cannot really place particularly stringent constraints on the models, and is not attempted here.

6.5 Observational Results

In the calculations which follow, results will be compared with the measures of large-scale structure and CMB anisotropy limits in Tables 1 and 2.

Parameter	Scale R (h^{-1} Mpc)	Value	Source
σ_s^2	8.0	1.0	
	10.0	0.81	
	20.0	0.25	Peebles *et al.* (1991)
J_3	10.0	270 $h^{-3}Mpc^3$	Davis & Peebles (1983)
σ_g^2	5.0	0.436± 0.091	
	10.0	0.184± 0.050	Saunders *et al.* (1991)
	15.0	0.0669± 0.019	
σ_c^2	10.0	0.68 - 1.10	
	20.0	0.31 - 0.57	
	30.0	0.17 - 0.38	Efstathiou *et al.* (1990)
	40.0	0.14 - 0.32	
	60.0	0.017 - 0.11	
$\langle v_p^2 \rangle^{\frac{1}{2}}$	40.0[a]	388± 67 kms^{-1}	
	60.0[a]	327± 82 kms^{-1}	Bertshinger *et al.* (1990)

Table 6.1: Observational constraints on large-scale structure. *a*: with additional smoothing on a scale 12 h^{-1} Mpc.

6.6 The CDM model

The currently most popular model for the origin of structures in the universe is the Cold Dark Matter model. In such a model, dark matter particles (motivated by the twin desires to reconcile dynamical estimates of Ω in clusters with estimates of the visible content of the universe, and to make Ω equal to the closure density in accord with the inflationary universe model) are in the form of weakly interacting massive

Group	σ	θ_b	2/3 beam[a]	$\Delta T/T$ ($\times 10^6$)	Reference
UW	0.62'	4.5'	3	24.0	Uson & Wilkinson (1984)
OVRO	0.77'	7.15'	3	17.0	Readhead *et al.* (1989)
UCSB	13.0'	1.0°	2	35.0	Meinhold & Lubin (1991)
Jodrell-IAC	3.5°	8.2°	3	37.0[b]	Davies *et al.* (1987)
Rome	2.2°	6.0°	2	6.7[c]	de Bernardis *et al.* (1991)
COBE	3.0°	60.0°	2	40.0	Smoot *et al.* (1991)
a_2				30.0	

Table 6.2: Upper limits on CMB anisotropies. *a*: see Chapter 1; *b*: see Chapter 2; *c*: this limit for n = 1 spectral index, limit becomes 7.3×10^{-6} for n = 0.2, and 7.28×10^{-6} for n = 0.

particles with mass > 1 GeV. Such particles, to a good approximation, can be considered to have always had negligible thermal velocities, hence the nomenclature 'cold'. The formation of structure in such a model is hierarchical, the first objects to form being of sub-galactic size. These objects then break away from the general expansion and virialise into gravitationally bound objects. Bigger structures form later through tidal interaction and mergers of smaller objects. The formation of structure in a CDM universe has been investigated in some detail in a series of numerical simulations by Davis *et al.* (1985). The 'standard' model assumes h = 0.5 and $b_\rho = 2$.

Calculations of the linear transfer function for adiabatic CDM models have been performed by a number of authors (see section 2 for references).Here, the transfer function determined by Bond & Efstathiou (1984) is employed.

$$T(k) = (1 + (ak + (bk)^{1.5} + (ck)^2)^\nu)^{-\frac{1}{\nu}}$$

where $a = 6.4\ (\Omega h^2)^{-1}$, $b = 3.0\ (\Omega h^2)^{-1}$, $c = 1.7\ (\Omega h^2)^{-1}$, and $\nu = 1.13$. These parameters are strictly valid only in the limit $\Omega_b < \Omega_{CDM}$. Examining the parameters a, b, c, ν in Table 1 of Bond & Efstathiou, a clear dependence on Ω_b is observed. In the calculations which follow, however, the quoted transfer function will be of sufficient accuracy (that is, only models with low baryon contents are being considered). When $\Omega_b$becomes comparable to Ω_{CDM}, that is, when the baryons become dynamically important, this simple fit and the $(\Omega h^2)^{-1}$ scaling breaks down and the transfer function develops oscillations. As $\Omega_b \gg \Omega_{CDM}$, the oscillatory transfer function of adiabatic baryon dominated models is recovered (see Efstathiou, 1990).

In Table 3, calculations are presented for various quantities evaluated from linear theory for CDM models with $\Omega = 1$ and $h = 0.5, 1$ (the $h = 1$ case is possibly a little extreme, resulting in some timescale problems for globular clusters). The values assume $\sigma_s^2(8\,h^{-1})$ normalisation.

Quantity	Scale (h^{-1}Mpc)	h = 1	h = 0.5
σ_s^2	8.0	1.0	1.0
	10.0	0.589	0.644
	20.0	0.093	0.137
J_3	10.0	$279\,h^{-3}$Mpc^{-3}	$308\,h^{-3}$Mpc^{-3}
σ_g^2	5.0	0.519	0.578
	10.0	0.080	0.121
	20.0	0.009	0.019
σ_c^2	10.0	1.682	1.532
	20.0	0.328	0.392
	30.0	0.110	0.160
	40.0	0.048	0.070
	60.0	0.012	0.018
$\langle v_p^2 \rangle^{\frac{1}{2}}$	40.0	195.8 kms^{-1}	316.6 kms^{-1}
	60.0	149.8 kms^{-1}	251.9 kms^{-1}

Table 6.3: Linear theory calculations for a CDM model

For the σ_g^2, σ_c^2 calculations, nonlinear effects will suppress the calculated values on the smallest scales from those recorded in the table calculated using the linear approximation. This explains the discrepancies with values in Saunders *et al.* (1991) and Efstathiou *et al.* (1990) which quote values estimated from averages over a number of numerical simulations. It should also be noted that since the calculations are normalised using a value for $\sigma_s^2(8\,h^{-1})$ estimated from an optically selected sample, and since the IRAS galaxies are mainly spirals which tend to avoid densely clustered environments, the predictions for σ_g^2, σ_c^2 on the smallest scales will be slightly overestimated. The difference in the quoted values for the peculiar velocities and those in Bertshinger *et al.* (1991) can be traced to their adoption of the linear transfer function given in Vittorio & Silk (1985). The results assume $b_\rho = 1$. However, if we interpret the results as pertaining to measures of the galaxy distribution rather than in the mass distribution where $b_\rho^2\ \sigma_s^2(R\,h^{-1})_{mass} = \sigma_s^2(R\,h^{-1})_{galaxy}$, and since the quantities are normalised using $\sigma_s^2(8\,h^{-1})(mass) = 1/b_\rho^2$, the bias factor is eliminated in this interpretation except in the case of peculiar velocities which relate

directly to the mass distribution. For a non-unity value of b_ρ, $\left\langle v_p^2 \right\rangle^{\frac{1}{2}}$ should be scaled by $1/b_\rho$ in order to compare with the observational constraints. The results for the CMB calculations for the same normalisation and again assuming $b_\rho = 1$ are provided in Table 4.

	$\Delta T/T$ ($\times 10^6$)	
Experiment	h = 1	h = 0.5
UW†	2.16	4.09
OVRO†	4.05	7.89
UCSB†	8.47	15.93
Jodrell-IAC	2.75	5.30
Rome	3.27	6.31
COBE	6.10	11.8
a_2	4.24	8.18

Table 6.4: Linear theory calculations of CMB fluctuations for a CDM model. † calculated from the analytic fits to the correlation function provided in Efstathiou (1990), scaled to the quadrupole calculation quoted here.

If there is biasing, then values of $\Delta T/T$ should be scaled by $1/b_\rho$. That the UCSB South Pole experimental configuration yields the largest predicted values should not be regarded as surprising since the apparatus was designed to provide the maximal test for CDM.

Comparing the results with the observational data in Table 2, it is clear that there is no problem with either model as far as the predicted $\Delta T/T$ is concerned, although the new Rome figure, if confirmed, indicates that the observation of genuine anisotropies is very close (the limit is very sensitive to the technique used to remove foreground dust emission, however). Considering the results on large-scale structure in Table 3, both models go some way to accounting for the structure observed, although almost without exception the results lie below the observations. Those which do not are themselves on a sufficiently small scale that the linear theory calculation must be called into doubt.

To help the analysis, it is useful to compare the normalisation amplitude required to reproduce the observational results relative to the usual $\sigma_s^2(8\,h^{-1})$ normalisation. Figs. 2 and 3 show the situation for the h = 1 and 0.5 cases respectively. Note that the normalisation scale is not the same as the scale quoted in the above tables.

This is a consequence of the different window functions employed: to make a more meaningful comparison the normalisation radius R_{eff} is defined by equating the volume in a spherical of radius R_{eff} to the volume defined by the appropriate window function. Thus for the gaussian window,

$$\frac{4}{3}\pi R_{eff}^3 = (2\pi)^{\frac{3}{2}} R^3$$

$$R_{eff} = 1.555 R$$

whilst for the cubic cell window function

$$\frac{4}{3}\pi R_{eff}^3 = R^3$$

$$R_{eff} = R/1.612$$

A correction also needs to be made when comparing calculation to observation in that the IRAS results correspond to quantities determined in redshift space. Kaiser (1987) demonstrated that a density perturbation as measured in redshift space has an enhanced amplitude over the value that would be determined in real space, the amplification factor being $(1 + \frac{2}{3}\frac{\Omega^{0.6}}{b_\rho} + \frac{1}{5}\frac{\Omega^{1.2}}{b_\rho^2})$. All calculated values in the figures are corrected appropriately.

Now consider Fig. 2; it is clear that the standard normalisation scheme underpredicts the observational data on scales $> 10\ h^{-1}$Mpc, the effect in some cases being greater than 2.5σ. However, the h = 1 case is rather extreme as already noted, so instead consider Fig. 3 which represents the standard h = 0.5 model with no bias. Again, there is some underprediction of the larger scale measures, but now the results are all consistent with the standard normalisation to better than 1.5σ (the worst case being for $\sigma_g^2(20\,h^{-1})$). For both figures, the point at $\sim 6\,h^{-1}$Mpc lies below the standard normalisation, that is, the value is overpredicted. This is easily understood in terms of nonlinear effects - the amplitude predicted by linear theory is unlikely to be accurate on this scale.

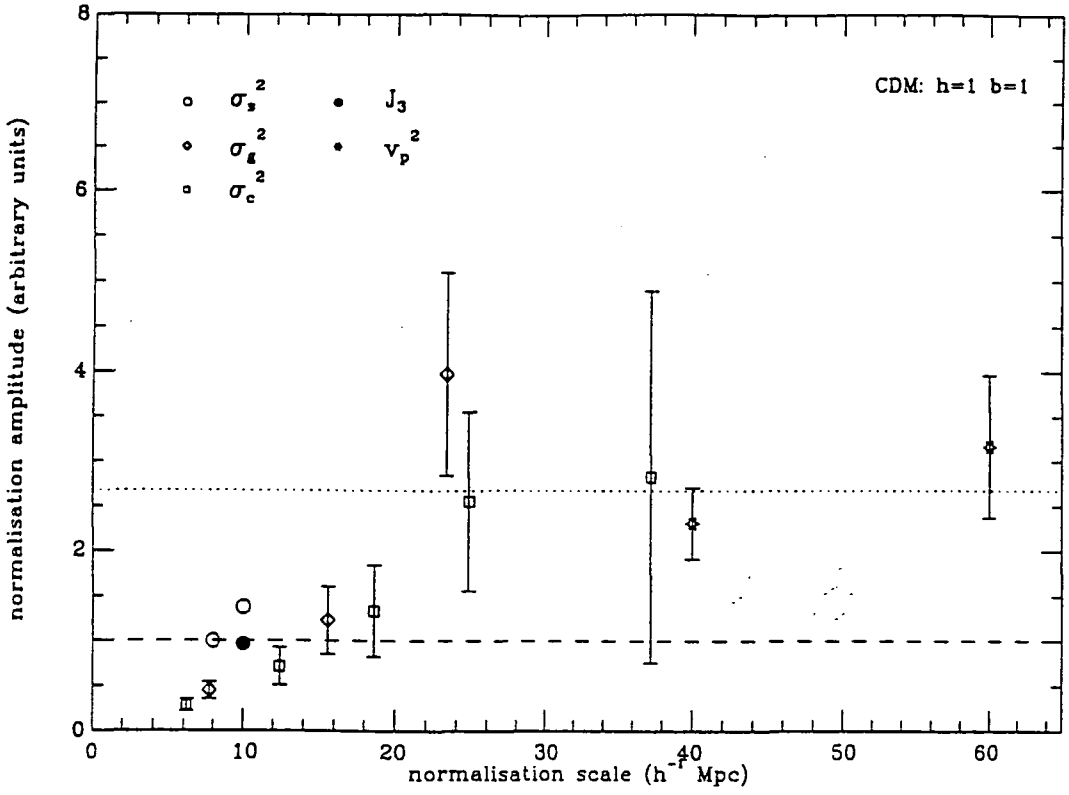

Figure 6.2: Relative normalisation amplitude for CDM model h = 1, b = 1.

Better agreement with the data is achieved on the largest scales in both cases if the suggestion of Peebles *et al.* (1991) is adopted and normalisation is made by comparison with the value $\sigma_s^2(20\,h^{-1}) \simeq 0.25$ (this denoted by the dotted line in both figures). Agreement on large scales in the h = 1 case is now better than 2.5σ, but there is considerable overprediction on scales smaller than $\sim 12\,h^{-1}$Mpc. However, the new normalisation pushes such scales further into the nonlinear regime, where the linear calculations are inapplicable. Note that at $8\,h^{-1}$Mpc, the amplitude is too large by a factor ~ 0.37, which is close to the value predicted by Hoffman. Scaling the linear calculation by this amount accounts for the non-linearities rather well. For the h = 0.5 case, agreement is better than 2σ for all scales $> 12\,h^{-1}$Mpc, the values at smaller scales again being too large as a result of non-linearities (the scaling is again close to the Hoffman factor). There is a problem, however, in that with the new normalisation, the upper limit on the Rome CMB data is exceeded. If we are to achieve consistency, then a bias factor of order 1.3 or greater is required to correct the effect, but this has the consequence of increasing the relative normalisation amplitude for the peculiar velocity data by b_ρ (although the size of the error bars also increases as this factor). However, even with a bias factor at the top of the range usually quoted, that is ~ 2 as in the standard biased CDM model, the peculiar

velocity data remain consistent with both normalisations to better than 2σ.

The 'standard' model was rejected by Efstathiou *et al.* (1990) largely on the basis of the value $\sigma_c^2(40\,h^{-1})$. Here, the CDM prediction from a small number of simulations indicated a value lower than that from the observations, and with a dispersion which indicated no agreement. However, it seems that this observational point may have been affected by spurious galaxy counts, and an alternate IRAS galaxy survey by Davis and his colleagues finds much better agreement with CDM. More simulations show that the result is quite sensitive to the observers location, and a larger number increases the dispersion in agreement with the standard model, as linear theory naively suggests. The simulations themselves are also sensitive to bias because of the redshift space correction (smaller bias increases the dispersion since the peculiar velocity field increases in amplitude). Park (1991) has also concluded that the $40h^{-1}$Mpc cell may be spurious since analytic models suggest that it is internally inconsistent with the other measures.

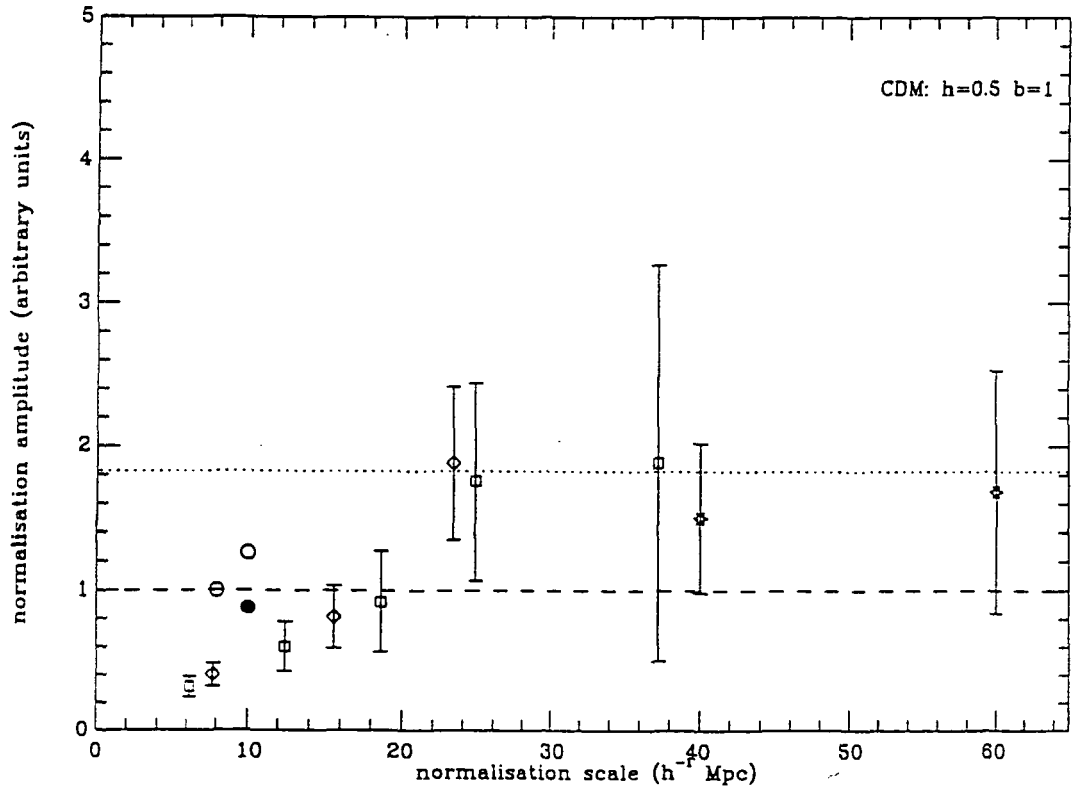

Figure 6.3: Relative normalisation amplitude for CDM model h = 0.5, b = 1.

Thus, it seems that 'standard' CDM with $h = 0.5$ and b_ρ in the range 1.5 - 2 is still consistent with the new data. Normalisation on a larger scale where linear theory is more reliable, and a better understanding of nonlinear effects on scales

below $10\,h^{-1}$Mpc may provide the best minimal solution to the problem of large-scale structure (such a model will obviously require study in some detail via numerical simulations to test its overall validity as a model for galaxy formation). The most natural normalisation, to the peculiar velocity data, seems to be consistent with either normalisation although there is good agreement with the Peebles *et al.* figure.

6.7 Fits to the APM angular correlation function

In this section, several power spectra are considered which provide a reasonable fit to the APM galaxy 2-point angular correlation function $w(\theta)$. This measure suggests that there is more power on large scales than the usual spatial correlation function ($\xi(r) \simeq \left(\frac{r}{r_0}\right)^{-1.8}$, with $r_0 \sim 5\,h^{-1}$Mpc) would give when projected using Limber's equation. Several authors have proposed model power spectra to account for this additional power — the consequences are examined by investigating the expected level of fluctuations in the CMB.

6.7.1 Analytic fit from Peacock (1991)

This was obtained by seeking a formula for $\Delta^2(k)$ which was consistent with scale-invariance for small k. The resultant spectrum was found to give a good fit to the APM $w(\theta)$, to be fairly consistent with the power spectrum analysis of the CfA survey (Baumgart & Fry, 1991), and with a survey of radio galaxies at redshifts less than 0.1 (Peacock & Nicholson, 1991). The QDOT IRAS values also show reasonable consistency. It was found that

$$|\,\delta_k\,|^2 = A k^n (1 + B k^{2.4})^{-1}$$

where $A = 1.182 \times 10^6\ h^{-4}$and $B = 3.345 \times 10^3\ h^{-2.4}$.

Fig. 4 shows the amplitude relative to that derived by the fit to the APM data required to match the observational data. A correction has been made to the values associated with optically selected samples (eg. J_3), since the power spectrum refers to clustering measured in redshift space. The results for σ_c^2 show clearly too much

Experiment	$\Delta T/T \times 10^6$
UW	-
OVRO	-
UCSB	-
Jodrell-IAC	9.02
Rome	10.7
COBE	20.0
a_2	13.9

Table 6.5: $\Delta T/T$ values for Peacock APM fit.

power on small scales, however, this is a result of the use of linear theory where it is not applicable. Since the power spectrum analysis is not very sensitive to small scales, and is motivated by the requirement to match the large scale APM power, then it should not be too surprising that the agreement is not exceptional on scales smaller than $10\,h^{-1}$Mpc, and that there should be evidence for nonlinear effects here.

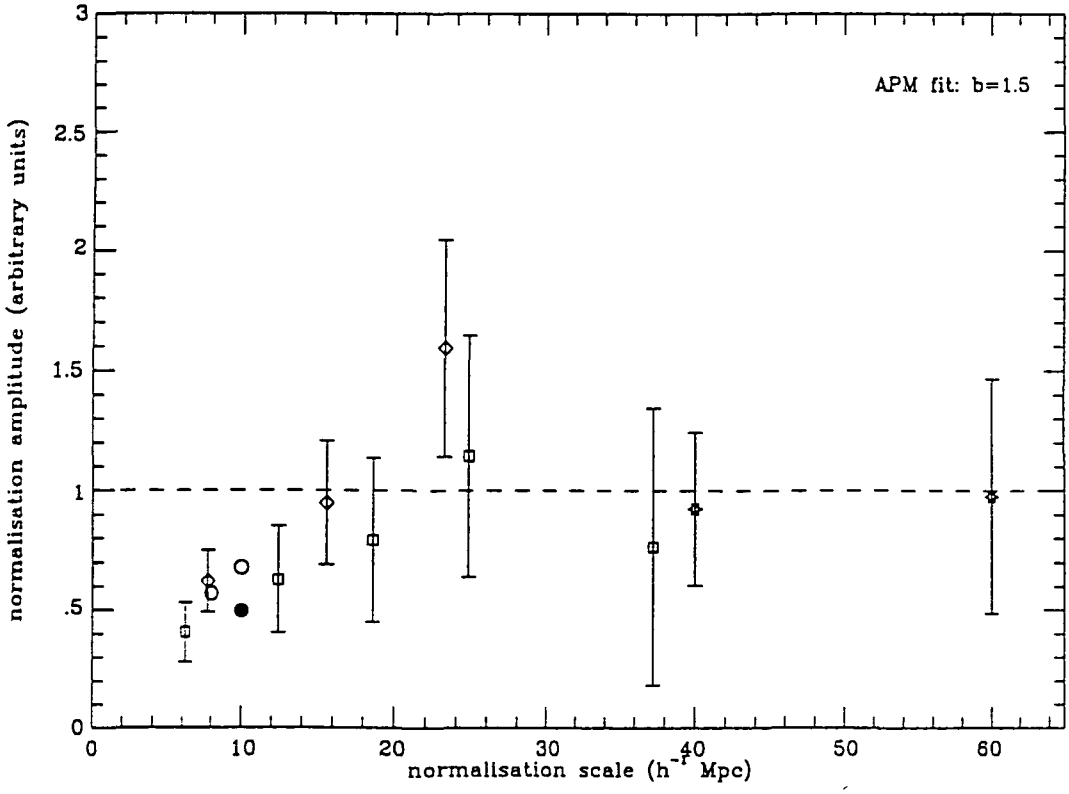

Figure 6.4: Relative normalisations for the APM fit from Peacock (1991).

The $\Delta T/T$ results are interesting in that they suggest that the detection of a genuine anisotropy cannot be too far off. The prediction for the Rome group is within the old Melchiorri *et al.* upper limit; however, the newer limit suggests a bias factor of ~ 1.5 is required. This then brings the predictions for the peculiar

velocities down by $1/b_\rho$ into good agreement with the POTENT analysis. Including the bias factor required from CMB measures, good agreement is evident on on all scales $> 10\,h^{-1}$Mpc. If there were no bias (ie. if the Rome group upper limit were revised upwards), the large scale measures would still be in agreement with the data to better than 1σ.

6.7.2 Alternative power spectra fits to the APM data

Sutherland (1991) has, after a thorough investigation of a large number of model power spectra taken from Efstathiou (1990) and Holtzman (1989), proposed several spectra which seem to reproduce the APM angular correlation function satisfactorily on large scales when the standard $\sigma^2(8\,h^{-1})$ normalisation is employed. These models are,

- Model 1: low density with $\Omega h^{-1} = 0.2$ and a cosmological constant $\lambda = 0.8$ (see also Efstathiou *et al.* , 1990)
- Model 2: a hybrid model with $\Omega_c \sim 0.7$, $\Omega_{HDM} \sim 0.3$, $h = 1$
- Model 3: as above, $h = 0.5$
- Model 4: CDM with $\Omega h^{-1} = 0.75$, white noise initial spectrum ($n = 0$)
- Model 5: Isocurvature CDM, $h = 0.5$ (Peacock, 1991).

	$\Delta T/T \times 10^6$				
Experiment	Model 1	Model 2	Model 3	Model 4	Model 5
UW	3.49	2.92	6.84	-	4.05
OVRO	6.93	5.80	14.2	-	8.37
UCSB	18.10	12.30	39.9		77.94
Jodrell-IAC	5.97	4.66	11.30	28.60	66.40
Rome	6.61	5.16	12.51	34.80	73.51
COBE	15.50	12.11	27.04	114.0	172.48
a_2	8.67	6.77	16.41	111.0	96.41

Table 6.6: CMB fluctuations for model spectra to fit the APM galaxy correlation function

Table 6 gives the CMB fluctuations expected for these models. Whilst it is obvious that the above models will produce large-scale power in the galaxy distribution to similar levels as they should since all were chosen to match the APM correlation function on large scales, the CMB limits allow some conclusions to be made about the models. The values for $\Delta T/T$ were evaluated in the usual fashion where possible using fits for $C(\theta)$ from Efstathiou (1990) and Holtzman (1989).

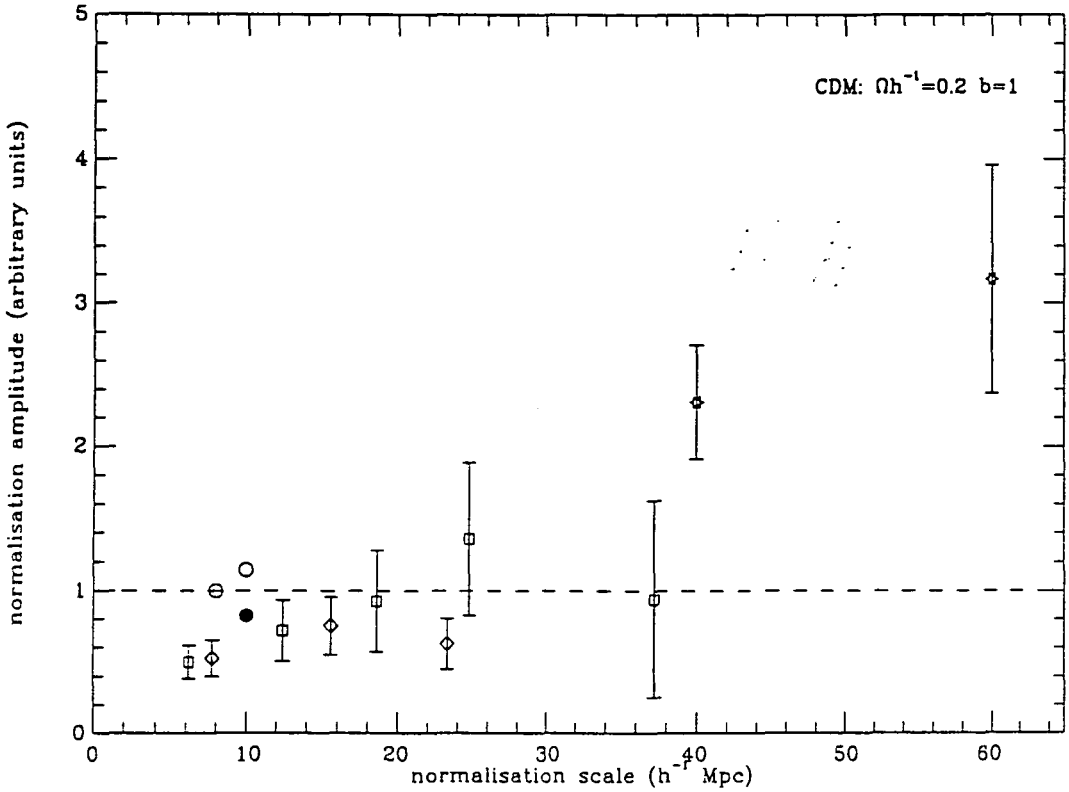

Figure 6.5: Relative normalisation amplitude for CDM model $\Omega h^{-1} = 0.2$, b = 1.

Clearly, models 4 and 5 are ruled out by the excessive amplitude of their quadrupole moments which cannot be reconciled with the COBE upper limit even with the most extreme biasing allowed. Models 1 and 2 survive all of the tests even without biasing, but the calculations imply that the detection of genuine anisotropies is very close. Model 3 exceeds the UCSB and Rome group results, but a bias factor of 2 reconciles the values (if the Rome value is refuted, the a more modest amount of biasing will suffice, $b_\rho \sim 1.2$). Fig. 5 shows the normalisation amplitude required to reproduce the results relative to the $\sigma^2(8\,h^{-1})$ normalisation for the $\Omega h^{-1} = 0.2$ CDM model. It can be seen that whilst the results are in good agreement with the observations on the IRAS QDOT scales (as they were chosen to be), there is some discrepancy with the peculiar velocity results. Thus standard CDM which is more successful over the whole range of scales may remain a better model.

Whilst it is easy to choose model power spectra consistent with the claimed large-scale galaxy distribution, the CMB can provide strong constraints on these models.

6.7.3 Modification of Standard CDM power spectra

This is discussed at length in the paper by Efstathiou (1991). In this paper, the initial scale-invariance of the CDM model is modified in order to retain a spatially flat model with h = 0.5. Recognising that a model with $\Omega h \sim 0.15$ fits the APM data rather well, a function F(k) is evaluated which multiplies the power spectrum for the standard h = 0.5 CDM model so that it matches the spectrum of the low density model. It is then shown that the power spectrum can be modified further still, so that there is no power on scales bigger than $100\,h^{-1}$Mpc, but all the power on scales less than this is reproduced. The resultant fluctuations in the CMB are then determined, and whilst the fluctuations are very small for all scales $> 1^\circ$ for the final model, it is very difficult to avoid generating fluctuations smaller than 10^{-5} if the power on scales of $10\,h^{-1}$- $100\,h^{-1}$Mpc is to be reproduced. Of course, the model itself is not very natural, requiring the existence of special scalar fields at the inflationary epoch in order to generate the initial power spectrum $k\,F(k)$.

6.8 Power Law Inflation and CDM

This model was recently considered by Schaeffer (1991) who noted that it provided consistency with observations over a large range of scales. In this section, the calculations are extended to account for the most recent observations.

In a power law inflationary model, the cosmological scale factor a(t) expands as a power in time rather than as the more usual exponent during the inflationary epoch (Lucchin & Matarrese, 1985). The density fluctuation amplitudes then have a weak scale dependence, $\sim R^{2\alpha}$, with α lying in the range -0.5 to 0.5. The primordial power spectrum is also modified from k^n to $k^{n-2\alpha}$. In the calculations which follow, quantities are evaluated using the standard CDM transfer function for $\Omega = 1$, h = 1 with a bias factor of 2. Normalisation is made using the $\sigma_s^2(8\,h^{-1})$ formalism. The linear equations are modified by the scaling factor, for example, consider the

relation for the variance in a volume defined by the window function W(r),

$$\sigma^2(R) = \frac{1}{2\pi^2}\left(\frac{R}{R_{norm}}\right)^{2\alpha}\int_0^\infty \frac{k^2}{k^{2\alpha}} \mid \delta_k \mid^2 \frac{\mid W_k \mid^2}{V_W^2} dk$$

where R_{norm} is the scale at which the power spectrum is normalised. Table 7 records the results of calculations where, following Schaeffer, α is taken as 0.4. In the Sachs-Wolfe calculations, the scale of interest is that defined by the distance to the last scattering surface, thus is taken as $R \sim \frac{2c}{H_0}$.

Experiment	$\Delta T/T \times 10^6$
UW	-
OVRO	-
UCSB	-
Jodrell-IAC	8.6
Rome	10.3
COBE	30.0
a_2	27.7

Table 6.7: CMB calculations for power law inflation model of CDM

Fig. 6 compares the amplitudes required to reproduce the observational data assuming that the characteristic scale R_{norm} is always $8\,h^{-1}$Mpc with the standard normalisation. The measures are nearly always slightly higher than the observed quantities (after correction for redshift space effects). The bias parameter is required to reconcile the velocity dispersion data to the calculations, and the prediction for $\Delta T/T$ for the Rome experiment to the observational upper limit of 7.3×10^{-6} for an $n = 0.2$ spectrum. It is interesting that there is much less dispersion amongst the best fit relative amplitudes than for the other models, suggesting that the power law CDM spectrum does reproduce the spectral shape required to explain the observations over a variety of scales. There is no need to invoke non-linear effects on small scales, as would be expected in a high bias model. Reducing the normalisation amplitude slightly, or perhaps modifying the power-law inflation expansion parameter α could improve the fit. The model provides a plausible explanation of large-scale power. Detailed simulations are required to ensure that the successes of standard CDM are reproduced by this variation before it can be taken too seriously.

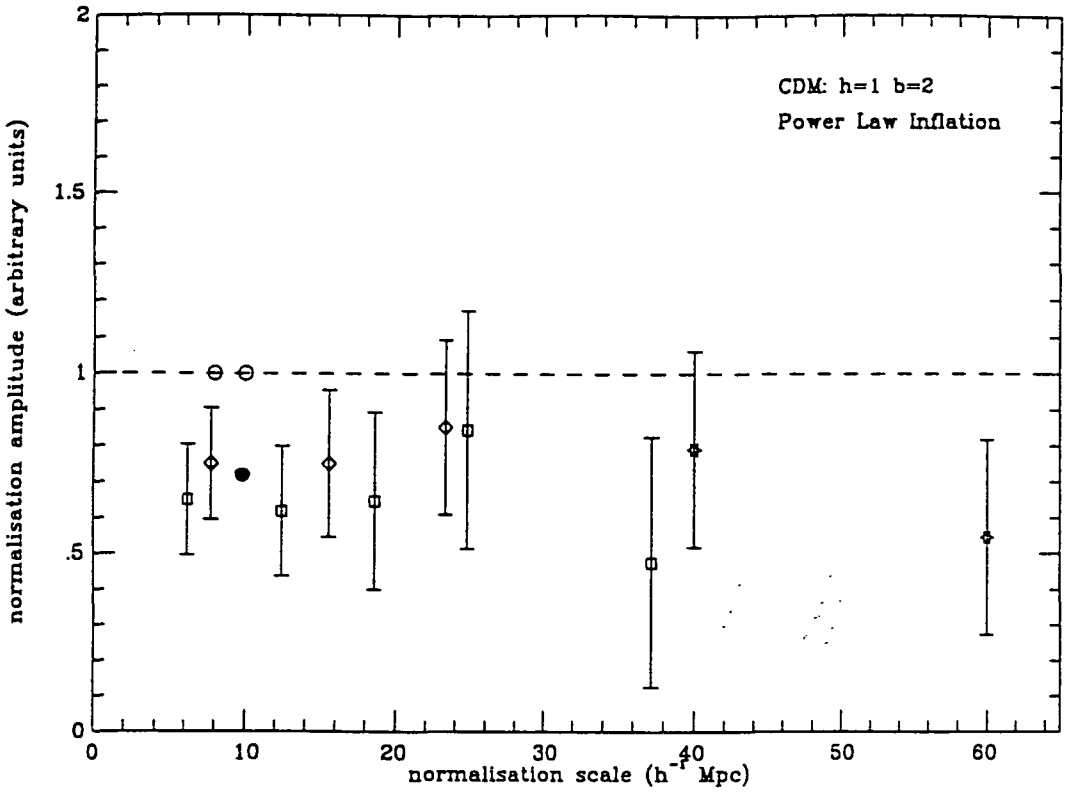

Figure 6.6: Relative normalisations for the power law inflation CDM model.

6.9 Conclusions

Calculations have indicated that the 'standard CDM model of galaxy formation is consistent with the most recent measures of large-scale structure (if the value for $\sigma_c^2(40\,h^{-1})$ is in error), and further that a modest increase in amplitude connected with normalisation on a larger scale where linear theory is more applicable produces even better agreement on these scales, the small-scale overpredictions being accounted for by nonlinear effects, since these scales now certainly lie in the nonlinear regime. Such effects are particularly significant in models with low bias, which have yet to be fully explored. Couchman & Carlberg (1991) have recently evolved an h = 0.5 CDM model with a bias factor on small scales ~ 0.8, and incorporating techniques to account for merging and non-linear dynamical effects. On large scales, non-linear evolution causes growth of the large scale correlation beyond that predicted by linear theory, bringing the simulations into agreement with the APM $w(\theta)$. Clearly, this is an important area of research. If power on still larger scales is determined, then it may yet not be possible to rescue the CDM model. If this is the case, then there is no shortage of models to resolve the excess power problem.

However, the reliability of the observations on the largest scales has been called into some doubt. It appears that the error analysis for the QDOT IRAS survey may be inaccurate in that the errors quoted are too small (this traces to an assumption about the gaussianity of the fluctuations in the survey). This would, of course, improve the agreement with standard CDM. Fong, Hale-Sutton & Shanks (1991) have demonstrated that photometric errors may have produced the large-scale power in the APM galaxy correlation function, the removal of an appropriate zero-point error reducing the spatial break scale to $\sim 10\,h^{-1}$Mpc, in better agreement with the standard model.

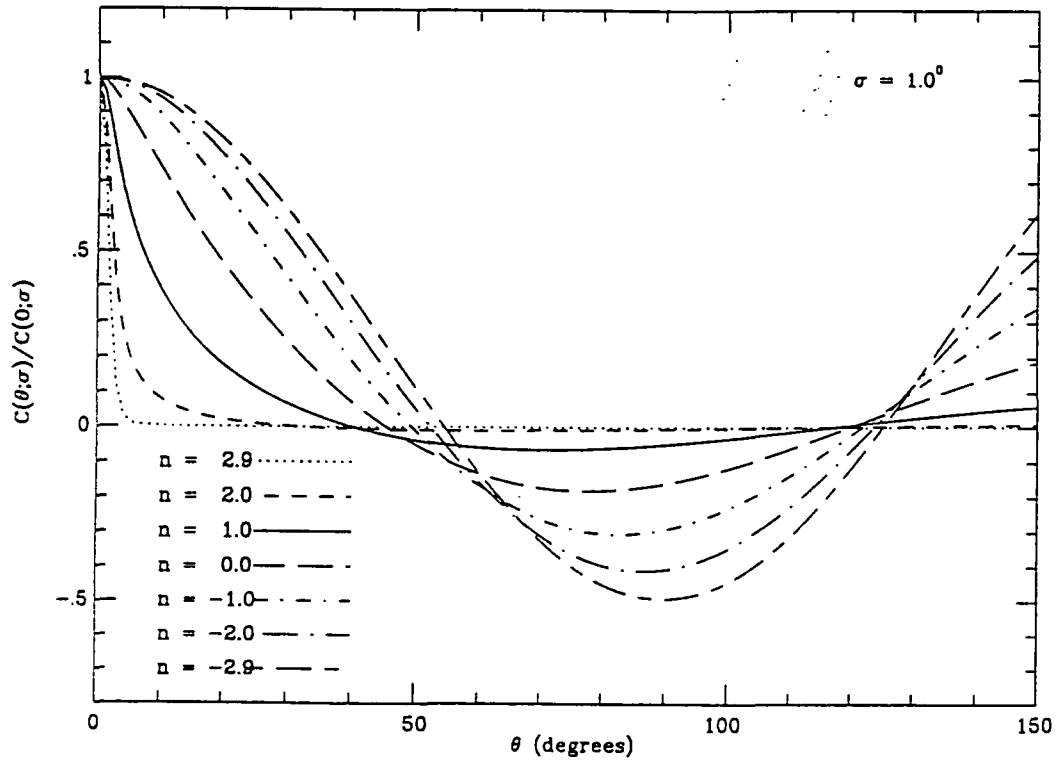

Figure 6.7: The temperature auto-correlation function for a number of spectral indices. The function is normalised to the value at zero lag. All calculations are for a beam of FWHM 1° .

Whatever the origin of the observed large-scale power, it is clear that the observation of anisotropies in the CMB will provide serious constraints on any theoretical model. The South Pole and Rome results (if confirmed) are very important in restricting the number of cosmological models. The nature of the primordial spectrum will also be most evident in observations of anisotropies on angular scales $\geq$ 5° , where microphysical processes play no role and the 'virgin' fluctuation spectrum is observed. The determination of the initial spectral index should be possible since the correlation function of the CMB temperature fluctuations has a different

shape dependent on the primordial spectral index (see Fig. 7). Figs. 8a and b show the variation in the measured $\Delta T/T$ expected from a 3-beam experiment with $\sigma =$ 1° for a number of beamthrows for n = 1 and 0 respectively. It might be hoped that when measures are available of sufficient accuracy, then the variations with θ_b will be discernable enabling the index to be determined.

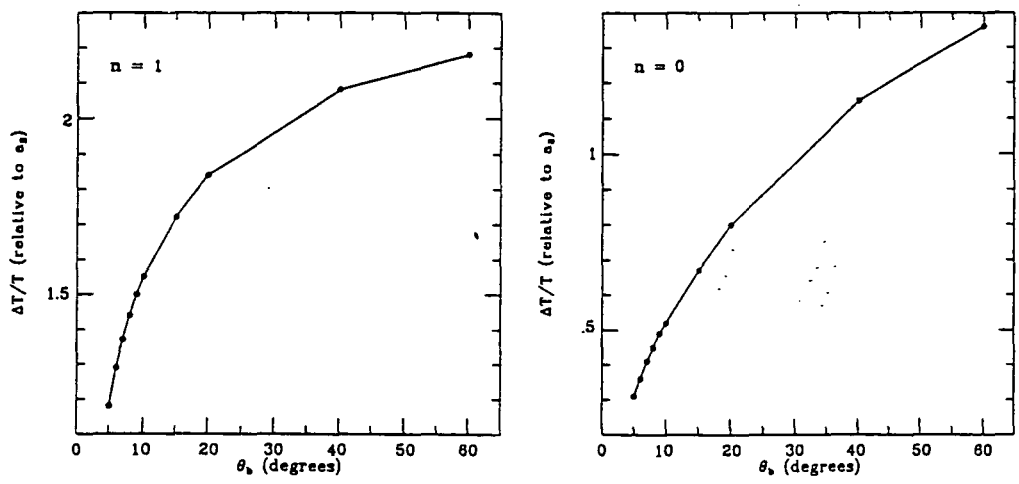

Figure 6.8: The variation of the observed fluctuations in temperature vs. beamthrow for initial spectral indices of n = 1 and 0.

Care should always be exercised when comparing theoretical $\Delta T/T$ values with experimental limits extracted from limited sky coverage observations, detailed comparisons requiring simulations of the expected $\Delta T/T$ for a given cosmological model including sky coverage, sampling strategy etc.

References

Bardeen, J., *et al.* , 1986. *Astrophys. J.*, **304**, 15.

Baumgart, D.J. & Fry, J.N. 1991. *Astrophys. J.*, **375**, 25.

Bertshinger, E.M. *et al.*, 1991. *Astrophys. J.*, **364**, 349.

Bond, J.R., 1990. in *Frontiers in Physics: from Colliders to Cosmology*, eds. Campbell, B. & Khanna, F., World Scientific.

Bond, J.R. & Efstathiou, G., 1984. *Astrophys. J. Letts.*, **285**, L45.

Bond, J.R. & Efstathiou, G., 1987. *Mon. Not. R. astr. Soc*, **226**, 655.

Broadhurst, T.J. *et al.*, 1990. *Nature*, **343**, 726.

Couchman H.M.P. & Carlberg, R.G., 1991. *preprint.*

Davies *et al.*, 1987. *Nature*, **326**, 462.

Davis, M., *et al.* , 1985. *Astrophys. J.*, 292, 371.

Davis, M. & Peebles, P.J.E., 1983. *Astrophys. J.*, **267**, 465.

de Bernardis, P. *et al.*, 1991. in *Observational Tests of Cosmological Inflation*, eds. Shanks, T. *et al.*, Kluwer

Efstathiou, G.. 1988. *Mon. Not. R. astr. Soc*, **235**, 715.

Efstathiou, G. *et al.*, 1990, *Nature*, **348**, 705.

Efstathiou, G., 1990. in *The Physics of the Early Universe'*, eds. Heavens, A.F. *et al.*, SUSSP.

Efstathiou, G. *et al.*, 1991, *Mon. Not. R. astr. Soc*, **247**, 10P.

Efstathiou, G., 1991. in *Observational Tests of Cosmological Inflation*, p. 425, eds. Shanks, T., *et al.* , Kluwer.

Fong, R., Hale-Sutton, D. & Shanks, T., 1991. *preprint.*

Fukugita, M. & Umemura, M., 1989. *Astrophys. J. Letts.*, **339**, L1.

Fukugita, M., Sugiyama, N. & Umemura, M., 1990. *Astrophys. J.*, **358**, 28.

Groth, E.J. & Peebles, P.J.E., 1976. *Astr. Astrophys.*, **53**, 131.

Hoffman, Y., 1987. *Astrophys. J. Letts.*, **318**, L7.

Holtzman, J.A., 1989, *Astrophys. J. Suppl.*, **71**, 1.

Kaiser, N., 1987. *Mon. Not. R. astr. Soc*, **227**, 1.

Lucchin, F. & Matarrese, S., 1985. *Phys. Rev. D*, **32**, 1316.

Lubin, P.M. *et al.*, 1990. in *The Cosmic Microwave Background: 25 Years Later'*, p. 115, eds. Mandolesi, N. & Vittorio, N., Kluwer Academic Press.

Maddox, S.J. *et al.*, 1990. *Mon. Not. R. astr. Soc*, **242**, 43P.

Martínez-Gonzalez, E. & Sanz, J.L., 1991. *Astrophys. J.*, **366**, 1.

Melchiorri, F., *et al.* , 1981. *Astrophys. J. Letts.*, **250**, L1.

Park, C., 1991. *preprint.*

Peacock, J.A., 1991. in *Observational Tests of Cosmological Inflation*, p. 471, eds. Shanks, T. *et al.*, Kluwer Academic Press.

Peacock, J.A. & Nicholson, R., 1991. *Mon. Not. R. astr. Soc*, **253**, 307.

Peebles, P.J.E., 1980. in *The Large Scale Structure of the Universe'*, p.65, Princeton University Press.

Peebles, P.J.E., 1984. *Astrophys. J.*, **277**, 470.

Peebles, P.J.E., *et al.* , 1991. *preprint.*

Readhead, A.C.S. *et al.*, 1989. *Astrophys. J.*, **346**, 566.

Saunders, W., *et al.* , 1991, *Nature*, **349**, 32.

Schaefer, R.S., 1991. in *Physical Cosmology*, p.429, eds, Blanchard, A., *et al.* , Editions Frontiéres.

Smoot, G.F., *et al.* , 1991. *Astrophys. J. Letts.*, **371**, L1.

Sutherland, W.J., 1991. in *Observational Tests of Cosmological Inflation*, p. 331, eds. Shanks, T., *et al.* , Kluwer.

Uson, J.M. & Wilkinson, D.T., 1984. *Nature*, **312**, 427.

Vittorio, N. & Silk, J., 1985. *Astrophys. J.*, **293**, L1.

Chapter 7

Conclusions

In this thesis, we have investigated a number of effects which can complicate searches for fluctuations in the Cosmic Microwave Background. In particular, a detailed investigation has been made of the foreground emission from the Galaxy, and the expected contribution from discrete sources, ie. the radio and FIR emission from other galaxies. These foregrounds have frequency dependencies which differ from that of the primordial CMB fluctuations which (aside from the conversion from brightness to thermodynamic temperature) are frequency independent, thus it should be possible to observe the microwave sky at a frequency which minimises the foreground emission. The accurate subtraction of all foregrounds is obviously of great importance since oversubtraction leaves residual sky fluctuations which impose excessively strong and unrealistic constraints on cosmological models as well as the possibility of subtracting away genuine signals, whilst undersubtraction ascribes cosmological importance to non-cosmological fluctuations. Particular attention has been paid to the problem of removing the Galactic foreground on large angular scales, viz greater than $\sim 1^{\circ}$ (where the CMB fluctuations are expected to be primordial and unaffected by the reionisation history of the universe).

In Chapter 2, it was demonstrated that the Galactic Synchrotron emission could reproduce the observed fluctuations at 10 GHz from the Davies *et al.* (1987) experiment. The region in question actually corresponds to a quiet region of the sky, so that non-cosmological fluctuations away from this region will be higher and the unambiguous detection of anisotropies requires moving to higher frequencies. Only for frequencies above 20 GHz in this quiet region is there the possibility of the detection

of a genuine signal. Since the Jodrell-IAC group plan to extend their observations to 30 GHz, use of the 10 GHz and 15 GHz survey now in progress to eliminate any residual Galactic signal will lead to either the detection of anisotropies or much improved upper limits on the likely cosmological signal, provided that the experimental noise and atmospheric contribution can be reduced sufficiently. In this chapter, we also investigated the possibility of distinguishing between CMB and GSR fluctuations from the corresponding temperature auto-correlation functions, but found that the coherence length of GSR effects was similar to that expected in CDM scenarios, even demonstrating a similar dispersion for limited sky regions. Only by reducing the amplitude of GSR fluctuations by moving to higher frequencies and using models and extrapolations from lower frequencies to understand the residual effects can observations be made attainable.

In Chapter 3, the effects of Galactic dust emission at higher frequencies was considered. Use of the IRAS 100 μm data along with a number of fits to the frequency dependence of the emission again suggested that even at the highest latitudes the Galactic contribution could be significant. However, the possible existence of cold dust and spectral variations of the emission with Galactic position implies that the IRAS data by itself is unlikely to yield an accurate enough prediction of the foreground.

Chapter 4 used a fit to the thermal emission from the plane originally derived by Broadbent (1989) together with an estimate of the thermal emission at high latitudes from Hα data in combination with maps of the GSR and dust emission to generate maps of the sky at the COBE DMR frequencies of 31.5, 53, and 90 GHz. The accuracy of extrapolation, and in particular of the thermal emission, was estimated from comparisons of sky maps generated at 10 GHz with a number of Galactic plane crossings at different declinations from Watson (1989). The results are in agreement to better than 20% for the regions considered. The COBE type maps show similar features to those published in Smoot *et al.* (1991) - the sky temperature is dominated by the Galactic plane emission, although this falls off quite rapidly with increasing frequency. Improvements to the model could be made by comparison with the 19 GHz map of Boughn *et al.* (1990) and the 24.5 GHz map of Fixsen, Cheng & Wilkinson (1983) to check the thermal emission from HII regions in the plane. A quiet region on the sky was also identified using the 408

MHz radio survey and the IRAS 100 μm survey as indicators – this would be an excellent region in which to plan more sensitive searches for CMB anisotropies to push down existing limits, and to use as a calibrator for all-sky surveys. The nature of the Galactic emission and its frequency dependence implies that the foreground emission should reach a minimum at $\sim$ 60 GHz (although there is some variation with sky position).

Chapter 5 summarises the contribution from known discrete sources – the radio and FIR emission from galaxies. At the largest scales, the contribution is small at the COBE frequencies, but at $\sim$ 10 GHz, and in the sub-mm region, the fluctuations remain important (for a beam of FWHM 7°). On the smallest scales, the radio emission from galaxies may remain the limiting factor in the detection of anisotropies.

The work in this thesis reinforces the notion that for the CMB, everything else is foreground, and whilst we have considered a number of the potentially important foreground effects, there are a number of other plausible astrophysical sources lying between us as observers and the source of the CMB. These have been discussed elsewhere (see Bond, Carr & Hogan; 1986, 1991) and such sources are also expected to emit at a level which becomes increasingly significant as observational upper limits on anisotropies fall. It is important to realise is that the observation and interpretation of anisotropies is now a field of astrophysics requiring multi-frequency maps, since when $\Delta T/T \leq 10^{-6}$ there will inevitably be structure in the observed sky brightness distribution. The use of existing surveys to estimate the likely level of Galactic contamination is open to question (see Chapter 4 for a discussion) since these are quite often not absolutely calibrated and are subject to problems with baseline errors. New more sensitive surveys are certainly required to aid the Galactic foreground modelling. The COBE project will undoubtedly provide the best results on degree scales to date, and with its wide spectral coverage will certainly generate some complete models of the all-sky dust emission, which will help the analysis of ongoing anisotropy measurements and plans for future projects. However, the likely contribution to the lowest frequency DMR band centred on 31.5 GHz from GSR still remains somewhat uncertain, and it may be that lower frequency radio surveys will have to be specially undertaken to enable better modelling of this component (an absolutely calibrated 408 MHz survey with baseline errors removed by some

Fourier cleaning technique would also be of assistance). The large scale distribution of radio sources and the extension of number counts to the faintest flux levels is of importance on both large and small angular scales.

Another possible technique to reduce foreground effects is to optimise the experimental configuration to avoid any characteristic scales in the foregrounds. Efstathiou (1990) describes how to compare the filter function of a given experiment with the likely power on that scale for a given cosmological scenario, allowing the design of the experiment to be adjusted to match any peaks in the CMB power spectrum. Whilst optimising the observational strategy towards a given theoretical model may not be advisable (how realistic is the model ?), the adoption of a similar technique to allow the configuration to avoid any power in the foregrounds might be helpful. Theoretical work towards understanding the correlation functions of GSR or dust in the interstellar medium is thus needed (Banday, Giller & Wolfendale; 1991 have attempted a number of models to explain the GSR correlation function at low frequencies).

One approach to improve observational constraints on the CMB might be to make a number of all-sky surveys at intermediate resolution over a number of frequencies (to help foreground subtraction), together with higher resolution observations at those same frequencies on smaller regions which are either quiet in terms of the total sky temperature or contain a number of interesting features. The smaller regions might then help to calibrate the all-sky surveys, as well as aiding the foreground modelling, since the instrumental noise can be reduced considerably over the integration times available in comparison to an all-sky survey. The interpretation of the limits set by small sky area observations is open to some question, however, particularly with respect to those models such as CDM where even the angular average over the whole of our observable sky does not coincide with the theoretically determined ensemble average; that is, our own microwave sky is not a fair sample for large scale CMB anisotropy as a consequence of the long range nature of the gravitational interactions and the assumed power spectrum. Fig. 1 demonstrates the variations expected for different observers in a CDM model for the observed correlation function Watson (1989) compared to the theoretically expected average for an all-sky survey. There is considerable variation, and since the observed rms second difference measure is proportional to this correlation function, some dispersion

is expected in the calculated average result for different observers (see Scaramella & Vittorio; 1990).The investigation of a limited sky region is only likely to increase the dispersion further. In baryonic models, our microwave sky is virtually indistinguishable from the ensemble average, but again limited sky observations will create some dispersion about the theoretically predicted $\Delta T/T$. An unambiguous approach for comparing theory and observation in a statistically significant sense is to perform Monte Carlo simulations of the sky as expected in a given scenario and analyse them as is done in the actual experiment. Numerical methods of this kind provide perhaps the only direct means of including effects such as differencing strategy, instrumental noise, sky coverage and data sampling. Simulations will also become increasingly important once CMB fluctuations are actually detected to compare the topological variations in small regions with theoretical expectations, as opposed to using the peak theory (Bond & Efstathiou; 1987) which merely predicts the numbers of peaks above/below a given threshold in an average sense.

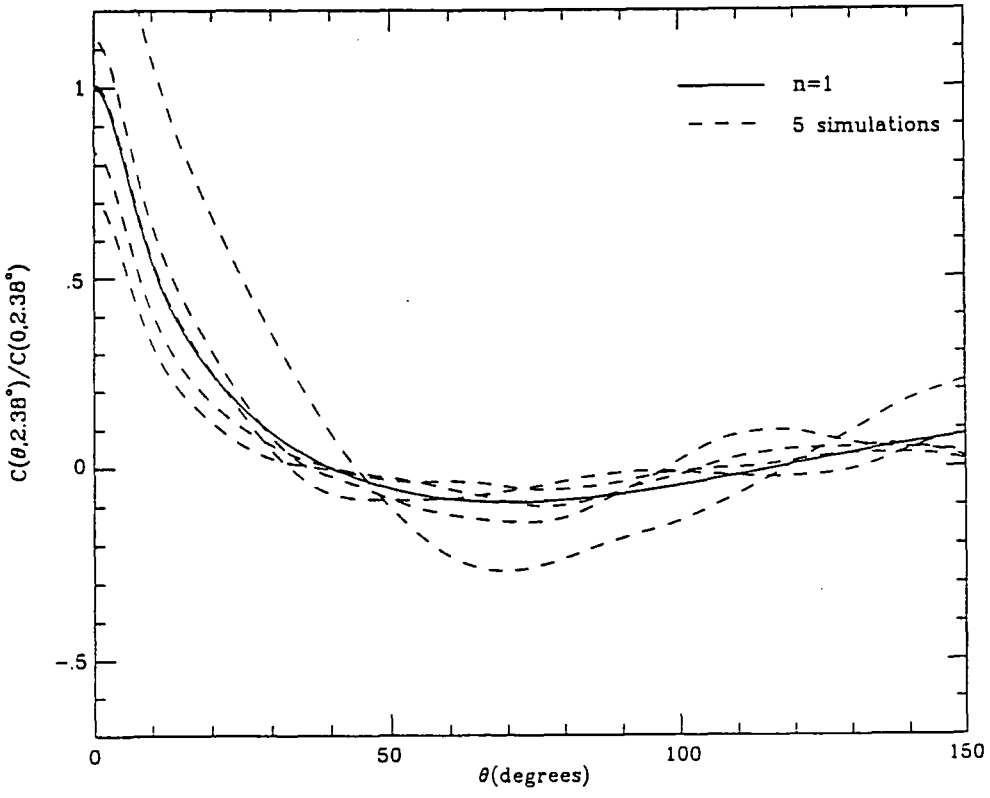

Figure 7.1: The calculated all-sky CDM correlation function for 5 different observers compared to the ensemble average (solid line).

Finally, new techniques of both a statistical and observational nature, plus the adoption of sites to reduce atmospheric effects should allow an increase in sensitivity by a factor of 2 or 3, which is just at the point where, if the large-scale structure

discussed in Chapter 6 is verified, CMB anisotropies can be expected to be seen. Detailed models of the astrophysical foregrounds should then allow some important constraints on cosmological models to be made through the unambiguous detection of CMB anisotropies.

References

Banday, A.J., Giller, M. & Wolfendale, A.W., 1991. *Proc. 22nd I.C.R.C.*, in press.

Bond, J.R., Carr, B.J. & Hogan, C.J., 1986. *Astrophys. J.*, **306**, 428.

Bond, J.R., Carr, B.J. & Hogan, C.J., 1991. *Astrophys. J.*, **367**, 420.

Bond, J.R. & Efstathiou, G., 1987. *Mon. Not. R. astr. Soc*, **226**, 655.

Boughn, S.P., *et al.* , 1990. *Rev. Sci. Instrum.*, **61**, 158.

Broadbent, A., 1989. *Ph.D Thesis*, University of Durham.

Davies R.D., *et al.* , 1987. *Nature*, **326**, 462.

Efstathiou, G., 1990. in *Physics of the Early Universe*, SUSSP.

Fixsen, D.J., Cheng, E.S. & Wilkinson, D.T., 1983. *Phys. Rev. Letts.*, **50**, 620.

Scaramella, R. & Vittorio, N., 1990. *Astrophys. J.*, **353**, 372.

Smoot, G.F., *et al.* , 1991. *Astrophys. J. Letts.*, **371**, L1.

Watson, R.A., 1989. *Ph.D Thesis*, Victoria University of Manchester.

Appendix A

Monte Carlo Techniques

In Chapter 2, extensive use is made of Monte Carlo techniques to simulate on a computer random behaviour which is either too difficult to evaluate analytically, or for which insufficient information is available to allow better than a statistical approximation to be made to the data.

Such calculations are based on pseudorandom numbers, a reproducible set of numbers generated on the unit interval (0,1) which satisfy certain statistical tests for independence. In those calculations which utilise Monte Carlo techniques, these random numbers have been generated using the internal machine specific function provided by *Digital Electronic Corporation's* VAX 3400 machines which form part of the Durham Starlink cluster. A commercial random number generator such as this often sacrifices accuracy for speed, and it is not uncommon for errors to creep into a calculation as a consequence of unforeseen correlations. To improve upon the performance, the **Bays-Durham** algorithm may be employed.

The Bays-Durham Algorithm:

1. Initialize by generating a large odd number N (N=97, say) of random numbers in an array v using the available generator. Generate a new random number u and save it.

2. On the next call, use the number u as an address $j = 1+$ (integer part of Nu) to choose v_j as the random number to be returned. Save v_j as u for the next

call. Replace v_j in the array with a new random number from the available generator. On the next call, go to b).

Monte Carlo techniques evaluate the outcome of a process from a set of possibilities according to a particular probability density function. In Chapter 2, a random spectral index component was chosen according to a gaussian distribution of spectral indices. The following algorithm provides a relatively accurate and fast way of selecting a random variable according to a gaussian distribution of zero mean and unit dispersion.

Gaussian distribution: Generate two uniformly distributed variables u_1 and u_2. then $v_1 = 2u_1$ - 1 and $v_2 = 2u_2$ - 1 are uniform on (-1,1). Calculate $S = v_1^2 + v_2^2$. If $S > 1$, start again, otherwise

$$z_i = v_i \sqrt{\frac{-2 \ln S}{S}}$$

for $i = 1,2$ are independent and gaussian distributed. For another mean μ and dispersion σ^2 use $z_i' = \sigma z_i + \mu$.

Later on in Chapter 7, random sampling from a chi-square distribution is performed (whilst evaluating the variation of the temperature auto-correlation function in a CDM model for different observers).

$\chi^2(n_D)$ distribution: If n_D is the number of degrees of freedom, then for n_D even, generate $n_D/2$ random numbers u_i, y from the chi-square distribution is given by:

$$y = -2 ln \left(\Pi_{i=1}^{n_D/2} u_i \right)$$

If n_D is odd, generate $(n_D\text{-}1)/2$ random numbers, and one gaussian z as before, then

$$y = -2 ln \left(\Pi_{i=1}^{(n_D-1)/2} u_i \right) + z^2$$

For more details of all these techniques, see 'Review of Particle Properties', Phys. Lett **B239**, April 1990.